Design and Development of Brush-Arm Star Polymers for Applications in Drug Delivery

By

Jenny Liu

B.Sc. Chemistry
McGill University, 2011

Submitted to the Department of Chemistry
in Partial Fulfillment of the Requirements for the Degree of

DOCTOR OF PHILOSOPHY
IN BIOLOGICAL CHEMISTRY

at the

MASSACHUSETTS INSTITUTE OF TECHNOLOGY

February 2017

Signature of Author: Signature redacted
Department of Chemistry
September 28, 2016

Certified by: Signature redacted
Jeremiah A. Johnson
Firmenich Career Development Associate Professor of Chemistry
Thesis Supervisor

Accepted by: Signature redacted
Robert W. Field
Haslam and Dewey Professor of Chemistry
Chairman, Departmental Committee on Graduate Students

This doctoral thesis has been examined by a committee of Professors from the Department of Chemistry as follows:

Signature redacted

Professor Barbara Imperiali _

Thesis Committee Chair

Signature redacted

Professor Jeremiah A. Johnson _

Thesis Supervisor

Signature redacted

Professor Bradley L. Pentelute _

Thesis Committee Member

Design and Development of Brush-Arm Star Polymers for Applications in Drug Delivery

By

Jenny Liu

Submitted to the Department of Chemistry
on September 28, 2016 in Partial Fulfillment of the
Requirements for the Degree of Doctor of Philosophy
in Chemistry

ABSTRACT

Treatment and prevention of disease is a major area of research effort and interest; development of new technologies could overcome limitations of current medicines, and provide new treatment modalities that improve patient outcomes. In cancer, small molecule chemotherapeutics often suffer from lack of selectivity, poor pharmacokinetics and biodistribution, limited solubility, fast clearance from the body, and development of resistance. Nano-sized particles that conjugate to or encapsulate small molecule drugs could address these issues by increasing circulation times and facilitating selective delivery of a higher drug load to the tumor, which overall can help improve efficacy and lower toxic side effects. This thesis describes the development of a unique polymer architecture – the Brush-Arm Star Polymer (BASP) – that represents a modular, customizable therapeutic platform with potential in drug delivery.

In this thesis, BASPs are synthesized by ring opening metathesis polymerization (ROMP) of a norbornene functionalized PEG-based macromonomer to first form a living bottle-brush initiator. Next, a bifunctional norbornene crosslinker is added to the bottle-brush polymer to yield star polymers with a crosslinked-core and bottle-brush polymer arms. We synthesized a variety of functional macromonomers and crosslinkers to use in BASP synthesis. For example, drug-loaded doxorubicin macromonomers were synthesized that could release free doxorubicin under a light stimuli or by hydrolysis. Crosslinkers were designed to facilitate BASP degradation, and ultimately enable excretion of BASP components from the body. Various crosslinkers that respond to UV irradiation, change in pH, or reducing conditions were investigated. A multi-drug-conjugated BASP was synthesized and characterized that contained the drug components of FOLFIRINOX, a combination therapy regimen for pancreatic cancer. Nanoparticle combination therapy offers the advantage of delivering combination of drugs at desired ratios in one vehicle, which may improve efficacy due to drug synergism, enhance synthetic reproducibility, and reduce regulatory challenges. This thesis highlights the development of BASP nanotechnology in an effort to improve efficacy and reduce side effects compared to conventional therapeutics.

Thesis Supervisor: Jeremiah Johnson
Title: Firmenich Career Development Associate Professor of Chemistry

Acknowledgements

Throughout my journey in graduate school, I have had the opportunity to meet many wonderful and talented people who have inspired and helped me be who I am today. I have so many people to thank and acknowledge for their support, friendship, and encouragement.

To my PhD advisor, Professor Jeremiah Johnson, thank you for the opportunity to work in your lab and on all your knowledgeable insights. I've learned so much from all the various projects that I got to work on and from the people that you have welcomed into your group. Your guidance on my projects has been invaluable, and I am grateful for all the opportunities you have given me.

I would also like to thank my thesis committee chair, Professor Barbara Imperiali, for all the advice provided through the years. Thank you also to thesis committee member, Professor Bradley Pentelute, for your advice as well. Both of you have helped me through the orals process and given good feedback.

I would also like to thank everyone in the Johnson group, past and present, including graduate students, postdoctorates, visiting students, and undergraduates. Thank you all for answering my questions and talking with me, both about science and life in general. I have learned so much from the people around me. You all have made a difference in my life and I could not have survived the past five years in graduate school without you.

Thank you to all the people who have joined me in the Johnson Lab as first years, Jessica McCombs, Dr. Aleksandr Zhukhovitskiy, Alan Burts, and Alexandra Cok. Although many of you have left, your impact on the lab, such as projects started and setting up the lab, have been meaningful. Special thanks to Jess, you have been a good friend, not just to me but everyone, and made lab more enjoyable. To Alex, thank you for answering all my questions and helping me with chemistry. You will make a great professor in the near future. Alan, your time was short so I didn't get to know you for too long, but you helped me a lot when I started to work on the BASP project, and this thesis wouldn't be here today without you.

To Michelle Macleod and Ken Kawamoto, who joined the Johnson lab a year after me, thank you for everything – I appreciate all the advice and conversations we had. I cannot emphasize enough that I would not have been able to graduate without you both. Also, thank you Michelle for bringing Buddy into lab every day. Seeing him always brings a smile to my face. To

Molly Sowers and Angela Gao, your friendliness and positivity will never be forgotten. I really enjoyed working with all four of you, and know you will all do amazing things to come.

To Deborah Ehrlich, you are such an amazing and nice person. I really appreciate all your help and the little things you've done for us. Keep up the great work! To the younger years, Yuwei Gu, Hung Nguyen, Yivan Jiang, and Julia Zhao, hang in there and enjoy the journey. Lots of rough years may lay ahead, but it could be worthwhile at the end.

To the postdoctorates that I have had the opportunity to meet and learn from, your expertise has taught me a lot. Dr. Huaxing Zhou and Dr. Longyan Liao, thank you for teaching me science. I am grateful that Jeremiah hired you both because your mentorship, leadership, and general lab knowledge were incredibly helpful when I first joined the lab. Dr. Mingjiang Zhong, Dr. Mao Chen, and Dr. Yufeng Wang, all of you were great mentors and very knowledgeable. Thank you for the scientific advice and help – all three of you will make amazing professors, and I can't wait to see the science to come from your labs. Dr. Matthew Golder, Dr. Qixian Chen, and Dr. Farrukh Vohidov, I can't thank you enough for all your help on the XTuit or FOLFIRINOX project; it was a great experience working with each of you.

To all the undergraduates that I have mentored, Ryan Liu, Leila Terrab, Kevin Erazo, and Julie Kim, it has been a pleasure to mentor all of you. I can't say enough how lucky I've been to have met each of you and will be excited to hear about all the things you will accomplish.

Thank you to all my collaborators, who have given valuable feedback on my projects. Dr. Peter Ghoroghchian and Dr. Mandar Muzumdar, your knowledge and expertise has been a huge help in the drug delivery project. From the Ghoroghchian lab, I would like to thank Xi Yang, Zhimin Tao, and Haihua Xiao for your help in running assays, providing me with cells, and experimental advice. From the Hammond Lab, I would like to thank Dr. Erik Dreaden, your scientific expertise was a huge help in our lab. Without you, we would never have been able to begin *in vitro* and *in vivo* studies. Thank you for your mentorship and answering all our biological related questions. To my collaborators at XTuit, it has been a great pleasure to work with everyone at the company including Peter, Don, Jannik, Jenny, Paul, Melody, Misha, Ritsuko and many others.

To my past undergraduate advisors, Professor Deborah Zamble at the University of Toronto, Professor Dmitrii Perepichka at McGill University, and Professor Christopher Barrett at

McGill University, thank you for teaching and preparing me for graduate school. I've learned a lot from you and people in your labs, which helped prepare me for the difficult road ahead. Andrew Sydor, who mentored me in the Zamble Lab, you were an amazing teacher and role model; thank you for your guidance and mentorship.

To Wankyu Lee, words can't even express how much you mean to me. Thank you for supporting me through all the tough times in graduate school and understanding me as a person. You are funny, nice, confident, positive, smart, and many more great personality traits that have made you an amazing role model and friend. You have always found a way to lighten up my day, even when things go wrong. You have been a huge help in my science, as well, and my projects would not have been successful without you. Thank you so much for being you and making me a better person!

I would also like to thank all my friends, who have made graduate school fun and improved my graduate school experience. To those who joined me in my very first year at graduate school, thank you for all the fun times! Kurt Cox, Phoom Chairatana, Mike Mavros, Matt Welborn, Stephanie Cheung, Jessica McCombs, and Paul Stevenson thank you for all the memories – playing volleyball or board games, eating out together, and hanging out – graduate school was much more enjoyable with friends to de-stress with. To everyone I play volleyball with, thank you for coming out every weekend and all the laughs. To everyone in the biochemistry division in my year, Kurt Cox, Wankyu Lee, Jingjing Ling, Mark Simon, Phoom Chairatana, Victoria Hung, and Stephanie Cheung, thanks for all the practice help during second and third year orals. To everyone I had the opportunity to TA with in 5.112 and 5.12, it was great getting to know everyone; thank you for making the TA experience even better.

Also, I would like to acknowledge everyone in the MIT community, who have worked hard to make graduate school a better experience. Tyler Brezler, thank you for everything you have done for the Johnson Group. Jennifer Weisman, I don't know how you manage everything, but thank you for working hard to help us. To everyone who works at the DCIF, thank you for your dedication to running the facility and helping us in our experiments.

Finally to my family, thank you for your continuous support. Mom, Dad, Grandma, and Gina, I wouldn't be here today without you; thank you for listening and supporting when times were rough and stressful. I can never thank you enough for everything you have taught me throughout the years and raising me to be the person I am today.

Table of Contents

Appendix Chapter II

Abbreviations

^{1}H-NMR	Proton nuclear magnetic resonance
^{13}C-NMR	Carbon-13 nuclear magnetic resonance
5FU	5-fluorouracil
Acetal-XL	Acetal crosslinker
AHA	L-Azidohomoalanine
A.U.C.	Area under the curve
Az	Azide
ARBs	Angiotensin II receptor blockers
BAIB	Bisacetoxyiodobenzene a.k.a. (Diacetoxyiodo)benzene
BASP	Brush-arm star polymer
CAFs	Cancer-associated fibroblasts
CHCA	α-cyano-4-hydroxycinnamic acid (MALDI-TOF matrix)
CI	Combination index
CTG	CellTiter-Glo luminescent cell viability assay
CuAAC	Copper (I) – catalyzed alkyne-azide cycloaddition
CuOAc	Copper (I) acetate
CPT	Camptothecin
CPT-MM	Campthothecin conjugated macromonomer
Cy	Cyanine
Đ	Dispersity index
D_{ave}	Average diameter (by TEM)
DCIF	MIT Department of Chemistry Instrument Facility
DCM	Dichloromethane
DDQ	2,3-dichloro-5,6-dicyano-1,4-benzoquinone (an oxidizing agent)
D_H	Hydrodynamic diameter (determined by DLS)
DIPEA	N,N-Diisopropylethylamine
DLS	Dynamic light scattering
Dn/dc	Refractive index increment
DMAP	4-dimethylaminopyridine

DMEM	Dulbecco's Modification of Eagle's Medium
DMF	N,N-dimethylformamide
DMSO	Dimethyl sulfoxide
DP	Degree of polymerization
DTT	Dithiothreitol
ECM	Extracellular matrix
EDC·HCl	N-(3-Dimethylaminopropyl)-N'-ethylcarbodiimide hydrochloride
EDTA	Ethylenediaminetetraacetic acid
EPR	Electron paramagnetic resonance
eq	Equivalents
Et_2O	Diethyl ether
EtOAc	Ethyl acetate
G3	Grubbs 3rd generation catalyst with pyridine ligands
GPC-MALLS	Gel permeation chromatography with multi-angle light scattering detection
HABA	2-(4'-hydroxybenzeneazo)benzoic acid (MALDI-TOF matrix)
HPLC	High-performance liquid chromatography
HRMS	High-resolution mass spectrometry
Im.	Imidazole
IPTG	Isopropyl β-D-1-thiogalactopyranoside
IRT	Irinotecan
IVIS	In vivo imaging system
KAN	Kanamycin
LCMS	Liquid chromatography mass spectrometry
LS	Light scattering
m	MM equivalents in forming living brush initiator (ie. DP of bottle-brush)
mAB	Monoclonal antibodies
MALDI-TOF	Matrix-assisted laser desorption ionization time-of-flight
MeCN	Acetonitrile
MeOH	Methanol
min	Minutes

MM	Macromonomers
MMP	Matrix-metalloprotease
M_n	Number average molar mass (number average molecular weight)
MTD	Maximum tolerated dose
MTT assay	Tetrazolium-based dye assay for monitoring cell viability
M_w	Mass average molar mass (weight average molecular weight)
N	Crosslinker equivalents in star polymer synthesis
NBOC	Nitrobenzyloxycarbonyl
NBOC-XL	Bis-norbornene nitrobenzyloxylcarbonyl crosslinker
NDS	Network disassembly spectrometry
NHS	N-hydroxysuccinimide
Ni-NTA	Nickel-nitrilotriacetic acid resin
NP	Nanoparticle
Oxali	Oxaliplatin
Oxali-XL	Oxaliplatin crosslinker
PAGE	Polyacrylamide gel electrophoresis
PBS	Phosphate buffered saline
PCR	Polymerase chain reaction
PDAC	Pancreatic ductal adenocarcinoma
PDI	polydispersity index (same as Đ)
PEG	Polyethylene glycol
PEG1kDA-NH_2	Hydroxyl PEG 1kDa amine
PEG2kDa-NH_2	Hydroxyl PEG 2kDa amine
PEG4	Tetraethylene glycol
PEG-alkyne-MM	PEG 3kDa branched alkyne macromonomer
PEG-MM	Polyethylene glycol 3kDA –macromonomer
Photo-B-DOX-MM	Photocleavable doxorubicin conjugated macromonomer, 1st generation
Photo-DOX-MM	Photocleavable doxorubicin conjugated macromonomer, newest generation
PLA	Polylactide
PPTS	Pyridinium p-toluenesulfonate
Pt	Platinum

Pt-XL	Cisplatin crosslinker
RI	Refractive Index
ROMP	Ring opening metathesis polymerization
rt	Room temperature
τ	Rotational diffusion time
TBAF	Tetra-n-butylammonium fluoride
TBE buffer	Tris/borate/EDTA buffer
TBDMS-Cl	tert-Butyldimethylsilyl chloride
TCICA	Trichloroisocyanuric acid
TEL	Telmisartan
TEM	Transmission electron microscopy
TFA	Trifluoroacetic acid
THF	Tetrahydrofuran
UV-vis	Ultraviolet-visible spectroscopy
XL	Crosslinker

Chapter 1: Development of brush-arm star polymers (BASPs)

1.1 Introduction

Brief Summary of Chapter and Respective Contributions

Chapter 1 of this thesis is focused on the development of a method to synthesize brush-arm star polymers (BASPs) with ring opening metathesis polymerization (ROMP). Two main publications have resulted from this work as follows:

- Liu, J. *et al.* "Brush-first" method for the parallel synthesis of photocleavable, nitroxide-labeled poly(ethylene glycol) star polymers. *Journal of the American Chemical Society.* **134**, 16337-16344 (2012).
- Liu, J., Gao, A. X. & Johnson, J. A. Particles without a box: brush-first synthesis of photodegradable PEG star polymers under ambient conditions. *Journal of Visualized Experiments* **80** (2013).

All work presented in the results section is my own, unless otherwise stated. Most significantly, I did not contribute to the nitroxide-labeled BASPs study – this work was a combination of effort from Professor J. A. Johnson, A. O. Burts, and Professor M.F. Ottaviani.

Introduction to Polymeric Nanoparticles

Nanoparticles have been widely studied for their potential uses in various settings, including materials, biological, and biomedical applications.[1-9] Nanoparticles are roughly defined as materials with sizes in the range of a few hundred of nanometers or smaller. The field of nanoparticle synthesis is extremely diverse ranging from inorganic nanoparticles derived from bottom-up or top-down approaches, self-assembled liposomes and micelles, polymerization of monomer units into soft matter materials, or conjugation of naturally derived organic biomolecules.[3] In the Johnson group, we focused on the development and synthesis of complex polymer architectures in the nanoscale range with highly tunable properties for potential applications in imaging and therapeutics. For applications in biology, the nanoparticles should be reproducible, easily synthesized, and possess desirable functionalities whether it be water-solubility, biocompatibility, imaging agents, or drug release.[10] Given the success of current nanomedicines in clinical applications, such as Doxil, Abraxane, and Onivyde, nanotherapeutics hold potential as a safer and/or more efficient way of delivering toxic chemotherapeutics to the patient – the advantages and disadvantages of which will be further discussed in chapter 2 of this

thesis.[11] However, ongoing research is needed to find an easy, reliable, reproducible method to make particles with the potential to be biocompatible, highly multi-functionalized, and superior to their equivalent free drug or drug combination in clinical applications.

The field of nanoparticles is diverse encompassing a large number of possibilities with various physical properties. Due to its diversity, it is difficult to generalize any properties of NPs as relevant to all types of applications. However, size on the nano-scale and opportunities to encapsulate small molecules are advantageous for drug delivery, and the biological properties of BASPs will be further discussed in chapter 2 of this thesis. This chapter will explore the synthesis of a new class of star polymers by ring opening metathesis polymerization and opportunities to chemically tune the physical characteristics of these polymeric nanoparticles. Thus, this chapter's introduction will focus on introducing the method and the rationale for using ring opening metathesis polymerization and the background of star polymers. Chapter 2 will then further explore the use of chemistry to introduce functionality to the BASPs with the goal of building functional NPs with desirable properties.

In particular, star polymers differ from linear polymers in that many linear polymers are attached to a core, thus star polymers allow for densely packed architectures with multiple chain ends.[12] The synthesis of star polymers can generally follow one of three routes: (1) 'core-first' by graft-from polymerization of a multifunctional initiator; (2) 'arm-first' by polymerization of a macroinitiator or macromonomer, followed by addition of a multifunctional monomer to form a crosslinked core; (3) an alternative arm-first approach that involves separate synthesis of the star arms, followed by chemical conjugation of the arms to a multifunctional molecule via a graft-to approach.[13] Due to their desirable properties, star polymers have been used in a number of applications including drug and gene delivery, catalysis, and diagnostics.[12,14] We sought to explore the advanced architecture of star polymers as an opportunity to synthesize multifunctional and densely packed nanoparticles, and apply a graft-through polymerization method to build these larger polymeric architectures.

Introduction to Ring Opening Metathesis Polymerization

Ring-opening metathesis polymerization (ROMP) was chosen as the method for polymerizing macromonomers to form star polymers because it is well-known to display remarkable efficiency and functional group tolerance (**Scheme 1.1**).[15-23] ROMP utilizes cyclic

olefins with greater than ~5 kcal/mol strain energy, such as cyclobutene, cyclopentene, cis-cyclooctene, and norbornene, as monomers.[24-26] However, norbornene is often the strained olefin of choice for ROMP due to its high strain energy and the ease of synthesizing norbornene functionalized compounds.[27-31] As is typical for metathesis reactions, ROMP is thermodynamically controlled; the release of ring strain in the monomer provides the driving force for polymerization.

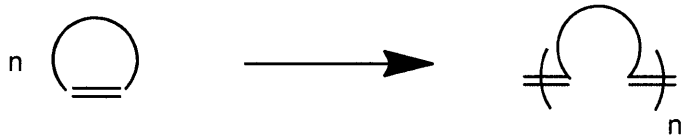

Scheme 1.1: General ring opening metathesis polymerization (ROMP) reaction

Different catalysts have been designed for ROMP, each with its own advantages and disadvantages. Developments in ROMP initiators have led to modern Grubbs Ru-based catalysts, including the Grubbs 3rd generation catalyst. Compared to traditional Ru-based catalysts, the modern Grubbs Ru-based catalysts offer (1) improved functional group, moisture, and oxygen tolerance; (2) improved control of polymer microstructure (e.g., *cis* vs. *trans* olefin configuration and/or tacticity); (3) reduced secondary metathesis reactions – reaction of growing polymer chain with internal polymer olefins either intermolecular or intramolecular (backbiting); (4) improved rates of initiation (k_i) and rates of propagation (k_p).[29,32-34] A large k_i/k_p leads to polymers with very narrow molar mass distribution, which is a highly desirable feature for controlled macromolecular synthesis.[29,30] Due to these developments, ROMP has become a powerful technique for the synthesis of a wide range of functional, well-defined polymers for a variety of applications. [31] The mechanism for ROMP as proposed by Chauvin is shown in **Scheme 1.2**.[27,35]

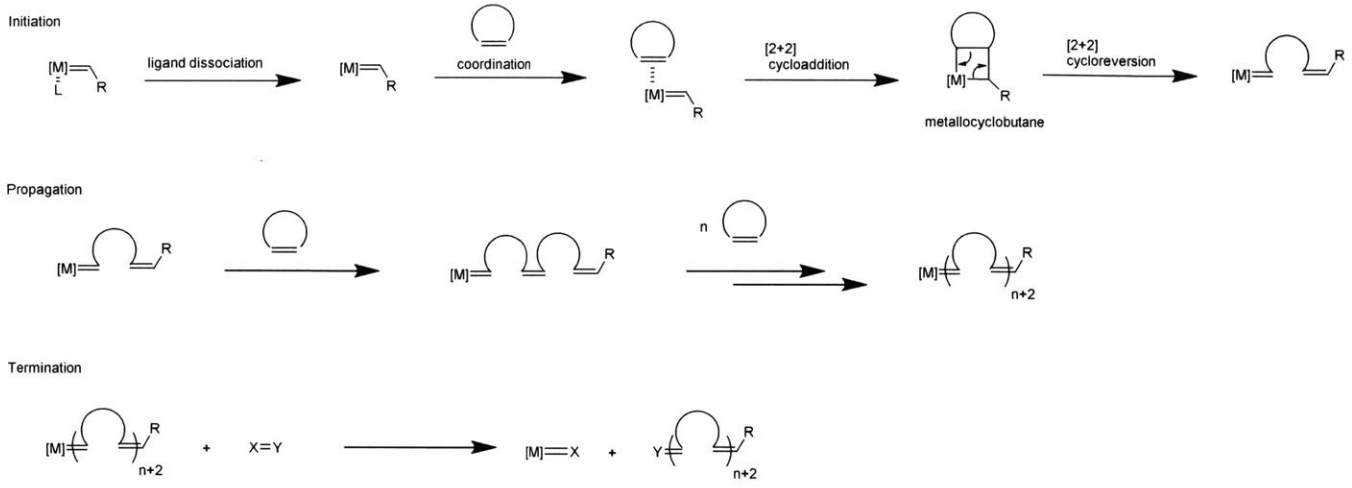

Scheme 1.2: Mechanism of ROMP

The initiation step typically involves dissociation of an L-type ligand from the metal alkylidene complex. Coordination of monomer is followed by [2+2] cycloaddition to produce a metallacyclobutane intermediate. This cycloaddition is followed by a cycloelimination to produce a new metal alkylidene species. Propagation via repetition of this sequence of monomer coordination, cycloaddition, and cycloelimination continues until the reaction is terminated or until all of the monomer is consumed. In the latter case, the living nature of the alkylidene polymer chain end enables the synthesis of block copolymers via the addition of a new monomer to the reaction medium.

The Grubbs 3rd generation catalyst is particularly useful because of its fast-initiation that can lead to living polymers with narrow mass distributions and its functional group tolerance. Thus, the next few paragraphs will discuss the main design considerations and limitations of ROMP with the Grubbs 3rd generation catalyst. To synthesize the Grubbs 3rd generation catalyst, commercially available Grubbs 2nd generation catalyst (**Scheme 1.3a**) is stirred in a solution of 3-bromopyridine or pyridine followed by precipitation (in pentanes) to yield so-called "fast-initiating" Grubbs 3rd generation catalysts with either bromopyridine (**Scheme 1.3b**) or pyridine ligands (**Scheme 1.3c**), respectively.[36,37] The Grubbs' 3rd generation catalyst with pyridine ligands (**Scheme 1.3c**) will be abbreviated as G3 throughout this thesis.

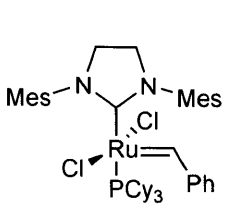

a) Grubbs' 2nd generation

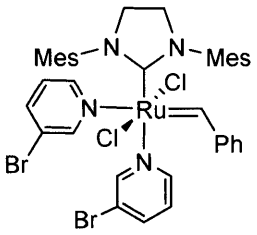

b) Grubbs' 3rd generation with bromopyridine ligands

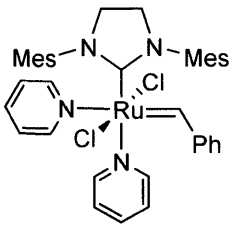

c) Grubbs' 3rd generation with pyridine ligands (G3)

Scheme 1.3: a) Grubbs' 2nd generation catalyst; b) Grubbs' 3rd generation catalyst with 3-bromopyridine ligands; c) Grubbs' 3rd generation catalyst with pyridine ligands (G3)

ROMP with the Grubbs 3rd generation catalyst is a method of living polymerization that is compatible with many functional groups, such as alcohols, carboxylic acids, aldehydes, esters, and quaternary amines. However, the Grubbs 3rd generation catalyst is generally not compatible with some common functional groups found in biological molecules, such as amines and thiols. Grubbs 3rd generation catalyst is effective in organic solvents such as dichloromethane (DCM), tetrahydrofuran (THF), dioxane, and toluene.[34] It also has been used for ROMP in N,N-dimethylformamide (DMF) and protic solvents for the polymerization of polar monomers, such as peptides.[38-40] Monomers designed for ROMP should satisfy the following constraints: a strained ring for polymerization, compatible functional groups with the Ru-based catalyst, and solubility in a solvent compatible with ROMP.

Temperature and monomer concentration also play important roles in ROMP. High monomer concentrations ensure that the rate of propagation is large relative to any potential termination and undesired chain-transfer reactions. For example, sub-optimal concentrations can lead to secondary metathesis reactions, such as intermolecular and intramolecular chain-transfer ("back-biting"). These side reactions can lead to cyclic oligomers particularly in cases of polymers with flexible back-bones.[27] In general, higher monomer concentrations and room temperature or lower are preferred for ROMP. Due to its advantages, ROMP has been used in making polymers for various applications, and is outlined in multiple reviews.[28,30-32,41,42]

Ring Opening Metathesis Polymerization for Synthesis of Star Polymers

ROMP can be employed for the 'arm-first' synthesis of core-crosslinked star nanoparticles. For example, Shrock and co-workers reported the synthesis of low dispersity star

polymers from small-molecule monomers, such as norbornene, dicarbomethoxynorbornadiene, and trimethylsilyl protected dicarboxynorbornenes, using a bifunctional norbornene crosslinker and a molybdenum ROMP initiator.[15,16] Buchmeiser and coworkers have synthesized crosslinked polymers similar to Shrock's using a dinorbornene crosslinker; though these materials are crosslinked resins and not technically star polymers, they are useful materials for various applications, such as catalyst supports, tissue-engineering, and chromatographic separations.[17-19] Otani and coworkers have reported the synthesis of star nanoparticles via ROMP using a molybdenum catalyst, including ones containing sugar residues.[22,23] In contrast to these systems, we realized that it would be possible to form star polymers with advanced functionality via the polymerization of norbornene-derived macromonomers rather than small molecule norbornene derivatives. Notably, Matyjaszewski and coworkers used ATRP to make star polymers from acrylate terminated macronomoners, divinyl crosslinkers, and 2-bromopropionate or ethyl 2-bromoisobutyrate as initiators.[43] However, in this system, all of the components were added at the outset of the reaction. We reasoned that it might be possible to first polymerize macromonomers to generate bottlebrush polymers, and then add crosslinkers to induce bottlebrush crosslinking and generate a new type of star polymer architecture, which we have called a *Brush-Arm Star Polymer* (BASP). The various advantages and disadvantages of BASPs are discussed further below.

We developed and explored ROMP to prepare BASPs from polyethylene glycol (3kDa)-based macromonomers (PEG-MM) and a bifunctional norbornene nitrobenzyloxycarbonyl (NBOC) derivative as the crosslinker (**Figure 1.1**).[37,44] Due to the high molecular weight of the polyethylene glycol (PEG) used, we refer to these PEG-based monomers as macromonomers. The crosslinker used is photodegradable, which leads to BASP degradation upon irradiation at wavelengths shorter than 365 nm.[45] These photocleavable BASPs are just one example of incorporating a stimuli responsive functional group into a complicated architecture. Furthermore, the sizes of these stars can be tuned by changing the amount of crosslinker equivalents relative to the Grubbs' initiator, the number of macromonomer units in the brush macroinitiator, or the length of the PEG chain. This work suggests that the bottlebrush plays an important steric role in preventing the polymerization of crosslinker from losing control and thus keeping the dispersity fairly low. Functionality can be built into the macromomonomer or crosslinker, which is then translated directly to the final particle. Much of the work in the next few chapters of this thesis is

based on developing and synthesizing functional macromonomers and crosslinkers with desirable properties to be built into BASPs. Based on macromonomer design, these BASPs can possess functionality either close to the core of the BASP or at the chain ends of the PEG, allowing for functional groups to be either protected from or exposed to the external environment. Developing these BASPs may allow for opportunities to further understand and advance the field of nanoparticles.

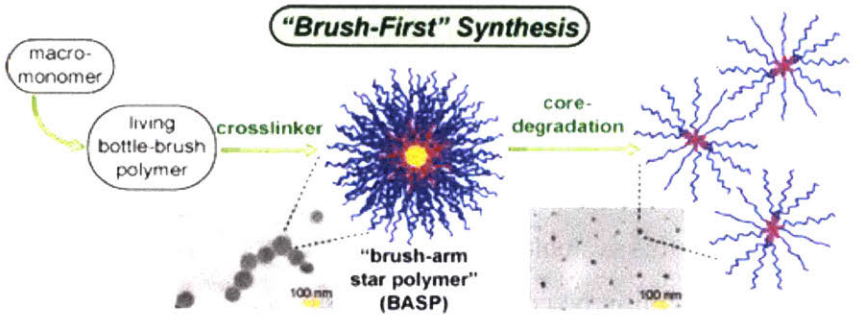

Figure 1.1: A brush-arm star polymer (BASP) can be synthesized using graft-through ROMP of macromonomer then crosslinker addition. Given the use of a photodegradable crosslinker, these BASPs can be degraded at the core with light irradiation to break the BASP into smaller components.

1.2 Results and Discussion

In this chapter, the development and synthesis of BASPs using ROMP was explored. PEG-3kDa functionalized with a norbornene group is used as the macromonomer (MM), which is polymerized by ROMP to make a living bottle-brush initiator. The living bottle-brush is added to a bifunctional norbornene crosslinker to tie the brushes together and create a crosslinked core.[44] PEG is desirable in drug delivery applications because of its solubility, biocompatibility, low uptake by the mononuclear phagocyte system, and low non-specific adsorption of cellular proteins and other biomolecules.[10] The sizes of these stars can be tuned and optimized for biological applications.

The synthesis of key reagents that were used to make BASPs will be discussed. **Scheme 1.4** shows the synthesis of the PEG macromonomer (PEG-MM), which involves ring opening of *cis*-5-norbornene-*exo*-2,3-dicarboxylic anhydride with γ-aminobutyric acid, followed by ring

closing driven forward through the removal of water. The next step involves N-(3-dimethylaminopropyl)-N′-ethylcarbodiimide (EDC) facilitated coupling of N-hydroxysuccinimide (NHS) to form an activated ester, which is coupled to O-(2-aminoethyl)polyethylene glycol 3000.

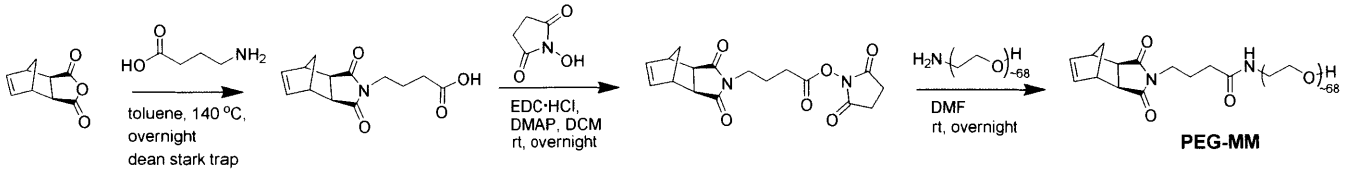

Scheme 1.4: Synthesis of PEG-MM.

The next component is the bifunctional crosslinker, which will form the core of the BASP. The steps to making this molecule are outlined in **Scheme 1.5**. The first step involves the formation of an imide with *cis*-5-norbornene-*exo*-2,3-dicarboxylic anhydride and glycine. 1,3-dimethyl-2-nitrobenzene was oxidized to 2-nitro-1,3-benzenedicarboxylic acid, which was then reduced to 1,3-dimethanol-2-nitrobenzyl.[46] The final step involves coupling of N-(glycine)-*cis*-5-norbornene-*exo*-dicarboximide with 2-nitro-1,3-benzenedimethanol to form the bis-norbornene-nitrobenzyloxycarbonyl crosslinker (NBOC-XL). The NBOC group is a photodegradable functional group designed to break apart the core of the star upon ultraviolet light irradiation.

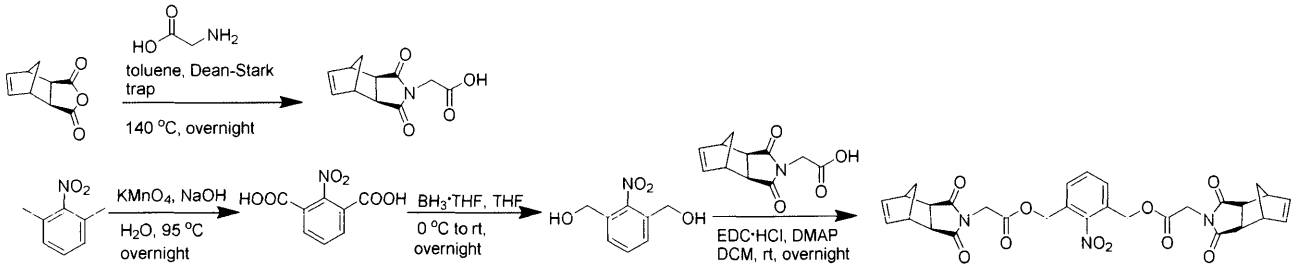

Scheme 1.5: Synthesis of the bifunctional norbornene photodegradable crosslinker (NBOC-XL)

Next, G3 is prepared by stirring Grubbs' second-generation catalyst with pyridine (**Scheme 1.6**). The third-generation catalyst is precipitated in pentanes and collected by filtration.

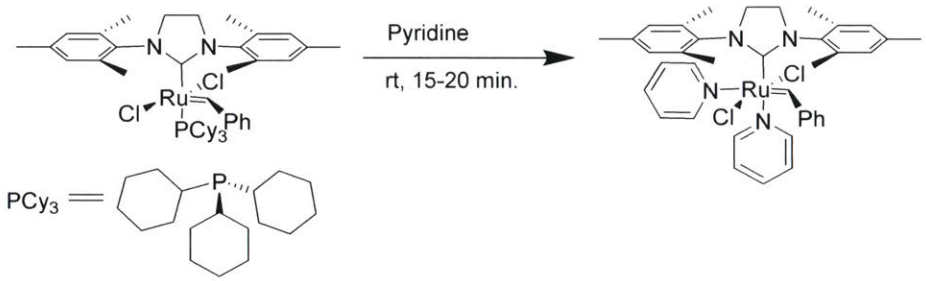

Scheme 1.6: Preparation of G3 from Grubbs' second-generation catalyst

The macromonomer and crosslinker were used in varying ratios to synthesize BASPs with a range of sizes. **Figure 1.2** details the synthesis of a ten unit living bottle brush polymer made through ROMP of PEG-MM. Next, one equivalent of this living brush initiator was added to either ten ($N = 10$), fifteen ($N = 15$), or twenty ($N = 20$) equivalents of NBOC-XL, and allowed to react for four hours before quenching with ethyl vinyl ether. **Figure 1.3** displays differential weight fraction plots with the weight average molar mass (M_w) and dispersities (Đ) of these BASP nanoparticles.

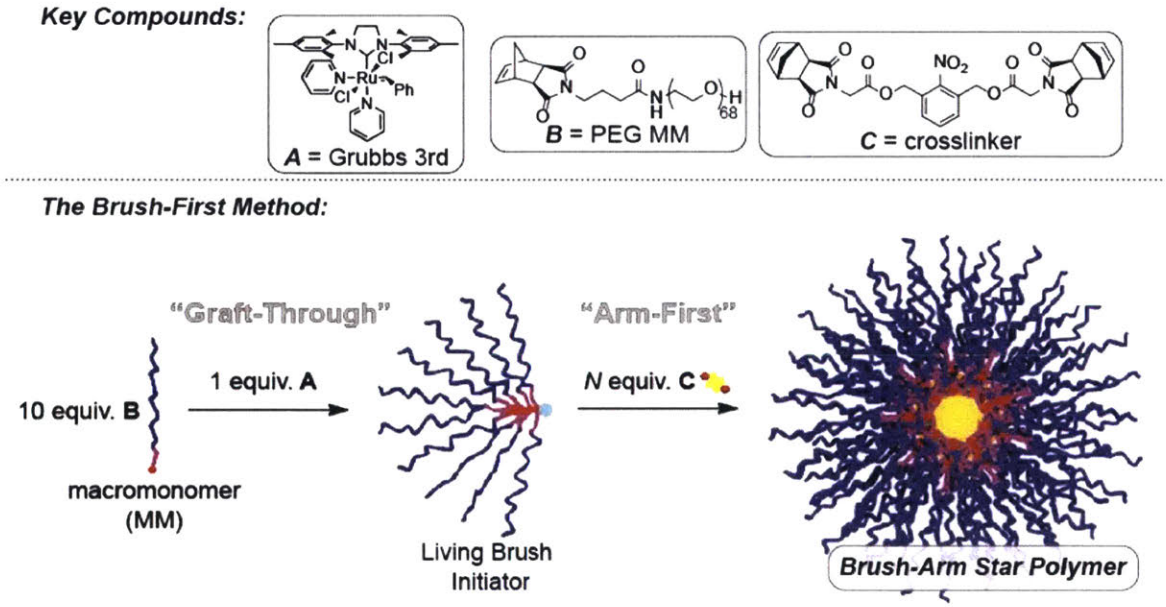

Figure 1.2: Synthesis of a star nanoparticle using ROMP: First, ten equivalents of PEG-MM (**B**) are polymerized into a living bottle-brush initiator by G3 (**A**), and then this solution is added to N equivalents of crosslinker (**C**).

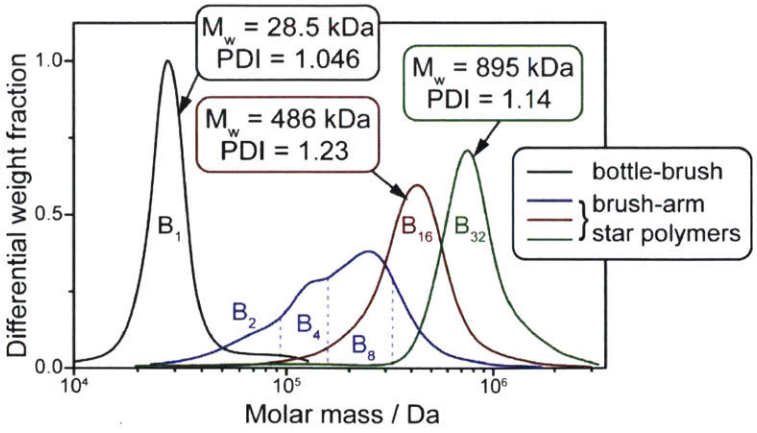

Figure 1.3: Differential weight fraction graphs for the 10-unit brush (B1), and $N = 10$, 15, 20 BASPs obtained from gel permeation chromatography multi-angle light scattering (GPC-MALLS)

Although the dispersity of the $N = 10$ BASP was high, increasing the crosslinker equivalents to $N = 15$ or $N = 20$ resulted in a more uniform distribution and low dispersity indices as shown in **Figure 1.3**. Importantly, care must be taken when interpreting the dispersity of highly branched polymers;[14] nonetheless, these data provide strong evidence for a unimodal molar mass distribution. With increasing crosslinker equivalents, the molecular weight of the BASP increased. Further studies showed that the molecular weight approximately doubled with every five additional equivalents of the NBOC-XL. The size of the BASP can also be tuned by changing the number of monomeric units, m, also referred to as the degree of polymerization (DP), of the living bottle-brush initiator. Bottle-brushes made from seven units of PEG-MM ($m = 7$) had a lower average molecular weight than those made from fourteen units ($m = 14$) as seen in **Figure 1.4**. The general trend observed was that the smaller the brush, the greater the final size of the BASP nanoparticle.

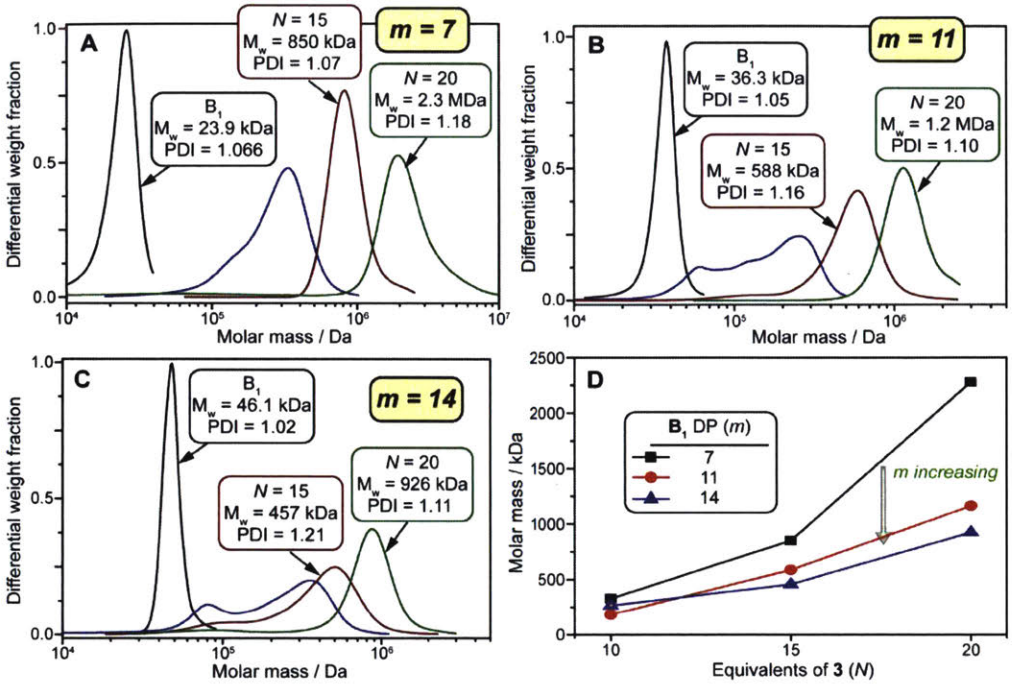

Figure 1.4: A) Differential weight fraction traces for the $m = 7$ unit brush initiator using $N = 10$, 15, and 20 equivalents. B) Differential weight fraction traces for the $m = 11$ unit brush initiator using $N = 10$, 15, and 20 equivalents. C) Differential weight fraction traces for the $m = 14$ unit brush initiator using $N = 10$, 15, and 20 equivalents. D) Plot of M_w vs. increasing N, showing that as m increases, the M_w becomes smaller.

These studies show that the size of the BASP can be tuned by increasing the number of crosslinker equivalents, N, or the degree of polymerization, m, of the living brush macroinitiator. These two handles allow for simplified control over the final size of the nanoparticle, which will be advantageous when optimizing these particles for *in vivo* delivery.

To explain the increase in size with increasing N and decreasing m, it was hypothesized that the mechanism involves a geometric growth of star-star (or BASP-BASP) coupling, which contributes to low dispersities, until steric hindrance hinders further BASP coupling. Thus, more crosslinker equivalents or smaller brushes sizes may help reduce steric constraints and promote an additional star-star coupling step. Studying the mechanism will help us understand how the size of the BASP can be tuned and applied to other core-crosslinked star polymers.

The star-star coupling hypothesis was further supported through kinetic analysis. After incremental periods of time, ROMP was quenched using ethyl vinyl ether and analyzed by GPC-MALLS. **Figure 1.5** shows the differential weight distribution chromatograms illustrating the molecular weight distributions of the star nanoparticles at different time points. In the initial

stages, two brushes (B_1) can couple to form the B_2 dimer. Once a large fraction of brushes have dimerized, the probability of dimer(B_2)-dimer(B_2) coupling increases, but also B_2-B_1 couplings can form the B_3 species. As the reaction proceeds, B_2-B_2 star-star coupling leads to formation of the B_4 species; further star-brush couplings are possible until all the brush is consumed. At later coupling steps, star-star coupling predominates and the system converges to a monomodal distribution. It is possible that the BASP from ten equivalents of crosslinker ($N = 10$) is hindered from further coupling at earlier stages leading to increased dispersity. Also, this geometric coupling may explain why the BASPs appear to approximately double in molecular weight per each increase of five crosslinker equivalents: the BASPs are less hindered and can complete an additional coupling step.

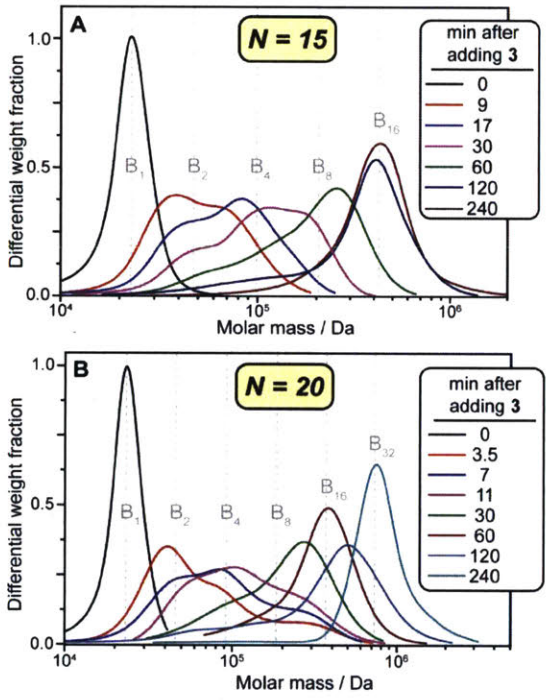

Figure 1.5: The ROMP reaction to make BASP nanoparticles was quenched with ethyl vinyl ether after a certain period of time and results were analyzed by GPC-MALLS to give the differential weight fraction traces for A) the $m = 10$, $N = 15$ BASP and B) the $m = 10$, $N = 20$ BASP.

Further studies by Dr. Aleksandr V. Zhukhovitskiy and Alan O. Burts using transmission electron microscopy (TEM) and dynamic light scattering (DLS) confirmed that the BASP cores can degrade into smaller fragments upon UV irradiation at 365 nm (**Figure 1.6**).[45] The Johnson group has also investigated other stimuli responsive cores that will degrade to release free brushes, such as acid-cleavable cores and redox-sensitive cores, which are more applicable in biological applications and will be introduced in the next chapter.[47,48]

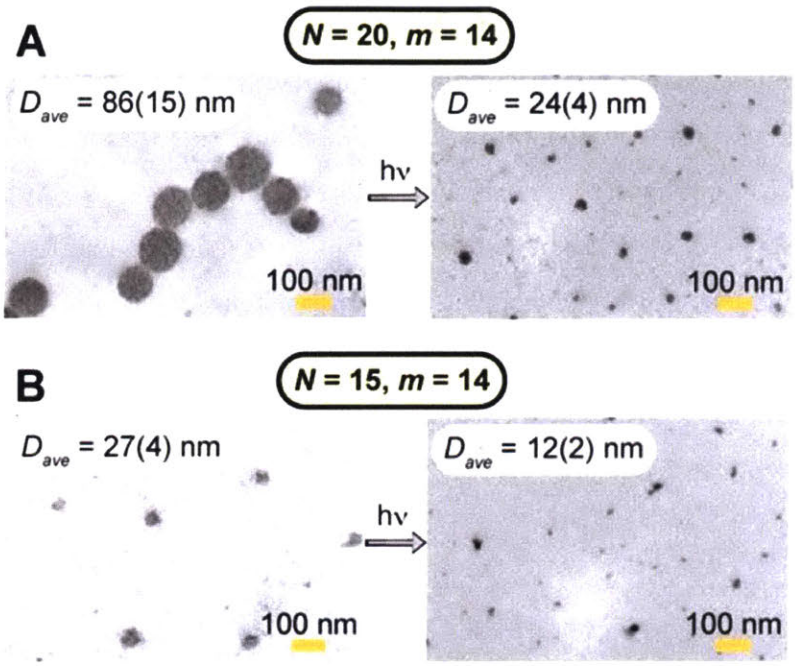

Figure 1.6: A) TEM images of $N = 20$, $m = 14$ BASPs obtained before and after degradation with light irradiation (hv). B) TEM images of $N = 15$, $m = 14$ BASPs obtained before and after degradation with light irradiation (hv). Average diameters (D_{ave}) are listed as insets in each image with error in parentheses.

Overall, these studies have shown that the synthesis of BASP nanoparticles with PEG arms and a photo-responsive core is possible. A. O. Burts and others also showed that the core of the BASP was in a more environmentally hindered environment as suggested by the broadened electron paramagnetic resonance (EPR) spectra of BASPs synthesized with nitroxides appended to a branched PEG-macromonomer, denoted as core-labeled nitroxides (**Figure 1.7**).[44] However, nitroxides appended to the terminal alcohol of PEG-MM were generally located along the periphery of the BASP. These periphery-labeled nitroxides displayed sharper peaks and faster relaxation times in its EPR spectrum. Also, when treated with a polymeric phenyl hydrazine reducing agent, the core-labeled nitroxide BASPs were quenched about 3 times slower than periphery-labeled nitroxide BASPs.

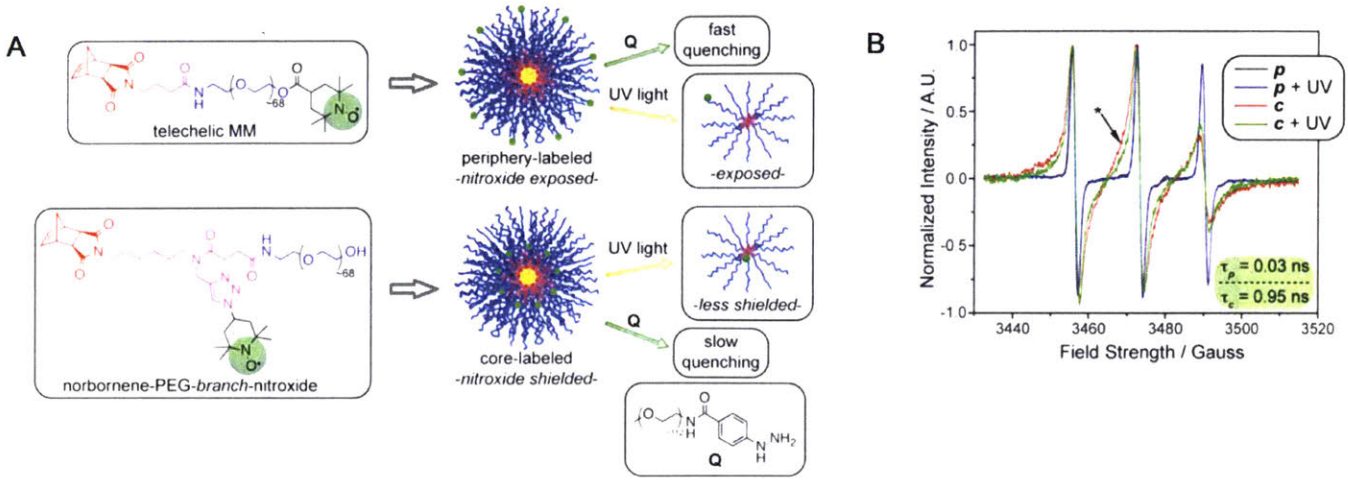

Figure 1.7[44]: Nitroxides can be labeled at the periphery or the core of BASPs and studied by EPR to determine how solvent-exposed the nitroxides are. A) BASPs synthesized with about 95% of PEG-MM and 5% of telechelic MM have nitroxides displayed near the periphery of the star. On the other hand, BASPs synthesized with about 95% of PEG-MM and 5% of branched-nitroxide MM have nitroxides bound closer to the core of the star. Quenching the periphery-labeled nitroxides with a phenyl-hydrazine derivative, **Q**, was relatively fast compared to quenching core-labeled BASPs. B) EPR spectra show sharper lines of periphery-labeled BASPs, **p**, and a faster rotational diffusion time, τ, of 0.03 ns. However, EPR signals from the core-labeled BASPs, **c**, have increased spectral broadening and slower rotational diffusion time, τ, of 0.95 ns, suggesting more hindered and less exposed nitroxides. Light irradiation (+UV) degrades the core of the star and breaks up the BASP into smaller brush components, but does not lead to any significant changes in the EPR spectrum of **p** and only slightly more sharpening for **c** as shown by the *.

In addition to modulating *m* and *N* to tune BASP size, a third variable, PEG chain length, can give us further control of the BASP size and composition. To further test the effect of this variable on BASP size, PEG MMs were synthesized from PEG1kDa-NH_2 and PEG2kDa-NH_2. Using the NBOC-XL, ROMP of PEG1kDa-MM and PEG2kDa-MM was tested with varied *m* and *N* values to study the extent to how the three variables, PEG-chain length, degrees of polymerization of the brush, and crosslinker equivalents, can affect the final size of the particle. **Table 1.1** shows a summary of the GPC and DLS results obtained for BASPs made with PEG1kDa-MM or PEG2kDa-MM and NBOC-XL at $m = 10$ and $N = 10$, 15, or 20 (differential weight fraction traces are shown in **Figure 1.8**). In the $m = 10$, $N = 15$ case, the general trend observed was that smaller PEG chains leads to larger particle sizes, perhaps due to decreased steric hindrance. These preliminary studies suggest that all three variables play a role in BASP size, but future studies will be needed to further explore and confirm the relationship among these variables.

MM	Target Stoichiometry	Mw GPC (dn/dc =0.450)	Avg. Size (DLS)	Dispersity (GPC)
PEG1kDa-MM	m= 10, N = 10	403 400 g/mol	22.2 nm	1.303
PEG1kDa-MM	m= 10, N =15	1 138 000 g/mol	45.9 nm	1.283
PEG1kDa-MM	m= 10, N =20	2 401 000 g/mol	85.3 nm	1.496
PEG2kDa-MM	m= 10, N = 10	272 100 g/mol	22.8 nm	1.591
PEG2kDa-MM	m= 10, N =15	530 900 g/mol	26.2 nm	1.221
PEG2kDa-MM	m= 10, N =20	1 073 000 g/mol	41.2 nm	1.204
PEG-MM 3kDa (lit.)[44]	m =10, N =15	486 000 g/mol	24 nm	1.23

Table 4.1: To study the effect of PEG chain length on final BASP size, BASPs were synthesized with m = 10 units of different molecular weight PEG MMs and N units of NBOC-XL. The BASPs were characterized via GPC-MALLS and DLS, and data is summarized in this table.

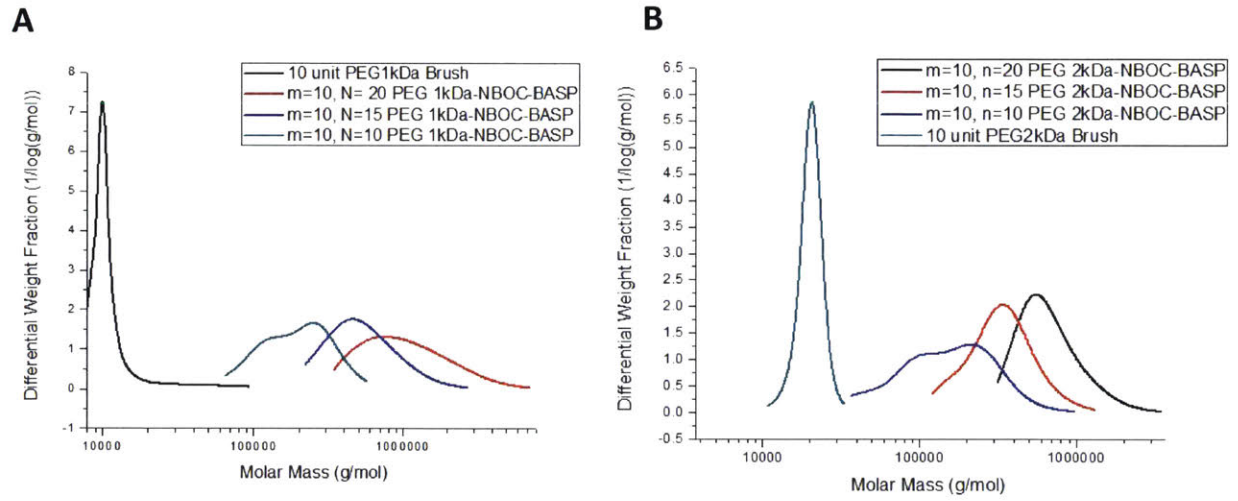

Figure 4.5: Differential weight fraction chromatogram from GPC-MALLS of test BASPs synthesized with A) m = 10 units of PEG1kDa-MM and N units of Acetal-XL, and B) m = 10 units of PEG2kDa-MM and N units of Acetal-XL.

These studies show the potential for BASPs to be used in a number of applications including drug delivery or diagnostics. Carefully designed crosslinkers can be optimized to cleave under biologically relevant conditions; also, biomolecules can be appended at the core or periphery of the BASP. Less physiologically stable compounds or biomolecules that can interact with enzymes, such as nucleic acids, can be appended to the core to protect them from their

surroundings. On the other hand, targeting ligands or ligands that promote cellular uptake can potentially be appended to the periphery of the BASP. The size of the BASP can be optimized for *in vivo* delivery and adapted for different types of diseases. For example, cancers associated with a dense stroma, such as pancreatic cancer, may benefit from small nanoparticles. The next chapters use some of these design considerations in applying BASPs as cancer therapeutics.

1.3 Conclusion

In this chapter, BASPs were synthesized with various properties that could be useful in future biological applications, such as tunable sizes, reproducible size distributions, dense packing, degradable cores, and water-solubility. Due to the use of ROMP, an efficient, controlled, and functional-group tolerant polymerization, these BASPs hold potential for multifunctionalization and ratiometric, controlled drug loading. Also, by developing a degradable core to respond to stimuli in the biological environment, the particle can break up into smaller brush polymers and small molecules for easier excretion from the body. These features make BASPs desirable for many applications, in particular as vehicles for drug delivery. In the next two chapters, multifunctional BASPs are synthesized with drug-conjugated macromonomers; these nanoparticles were explored for their possible applications in cancer therapeutics.

1.4 Experimental

General Considerations

Unless otherwise noted, all reagents and solvents were purchased from Sigma Aldrich or Alfa Aesar and used as supplied. Grubbs' 2nd generation catalyst was obtained from Materia. PEG1kDa-NH_2 and PEG2kDa-NH_2 were purchased from JenKem Technology USA as the hydrochloride salt. Silica gel used in column chromatography was the ZEOprep 60 HYD, 40-63 μm. Compounds purified by flash chromatography were purified on a Biotage Isolera One.

GPC-MALLS characterization was performed on an Agilent 1260 LC system equipped with a Wyatt T-rEX refractive index detector and Wyatt DAWN EOS 18 angle laser light scattering detector. Samples were run on two Shodex KD-806M GPC columns in series at a temperature of 60°C, flow rate of 1 ml/min, and dimethylformamide with 0.1 M LiBr as the eluent.

^{1}H nuclear magnetic resonance (^{1}H-NMR) and ^{13}C nuclear magnetic resonance (^{13}C-NMR) spectra were recorded on Bruker AVANCE-400 Mhz NMR spectrometer or a VARIAN Inova-500 Mhz NMR spectrometer. Spectra were analyzed on MestReNova NMR software. Chemical shifts are expressed in parts per million (ppm); splitting patterns are designated as s (singlet), d (doublet), t (triplet), m (multiplet), and br (broad); and coupling constants, J, are reported in Hertz (Hz).

Samples submitted to the MIT Department of Chemistry Instrumentation Facility (DCIF) for high-resolution mass spectrometry (HRMS) were obtained on a Bruker Daltonics APEXIV 4.7 Tesla Fourier Transform Ion Cyclotron Resonance Mass Spectrometer (FT-ICR-MS).

Matrix-assisted laser desorption ionization time-of-flight (MALDI-TOF) mass spectrometry was analyzed for macromonomers on a Bruker Omniflex MALDI-TOF with a Reflectron accessory. For MALDI-TOF, sample was prepared by dissolving 1 mg of MM in 200 μL MeCN. Matrix was prepared by dissolving approximately 3 mg of 2-(4'-hydroxybenzeneazo)benzoic acid (HABA) in a 0.3mL/0.2mL MeCN/water mixture, or approximately 20 mg of α-cyano-4-hydroxycinnamic acid (CHCA) in 500 uL of 1:1 MeCN:water + 0.1% TFA solution. 3 μL of sample solution was mixed with 50 μL of matrix solution, then about 0.7 μL of this mixture was spotted onto the MALDI target.

Liquid chromatography-mass spectrometry (LC-MS) was performed on an Agilent 1260 LC system equipped with an Agilent 6130 single quadrupole mass spectrometer. Samples were obtained on a Zorbax SB-C18 rapid resolution HT analytical column in a gradient eluent of 0.1% acetic acid in purified water from a MilliQ Biocel A10 water purification system to 100% HPLC-grade acetonitrile.

Light irradiation for photodegradation experiments was sourced from a Multiple Ray Lamp or a Rayonet Photoreactor fitted with 8W filtered blacklight bulbs (365 nm).

Synthesis of PEG-MM:

The procedures for synthesis of branched PEG-MM and NBOC-XL are reported in literature,[44] with updated experimental procedures below. Unless otherwise stated, ^{1}H-NMR, ^{13}C-NMR, and HRMS are as reported in literature,[44] and are not reproduced in this document.

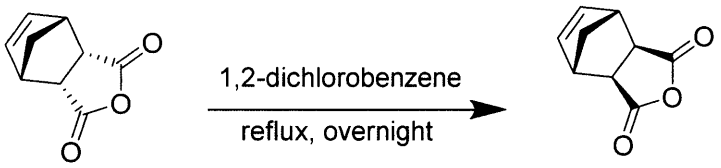

***Exo*-norbornene anhydride**

***Exo*-norbornene anhydride:** Norbornene anhydride (≥ 95% *endo*, Sigma Aldrich) (250g, 1.5 mol, 1 eq) was dissolved in 1,2-dichlorobenzene (250 mL) in a dry 500 mL round bottom equipped with a stirbar and reflux condenser. The reaction was heated to reflux with stirring overnight. After the hotplate was turned off and the reaction reached room temperature, the reaction was transferred to a 2 L Erlenmeyer flask and 1 L of hexanes was added to precipitate out the norbornene anhydride. The reaction was placed in a -20 °C freezer for one hour, and then filtered to collect the precipitate. The precipitate was washed with hexanes, then transferred to a round bottom and dried under high vacuum overnight. The solids were placed in an Erlenmeyer and a thin layer of ethyl acetate was added just barely covering the solids. The solvent was heated until all solids dissolved, adding small amounts of ethyl acetate as necessary. The flask was placed in a cold room at 4 °C overnight for crystallization, then the solids that formed were

filtered and collected. This recrystallization in ethyl acetate procedure was repeated multiple times until *endo*-norbornene anhydride was not present in the ^{1}H-NMR. Any supernatant from the recrystallizations can be collected and reheated in 1,2-dichlorobenzene, and then recrystallized in ethyl acetate to improve yields of *exo*-norbornene anhydride. ^{1}H-NMR (500 MHz, $CDCl_3$): δ 6.33 (s, 2H), 3.45 (s, 2H), 3.00 (s, 2H), 1.66 (d, J = 10.4 Hz, 1H), 1.44 (d, J = 10.4 Hz, 1H).

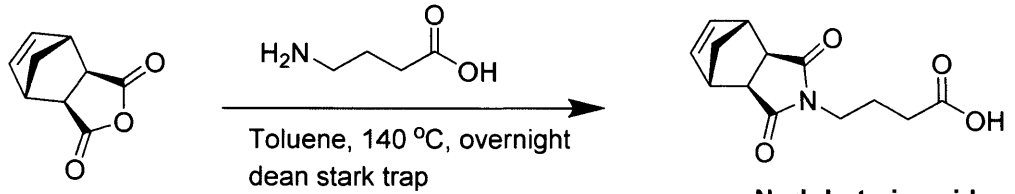

Norb-butyric-acid

Norb-butyric-acid: *Exo*-norbornene anhydride (8.0 g, 0.049 mol, 1 eq) and λ-aminobutyric acid (5.0g, 0.049 mol, 1.0 eq) were dissolved in 100 mL of toluene in a 250 mL round bottom flask equipped with stir bar, Dean-Stark trap, and reflux condenser. The oil bath was heated to 140 °C or until solvent was refluxing, and stirred overnight. The heat was turned off and the reaction was allowed to reach room temperature, then placed in a -20 °C fridge. If necessary, the inside of the glassware was scratched to induce the product to precipitate out of solution. The solid white product was filtered and washed with small amounts of toluene, then dried under high vacuum overnight to yield Norb-butyric-acid (10.4 g, 0.0405 mol, 83%). ^{1}H-NMR, ^{13}C-NMR, and HRMS are as reported in literature.[44]

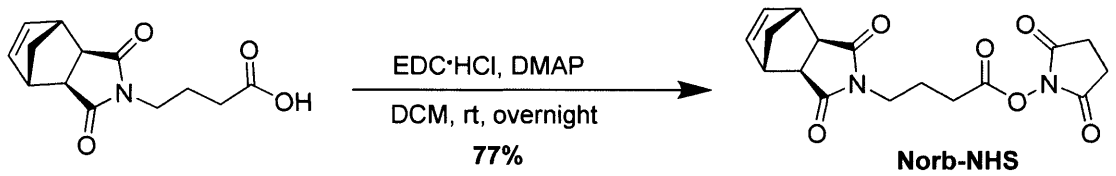

Norb-NHS

Norb-NHS: Norb-butyric-acid (3.0 g, 0.012 mol, 1 eq), EDC·HCl (3.5 g, 0.018 mmol 1.5 eq), and DMAP (0.3 g, 0.0025 mmol 0.2 eq) were dissolved in anhydrous DCM (100 mL), and stirred for 30 min. NHS (2.1 g, 0.018 mmol 1.5 eq) was added to the solution, and the reaction was stirred overnight at room temperature or until complete as monitored by LCMS. The solution was directly loaded onto a silica cartridge and purified by flash chromatography (0%

EtOAc/Hexanes to 100% EtOAc/Hexanes) to afford Norb-NHS (3.2 g, 77 %). ^{1}H-NMR, ^{13}C-NMR, and HRMS are as reported in literature.[44]

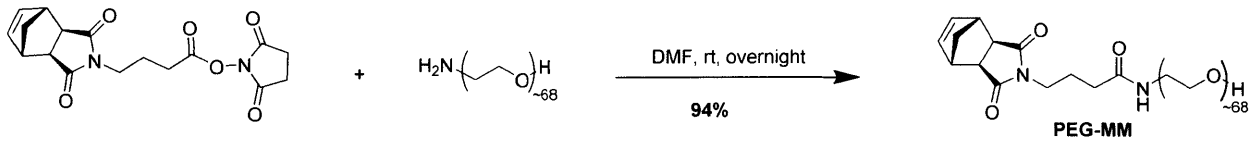

PEG-MM: Norb-NHS (36.4 mg, 0.105 mmol, 1.05 eq), and O-(2-aminoethyl)polyethylene glycol 3000 (300 mg, 0.100 mmol, 1.0 eq) were reacted in anhydrous DMF (3 mL) under N_2 overnight. The compound was precipitated in ether, followed by centrifugation of solids and decantation of the ether five times. The compound was dried under high vacuum overnight to yield PEG-MM (303 mg, 94% yield) as a white powder. ^{1}H-NMR and MALDI-TOF spectra are as reported in literature.[44]

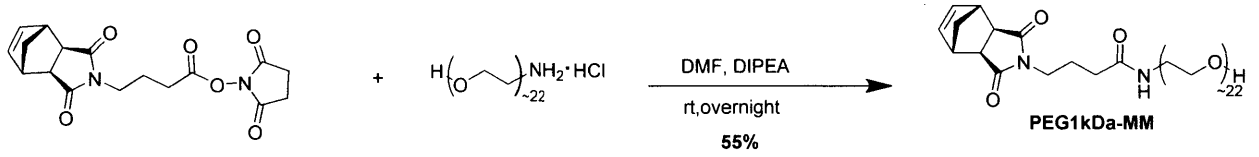

PEG1kDa-MM: Norb-NHS (182 mg, 0.525 mmol, 1.05 eq), PEG1kDa-NH_2·HCl (500 mg, 0.500 mmol, 1.0 eq), and DIPEA (0.084 mL, 0.500 mmol, 1.0 eq) were reacted in anhydrous DMF (3 mL) under N_2 overnight. The compound was precipitated in ether, followed by centrifugation of solids and decantation of the ether three times. The solids were then redissolved in a small amount of methanol and purified by HPLC (10% MeCN and 0.1% acetic acid in MilliQ deionized water to 100% MeCN). Once water was removed by rotary evaporation, the PEG1kDa-MM was redissolved in dichloromethane and dried over sodium sulfate. After concentration by rotary evaporation, the PEG1kDa-MM solid was washed with diethyl ether by centrifugation of solids and decantation of ether. The compound was dried on high vacuum overnight resulting in PEG1kDa-MM (370 mg, 55% yield) as a white powder. ^{1}H-NMR provided in **Supplemental Figure 1.S1**.

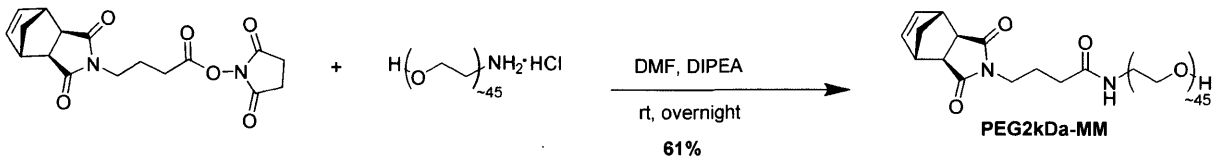

PEG2kDa-MM: Norb-NHS (90.9 mg, 0.263 mmol, 1.05 eq), PEG2kDa-NH_2·HCl (500 mg, 0.250 mmol, 1.0 eq), and DIPEA (0.043 mL, 0.250 mmol, 1.0 eq) were reacted in anhydrous DMF (3 mL) under N_2 overnight. The compound was precipitated in ether, followed by centrifugation and decantation of the ether three times. The solids were then redissolved in a small amount of methanol and purified by HPLC (10% MeCN/0.1% acetic acid in MilliQ deionized water to 100% MeCN). Once water was removed by rotary evaporation, PEG2kDa-MM was redissolved in dichloromethane and dried over sodium sulfate. After concentration by rotary evaporation, PEG2kDa-MM solid was washed with diethyl ether by centrifugation of solids and decantation of ether. The compound was dried on high vacuum overnight resulting in PEG2kDa-MM (360 mg, 61% yield) as a white powder. ^{1}H-NMR provided in **Supplemental Figure 1.S2**.

Synthesis of photocleavable crosslinker:

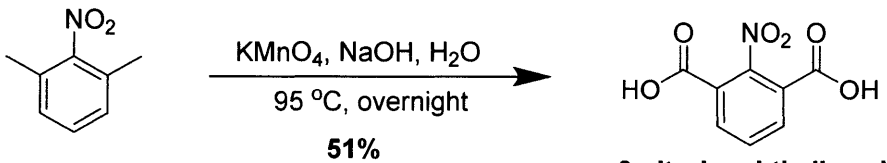

2-nitroisophthalic acid: 1,3-dimethyl-2-nitrobenzene (7.9 g, 0.052 mol, 1 eq) was added to a solution of sodium hydroxide (3.2 g, 0.080 mol, 1.5 eq) in water (400 mL) and heated to 95 °C in a two/three-arm round bottom flask equipped with a reflux condenser and stir bar. Potassium permanganate (33 g, 0.21 mol, 4 eq) was added to the stirring solution over a period of 3 h. The reaction was refluxed overnight, then cooled and filtered to remove solids. The filtrate was acidified with concentrated HCl until a precipitate formed. This precipitate was collected, redissolved in ethyl acetate, and dried over sodium sulfate. After the sodium sulfate was removed by filtration, the product was dried *in vacuo* to yield 2-nitroisophthalic acid (5.6 g, 51% yield). [1]

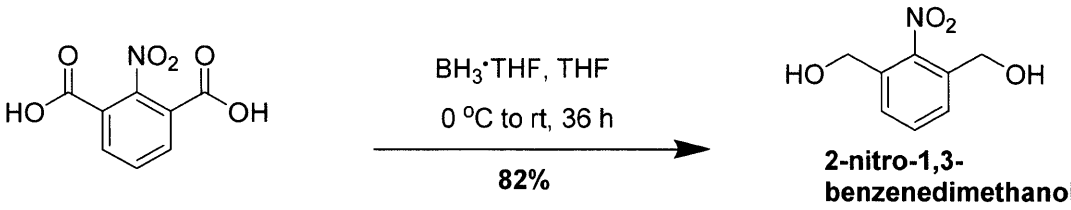

2-nitro-1,3-benzenedimethanol

2-nitro-1,3-benzenedimethanol: To a dry 500 mL flask equipped with an addition funnel under N_2, 2-nitroisophthalic acid (5.6g, 0.027 mol, 1 eq) was added, then dissolved in THF (30 mL). After the reaction was cooled to 0 °C in an ice bath, $BH_3 \cdot THF$ as a 1 M solution in THF (133 mL, 0.13 mol, 5 eq) was cannulated into the addition funnel, and added slowly over 1 h. The reaction was allowed to warm to room temperature and stirred for 36 h. The reaction was quenched by slow addition of methanol (25 mL) and then concentrated by rotary evaporation. The concentrated solution was dissolved in ethyl acetate (75 mL) and washed with water twice (50 mL each) and brine once (50 mL). After drying over magnesium sulfate, the solution was concentrated and purified by column chromatography (20% EtOAc/Hexanes to remove impurities, then 50% EtOAc/Hexanes to elute product) to yield 2-nitro-1,3-benzenedimethanol (4.0 g, 82% yield). ^{1}H-NMR and HRMS are as reported in literature.[46]

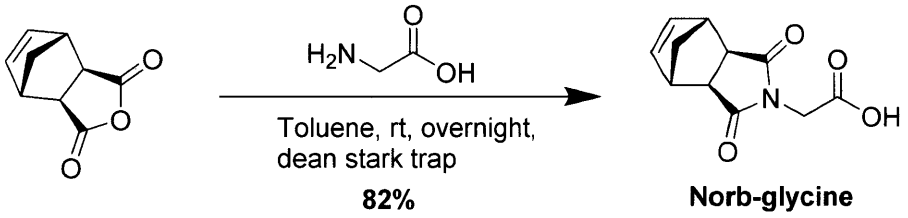

Norb-glycine

Norb-glycine: *Exo*-norbornene anhydride (5.0 g, 30.5 mmol, 1 eq), glycine (2.4 g, 31.7 mol, 1.04 eq), and triethylamine (0.51 mL, 3.7 mmol, 0.12 eq) were dissolved in 30 mL of toluene in a 100 mL round bottom flask equipped with stir bar, dean-stark trap, and reflux condenser. The oil bath was heated to 140 °C or until solvent was refluxing, and stirred overnight. The heat was turned off and the reaction was allowed to reach room temperature. The reaction was then transferred to separatory funnel with ethyl acetate (60 mL) and 0.2 N aqueous HCl (20 mL). The organic layer was collected and concentrated and resuspended in saturated sodium bicarbonate solution. The aqueous layer was washed with dichloromethane (10 mL) twice and then was acidified to pH 2 with concentrated HCl, at which point a white precipitate formed. The precipitate was extracted with chloroform three times (50 mL), then the organic layer was dried over magnesium sulfate. After filtering out the salts, the chloroform was removed *in vacuo* to

yield norb-glycine (5.5 g, 82% yield). ^{1}H-NMR, ^{13}C-NMR, and HRMS are as reported in literature.[51]

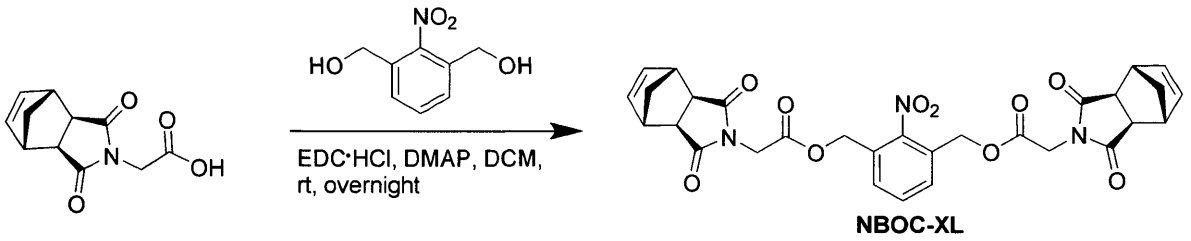

NBOC-XL: Norb-glycine (150 mg, 0.678 mmol, 2.2 eq), EDC·HCl (148 mg, 0.772 mmol, 2.5 eq), and DMAP (19 mg, 0.15 mmol, 0.5 eq) were dissolved in anhydrous DCM (5 mL) in a flask equipped with a stirbar under N_2. After stirring for ten minutes, 2-nitro-1,3-benzenedimethanol (56.4 mg, 0.308 mmol, 1 eq) was added and the reaction was stirred overnight. The reaction was diluted with dichloromethane (75 mL) and washed with 75 mL each of saturated sodium bicarbonate solution, water, and brine, and then the organic layer was dried over magnesium sulfate. After filtering out the salts, the solution was dry loaded onto silica and purified by column chromatography (0% MeOH/DCM to 10% MeOH/DCM) to yield NBOC-XL. ^{1}H-NMR, ^{13}C-NMR, and HRMS are as reported in literature.[44]

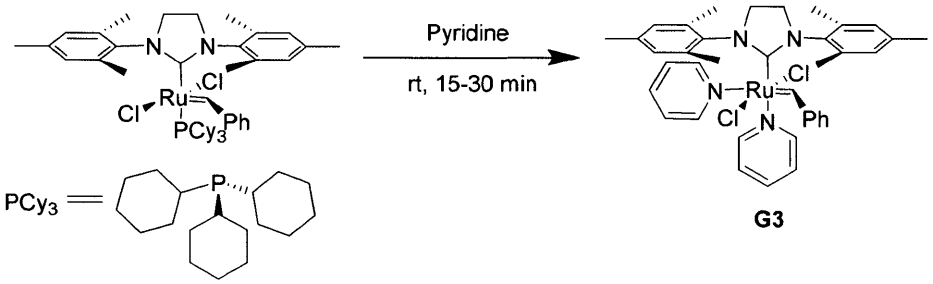

G3*: Grubbs 2nd generation catalyst (500 mg, 0.589 mmol, 1 eq) was added to a 20 ml vial equipped with a stir bar. The catalyst was dissolved in pyridine (approximately 0.474 ml, 5.89 mmol, 10 eq), upon which the solution color changes from red to green. The reaction was stirred until all of the red color had disappeared and the solution had become viscous (15-30 min). Cold pentane was added to precipitate out G3 as green solids, which was collected by filtration and washed 4x with 15 ml of cold pentane. The green solid was dried under high vacuum overnight to afford G3.

*G3 can be stored for months at room temperature in a benchtop desiccator without significant loss of activity. For extra precaution, we typically store the complex in a -20 °C freezer inside a glovebox. For convenience, we pre-weigh known amounts of G3 into 4 ml scintillation vials immediately after drying and store these vials in the glovebox freezer. When ready to run a ROMP reaction, we simply take one vial out of the glovebox and dissolve in solvent to make a stock solution of catalyst, which we discard after use.

General Procedure for synthesis of BASPs by ROMP (**Figure 1.2**):

All ROMP reactions were performed in a glovebox. Refer to published *Journal of Visualized Experiments* (JoVE) video for a visual representation of this procedure.[37]

1. **Living bottle-brush initiator solution:** PEG-MM (*m* eq, where *m* = 7, 10, or 14 eq were tested) was added to a 4 mL vial containing a stir bar, then dissolved in THF. The volume of THF to use is calculated as the volume required for a 0.05 M solution of MM minus the volume of G3 solution to add in the next step. G3 was dissolved in THF to make a 6 mg/mL solution, then G3 (1 eq relative to *m*) was added to the solution of PEG-MM. The final concentration of PEG-MM in solution should be 0.05 M. ROMP for formation of the living bottle-brush initiator was allowed to proceed for 15 min to make a living brush initiator stock solution, which was used immediately for formation of BASPs.

2. **BASP formation:** From this stock solution, aliquots of living bottle-brush initiator (1 eq) were transferred into pre-weighed vials containing crosslinker (*N* eq, where *N*= 10, 15, 20 were tested). After ROMP had proceeded for 4 h, the reaction was quenched with ethyl vinyl ether (approximately 50 eq). GPC-MALLS characterization of BASPs is shown in **Figure 1.3** and **Figure 1.4**.

Example: PEG-MM (65 mg, 0.020 mmol, 10 eq) was weighed into a 4 mL vial. Also, a 6 mg/mL stock solution of G3 in THF was prepared. For a 0.05 M solution of MMs, we would need 401 μL total volume of THF, and we would also need 243 μL of G3 from a 6 mg/mL stock

(0.0020 mmol, 1 eq). Thus, we dissolved MMs in 401 μL – 243 μL = 158 μL of THF and stirred until MMs were dissolved. Next we added the 243 μL of G3 from the stock solution. ROMP of MMs was allowed to proceed for 15 minutes to make a living brush solution.

We added 123 μL (0.618 μmol) from the living brush solution directly to three separate vials containing NBOC-XL (Vial 1: 3.6 mg, 6.18 μmol, 10 eq to brush; Vial 2: 5.5 mg, 9.28 μmol, 15 eq to brush; Vial 3: 7.3 mg, 12.4 μmol, 20 eq to brush). The leftover brush solution was quenched with a few drops of ethyl vinyl ether, and analyzed by GPC. The BASP reactions were stirred for 4 h before quenching with a few drops of ethyl vinyl ether, and then analyzed by GPC-MALLS.

Sample kinetics ROMP test:

PEG-MM (81.4 mg, 0.025 mmol, 10 eq) and NBOC-XL (22.1 mg, 0.038 mmol, 15 eq) were weighed into 4-mL vials and brought into the glovebox. THF (199 uL) was added to the PEG-MM until it was fully dissolved, followed by addition of 305 μL (0.0025 mmol, 1 eq) of a 6 mg/mL G3 solution. The reaction was stirred for 15 min to form the living brush initiator, then the brush solution was added directly to the vial containing NBOC-XL. The initial time was recorded, and then the reaction vial was brought out of the glovebox and placed under N_2. At each time point, 25 μL of the BASP solution was removed and quenched with one of drop of ethyl vinyl ether, then analyzed on GPC-MALLS. For brush characterization, any leftover residue in the living brush initiator solution vial was quenched with one drop of ethyl vinyl ether, then analyzed on GPC-MALLS. The GPC chromatograms for m=10, N=15 and m=10, N=20 BASPs are shown in **Figure 1.6**.

1.5 References

1 Hawker, C. J. & Wooley, K. L. The convergence of synthetic organic and polymer chemistries. *Science* **309**, 1200-1205 (2005).

2 Peer, D. *et al.* Nanocarriers as an emerging platform for cancer therapy. *Nature Nanotechnology* **2**, 751-760 (2007).

3 Whitesides, G. M. Nanoscience, nanotechnology, and chemistry. *Small* **1**, 172-179 (2005).

4 Hu, C.-M. J. & Zhang, L. Nanoparticle-based combination therapy toward overcoming drug resistance in cancer. *Biochemical Pharmacology* **83**, 1104-1111 (2012).

5 Duncan, R. Polymer conjugates as anticancer nanomedicines. *Nature Reviews Cancer* **6**, 688-701 (2006).

6 Duncan, R. The dawning era of polymer therapeutics. *Nature Reviews Drug Discovery* **2**, 347-360 (2003).

7 Wolinsky, J. B. & Grinstaff, M. W. Therapeutic and diagnostic applications of dendrimers for cancer treatment. *Advanced Drug Delivery Reviews* **60**, 1037-1055 (2008).

8 Davis, M. E. & Shin, D. M. Nanoparticle therapeutics: an emerging treatment modality for cancer. *Nature Reviews Drug Discovery* **7**, 771-782 (2008).

9 Kwon, G. S. & Kataoka, K. Block copolymer micelles as long-circulating drug vehicles. *Advanced Drug Delivery Reviews* **16**, 295-309 (1995).

10 Nel, A. E. *et al.* Understanding biophysicochemical interactions at the nano–bio interface. *Nature Materials* **8**, 543-557 (2009).

11 Barenholz, Y. C. Doxil®—the first FDA-approved nano-drug: lessons learned. *Journal of Controlled Release* **160**, 117-134 (2012).

12 Ren, J. M. *et al.* Star Polymers. *Chemical Reviews* **116**, 6743-6836 (2016).

13 Blencowe, A., Tan, J. F., Goh, T. K. & Qiao, G. G. Core cross-linked star polymers via controlled radical polymerisation. *Polymer* **50**, 5-32 (2009).

14 Gao, H. Development of star polymers as unimolecular containers for nanomaterials. *Macromolecular Rapid Communications* **33**, 722-734 (2012).

15 Bazan, G. C. & Schrock, R. R. Synthesis of star block copolymers by controlled ring-opening metathesis polymerization. *Macromolecules* **24**, 817-823 (1991).

16 Saunders, R. S., Cohen, R. E., Wong, S. J. & Schrock, R. R. Synthesis of amphiphilic star block copolymers using ring-opening metathesis polymerization. *Macromolecules* **25**, 2055-2057 (1992).

17 Buchmeiser, M. R. & Wurst, K. Access to well-defined heterogeneous catalytic systems via ring-opening metathesis polymerization (ROMP): applications in palladium (II)-mediated coupling reactions. *Journal of the American Chemical Society* **121**, 11101-11107 (1999).

18 Weichelt, F., Frerich, B., Lenz, S., Tiede, S. & Buchmeiser, M. R. Ring-opening metathesis polymerization-based synthesis of $CaCO_3$ nanoparticle-reinforced polymeric monoliths for tissue engineering. *Macromolecular Rapid Communications* **31**, 1540-1545 (2010).

19 Weichelt, F. *et al.* ROMP-Derived cyclooctene-based monolithic polymeric materials reinforced with inorganic nanoparticles for applications in tissue engineering. *Beilstein Journal of Organic Chemistry* **6**, 1199-1205 (2010).

20 Mayr, M., Mayr, B. & Buchmeiser, M. R. Monolithic materials: new high-performance supports for permanently immobilized metathesis catalysts. *Angewandte Chemie International Edition* **40**, 3839-3842 (2001).

21 Mayr, B., Hölzl, G., Eder, K., Buchmeiser, M. R. & Huber, C. G. Hydrophobic, pellicular, monolithic capillary columns based on cross-linked polynorbornene for biopolymer separations. *Analytical Chemistry* **74**, 6080-6087 (2002).

22 Nomura, K., Watanabe, Y., Fujita, S., Fujiki, M. & Otani, H. Facile controlled synthesis of soluble star shape polymers by ring-opening metathesis polymerization (ROMP). *Macromolecules* **42**, 899-901 (2009).

23 Otani, H., Fujita, S., Watanabe, Y., Fujiki, M. & Nomura, K. A facile, controlled synthesis of soluble star polymers containing a sugar residue by ring-opening metathesis polymerization (ROMP). *Macromolecular Symposia* **293**, 53-57 (2010).

24 Hejl, A., Scherman, O. A. & Grubbs, R. H. Ring-opening metathesis polymerization of functionalized low-strain monomers with ruthenium-based catalysts. *Macromolecules* **38**, 7214-7218 (2005).

25 Benson, S. W. *et al.* Additivity rules for the estimation of thermochemical properties. *Chemical Reviews* **69**, 279-324 (1969).

26 Bielawski, C. & Grubbs, R. Highly efficient ring-opening metathesis polymerization (ROMP) using new ruthenium catalysts containing N-heterocyclic carbene ligands. *Angewandte Chemie International Edition* **39**, 2903-2906 (2000).

27 Bielawski, C. W. & Grubbs, R. H. Living ring-opening metathesis polymerization. *Progress in Polymer Science* **32**, 1-29 (2007).

28 Grubbs, R. H. & O'Leary, D. J. *Handbook of Metathesis, Volume 2: Applications in Organic Synthesis*. (John Wiley & Sons, 2015).

29 Choi, T. L. & Grubbs, R. H. Controlled living ring-opening-metathesis polymerization by a fast-initiating ruthenium catalyst. *Angewandte Chemie* **115**, 1785-1788 (2003).

30 Slugovc, C. The ring opening metathesis polymerisation toolbox. *Macromolecular Rapid Communications* **25**, 1283-1297 (2004).

31 Leitgeb, A., Wappel, J. & Slugovc, C. The ROMP toolbox upgraded. *Polymer* **51**, 2927-2946 (2010).

32 Sutthasupa, S., Shiotsuki, M. & Sanda, F. Recent advances in ring-opening metathesis polymerization, and application to synthesis of functional materials. *Polymer Journal* **42**, 905-915 (2010).

33 Love, J. A., Sanford, M. S., Day, M. W. & Grubbs, R. H. Synthesis, structure, and activity of enhanced initiators for olefin metathesis. *Journal of the American Chemical Society* **125**, 10103-10109 (2003).

34 Sanford, M. S., Love, J. A. & Grubbs, R. H. Mechanism and activity of ruthenium olefin metathesis catalysts. *Journal of the American Chemical Society* **123**, 6543-6554 (2001).

35 Jean-Louis Hérisson, P. & Chauvin, Y. Catalyse de transformation des oléfines par les complexes du tungstène. II. Télomérisation des oléfines cycliques en présence d'oléfines acycliques. *Die Makromolekulare Chemie* **141**, 161-176 (1971).

36 Love, J. A., Morgan, J. P., Trnka, T. M. & Grubbs, R. H. A practical and highly active ruthenium-based catalyst that effects the cross metathesis of acrylonitrile. *Angewandte Chemie International Edition* **41**, 4035-4037 (2002).

37 Liu, J., Gao, A. X. & Johnson, J. A. Particles without a box: brush-first synthesis of photodegradable PEG star polymers under ambient conditions. *Journal of Visualized Experiments* **80** (2013).

38 Kammeyer, J. K., Blum, A. P., Adamiak, L., Hahn, M. E. & Gianneschi, N. C. Polymerization of protecting-group-free peptides via ROMP. *Polymer Chemistry* **4**, 3929-3933 (2013).

39 Blum, A. P. *et al.* Peptides displayed as high density brush polymers resist proteolysis and retain bioactivity. *Journal of the American Chemical Society* **136**, 15422-15437 (2014).

40 Hahn, M. E., Randolph, L. M., Adamiak, L., Thompson, M. P. & Gianneschi, N. C. Polymerization of a peptide-based enzyme substrate. *Chemical Communications* **49**, 2873-2875 (2013).

41 Imamoglu, Y. & Dragutan V. ed. Metathesis chemistry: from nanostructure design to synthesis of advanced materials. (Springer, 2007).

42 Anderson, E. B. & Buchmeiser, M. R. Catalysts immobilized on organic polymeric monolithic supports: from molecular heterogeneous catalysis to biocatalysis. *ChemCatChem* **4**, 30-44 (2012).

43 Gao, H., Ohno, S. & Matyjaszewski, K. Low polydispersity star polymers via cross-linking macromonomers by ATRP. *Journal of the American Chemical Society* **128**, 15111-15113 (2006).

44 Liu, J. *et al.* "Brush-first" method for the parallel synthesis of photocleavable, nitroxide-labeled poly(ethylene glycol) star polymers. *Journal of the American Chemical Society* **134**, 16337-16344 (2012).

45 Zhao, H., Sterner, E. S., Coughlin, E. B. & Theato, P. o-Nitrobenzyl alcohol derivatives: opportunities in polymer and materials science. *Macromolecules* **45**, 1723-1736 (2012).

46 Pavia, M. R., Moos, W. H. & Hershenson, F. M. Benzo-fused bicyclic imides. *The Journal of Organic Chemistry* **55**, 560-564 (1990).

47 Liao, L. *et al.* A convergent synthetic platform for single-nanoparticle combination cancer therapy: ratiometric loading and controlled release of cisplatin, doxorubicin, and camptothecin. *Journal of the American Chemical Society* **136**, 5896-5899 (2014).

48 Gao, A. X., Liao, L. & Johnson, J. A. Synthesis of acid-labile PEG and PEG-doxorubicin-conjugate nanoparticles via brush-first ROMP. *ACS Macro Letters* **3**, 854-857 (2014).

49 Wang, Q. C., Qu, D. H., Ren, J., Chen, K. & Tian, H. A lockable light-driven molecular shuttle with a fluorescent signal. *Angewandte Chemie* **116**, 2715-2719 (2004).

50 Brenet, S., Minozzi, C., Clarens, B., Amiri, L. & Berthiol, F. 3,3′-diiodobinaphthol and 3,3′-diiodobiphenol derivatives as hypervalent iodine organocatalysts for the α-oxytosylation of ketones. *Synthesis* **47**, 3859-3873 (2015).

51 Conrad, R. M. & Grubbs, R. H. Tunable, temperature-responsive polynorbornenes with side chains based on an elastin peptide sequence. *Angewandte Chemie International Edition* **48**, 8328-8330 (2009).

1.6 Supplemental Figures and Spectra

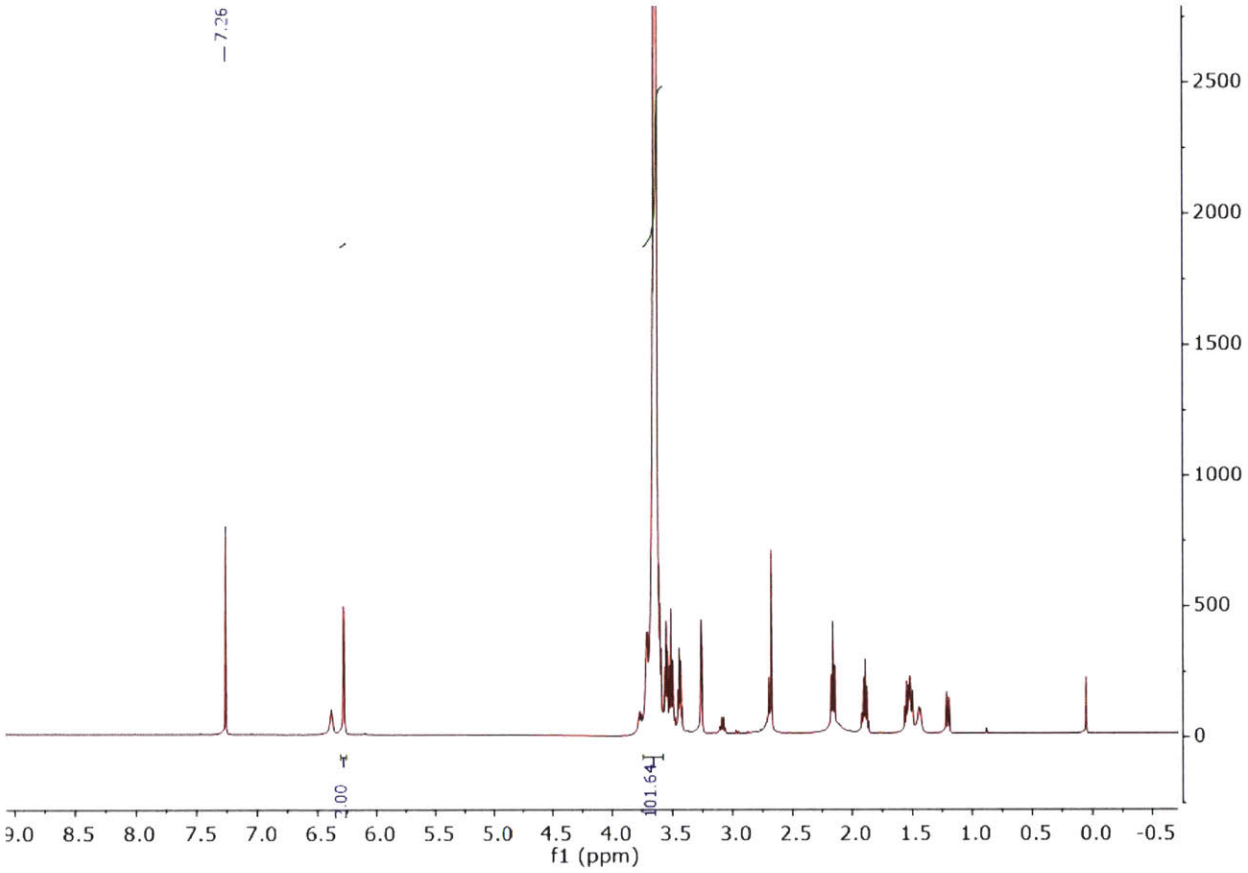

Supplemental Figure 1.S1: ^{1}H-NMR spectrum of **PEG1kDa-MM** taken on a 500 MHz NMR spectrometer in in $CDCl_3$.

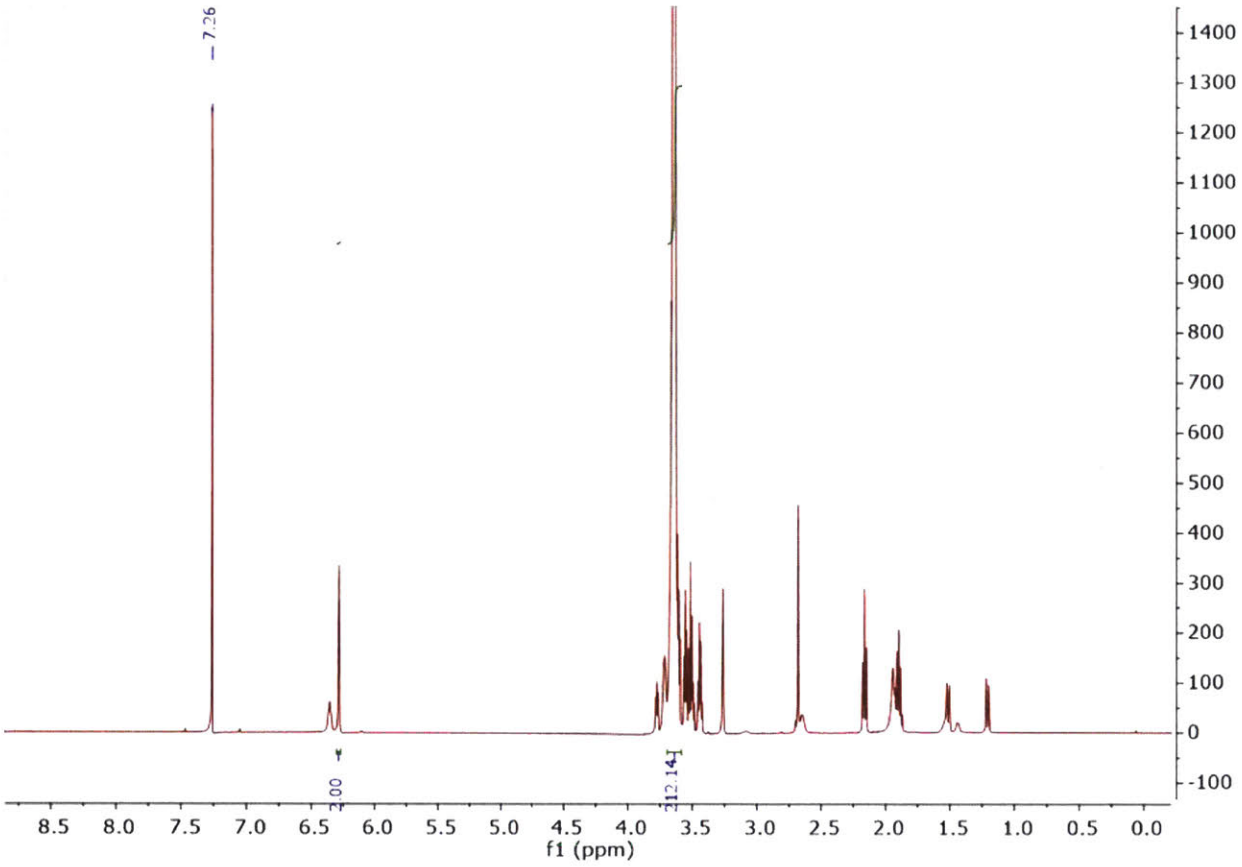

Supplemental Figure 1.S2: ^{1}H-NMR spectrum of **PEG2kDa-MM** taken on a 500 MHz NMR spectrometer in in $CDCl_3$.

Chapter 2: Drug-conjugated BASPs and development of doxorubicin-conjugated MMs

2.1 Introduction

Brief Summary of Chapter and Respective Contributions

Chapter 2 of this thesis is focused on the modular synthesis of drug-conjugated macromonomers as a method to introduce functionality to BASPs. Three publications have resulted from this work as follows:

- Liao, L. *et al.* A convergent synthetic platform for single-nanoparticle combination cancer therapy: ratiometric loading and controlled release of cisplatin, doxorubicin, and camptothecin. *Journal of the American Chemical Society*. **136**, 5896-5899 (2014).
- Gao, A. X., *et al.* Synthesis of acid-labile PEG and PEG-doxorubicin-conjugate nanoparticles via brush-first ROMP. *ACS Macro Letters*. **3**, 854-857 (2014).
- Barnes, J. C. et al. Using an RNAi signature assay to guide the design of three-drug-conjugated nanoparticles with validated mechanisms, *in vivo* efficacy, and low toxicity. *Journal of the American Chemical Society* **138**, 12494-12501 (2016).

All macromonomer synthesis work presented in the results section is my own, unless otherwise stated. The majority of the BASP synthesis and characterization was performed by either Dr. L. Liao or A. X. Gao, as stated in the results section.

Introduction to Nanoparticles for Cancer Therapy

Advances in cancer research have accumulated a wealth of knowledge regarding a cancer cell's growth, progression, interactions, biochemistry, and environment.[1] These developments have helped researchers build small molecule therapeutics for cancer treatment and tools for cancer detection. However, small molecule therapeutics often lack selectivity, rapidly clear from the body, are taken up by the immune system, and may have low solubility, thus contributing to decreased efficacy and undesirable side effects.[2] Many cancer cell types can also develop resistance to small molecule drugs, so strategies such as combination therapy are used to combat resistance or increase potency, but can also increase toxicity. To overcome these issues with current small molecule drugs, researchers have been working toward the design and development of drug delivery devices with desirable pharmacokinetics that can selectively deliver large drug payloads to tumor cells.[3-7] New developments in nanoparticles have indeed led to drug delivery

devices with reduced side effects and more selective delivery to cancer cells than current treatments available on the market.[6]

Some of these successful nanoparticles, which are used in the clinic (**Table 2.1**), include liposomal doxorubicin, Doxil and Myocet; nanoparticle coated albumin, nab-paclitaxel (Abraxane); polymeric micellular formulations of paclitaxel (Genexol-PM), liposome encapsulated vincristine (Marqibo), irinotecan liposome injection (Onivyde), and liposomal cytarabine and daunorubicin combination (Vyxeos).[8-10] These liposomal and protein-bound systems benefit from increased circulation times and greater accumulation in tumors. The mechanism of targeting for these particles is passive, whereby nanoparticles usually between 20-100 nm in diameter accumulate in tumors due to the enhanced permeation and retention effect.[11,12] Extensive research has gone into studying the enhanced permeation and retention effect for various cancers, and although controversial, it is likely in some cancers that the enhanced permeation and retention effect can lead to a small (~1-10%) percent build-up of nanoparticles at the site of a tumor.[13,14] Even if only a 5% increase in nanoparticle accumulation at the tumor is achieved, a particle with high drug loading or highly toxic drug payloads can reduce the total drug dosage required or use the same dosage with increased efficacy and reduced side effects.[15] Doxil uses a polyethylene glycol coating to increase circulation time of doxorubicin to 2-3 days compared to the five minute half-life of the free drug.[16-18] Furthermore, Doxil shifts the dose-limiting toxicity of free DOX away from cardiac toxicity, thus lowering side effects in patients. Doxil also biodegrades into biocompatible phospholipid and cholesterol components. On the other hand, Nab-paclitaxel (Abraxane) is coated in albumin to help bind hydrophobic drugs, such as paclitaxel, and may help in transcytosis of the drug.[8] Future nanoparticles should improve on pharmacokinetics, biodistribution, immunogenicity, side effects, and drug release, and also enable the incorporation of drug combinations in a highly scalable, reproducible synthetic format.

NPs for cancer	Type	Approval year	Approved for
Doxil	Liposomal doxorubicin (PEGylated)	1995 (FDA)	Ovarian cancer, HIV-assocated Kaposi's sarcoma (secondary)
DaunoXome	Liposomal doxorubicin	1996 (FDA)	HIV-associated Kaposi's sarcoma (primary)
Abraxane	Albumin-bound paclitaxel	2005 (FDA)	Advanced nonsmall cell lung cancer, metastatic breast cancer (secondary), metastatic pancreatic cancer (primary)
Marqibo	Liposomal vincristine	2012 (FDA)	Acute lymphoblastic leukemia (tertiary)
Onivyde	Liposomal irinotecan	2015 (FDA)	Metastatic pancreatic cancer (secondary)
Vyxeos	Liposomal cytarabine, doxorubicin	Phase III trials completed in Mar. 2016	Acute-myeloid leukemia

Table 2.1[19]: Examples of some clinically-approved nanoparticles for cancer therapy.

Antibody-drug conjugates, such as brentuximab vedotin and trastuzumab emtansine, are another type of nanocarrier wherein cytotoxic drugs are conjugated to nano-scale monoclonal antibodies to deliver drugs to specific tumor cells overexpressing an appropriate antigen, which is an example of active targeting.[20,21] Unconjugated monoclonal antibodies bind to receptors and can inhibit signal transduction and tag the cancer cell for phagocytosis; adding conjugated drugs can increase toxicity to targeted cells. Although promising, these systems suffer from poor pharmacokinetics, such as uptake by the mononuclear phagocyte system and fast clearance, in addition to poor penetration into solid tumors and poor drug loading.[22] Furthermore, recent evidence suggests that antibody-drug conjugates do not necessarily outperform passively targeted nanoparticles in terms of overall tumor biodistribution.[23]

Many challenges still exist for cancer nanotherapeutics to be safer and more reliable. These challenges include higher drug loading to minimize the impact of the carrier material on the body; specific release of drug load at the tumor; and delivery of multiple drugs, which may help overcome resistance.[24] Also, important to consider are the byproducts of the nanoparticle and whether they can be cleared from the body safely. The heterogeneity of cancer, the difficulty of nanoparticles to cross endothelial barriers and penetrate to the tumor, and the high cost of

production due to complexity of the nanoparticle are more issues that must be overcome in nanotherapy.[25] The recent bankruptcy of the nanoparticle start-up Bind Therapeutics was in part due to their pilot polymer coated docetaxel, BIND-014, that struggled to meet expectations in clinical trials even though mouse studies had shown promise as a more effective therapeutic in comparison to the free drug.[26] This example highlights the difficulty in using data from *in vivo* animal studies to predict the effectiveness of a drug or nanotherapy in human clinical trials. Moving forward, it is important to learn from trials and failure to help design and guide research into new and effective therapeutics that can improve patient outcome.[27] The success of other nanoparticle formulations in the field of nanoparticles for drug delivery is promising and a number of reviews have outlined design considerations for optimizing drug delivery of nanoparticles *in vivo*.[12,15,28,29] Currently, the Johnson group focuses on the development of BASPs for applications in drug delivery to address some of these therapeutic challenges. The design and synthesis of BASPs was introduced in chapter 1; chapter 2 will focus on the introduction of functionality to BASPs, in particular the synthesis of drug-conjugated macromonomers with stimuli-responsive drug release.

Since every nanoparticle behaves differently *in vivo*, the biological properties of BASPs must be investigated before conclusions can be drawn about their ultimate potential. Currently, *in vitro* cytotoxicity assays has shown that the empty BASP vehicle is not toxic to cells at the highest concentrations that are typically tested.[30] *In vitro* live confocal imaging experiments also suggest that the pegylated doxorubicin-conjugated BASPs are generally endocytosed and taken up in endosomes or lysosomes for OVCAR3 cells.[30] The mechanism of BASP endocytosis has not been studied yet; depending on the cell-type, some possible mechanisms may include receptor/clathrin-mediated endocytosis, clathrin-independent pathways, or other endocytosis pathways, such as phagocytosis.[31] Light was then irradiated on the OVCAR3 cells to release the doxorubicin conjugated to the BASP via a photocleavable linker. The live confocal imaging suggests that doxorubicin was able escape the endosomal compartment and distribute to the cytoplasm and the nucleus, of which the nucleus is the mechanistically active site of doxorubicin, a topoisomerase II inhibitor.[30] It is not well known how doxorubicin or some endocytosed drugs release from endosomal compartments; reviews highlight some possibilities.[31-33] Researchers have proposed one possibility for endosomal release, known as the "proton sponge" effect, in

which pH-sensitive, cationic polymers, such as polyethyleneimine, can protonate at low pH leading to osmotic swelling inside the endosome and subsequent bursting of the compartment.[33]

Many of the clinically-approved nanoparticles are liposomal formulations; however, BASPs are likely to have different *in vivo* properties than liposomes. Even among BASPs, different sizes and functionality can easily alter a BASP's biological half-life, pharmacokinetics, and degradation pathways. The therapeutics and drug release chemistries will easily affect both the *in vitro* cytotoxicity and the *in vivo* efficacy of these BASPs and should be evaluated for each BASP. In the Johnson group, we study these biological properties of BASPs, and also use chemistry and polymer science to tune and optimize BASP properties for drug delivery.

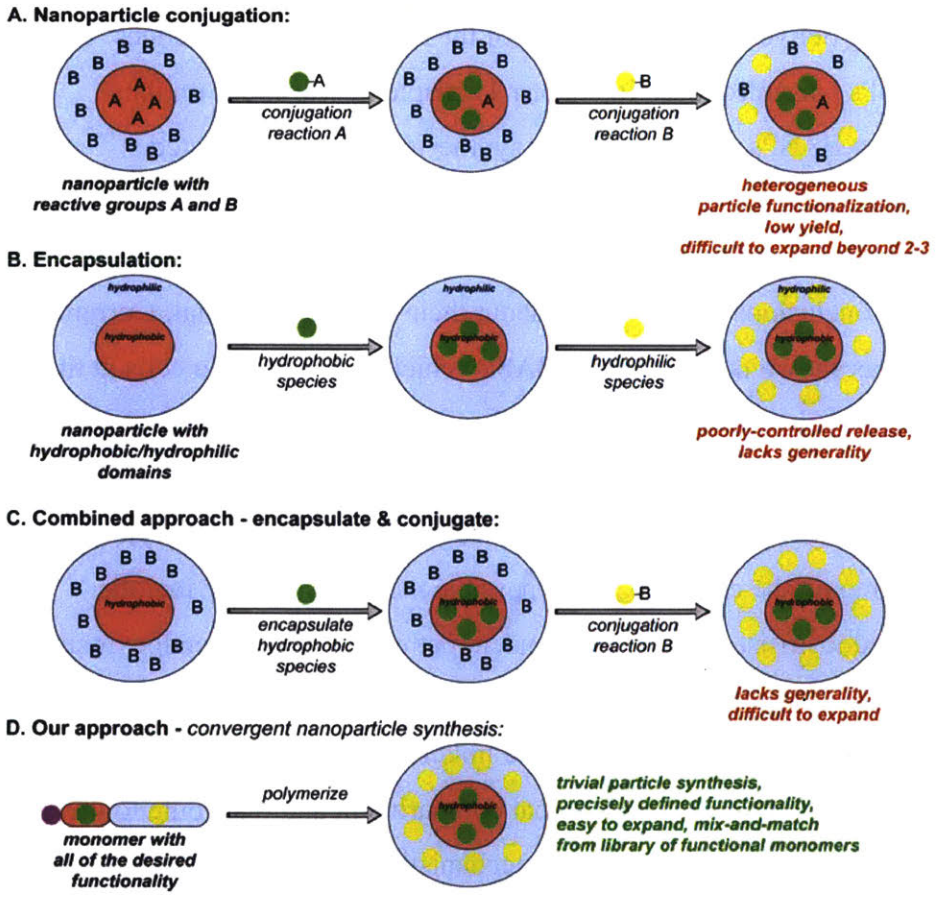

Figure 2.1: Nanoparticle conjugation (A), encapsulation (B), and a combined approach (C) in comparison to our approach (D) for introducing multiple functionalities.

A Modular Approach to Synthesizing Functional BASPs

Many methods have been applied to synthesize nanoparticles for drug delivery with multiple functional molecules, such as drugs, targeting ligands, and imaging agents.[34-36] Some general strategies are shown in **Figure 2.1**, which highlights several drawbacks and advantages. In **Figure 2.1A**, the nanoparticle is created first, followed by conjugation of the free drug, but this method suffers from incomplete conversion and requires orthogonal reactive groups limiting the degree of functionality. In the encapsulation approach (**Figure 2.1B**), the nanoparticle is synthesized first then the drugs can be encapsulated through passive diffusion or an active transport mechanism, like in Doxil, or the nanoparticle can be assembled in the presence of drug. However, the drug-loading is not usually well-defined and these systems suffer from poor drug release kinetics and limited scalability. Another possibility is the encapsulation of a hydrophobic drug and assembly of the nanoparticle, followed by post-assembly conjugation, but it inherits the drawbacks of both systems. In a convergent approach, the Johnson group proposes to synthesize monomers with functional groups attached that can then be polymerized via a graft-through strategy into a drug delivery device (**Figure 2.1D**). Through the synthesis of functional macromonomers, we can control the NP physical properties and functionality at the molecular level.

In the first chapter, BASPs were synthesized via a graft-through approach using ring opening metathesis polymerization (ROMP).[37,38] In BASP synthesis, G3 polymerizes a macromonomer to create a living bottle-brush initiator, followed by addition of a bifunctional crosslinker to yield a dense crosslinked core with PEG-brush arms.[39,40] In this chapter, ROMP is used to make multifunctional BASPs with applications in drug delivery. Development of the 3rd-generation Grubbs catalyst has led to a highly reliable method of synthesizing polymers of low dispersity.[41] Currently, the Johnson group is developing monomers conjugated with drugs, imaging agents, and targeting ligands that are compatible with ROMP, such as the doxorubicin conjugated monomers that are detailed in this chapter. To make the doxorubicin conjugated macromonomer, a branched-alkyne PEG 3kDa macromonomer (PEG-alkyne-MM) is first synthesized. Drugs or other molecules with an azide can be appended onto PEG-alkyne-MM by copper(I)-catalyzed alkyne-azide cycloaddition (CuAAC) to synthesize a functional branched macromonomer as shown in **Scheme 2.1**, which also points out some features of the drug-conjugated MM. In the case of doxorubicin, azide functionalized linkers are designed based on a

photocleavable and a hydrolyzable group that can cleave under light irradiation or aqueous conditions, respectively, to release free doxorubicin (**Scheme 2.2**: photo-DOX-MM and ester-DOX-MM). These doxoroubicin linked macromonomers were further used by other members in the Johnson lab to create multifunctional, water-soluble BASPs with a degradable core and applications in drug delivery.[30,42,43]

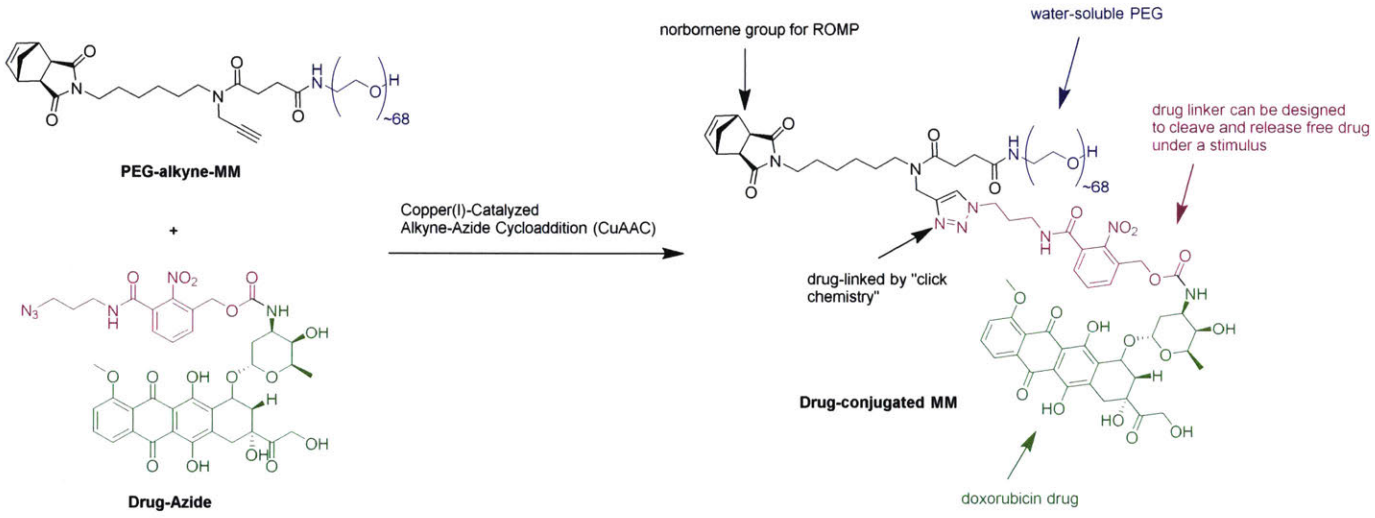

Scheme 2.1: Using copper(I) catalyzed azide-alkyne cycloaddition (CuAAC), a doxorubicin azide is appended to PEG-alkyne-MM to produce a doxorubicin functionalized macromonomer for use in ROMP.

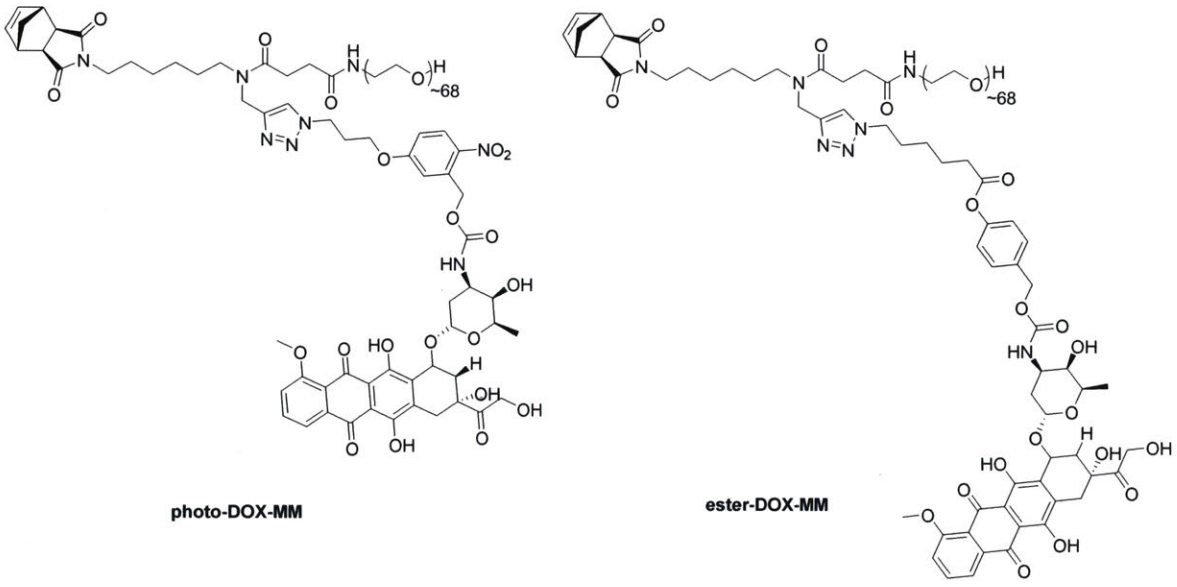

Scheme 2.2: Structures of the photo-DOX-MM and ester-DOX-MM designed and discussed in this report.

Aside from chemotherapeutics, the PEG-alkyne-MM can be used to couple other azide linked functional molecules, such as imaging agents or ligands. In this way, we can build a library of monomers to use in a convergent fashion for the synthesis of multifunctional BASP nanoparticles (**Figure 2.2**). Multifunctionality is achieved by polymerizing one functional monomer, followed by sequential addition of new monomers until the polymerization is quenched, or alternatively, a mixture of multifunctional macromonomers can be polymerized to synthesize polymers containing a statistical mixture of components. Each functional macromonomer can be combined in different ratios allowing for opportunities in controlled ratiometric drug loading. ROMP is ideal for the convergent synthesis of a drug delivery nanoparticle; it addresses the need for well-defined systems with high and predictable drug loading, opportunities for multifunctionality, and reproducible nanoscale particles. These particles are designed to address some of the drawbacks of current nanoparticle drug delivery systems, which were discussed in Chapter 1 of this thesis.

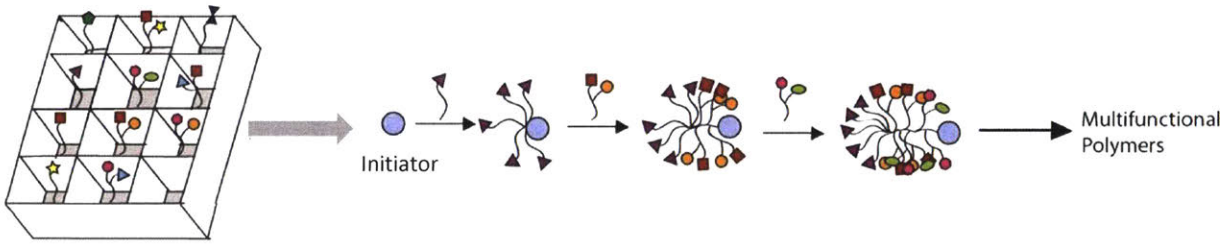

Figure 2.2: Starting with a library of multifunctional macromonomers, convergent synthesis of multifunctional polymers can be easily achieved.

2.2 Results and Discussion

In the previous chapter, BASPs with controlled sizes and degradable cores were synthesized by ROMP. Due to the well-established properties of PEG, including water-solubility and other favorable biological properties, such as low immunogenicity,[44] PEG was used as the main polymer by composition. Previously, Professor J. A. Johnson developed a branched macromonomer using PEG derivatized with a norbornene group and a branching alkyne functional group (PEG-alkyne-MM).[45] Biomolecules, such as chemotherapeutics bound to an azide-based linker, were appended to the alkyne branch using CuAAC. **Scheme 2.3** shows the synthetic route to producing PEG-alkyne-MM, which used PEG 3kDa as the number-average molar mass of PEG.

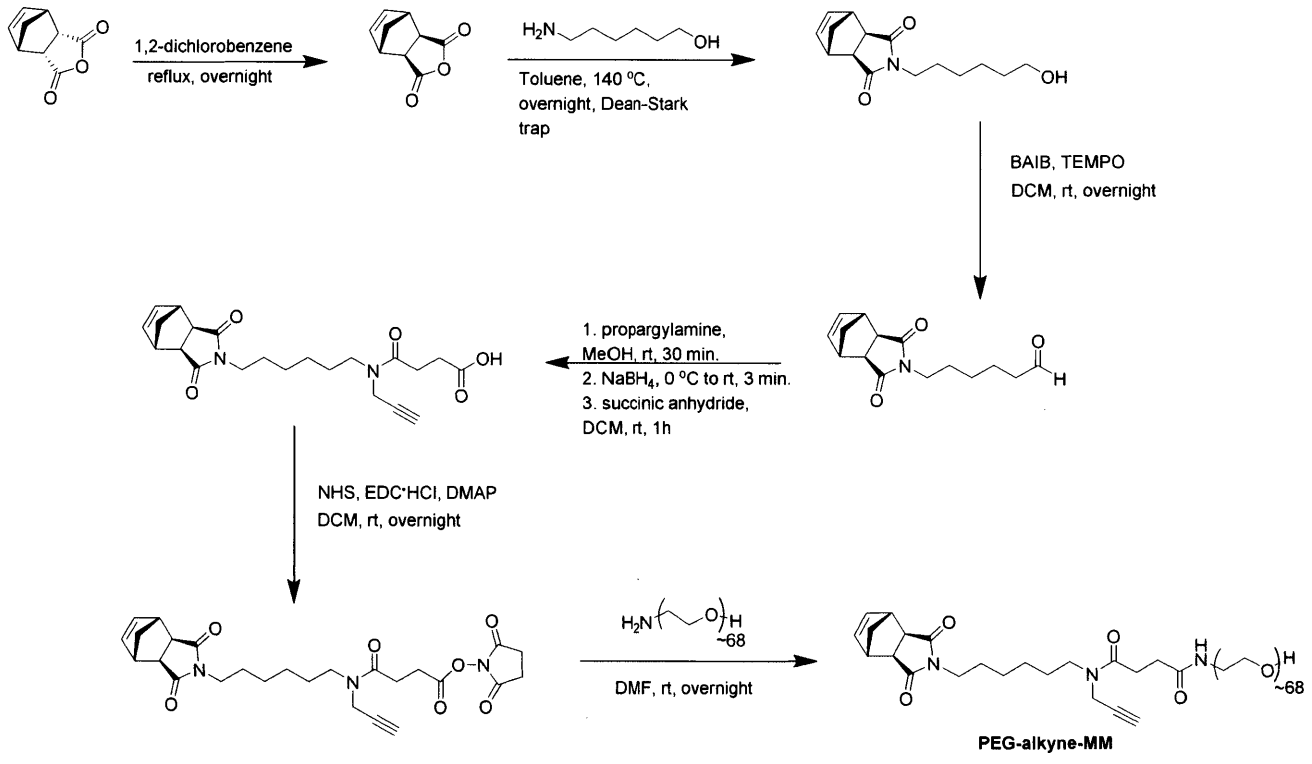

Scheme 2.3: Synthesis of PEG-alkyne-MM

A drug bound to a linker containing an azide can be conjugated to the alkyne branch of the PEG-alkyne-MM using copper (I)-catalyzed azide-alkyne cycloaddition click chemistry as shown in **Scheme 2.4**. Importantly, the PEG branch offers solubility to "clicked-on" groups that would have otherwise been insoluble in water.

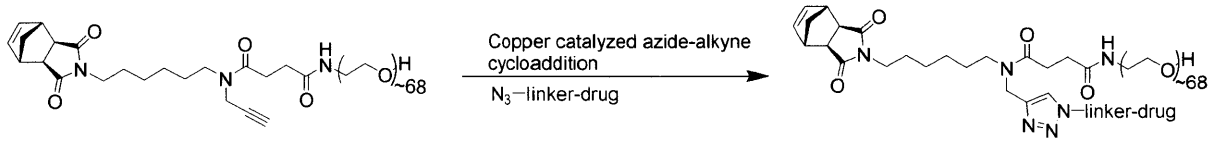

Scheme 2.4: Conjugation strategy to synthesize drug-loaded macromonomers

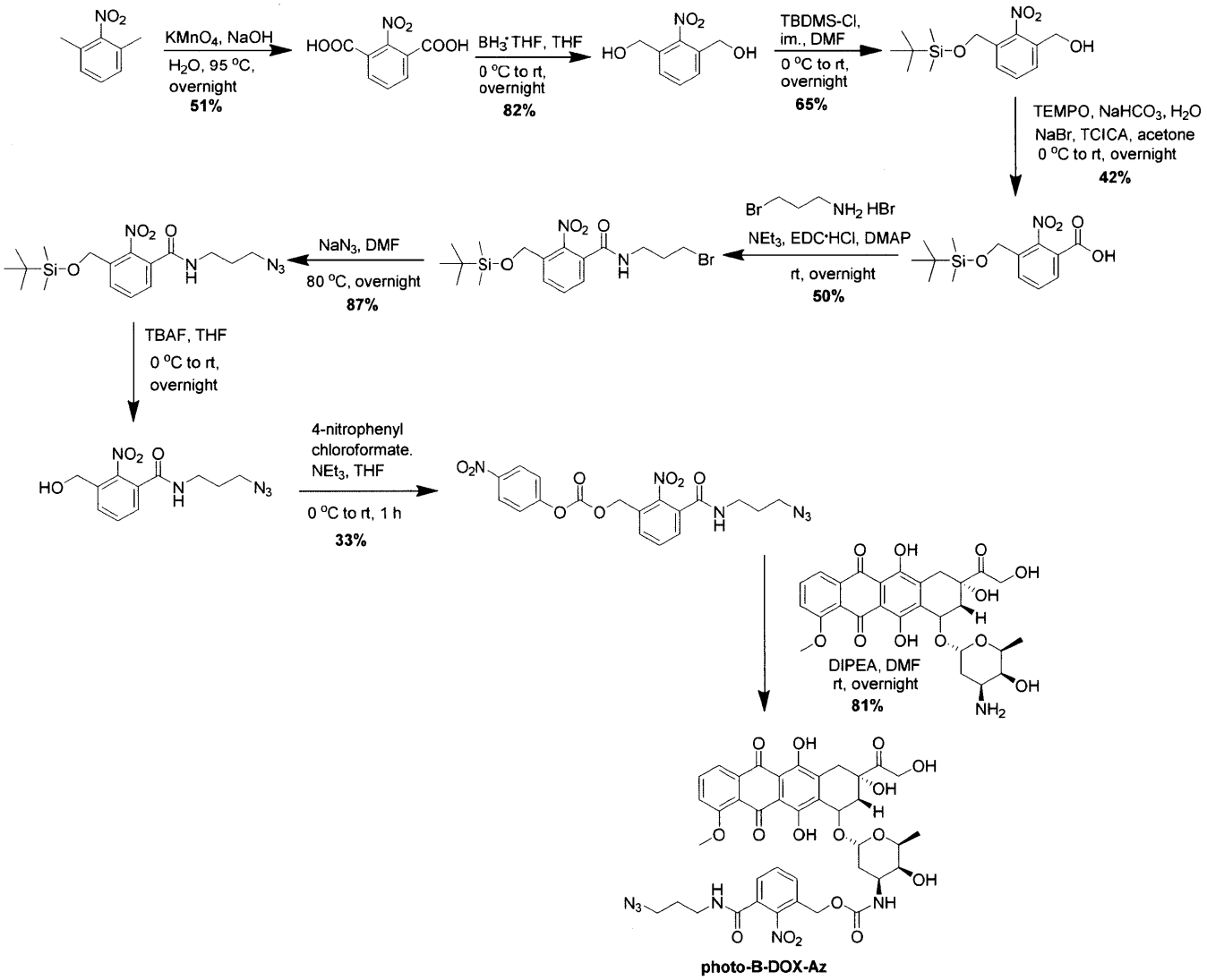

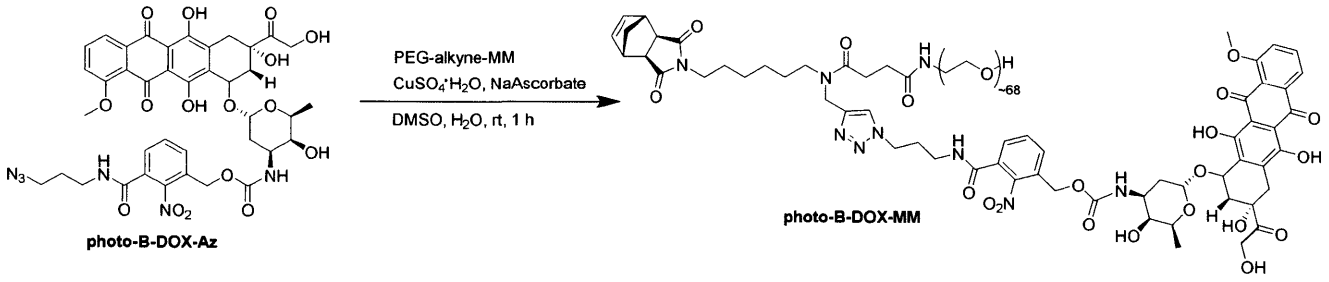

Scheme 2.5: Synthesis of photo-B-DOX-MM

With PEG-alkyne-MM in hand, we sought to produce drug-conjugated MM for application in BASP synthesis. With an initial interest in studying the impact of externally triggered drug release *in vitro* synthesize, we first targeted doxorubicin (DOX)-conjugated MMs. First, a photocleavable linker was synthesized and coupled to doxorubicin (photo-B-DOX-Az), as shown in **Scheme 2.5**.[45] As described in the previous chapter, upon light irradiation at 365 nm, the nitrobenyloxycarbonyl (NBOC) group undergoes a photochemical reaction to release CO_2 and free doxorubicin.[46] The initial synthesis of photo-B-DOX-Az was 9 steps from commercially available 1,3-dimethyl-2-nitrobenzene, and many of the steps had <50% yield, which led to overall low yields of the final DOX-azide. An alternative approach was identified to produce suitable NBOC linkers for DOX conjugation[47]; this route was adapted to produce a new photocleavable DOX-azide in a total of five steps in good yield, as shown in **Scheme 2.6**.

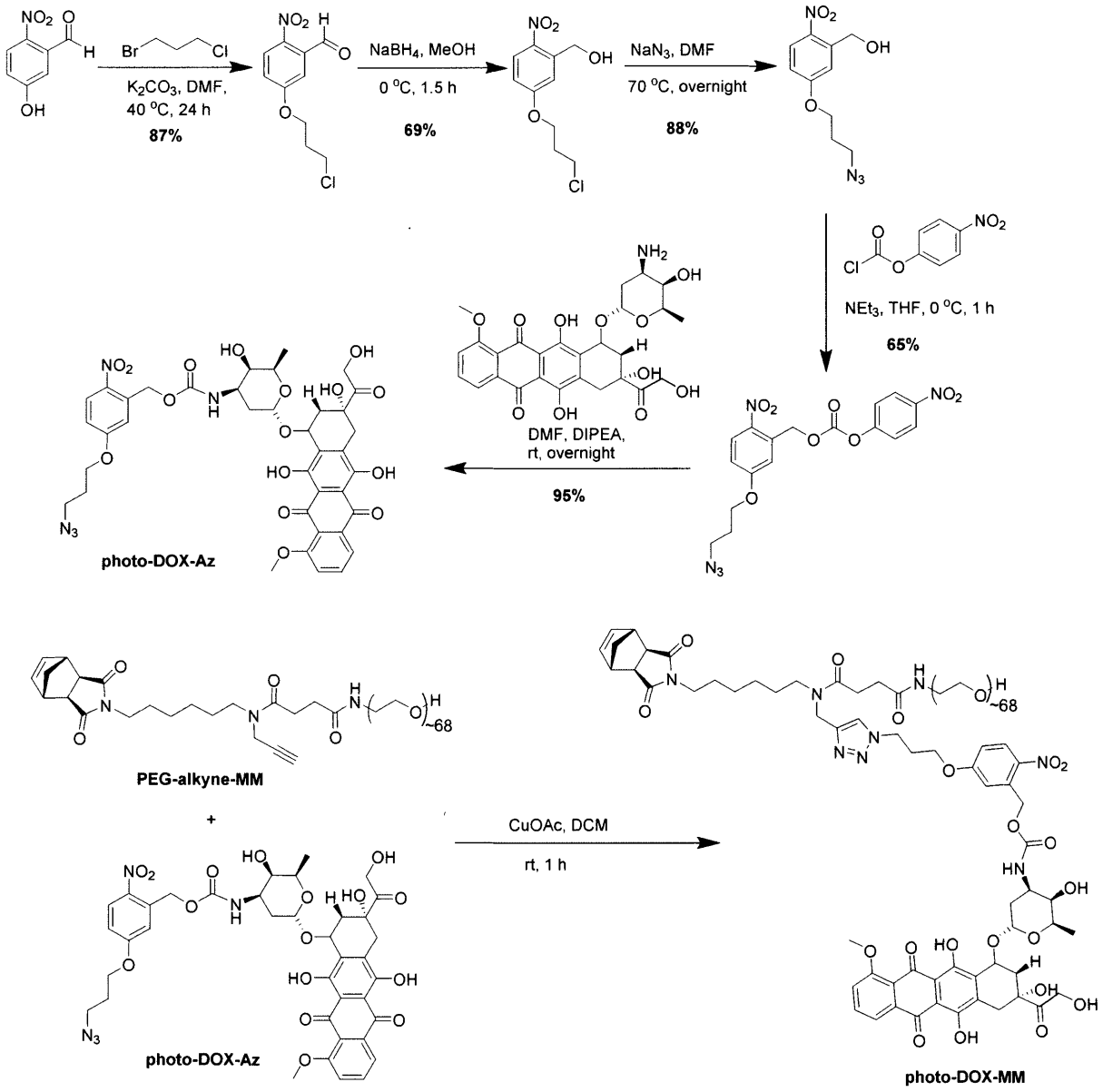

Scheme 2.6: Synthesis of photo-DOX-MM

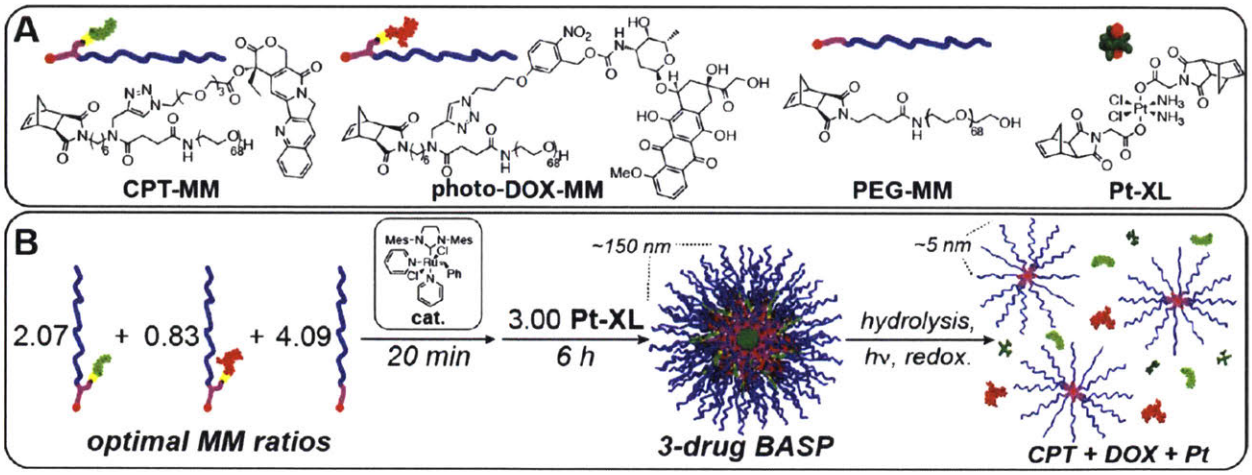

Figure 2.3:[30] A) Functional macromonomers used in the first 3-drug conjugated BASPs. B) Schematic illustrating CPT-MM, photo-DOX-MM and PEG-MM polymerized by G3 to produce a living bottlebrush initiator, and addition to Pt-XL to provide the core-crosslinked 3-drug conjugated BASP. In response to hydrolysis, light irradiation, and reducing conditions the BASP can release free camptothecin (CPT), doxorubicin (DOX), or cytotoxic platinum species (Pt), respectively.

Photo-DOX-Az was coupled to PEG-alkyne-MM by CuAAC to provide photo-DOX-MM (**Scheme 2.6**), which was used by Dr. L. Liao for the synthesis of a three-drug conjugated BASP.[30] The multifunctional, combination therapy BASP synthesized by Dr. Liao contained three chemotherapeutics: doxorubicin, camptothecin, and cisplatin as shown in **Figure 2.3**. Photo-DOX-MM releases free doxorubicin under light irradiation, whereas the camptothecin MM (CPT-MM) releases free camptothecin under aqueous conditions through a hydrolysable ester group. The platinum (IV) bifunctional norbornene crosslinker (Pt-XL) is a prodrug of cisplatin that cleaves under reducing conditions, such as in the cell's cytoplasm, to putatively release free cisplatin (II) and smaller brush components.

In the synthesis of the BASP, a mixture of 0.83 equivalents of photo-Dox-MM, 2.07 equivalents of CPT-MM, and 4.09 equivalents of PEG-MM was polymerized with 1 equivalent of G3 to create the 7-unit living brush initiator containing two drugs. The living brush initiator was added directly to 3 equivalents of Pt-XL and was allowed to react for six hours to create a BASP containing three chemotherapeutics (**Figure 2.3B**). Dr. Liao further tested these BASPs in cytotoxicity assays on OVCAR3 ovarian carcinoma cells confirming that the BASP was cytotoxic with an IC_{50} of 42 ± 6 μg BASP/mL. However, 10 min light irradiation at 365 nm of the same BASP formulation led to an increase in cytotoxicity (IC_{50} of 18±2 μg BASP/mL) due to

the release of free doxorubicin. In summary, photo-DOX-MM was used in the synthesis of a multifunctional, three-drug conjugated BASP with controlled ratiometric loading of each drug; these BASPs displayed increased cytotoxicity towards OVCAR3 cells after light irradiation.

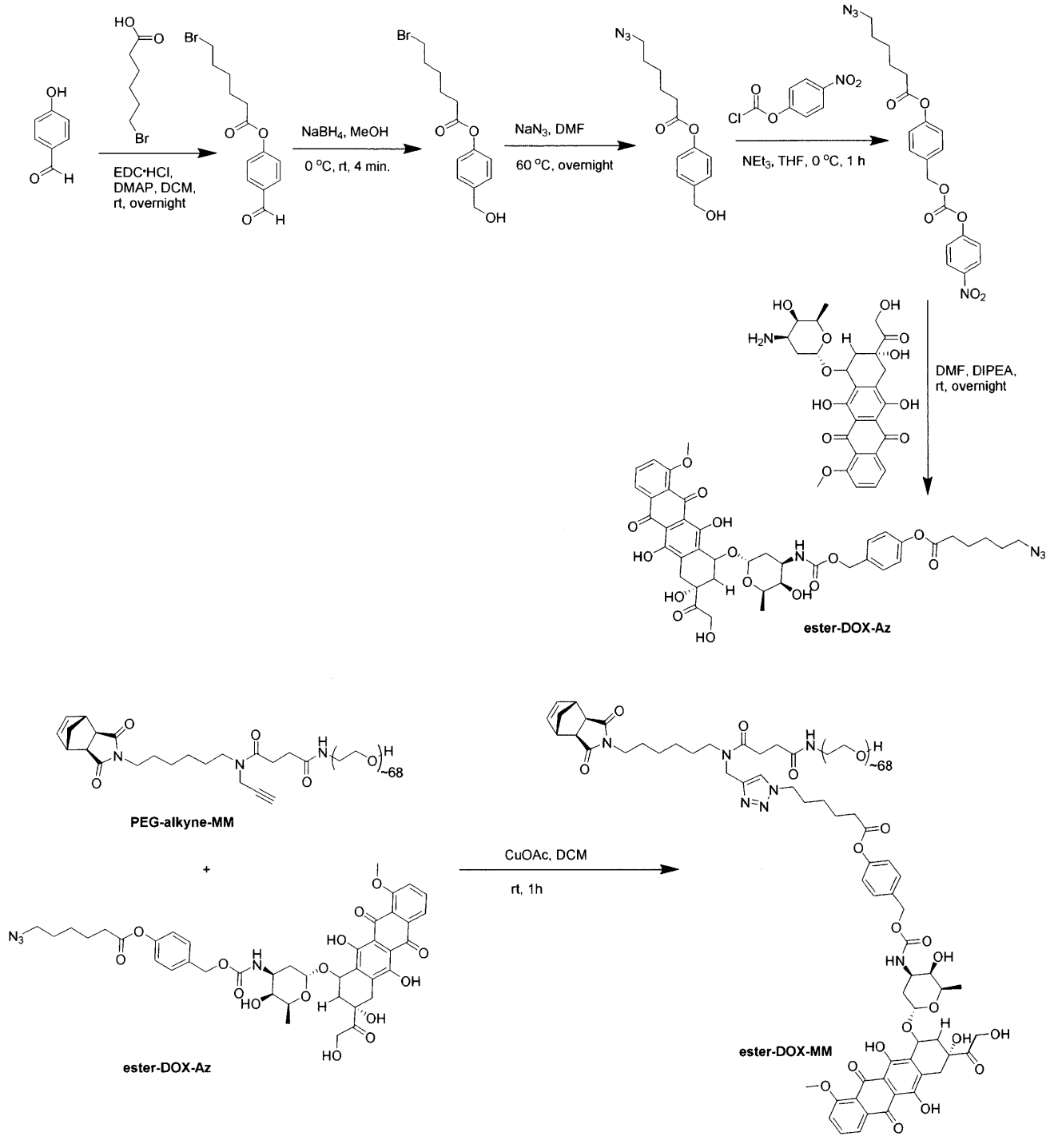

Scheme 2.7: Synthesis of ester-DOX-MM

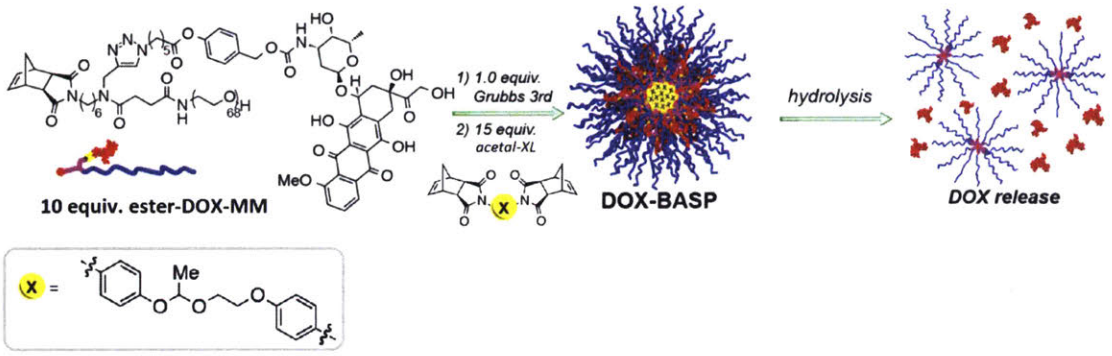

Figure 2.4:[42] 10 equivalents of ester-DOX-MM was polymerized by G3 to form the living bottlebrush initiator. 15 equivalents of Acetal-XL were added to form doxorubicin loaded BASPs. Incubation of BASP in pH 7.4 buffered PBS solution confirmed release of free doxorubicin, and *in vitro* assays using HeLa cells confirmed the cytotoxicity of these doxorubicin-loaded BASPs.

As stated above, the photocleavable doxorubicin linker used above was designed to study the effect of externally triggered DOX release *in vitro*. Such linkers are likely not applicable *in vivo* without the use of light guide or other special techniques due to the limited transmission of 365 nm light through biological tissues. Thus, we sought to develop alternative linkers that could hydrolyze to release free doxorubicin in response to chemical triggers *in vivo*. Our first-generation design, ester-DOX-Az, is provided in **Scheme 2.7**. The structure of ester-DOX-Az features an ester linker that can hydrolyze and undergo a 1,4-benzylic elimination to release free doxorubicin and carbon dioxide under biologically relevant conditions.[42,48] The azide linker was synthesized, and A. X. Gao further coupled the linker to doxorubicin to yield ester-DOX-Az; this DOX-azide was conjugated to PEG-alkyne-MM to produce ester-DOX-MM. Using 10 equivalents of the ester-DOX-MM to 1 equivalent of G3 and 15 equivalents of an acetal-based crosslinker, Acetal-XL (**Figure 2.4**), BASPs containing doxorubicin appended via a hydrolyzable linker were synthesized and characterized.

Release of doxorubicin was confirmed by incubating the doxorubicin-conjugated BASPs in pH 7.4 buffer and running cytotoxicity assays, which showed that the doxorubicin-conjugated BASPs were more toxic to HeLa cells (IC50 of 8.4±0.5 μM relative to doxorubicin) than non-drug-conjugated BASPs (no toxicity observed for concentration range tested). Furthermore, the acetal groups that comprised the BASP core degraded under acidic conditions, which could be advantageous for *in vivo* clearance of the BASP from the body. The acid-degradable crosslinker may facilitate the breakdown of BASPs in the extracellular space of solid tumors, which is slightly acidic (pH ~ 6-7),[28] or upon cellular uptake into acidic lysosomal compartments, which

can reach a pH as a low as 4.5.[49] Both the ester-based DOX linker and the acetal crosslinker can be used as components of a BASP drug delivery system that are responsive in tumor microenvironments.

2.3 Conclusion

This chapter detailed the development and synthesis of doxorubicin-conjugated PEG macromonomers, which were used synthesize multi-functional BASP nanoparticles via the ROMP-based strategy outlined in Chapter 1. The drug conjugated BASPs synthesized were generally <200 nm in diameter and possessed drugs linked through stimuli-responsive linkers that could be cleaved to release free drug under stimuli such as reduction, pH, or light. In particular, two novel doxorubicin conjugates were synthesized: one based on the NBOC group that cleaves upon light irradiation and another based on an ester linkage that cleaves to provide free DOX under aqueous conditions. Both of these strategies to release free doxorubicin could be extended to other drugs or biomolecules with free amines. Our modular approach to the synthesis of the DOX-conjugated MMs could easily be extended to building a library of various different drug-conjugated MMs and used in the convergent synthesis of BASPs. Given the heterogeneity of cancer, the mix-and-match nature of the BASP platform and control over final BASP size could be useful in optimizing a combination therapy for a given cancer type for a specific patient. Due to the high concentration of drugs conjugated within each BASP and the reproducible synthesis of these nanoparticles, it will be worthwhile to explore BASP nanotechnology as a safer way to deliver chemotherapeutics with improved efficacy and lower toxicity compared to free drug. The use of BASPs as a drug delivery platform for chemotherapeutics forms the basis of the next two chapters.

2.4 Experimental

General Considerations

Doxorubicin hydrochloride was purchased from LC laboratories. Unless otherwise noted, reagents were purchase from Sigma Aldrich or Alfa Aesar and used without further purification. Grubbs' 2nd generation catalyst was obtained from Materia, and converted to G3 following the procedure in chapter 1 of this thesis. Silica gel used in column chromatography was the ZEOprep 60 HYD, 40-63 μm. Compounds purified by flash chromatography were purified on a Biotage Isolera One.

^{1}H nuclear magnetic resonance (^{1}H-NMR) and ^{13}C nuclear magnetic resonance (^{13}C-NMR) spectra were recorded on Bruker AVANCE-400 Mhz NMR spectrometer or a VARIAN Inova-500 Mhz NMR spectrometer. Spectra were analyzed on MestReNova NMR software. Chemical shifts are expressed in parts per million (ppm); splitting patterns are designated as s (singlet), d (doublet), t (triplet), m (multiplet), and br (broad); and coupling constants, J, are reported in Hertz (Hz).

Samples submitted to the MIT Department of Chemistry Instrumentation Facility (DCIF) for high-resolution mass spectrometry (HRMS) were obtained on a Bruker Daltonics APEXIV 4.7 Tesla Fourier Transform Ion Cyclotron Resonance Mass Spectrometer (FT-ICR-MS).

Matrix-assisted laser desorption ionization time-of-flight (MALDI-TOF) mass spectrometry was analyzed for macromonomers on a Bruker Omniflex MALDI-TOF with a Reflectron accessory. For MALDI-TOF, sample was prepared by dissolving 1 mg of MM in 200 μL MeCN, and matrix was prepared by dissolving approximately 3 mg of 2-(4'-hydroxybenzeneazo)benzoic acid (HABA) in a 0.3mL/0.2mL MeCN/water mixture, or approximately 20 mg of α-cyano-4-hydroxycinnamic acid (CHCA) in 500 uL of 1:1 MeCN:water + 0.1% TFA solution. 3 μL of sample solution was mixed with 50 μL of matrix solution, then about 0.7 μL of this mixture was spotted onto the MALDI target.

Liquid chromatography-mass spectrometry (LC-MS) was performed on an Agilent 1260 LC system equipped with an Agilent 6130 single quadrupole mass spectrometer. Samples were obtained on a Zorbax SB-C18 rapid resolution HT analytical column in a gradient eluent of 0.1% acetic acid in purified water from a MilliQ Biocel A10 water purification system to 100% HPLC-grade acetonitrile.

High-pressure liquid chromatography (HPLC) was performed on an Agilent 1260 LC system equipped with an Agilent ZORBAX 300SB-C18 preparative column and using a gradient eluent of 0.1% acetic acid in MilliQ water to 100% HPLC-grade acetonitrile.

Synthesis of PEG-Alkyne-MM:

The procedure for synthesis of branched PEG-Alkyne-MM is reported in literature,[45] with any minor revisions detailed in the experimental procedures below. With the exception of *exo*-norbornene anhydride, all ^{1}H-NMR, ^{13}C-NMR, and HRMS are as reported in literature,[45] and are not reproduced in this document. The synthesis of *exo*-norbornene anhydride is reported in Chapter 1 of this thesis.

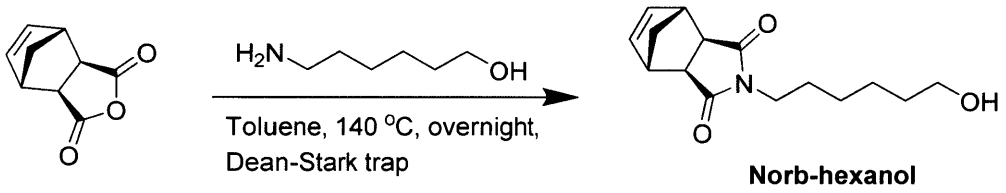

Norb-hexanol

Norb-hexanol: *Exo*-norbornene anhydride (12.0 g, 0.073 mol, 1 eq) and 6-amino-1-hexanol (9.0g, 0.077 mol, 1.05 eq) were dissolved in 150 mL of toluene in a 300 mL round bottom flask equipped with stirbar, Dean-Stark trap, and reflux condenser. The oil bath was heated to 140 °C or until solvent was refluxing, and stirred overnight. The heat was turned off and the reaction was allowed to reach room temperature. Next the solution was concentrated and loaded directly onto a silica cartridge. Purification by flash chromatography (0% EtOAc/Hexanes to 100% EtOAc/Hexanes) yielded norb-hexanol (yields typically >90%) as a clear viscous oil. ^{1}H-NMR, ^{13}C-NMR, and HRMS are as reported in literature.[45]

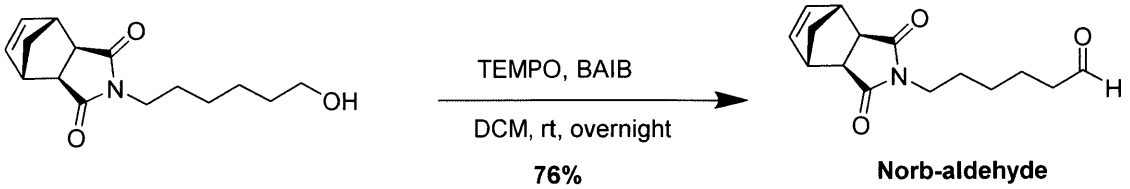

Norb-aldehyde

Norb-aldehyde: Norb-hexanol (10 g, 0.038 mol, 1 eq) was dissolved in 100 mL of anhydrous dichloromethane in a dry 250-mL round bottom flask. Bisacetoxyiodobenzene (13.5 g, 0.042

mol, 1.1 eq) was added, followed by addition of TEMPO (0.6 g, 0.0038 mol, 0.1 eq). The reaction was placed under N_2 and stirred at room temperature overnight. The reaction was diluted with an additional 100 mL of DCM and washed with 150 mL each of saturated sodium thiosulfate solution, saturated sodium bicarbonate solution, and brine in a 500 mL separatory funnel. The organic layer was then dried over magnesium sulfate, and concentrated by rotary evaporation. The concentrated solution was loaded onto a silica cartridge (100g) and purified by flash chromatography (0% EtOAc/Hexanes to 60% EtOAc/Hexanes) to afford Norb-aldehyde (7.5 g, 76 %) as a clear viscous oil. ^{1}H-NMR, ^{13}C-NMR, and HRMS are as reported in literature.[45]

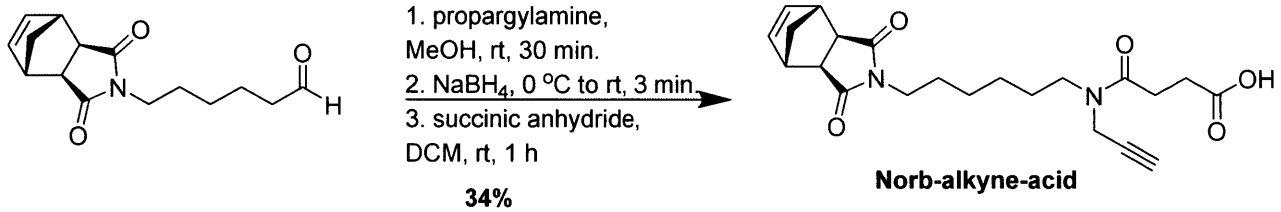

Norb-alkyne-acid: Norb-aldehyde (1g, 3.83 mmol, 1 eq) was stirred with propargylamine (0.26 mL, 4.02 mmol, 1.05 eq) in methanol (10 mL) for 30 min under N_2 at room temperature. The reaction was placed in an ice bath at 0 °C and sodium borohydride (218 mg, 5.75 mmol, 1.5 eq) was added. The ice bath was removed and the reaction was allowed to proceed for only 3 min, followed by quenching with 100 mL of saturated sodium bicarbonate solution. The crude product was extracted with dichloromethane (100 mL) five times. The organic layers were collected and dried over sodium sulfate. The crude product was dried in vacuo, then redissolved in 10 mL of anhydrous DCM, followed by addition of succinic anhydride. Once the reaction has gone to completion (~1 h), the sample was loaded directly onto a silica cartridge. Purification by flash chromatography (0% EtOAc/Hexanes to 100% EtOAc/Hexanes) yielded Norb-alkyne-acid (0.54 g, 1.3 mmol, 34% yield) as a viscous oil. ^{1}H-NMR, ^{13}C-NMR, and HRMS are as reported in literature.[45]

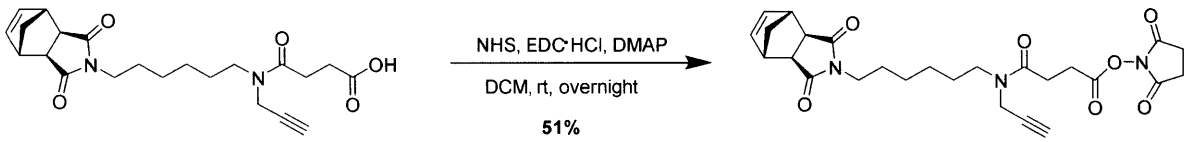

Norb-alkyne-NHS: Norb-alkyne-acid (500 mg, 1.25 mmol, 1 eq), EDC·HCl (479 mg, 2.50 mmol 2 eq), and DMAP (30 mg, 0.250 mmol 0.2 eq) were dissolved in anhydrous DCM (10 mL), and stirred for 30 min. NHS (288 mg, 2.50 mmol 2 eq) was added to the solution, and the reaction was stirred overnight at room temperature or until complete as monitored by LCMS. The solution was directly loaded onto a silica cartridge and purified by flash chromatography (0% EtOAc/Hexanes to 100% EtOAc/Hexanes) to afford Norb-alkyne-NHS (315 mg, 51 %). ^{1}H-NMR, ^{13}C-NMR, and HRMS are as reported in literature.[45]

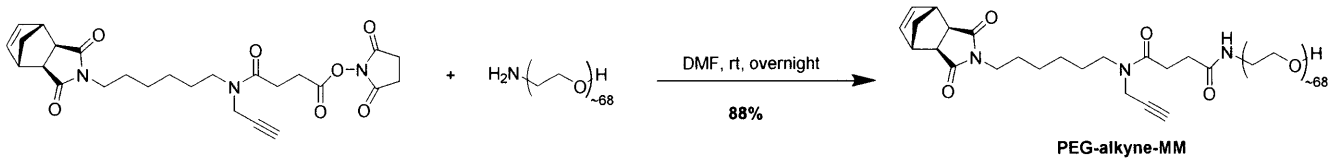

PEG-alkyne-MM: Norb-alkyne-NHS (315 mg, 0.633 mmol, 1.05 eq), and O-(2-aminoethyl)polyethylene glycol 3 kDa (1.8 g, 0.600 mmol, 1.0 eq) were reacted in anhydrous DMF (15 mL) under N_2 overnight. The compound was precipitated in ether, followed by centrifugation of solids and decantation of the ether five times. The product was dried on high vacuum to yield PEG-alkyne-MM (1.8 g, 88% yield) as a white solid. ^{1}H-NMR, and MALDI-TOF are as reported in literature.[45]

Synthesis of photo-B-DOX-MM:

The procedure for synthesis of photo-B-DOX-Az was reported in literature,[45] with any minor revisions detailed in the experimental procedures below. All ^{1}H-NMR, ^{13}C-NMR, and HRMS are as reported in literature,[45] and are not reproduced in this document. 2-nitro-1,3 benzenedimethanol is synthesized in chapter 1 of this thesis.

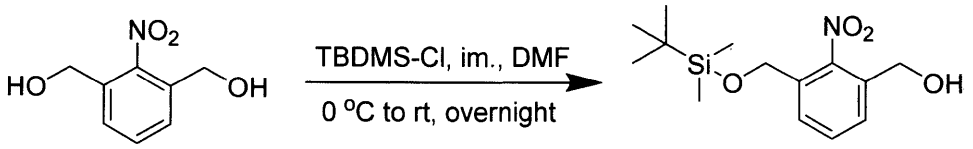

Compound 2.1: 2-nitro-1,3 benzenedimethanol (5.9 g, 32.2 mmol, 1 eq), imidazole (2.19 g, 32.2 mmol, 1 eq), and DMAP (0.393g, 3.2 mmol, 0.1 eq) were dissolved in anhydrous DMF (200 mL) in a dry flask under N_2. The flask was cooled to 0 °C and TBDMS-Cl (2.9 g, 19.3 mmol, 0.6 eq) in DMF (40 mL) was added dropwise with a syringe. The ice bath was removed and the reaction was stirred at room temperature overnight. The solution was concentrated by rotary evaporation, then the concentrated sample was diluted with ethyl acetate (150 mL) and washed with water (100 mL each) twice and brine (100 mL) once. The organic layer was dried over magnesium sulfate, which was filtered out, and then the solution was concentrated by rotary evaporation. Purification by column chromatography (0% EtOAc/Hexanes to 100% EtOAc/Hexanes) yielded compound 2.1 (3.5g, 65% yield with respect to TBDMS-Cl). ^{1}H-NMR, ^{13}C-NMR, and HRMS are as reported in literature.[45]

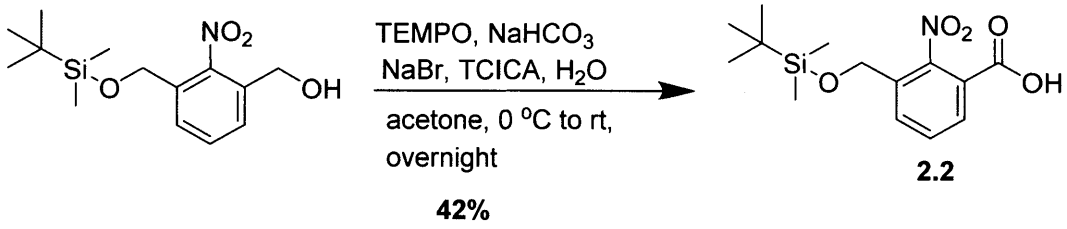

Compound 2.2: Compound 2.1 (450 mg, 1.5 mmol, 1 eq) was dissolved in acetone (33 mL), then 15% sodium bicarbonate solution (10 mL) was added to the solution. After cooling the reaction to 0 °C on an ice bath, TEMPO (11.8 mg, 0.076 mmol, 0.05 eq) and sodium bromide (77.9 mg, 0.76 mmol, 0.5 eq) were added to the solution, followed by slow addition of trichlorocyanuric acid (1.57 g, 6.8 mmol, 4.5 eq). The ice bath was removed and the reaction was stirred at room temperature overnight. After quenching with isopropanol (3 mL), the reaction was filtered over celite and concentrated by rotary evaporation. The concentrated sample was diluted with ethyl acetate (100 mL) and washed with water (75 mL each) twice and brine (75 mL) once. The organic layer was dried over magnesium sulfate, and the solution was

concentrated by rotary evaporation. Purification by column chromatography (0% MeOH/DCM to 10% MeOH/DCM) yielded compound 2.2 (196 mg, 42% yield). ^{1}H-NMR, ^{13}C-NMR, and HRMS are as reported in literature.[45]

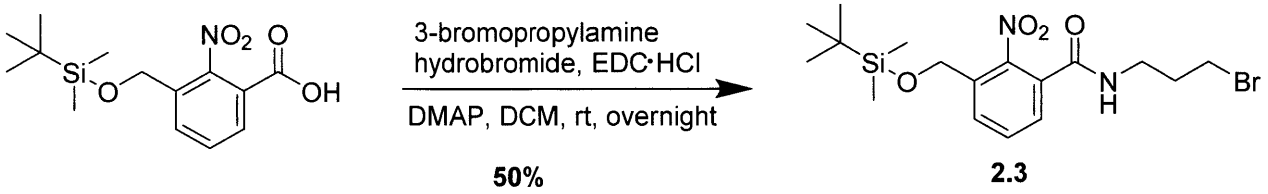

Compound 2.3: Compound 2.2 (1.18 g, 3.8 mmol, 1 eq), EDC·HCl (1.46 g, 7.6 mmol, 2 eq), and DMAP (0.093 g, 0.76 mmol, 0.2 eq) was dissolved in anhydrous DCM (100 mL), and stirred under N_2 for 10 min. 3-bromopropylamine hydrobromide (1.66 g, 7.6 mmol, 2 eq) and DIPEA (1 mL, 5.7 mmol, 1.5 eq) was added and the reaction was stirred at room temperature overnight. The reaction was washed with water twice (75 mL each) and brine once (75 mL). The organic layer was dried over magnesium sulfate, which was filtered out, and then the solution was concentrated by rotary evaporation. Purification by column chromatography (20% EtOAc/Hexanes to 100% EtOAc/Hexanes) yielded compound 2.3 (810 mg, 50% yield). ^{1}H-NMR, ^{13}C-NMR, and HRMS are as reported in literature.[45]

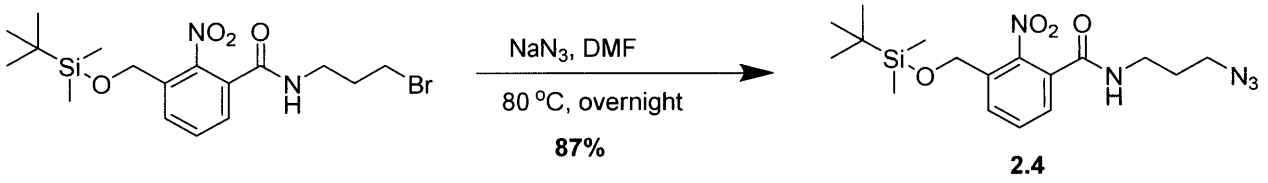

Compound 2.4: Compound 2.3 (300 mg, 0.70 mmol, 1 eq) and sodium azide (68 mg, 1.05 mmol, 1.5 eq) were dissolved in DMF (10 mL) and stirred at 80 °C overnight. The reaction mixture was diluted with ethyl acetate (50 mL) and washed with water twice (50 mL each) and brine once (50 mL), then the organic layer was dried over magnesium sulfate. After filtering out the salts and concentrating the organic layer, the product was purified by column chromatography (20% EtOAc/Hexanes to 70% EtOAc/Hexanes) to yield compound 2.4 (240 mg, 87% yield). ^{1}H-NMR, ^{13}C-NMR, and HRMS are as reported in literature.[45]

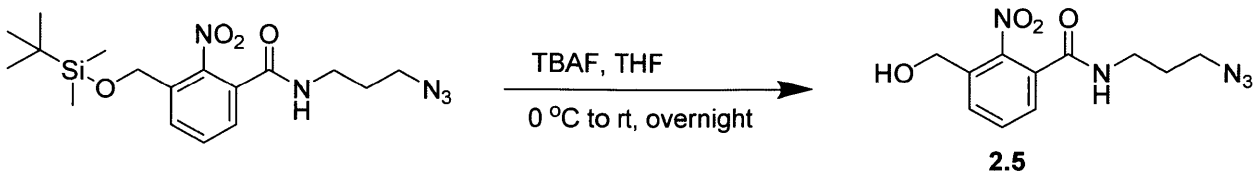

2.5

Compound 2.5: 1 M TBAF in THF (1.22 mL, 1.22 mmol, 2 eq) was added dropwise to a solution of compound 2.4 (240 mg, 0.61 mmol, 1 eq) in THF (10 mL) at 0 °C. The ice bath was removed and the reaction was stirred overnight at room temperature. The solution was diluted with ethyl acetate and washed with water twice (50 mL each) and brine once (50 mL), then the organic layer was dried over magnesium sulfate. After filtering out the salts and concentrating the organic layer, the product was purified by silica column chromatography (20% EtOAc/Hexanes to 100% EtOAc/Hexanes) to yield compound 2.5. ^{1}H-NMR, ^{13}C-NMR, and HRMS are as reported in literature.[45]

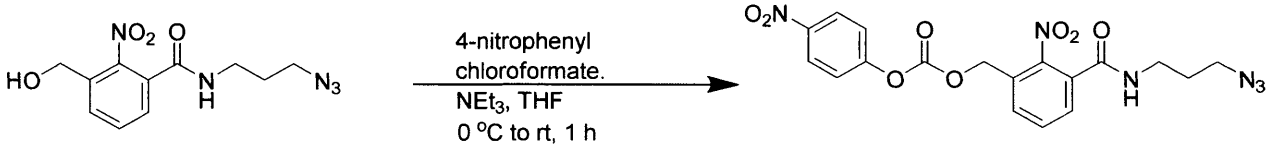

33% **2.6**

Compound 2.6: A solution of compound 2.5 (65 mg, 0.23 mmol, 1 eq) and triethylamine (0.0523 mL, 0.37 mmol, 1.6 eq) in anhydrous THF (2 mL) was added dropwise to a stirring solution of 4-nitrobenzyl chloroformate (75.6 mg, 0.37 mmol, 1.6 eq) in anhydrous THF (3 mL) at 0 °C in a dry flask under N_2. The ice bath was removed and the reaction was stirred for 1 h or until complete. The THF was removed by rotary evaporation and sample was redissolved in a small amount of dichloromethane, then loaded on a silica column. Purification by column chromatography (20% EtOAc/Hexanes to 60% EtOAc/Hexanes) yielded compound 2.6, which was dried in vacuo (34 mg, 33% yield). ^{1}H-NMR, ^{13}C-NMR, and HRMS are as reported in literature.[45]

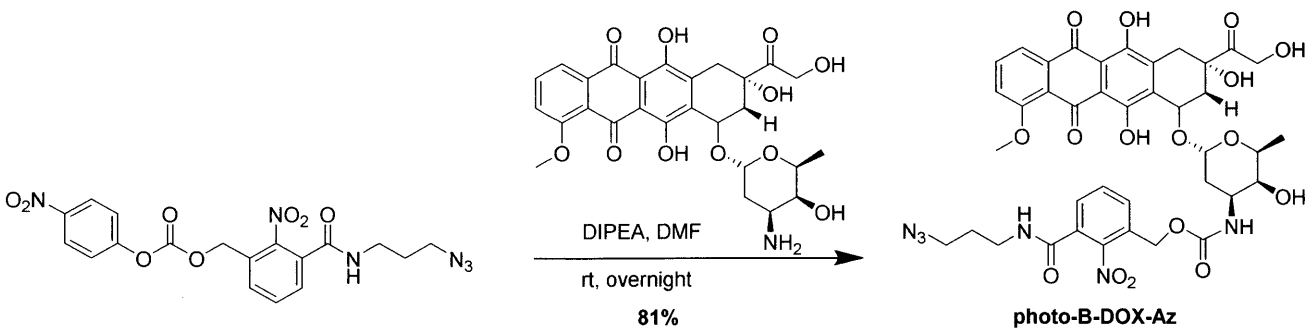

Photo-B-DOX-Az: Compound 2.6 (34 mg, 0.077 mmol,1 eq) was dissolved in anhydrous DMF (3 mL), followed by addition of doxorubicin hydrochloride (44 mg, 0.077 mmol, 1 eq) and DIPEA (0.013 mL, 0.077 mmol, 1 eq). The reaction was stirred overnight at room temperature, then diluted in ethyl acetate and washed with water twice (50 mL each) and brine once (50 mL), then the organic layer was dried over sodium sulfate. After filtering out the salts and concentrating the organic layer, the product was purified by column chromatography (0% MeOH/DCM to 5% MeOH/DCM) to yield photo-B-DOX-Az (53 mg, 81% yield) as red solid. ^{1}H-NMR, ^{13}C-NMR, and HRMS are as reported in literature.[45]

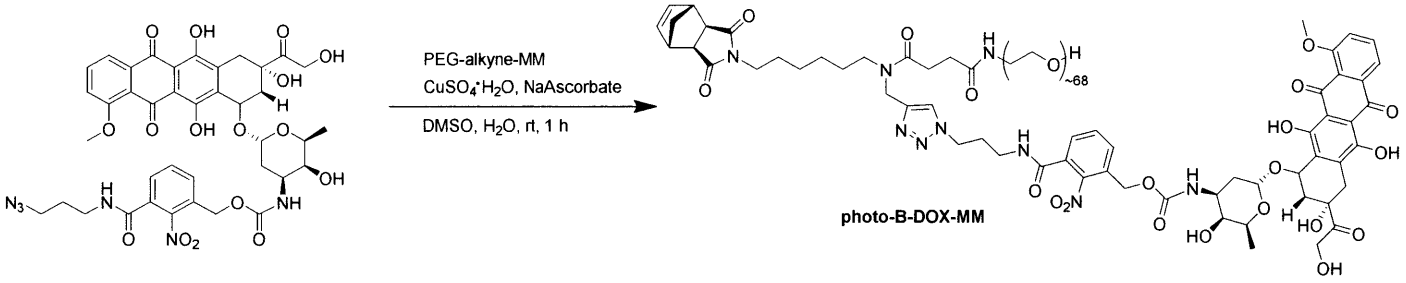

Photo-B-DOX-MM: PEG-alkyne-MM (335 mg, 0.01 mmol, 1 eq) and photo-B-DOX-Az (63.7 mg, 0.01 mmol, 1 eq) were dissolved in a 1:1 mixture of DMSO: H_2O (2 mL: 2mL), followed by addition of 1M solution of copper (I) sulfate pentahydrate in water (0.324 mL, 0.3 mmol, 3 eq) and spatula tip of sodium ascorbate. The reaction was allowed to proceed at room temperature for one hour or until done as monitored by LCMS. The compound was purified by HPLC (10% MeCN and 0.1% acetic acid in MilliQ deionized water to 100% MeCN). Once water was removed by rotary evaporation, photo-B-DOX-MM was redissolved in dichloromethane and dried over sodium sulfate. After concentration by rotary evaporation, photo-B-DOX-MM solid was washed with diethyl ether by centrifugation of solids in ether and decantation of ether. This

wash step was repeated three times to afford the photo-B-DOX-MM as a red powder. ^{1}H-NMR and MALDI-TOF are as reported in literature.[45]

Synthesis of photo-DOX-MM:

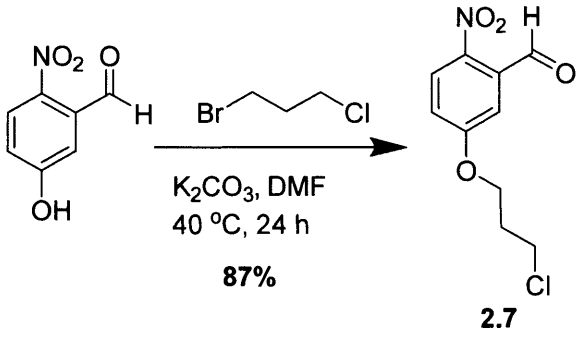

2.7

2-nitro-1-(3-chloropropoxy)benzyaldehyde, compound 2.7: 1-bromo-3-chloropropane (0.650 mL, 0.00658 moles) was added to a solution of p-hydroxybenzaldehyde (1.0g, 0.00598 moles) and potassium carbonate (1.66g, 0.0120 moles) in anhydrous dimethylformamide (6 mL). The solution was stirred at 40 °C for 24 h. The reaction was diluted with ethyl acetate (75 mL) and washed with saturated sodium bicarbonate solution (75 mL), water (75 mL), and brine (75 mL). The organic layer was dried with anhydrous magnesium sulfate, which was removed by filtration. The solution was concentrated and silica gel chromatography was performed using a gradient of 100% hexanes to 50% ethyl acetate in hexanes. The fractions containing product were collected, then solvent was removed by rotary evaporation, and dried overnight to yield 2-nitro-1-(3-chloropropoxy)benzaldehyde as a bright-green yellow solid (yield 87%*). ^{1}H NMR (400 MHz, Methylene Chloride-d_2) δ 10.42 (s, 1H), 8.15 (d, J = 9.1 Hz, 1H), 7.32 (d, J = 2.9 Hz, 1H), 7.18 (dd, J = 9.0, 2.9 Hz, 1H), 4.27 (t, J = 5.9 Hz, 2H), 3.76 (t, J = 6.3 Hz, 2H), 2.35 – 2.24 (m, 2H). ^{13}C-NMR (100 MHz, CD_2Cl_2) δ 189.05, 163.84, 135.04, 127.84, 119.16, 114.57, 66.28, 41.74, 32.35 HRMS: calcd. for $C_{10}H_{10}ClNO_4$ $[M+H]^+$, 244.0371; found, 244.0366.

*Observed extra peaks, but does not interfere with next step: ^{1}H NMR (400 MHz, Methylene Chloride-d_2) δ 4.27 (t, J = 5.9 Hz, 0.16), 3.62 (t, J = 6.4 Hz, 0.15H), 2.39-2.36 (m, 0.14H).

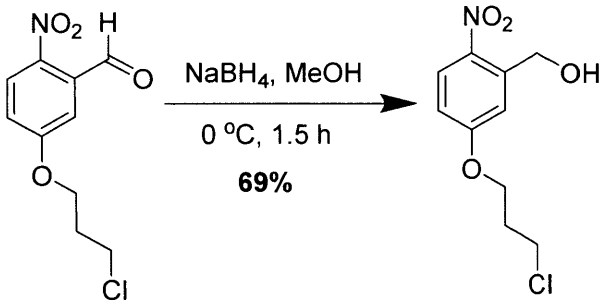

2.8

2-nitro-1-(3-chloropropoxy)benzyl alcohol, compound 2.8: Sodium borohydride (133 mg, 0.00351 moles) was added to 2-nitro-1-(3-chloropropoxy)benzyaldehyde (570 mg, 0.00234 moles) in anhydrous methanol (12 mL) at 0 °C under nitrogen. The reaction was stirred for 1.5 h, then concentrated with a rotary evaporator. The mixture was diluted with ethyl acetate (75 mL), and washed with 30 mL each of saturated sodium bicarbonate solution, water, and brine. The organic layer was dried with anhydrous magnesium sulfate, which was removed by filtration. The solution was concentrated and silica gel chromatography was performed using a gradient of 100% hexanes to 60% ethyl acetate in hexanes. The fractions containing product were collected, then solvent was removed by rotary evaporation, and dried overnight to yield 2-nitro-1-(3-chloropropoxy)benzyl alcohol as a pale yellow solid (yield 69%*). ^{1}H NMR (400 MHz, Methylene Chloride-d_2) δ 8.16 (d, J = 9.1 Hz, 1H), 7.27 (d, J = 2.7 Hz, 1H), 6.92 (dd, J = 9.1, 2.8 Hz, 1H), 4.98 (s, 2H), 4.24 (t, J = 5.9 Hz, 2H), 3.77 (t, J = 6.3 Hz, 2H), 2.28 (p**, J = 6.1 Hz, 2H). ^{13}C-NMR (100 MHz, CD_2Cl_2) δ 163.99, 141.21, 128.42, 114.95, 113.90, 65.80, 63.24, 41.91, 32.52 HRMS: calcd. for $C_{10}H_{12}ClNO_4$ $[M+H]^+$, 246.0528; found, 246.0529.

*Observed extra peaks, but does not interfere with next step: ^{1}H NMR (400 MHz, Methylene Chloride-d_2) δ 3.63 (t, J = 6.3 Hz, 0.14H), 2.39-2.31 (m, 0.24H).

** pseudo pentet

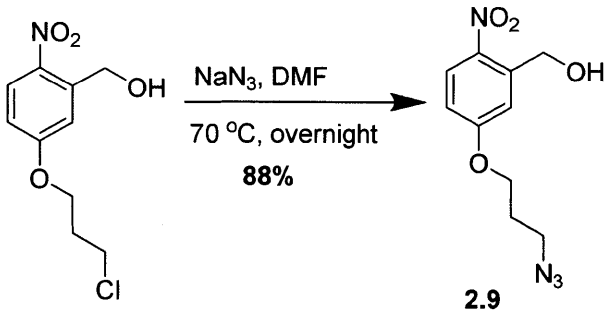

2.9

2-nitro-1-(3-azidopropoxy)benzyl alcohol, compound 2.9: DMF (7.5 mL) was added to 2-nitro-1-(3-chloropropoxy)benzyl alcohol (635 mg, 0.00258 moles) and sodium azide (252 mg, 0.00387 moles) in a flask, which was heated to 70 °C and stirred overnight. The reaction was diluted in ethyl acetate (100 mL), and washed twice with water (75 mL each) and once with brine (75 mL). The organic layer was dried with anhydrous magnesium sulfate, which was filtered out. The solution was concentrated on a rotary evaporator and dried on vacuum overnight to yield 2-nitro-1-(3-azidopropoxy)benzyl alcohol as a yellow solid (yield 88%). ^{1}H NMR (400 MHz, Methylene Chloride-d_2) δ 8.16 (d, J = 9.1 Hz, 1H), 7.27 (d, J = 2.8 Hz, 1H), 6.91 (dd, J = 9.1, 2.8 Hz, 1H), 4.98 (s, 2H), 4.18 (t, J = 6.0 Hz, 2H), 3.53 (t, J = 6.6 Hz, 2H), 2.12-2.06 (m, 2H). ^{13}C-NMR (100 MHz, CD_2Cl_2) δ 163.99, 141.22, 128.43, 114.97, 113.93, 66.15, 63.26, 48.68, 29.13 HRMS: calcd. for $C_{10}H_{12}N_4O_4$ $[M+H]^+$, 253.0931; found, 253.0939.

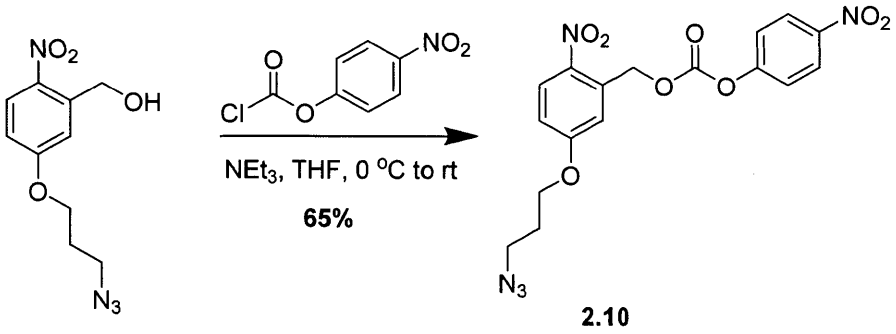

2.10

Compound 2.10: A solution of 2-nitro-1-(3-azidopropoxy)benzyl alcohol (250 mg, 0.00099 moles) and triethylamine (0.21 mL, 0.0015 moles) in tetrahydrofuran (5 mL) was added dropwise to a flask of 4-nitrophenyl chloroformate (423mg, 0.0021 moles) in tetrahydrofuran (15 mL) at 0 °C under nitrogen. The ice-bath was removed and the reaction was left to stir for 1 h. The mixture was concentrated on a rotary evaporator and purified by silica gel chromatography from 100% hexanes to 100% ethyl acetate. The fractions containing product was concentrated on a rotary evaporator and dried on vacuum overnight to yield compound 2.10 as a yellow solid

(yield 65%*). ^{1}H NMR (400 MHz, Methylene Chloride-d_2) δ 8.31 – 8.25 (m, 2H), 8.23 (d, J = 9.2 Hz, 1H), 7.49 – 7.40 (m, 2H), 7.20 (d, J = 2.7 Hz, 1H), 6.99 (dd, J = 9.2, 2.8 Hz, 1H), 5.72 (s, 2H), 4.19 (t, J = 6.0 Hz, 2H), 3.55 (t, J = 6.5 Hz, 2H), 2.16 – 2.05 (m, 2H). ^{13}C-NMR (100 MHz, CD_2Cl_2) δ 163.88, 156.02, 152.65, 146.13, 140.66, 134.37,128.73, 126.5, 125.81, 122.35, 116.1 , 115.11, 114.15, 68.12, 66.33, 48.58, 29.02 HRMS: calcd. for $C_{17}H_{15}N_5O_8$ $[M+NH_4]^+$, 435.1259; found, 435.1251. *May observe 4-nitrophenol, but does not interfere with next step: ^{1}H NMR (400 MHz, Methylene Chloride-d_2) δ 8.12-8.08 (m), 6.92-6.88 (m).

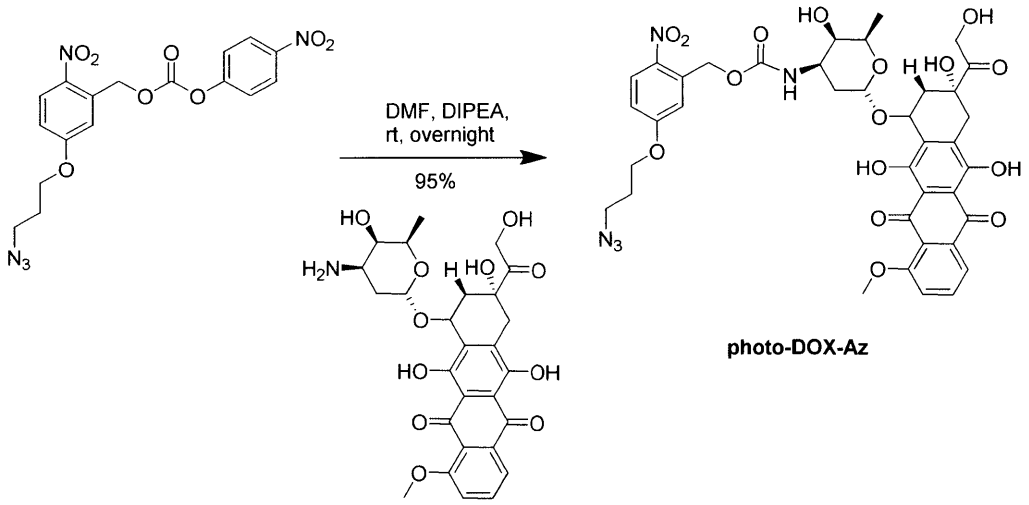

Photo-DOX-Az: Doxorubicin hydrochloride (70.6 mg, 0.000122 moles) was dissolved DMF (1.5mL), followed by addition of diisopropylethylamine (0.021 mL, 0.000122 moles) and 4 (48 mg, 0.000116 moles). The solution was stirred at room temperature overnight, then diluted in ethyl acetate (75 mL), washed twice with water (50 mL each) and brine (50 mL). The organic layer was dried with anhydrous magnesium sulfate, which was removed by filtration. The solution was concentrated and silica gel chromatography was performed using a gradient of 100% dichloromethane to 10% methanol in dichloromethane. The fractions containing product were collected, then solvent was removed by rotary evaporation, and dried overnight to yield photo-DOX-Az as a red solid (yield 92%*). ^{1}H NMR (400 MHz, Methylene Chloride-d_2) δ 13.94 (s, 1H), 13.10 (s, 1H), 8.09 (d, J = 9.1 Hz, 1H), 7.91 (dd, J = 7.7, 1.1 Hz, 2H), 7.74 (t, J = 8.1 Hz, 1H), 7.35 (dd, J = 8.5, 1.1 Hz, 1H), 7.03 – 6.97 (m, 1H), 6.86 – 6.81 (m, 1H), 5.54 (d, J = 8.6 Hz, 1H), 5.51-5.47 (m, 1H), 5.40 (dd, 24.6, 15.7, 1H), 5.24-5.19 (m, 1H), 4.74 (s, 2H), 4.60 (s, 1H), 4.19-4.11 (m, 1H), 4.09 (t, J = 6.0 Hz, 2H) 3.99 (s, 3H), 3.89-3.82 (m, 1H), 3.68 (s, 1H), 3.48 (t, J = 6.5 Hz, 2H), 3.22 – 3.12 (m, 1H), 2.94-2.87(m, 1H), 2.50 (s, 1H), 2.34 (d, J = 14.7 Hz, 1H),

2.13 (dd, J = 14.6, 4.1 Hz, 1H), 2.02 (p**, J = 6.3 Hz, 2H), 1.91-1.80 (m, 2H), 1.29 (d, J = 6.5 Hz, 3H). ^{13}C-NMR (100 MHz, CD_2Cl_2) δ 214.52, 187.20, 163.64, 161.60, 156.56, 155.90, 155.49, 140.54, 136.24, 135.77, 134.17, 133.96, 128.32, 120.00, 119.21, 114.20, 113.48, 112.02, 111.87, 101.11, 77.18, 69.96, 67.96, 66.08, 66.03, 63.99, 57.03, 48.57, 47.48, 36.09, 34.40, 30.61, 28.97, 17.15 HRMS: calcd. for $C_{38}H_{39}N_5O_{16}$ $[M+Na]^+$, 844.2284; found, 844.2271. *Observed DMF, but does not interfere with the next step: ^{1}H NMR (400 MHz, Methylene Chloride-d_2) δ 7.96 (s), 2.91 (s), 2.82 (s); ^{13}C-NMR (100 MHz, CD_2Cl_2) δ 162.89, 36.79, 31.61. **pseudo-pentet

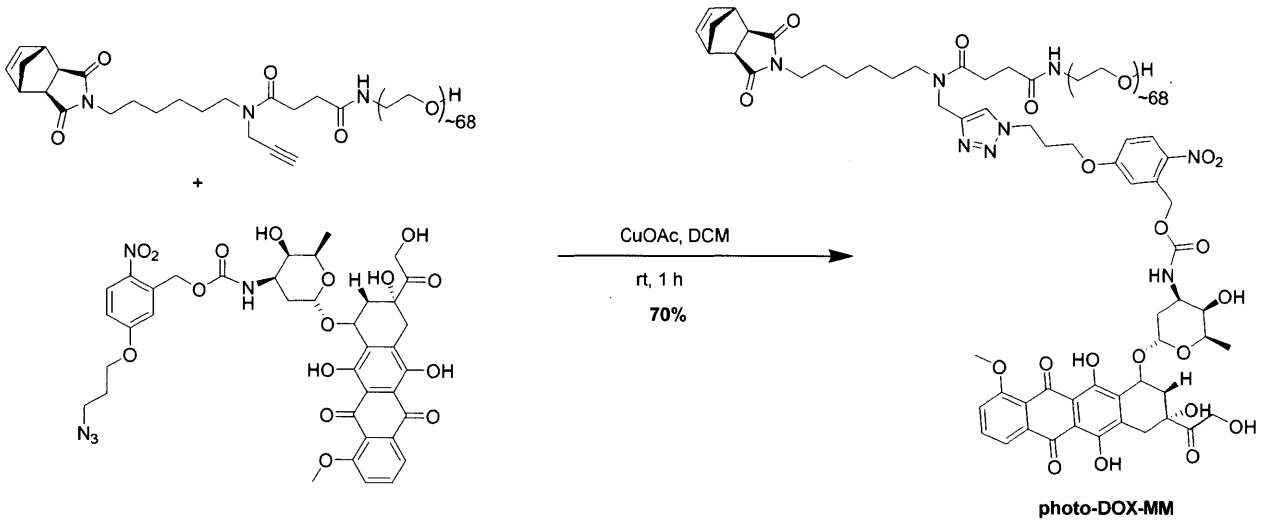

Photo-DOX-MM: A 20-mL scintillation vial was charged with Photo-DOX-Az (49 mg, 0.060 mmol, 1 eq) , PEG-Alkyne-MM (300 mg, 0.060 mmol, 1eq), and a stirbar, then brought into the glovebox. The reagents were dissolved in dichloromethane (3 mL), followed by addition of a pinch of copper (I) acetate, and allowed to stir outside the glovebox until complete consumption of PEG-alkyne-MM by LCMS (1 hour). Photo-DOX-MM was purified by HPLC (10% MeCN and 0.1% acetic acid in MilliQ deionized water to 100% MeCN) twice to remove all the unreacted photo-DOX-Az. Once water was removed by rotary evaporation, photo-DOX-MM was redissolved in dichloromethane and dried over sodium sulfate. After concentration by rotary evaporation, photo-DOX-MM solid was washed with diethyl ether by centrifugation of solids in ether and decantation of ether. This wash step was repeated three times to afford photo-DOX-MM (174 mg, 70% yield) as a red powder. ^{1}H-NMR and MALDI are provided in **Figure S2.11** and figure **Figure S2.12**, respectively.

Synthesis of ester-DOX-MM:

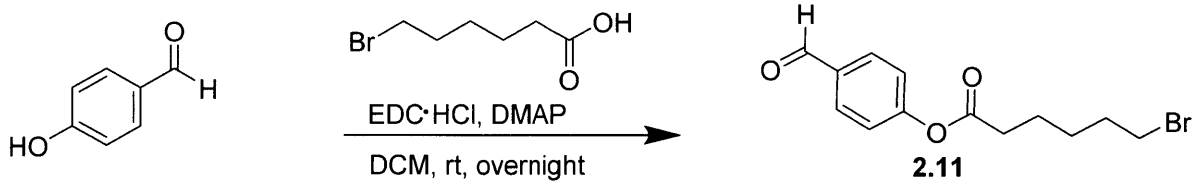

2.11

4-formylphenyl 6-bromohexanoate, compound 2.11: 1-bromohexanoic acid (2.4 g, 0.012 mol, 1.5 eq), EDC·HCl (2.4g , 0.012 mol, 1.5 eq), and DMAP (0.20 g, 0.0016 mol, 0.2 eq) were dissolved in dichloromethane (120 mL) in a dry 500-mL flask equipped with a stirbar. After stirring for 30 min, 4-hydroxybenzoic acid (1 g, 0.0082 mol, 1 eq) was added and the reaction stirred at room temperature overnight. The reaction was washed with 100 mL of water twice and brine once, then dried over magnesium sulfate. After concentration by rotary evaporation, the organic layer was loaded onto a silica cartridge and purified by flash chromatography (0% EtOAc/Hexanes to 50% EtOAc/Hexanes) to afford 4-formylphenyl 6-bromohexanoate (2.5 g crude yield). ^{1}H-NMR, ^{13}C-NMR, and HRMS are as reported in literature.[42]

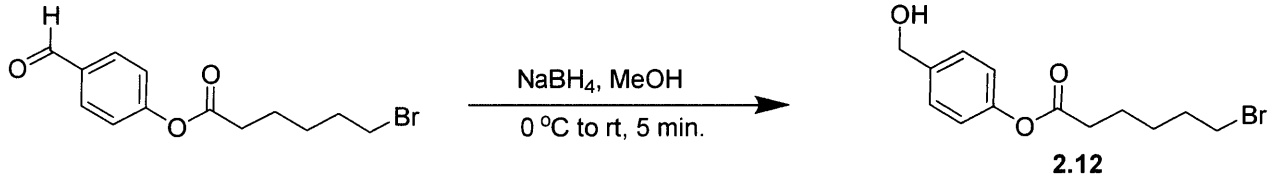

2.12

4-(hydroxymethyl)phenyl 6-bromohexanoate, compound 2.12: Sodium borohydride (0.45 g, 0.012 mol, 1.5 eq) was added to 4-formylphenyl 6-bromohexanoate (2.5 g crude, ~1 eq) dissolved in methanol (60 mL) in a dry 250 mL flask at 0 °C, and stirred for 5 min at room temperature. The reaction was quenched with slow addition of water (100 mL), and product was extracted with 100 mL of dichloromethane three times, then dried over sodium sulfate. After concentration by rotary evaporation, the organic layer was loaded onto a silica cartridge and purified by flash chromatography (0% EtOAc/Hexanes to 60% EtOAc/Hexanes) to afford 4-(hydroxymethyl)phenyl 6-bromohexnoate (1.2 g crude yield) .^{1}H-NMR, ^{13}C-NMR, and HRMS are as reported in literature.[42]

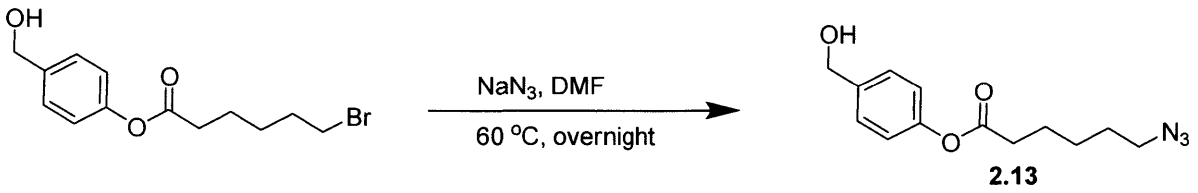

2.13

4-(hydroxymethyl)phenyl 6-azidohexanoate, compound 2.13: In a 100 mL round bottom flask equipped with a stirbar, sodium azide (155 mg, 2.4 mmol, 1.5 eq) was added to solution of 4-(hydroxymethyl)phenyl 6-bromohexanoate (500 mg, 1.6 mmol, 1 eq) in DMF (20 mL), then stirred overnight at 60 °C. The reaction was diluted in ethyl acetate (100mL) and washed twice with water (75 mL each), once with brine (75 mL), then dried over magnesium sulfate. After concentration by rotary evaporation, the organic layer was loaded onto a silica cartridge and purified by flash chromatography (0% EtOAc/Hexanes to 70% EtOAc/Hexanes) to afford 4-(hydroxymethyl)phenyl 6-azidohexanoate. ^{1}H-NMR, ^{13}C-NMR, and HRMS are as reported in literature.[42]

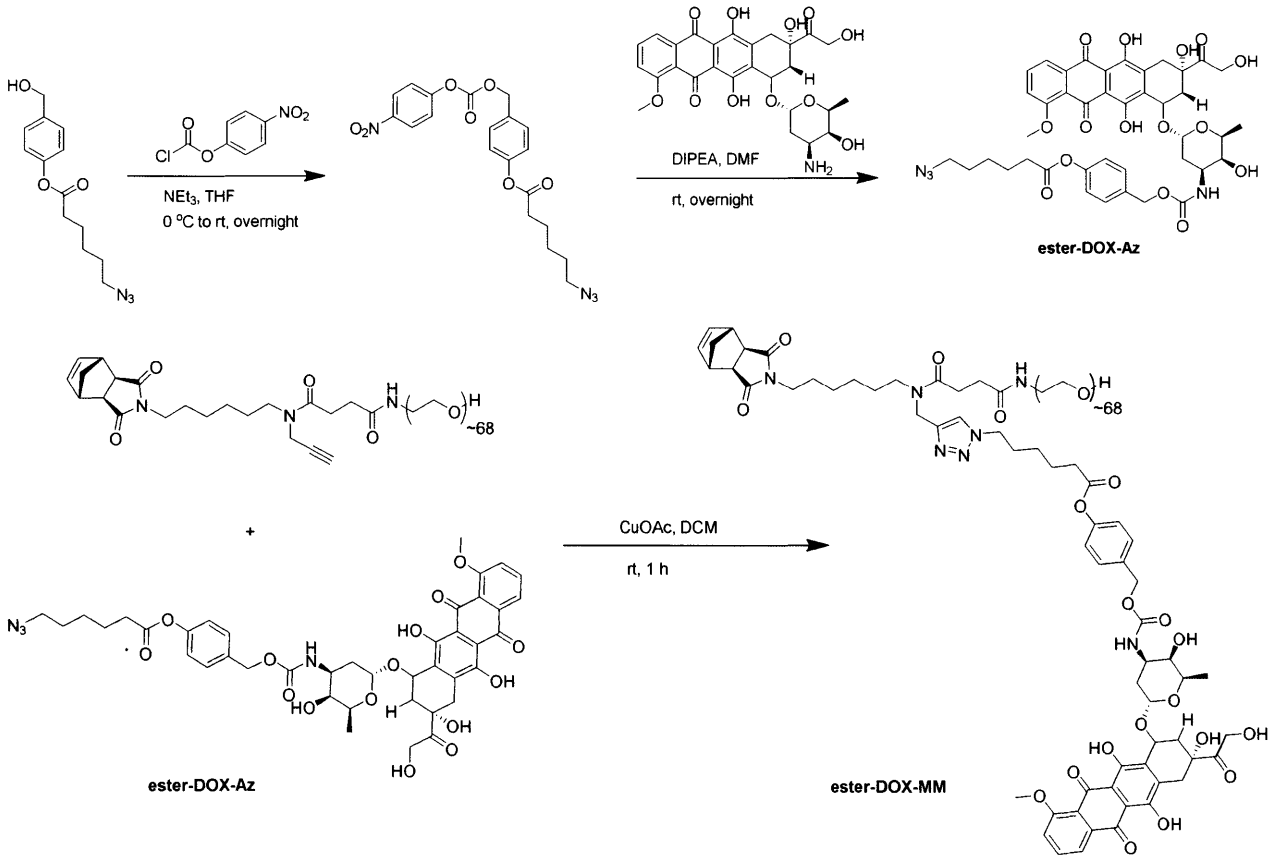

Ester-DOX-Az and Ester-DOX-MM: Synthesized from 4-(hydroxymethyl)phenyl 6-azidohexanoate by A. X. Gao as reported in literature.[42]

2.5 References

1 Weinberg, R. *The biology of cancer*. (Garland science, 2013).

2 Cho, K., Wang, X., Nie, S. & Shin, D. M. Therapeutic nanoparticles for drug delivery in cancer. *Clinical Cancer Research* **14**, 1310-1316 (2008).

3 Peer, D. *et al.* Nanocarriers as an emerging platform for cancer therapy. *Nature Nanotechnology* **2**, 751-760 (2007).

4 Whitesides, G. M. Nanoscience, nanotechnology, and chemistry. *Small* **1**, 172-179 (2005).

5 Venditto, V. J. & Szoka, F. C. Cancer nanomedicines: so many papers and so few drugs! *Advanced Drug Delivery Reviews* **65**, 80-88 (2013).

6 Duncan, R. & Vicent, M. J. Polymer therapeutics-prospects for 21st century: the end of the beginning. *Advanced Drug Delivery Reviews* **65**, 60-70 (2013).

7 Duncan, R. The dawning era of polymer therapeutics. *Nature Reviews Drug Discovery* **2**, 347-360 (2003).

8 Wang, A. Z., Langer, R. & Farokhzad, O. C. Nanoparticle delivery of cancer drugs. *Annual Review of Medicine* **63**, 185-198 (2012).

9 DiGiulio, S. FDA approves Onivyde combo regimen for advanced pancreatic cancer. *Oncology Times* (2015).

10 Rodriguez, M. *et al.* Vincristine sulfate liposomes injection (Marqibo) in heavily pretreated patients with refractory aggressive non-Hodgkin lymphoma. *Cancer* **115**, 3475-3482 (2009).

11 Matsumura, Y. & Maeda, H. A new concept for macromolecular therapeutics in cancer chemotherapy: mechanism of tumoritropic accumulation of proteins and the antitumor agent smancs. *Cancer Research* **46**, 6387-6392 (1986).

12 Perrault, S. D., Walkey, C., Jennings, T., Fischer, H. C. & Chan, W. C. Mediating tumor targeting efficiency of nanoparticles through design. *Nano Letters* **9**, 1909-1915 (2009).

13 Kwon, I. K., Lee, S. C., Han, B. & Park, K. Analysis on the current status of targeted drug delivery to tumors. *Journal of Controlled Release* **164**, 108-114 (2012).

14 Harrington, K. J. *et al.* Effective targeting of solid tumors in patients with locally advanced cancers by radiolabeled pegylated liposomes. *Clinical Cancer Research* **7**, 243-254 (2001).

15 Park, K. Facing the truth about nanotechnology in drug delivery. *ACS Nano* **7**, 7442-7447 (2013).

16 Gabizon, A. *et al.* Prolonged circulation time and enhanced accumulation in malignant exudates of doxorubicin encapsulated in polyethylene-glycol coated liposomes. *Cancer Research* **54**, 987-992 (1994).

17 Solomon, R. & Gabizon, A. A. Clinical pharmacology of liposomal anthracyclines: focus on pegylated liposomal doxorubicin. *Clinical Lymphoma and Myeloma* **8**, 21-32 (2008).

18 Barenholz, Y. C. Doxil®—the first FDA-approved nano-drug: lessons learned. *Journal of Controlled Release* **160**, 117-134 (2012).

19 Anselmo, A. C. & Mitragotri, S. Nanoparticles in the clinic. *Bioengineering & Translational Medicine* **1**, 10-29 (2016).

20 Sievers, E. L. & Senter, P. D. Antibody-drug conjugates in cancer therapy. *Annual Review of Medicine* **64**, 15-29 (2013).

21 Zolot, R. S., Basu, S. & Million, R. P. Antibody–drug conjugates. *Nature Reviews Drug Discovery* **12**, 259-260 (2013).

22 Schrama, D., Reisfeld, R. A. & Becker, J. C. Antibody targeted drugs as cancer therapeutics. *Nature Reviews Drug Discovery* **5**, 147-159 (2006).

23 Prasad, V. Perspective: The precision-oncology illusion. *Nature* **537**, S63-S63 (2016).

24 Couvreur, P. Nanoparticles in drug delivery: past, present and future. *Advanced Drug Delivery Reviews* **65**, 21-23 (2013).

25 Juliano, R. Nanomedicine: is the wave cresting? *Nature Reviews Drug Discovery* **12**, 171-172 (2013).

26 Ledford, H. Bankruptcy of nanomedicine firm worries drug developers. *Nature* **533**, 304-305 (2016).

27 Allen, C. Why I'm holding onto hope for nano in oncology. *Molecular Pharmaceutics* **13**, 2603-2604 (2016).

28 Danhier, F., Feron, O. & Préat, V. To exploit the tumor microenvironment: passive and active tumor targeting of nanocarriers for anti-cancer drug delivery. *Journal of Controlled Release* **148**, 135-146 (2010).

29 Albanese, A., Tang, P. S. & Chan, W. C. The effect of nanoparticle size, shape, and surface chemistry on biological systems. *Annual Review of Biomedical Engineering* **14**, 1-16 (2012).

30 Liao, L. *et al.* A convergent synthetic platform for single-nanoparticle combination cancer therapy: ratiometric loading and controlled release of cisplatin, doxorubicin, and camptothecin. *Journal of the American Chemical Society* **136**, 5896-5899 (2014).

31 Rajendran, L., Knölker, H.-J. & Simons, K. Subcellular targeting strategies for drug design and delivery. *Nature Reviews Drug Discovery* **9**, 29-42 (2010).

32 Varkouhi, A. K., Scholte, M., Storm, G. & Haisma, H. J. Endosomal escape pathways for delivery of biologicals. *Journal of Controlled Release* **151**, 220-228 (2011).

33 Sakhrani, N. M. & Padh, H. Organelle targeting: third level of drug targeting. *Drug Design, Development and Therapy* **7**, 585-599 (2013).

34 Bao, G., Mitragotri, S. & Tong, S. Multifunctional nanoparticles for drug delivery and molecular imaging. *Annual Review of Biomedical Engineering* **15**, 253-282 (2013).

35 Svenson, S. & Prud'homme, R. K. *Multifunctional nanoparticles for drug delivery applications: imaging, targeting, and delivery*. (Springer Science & Business Media, 2012).

36 Torchilin, V. *Multifunctional pharmaceutical nanocarriers*. Vol. 4 (Springer Science & Business Media, 2008).

37 Bielawski, C. W. & Grubbs, R. H. Living ring-opening metathesis polymerization. *Progress in Polymer Science* **32**, 1-29 (2007).

38 Grubbs, R. H. & O'Leary, D. J. *Handbook of metathesis, volume 2: applications in organic synthesis*. (John Wiley & Sons, 2015).

39 Liu, J. *et al.* "Brush-first" method for the parallel synthesis of photocleavable, nitroxide-labeled poly(ethylene glycol) star polymers. *Journal of the American Chemical Society* **134**, 16337-16344 (2012).

40 Liu, J., Gao, A. X. & Johnson, J. A. Particles without a box: brush-first synthesis of photodegradable PEG star polymers under ambient conditions. *Journal of Visualized Experiments* **80** (2013).

41 Love, J. A., Morgan, J. P., Trnka, T. M. & Grubbs, R. H. A practical and highly active ruthenium-based catalyst that effects the cross metathesis of acrylonitrile. *Angewandte Chemie International Edition* **41**, 4035-4037 (2002).

42 Gao, A. X., Liao, L. & Johnson, J. A. Synthesis of acid-labile PEG and PEG-doxorubicin-conjugate nanoparticles via brush-first ROMP. *ACS Macro Letters* **3**, 854-857 (2014).

43 Barnes, J. C. et al. Using an RNAi signature assay to guide the design of three-drug-conjugated nanoparticles with validated mechanisms, *in vivo* efficacy, and low toxicity. *Journal of the American Chemical Society* **138**, 12494-12501 (2016).

44 Nel, A. E. *et al.* Understanding biophysicochemical interactions at the nano–bio interface. *Nature Materials* **8**, 543-557 (2009).

45 Johnson, J. A. *et al.* Drug-loaded, bivalent-bottle-brush polymers by graft-through ROMP. *Macromolecules* **43**, 10326-10335 (2010).

46 Zhao, H., Sterner, E. S., Coughlin, E. B. & Theato, P. o-Nitrobenzyl alcohol derivatives: opportunities in polymer and materials science. *Macromolecules* **45**, 1723-1736 (2012).

47 Gumbley, P., Koylu, D. & Thomas III, S. W. Photoresponsive polymers containing nitrobenzyl esters via ring-opening metathesis polymerization. *Macromolecules* **44**, 7956-7961 (2011).

48 Greenwald, R. B. *et al.* Drug delivery systems employing 1,4-or 1,6-elimination: poly(ethylene glycol) prodrugs of amine-containing compounds. *Journal of Medicinal Chemistry* **42**, 3657-3667 (1999).

49 Mindell, J. A. Lysosomal acidification mechanisms. *Annual Review of Physiology* **74**, 69-86 (2012).

2.6 Supplemental Figures and Spectra

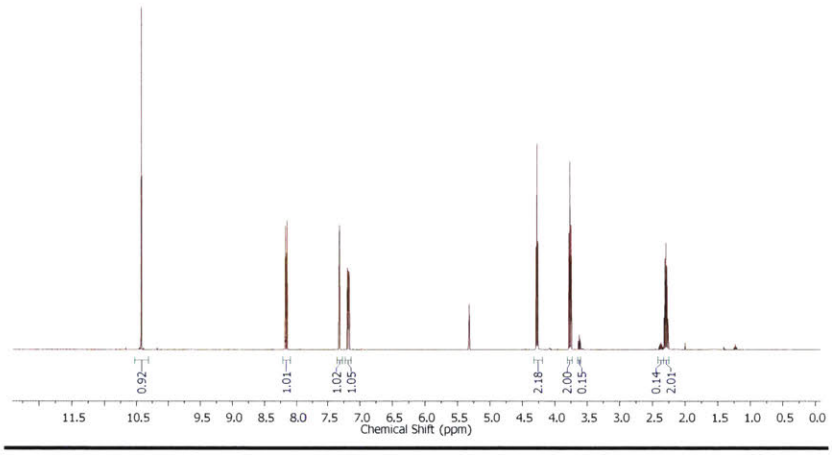

Figure S2.1. ^{1}H-NMR spectrum of **2-nitro-1-(3-chloropropoxy)benzyaldehyde 2.7** in CD_2Cl_2.

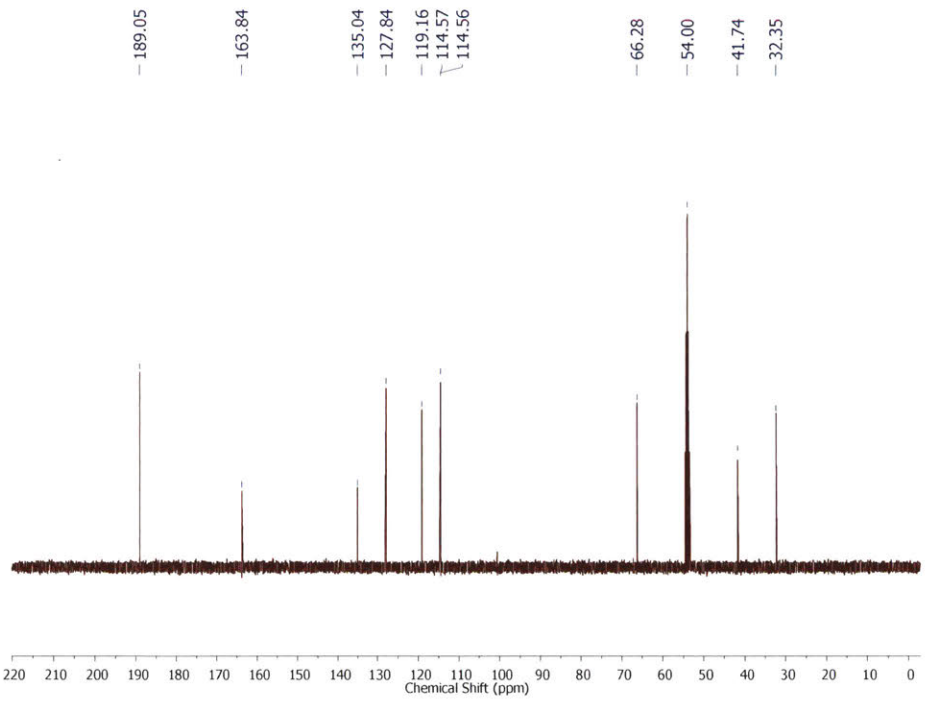

Figure S2.2. ^{13}C-NMR spectrum of **2-nitro-1-(3-chloropropoxy)benzyaldehyde 2.7** in CD_2Cl_2.

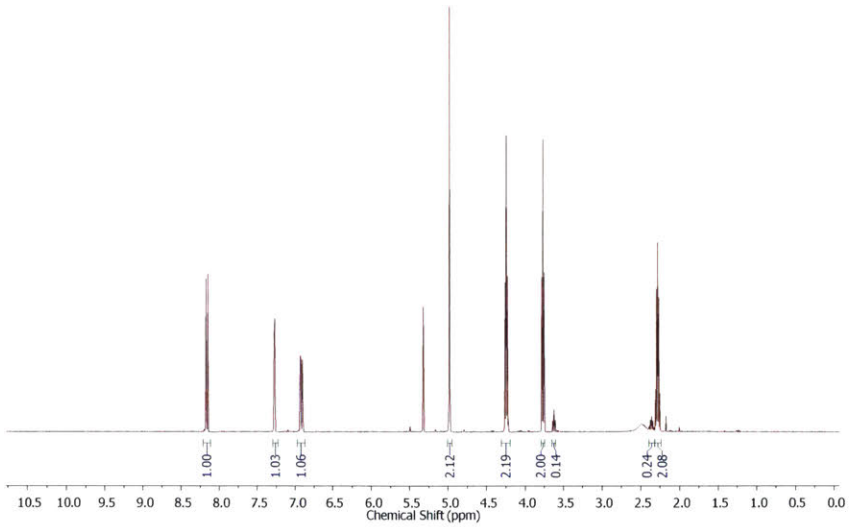

Figure S2.3. ^{1}H-NMR spectrum of **2-nitro-1-(3-chloropropoxy)benzyl alcohol 2.8** in CD_2Cl_2.

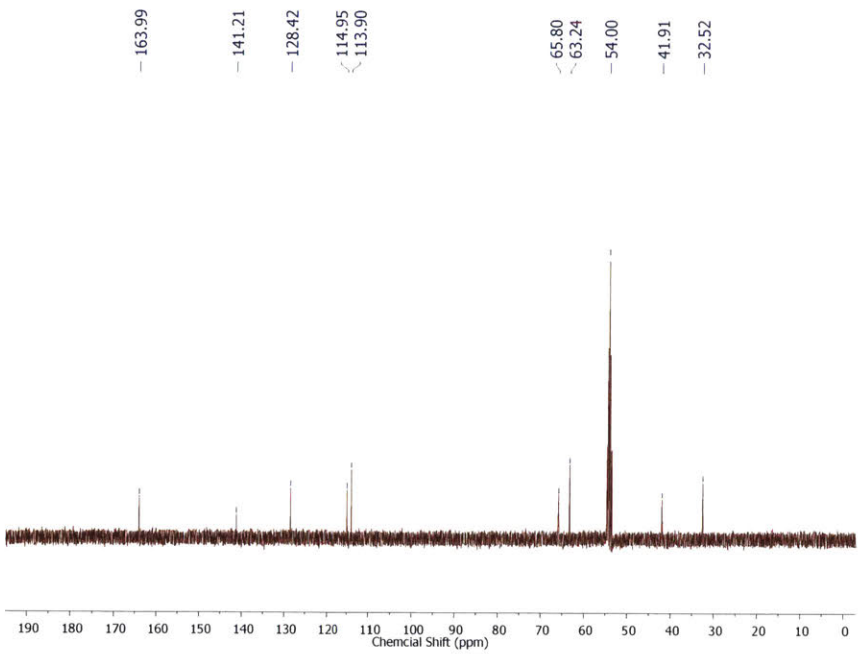

Figure S2.4. ^{13}C NMR spectrum of **2-nitro-1-(3-chloropropoxy)benzyl alcohol 2.8** in CD_2Cl_2

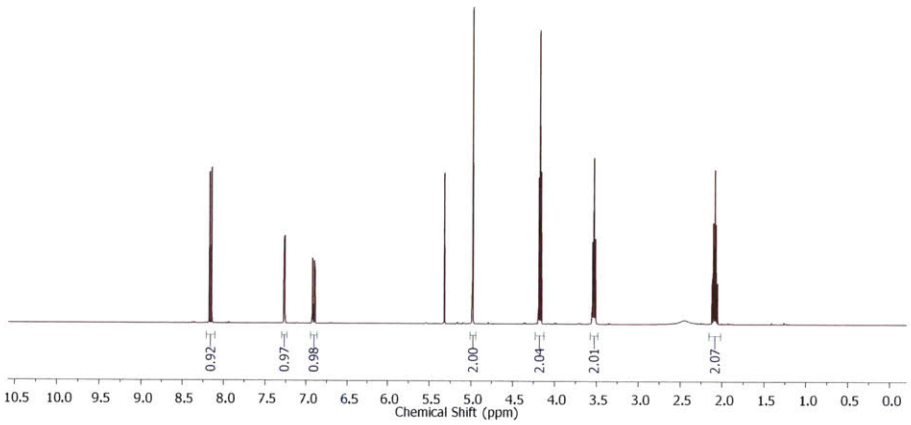

Figure S2.5. ^{1}H-NMR spectrum of **2-nitro-1-(3-azidopropoxy)benzyl alcohol 2.9** in CD_2Cl_2.

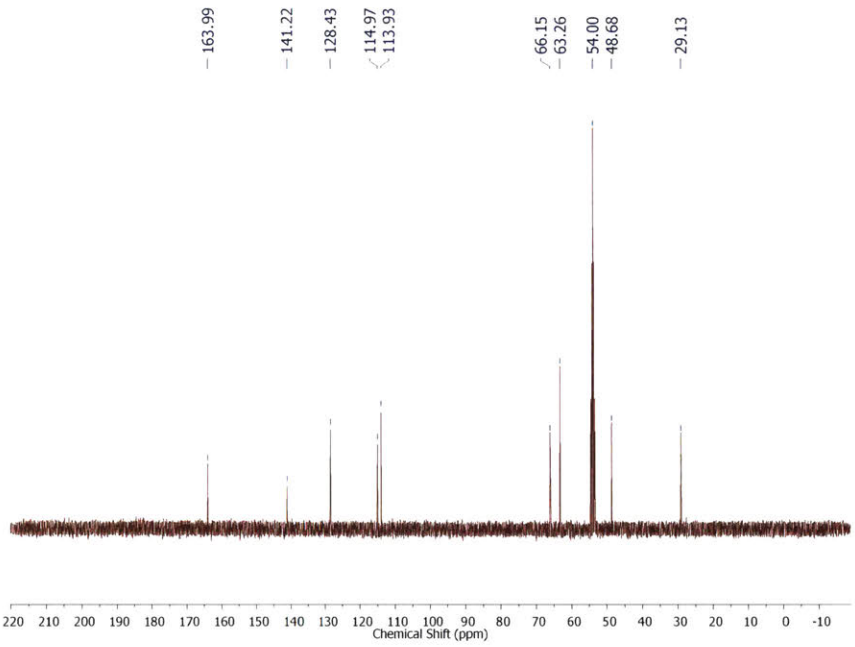

Figure S2.6. ^{13}C-NMR spectrum of **2-nitro-1-(3-azidopropoxy)benzyl alcohol 2.9** in CD_2Cl_2.

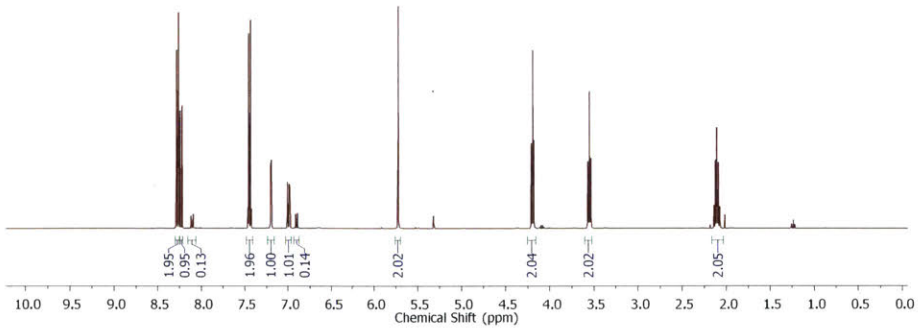

Figure S2.7. ^{1}H-NMR spectrum of **compound 2.10** in CD_2Cl_2.

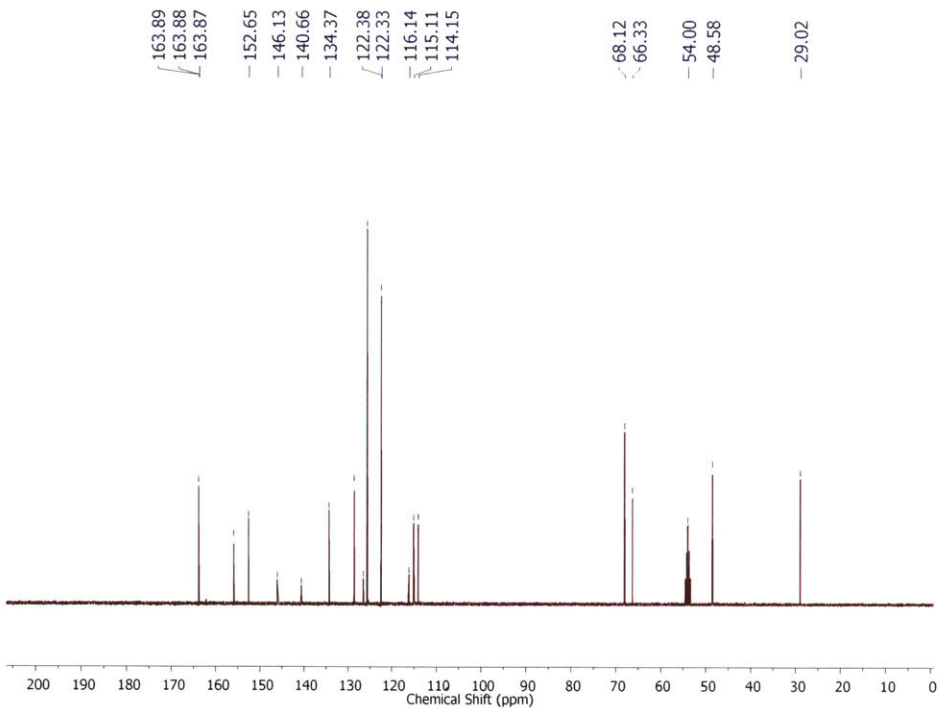

Figure S2.8. ^{13}C NMR spectrum of **compound 2.10** in CD_2Cl_2.

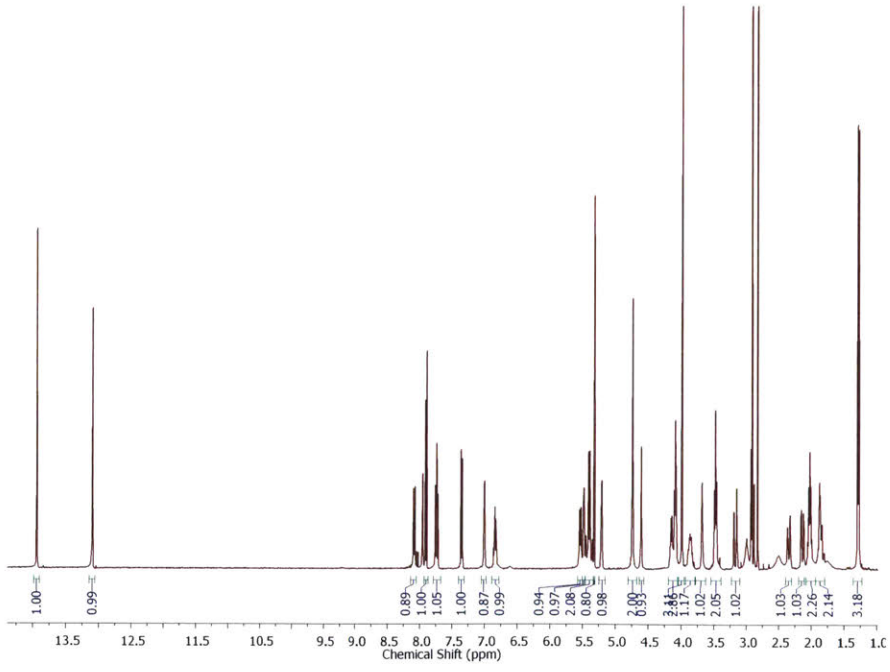

Figure S2.9. ^{1}H-NMR spectrum of photo-**DOX-Az** in CD_2Cl_2.

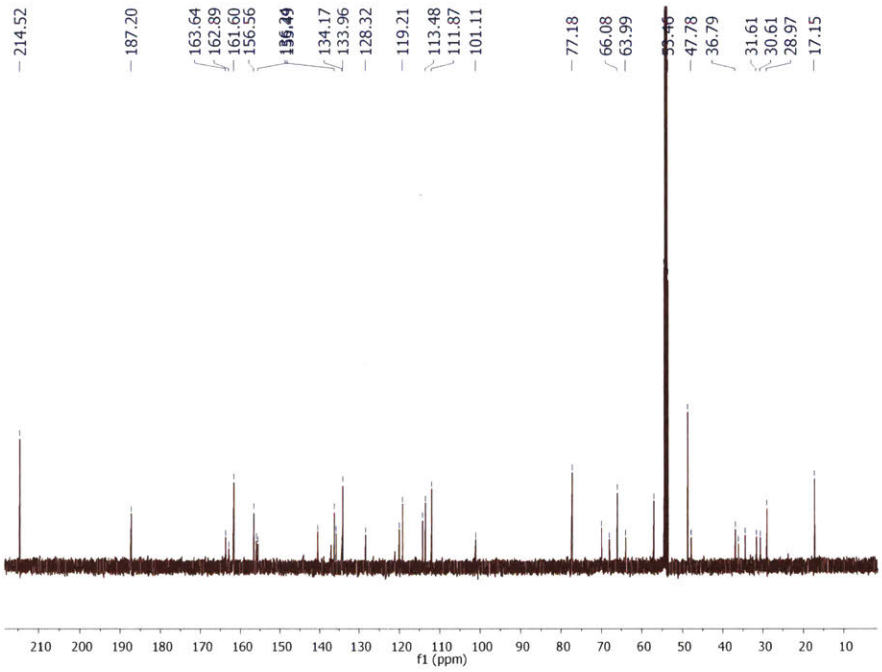

Figure S2.10. ^{13}C-NMR spectrum of photo-**DOX-Az** in CD_2Cl_2.

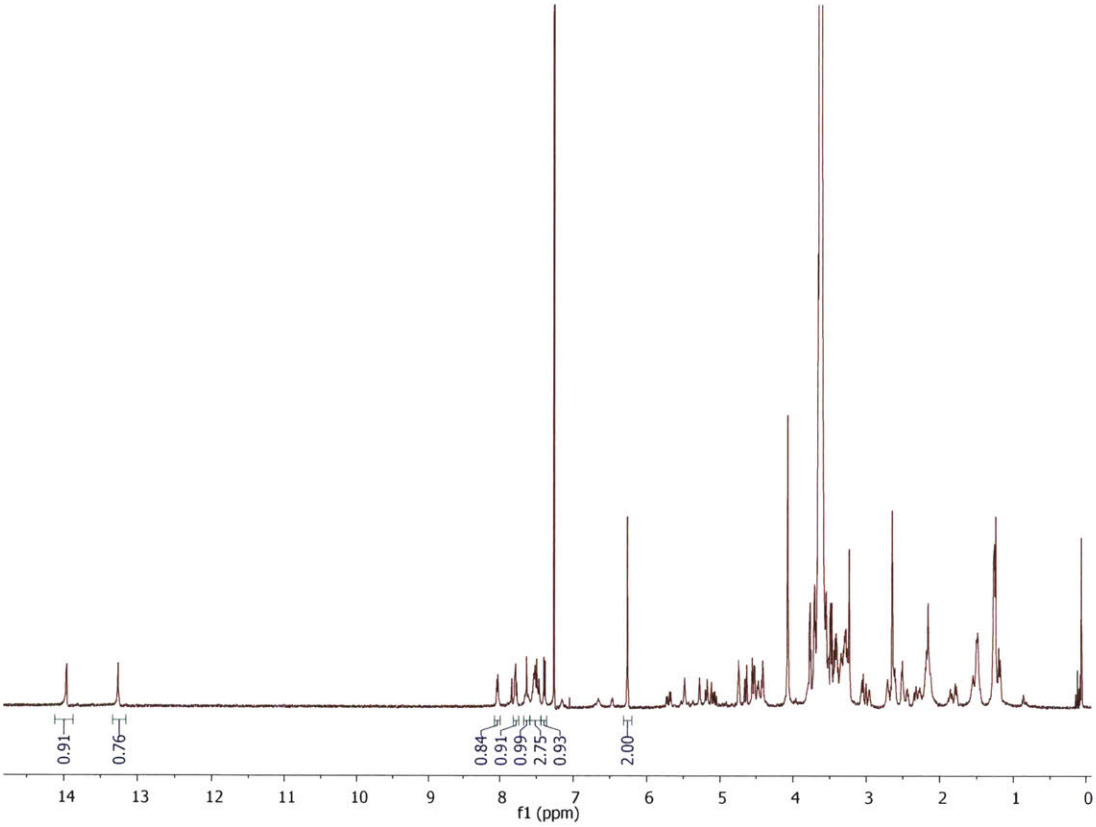

Figure S2.11. ^{1}H-NMR spectrum of **photo-DOX-MM** in $CDCl_3$.

Figure S2.12. MALDI spectrum of **photo-DOX-MM**. ((M+Li)+ calcd. for $C_{194}H_{336}N_8O_{87}Li$: 4177.23, Observed: 4176.73; (M+MeOH+H)+ calcd. for $C_{195}H_{341}N_8O_{88}$: 4203.25, Observed: 4201.77.

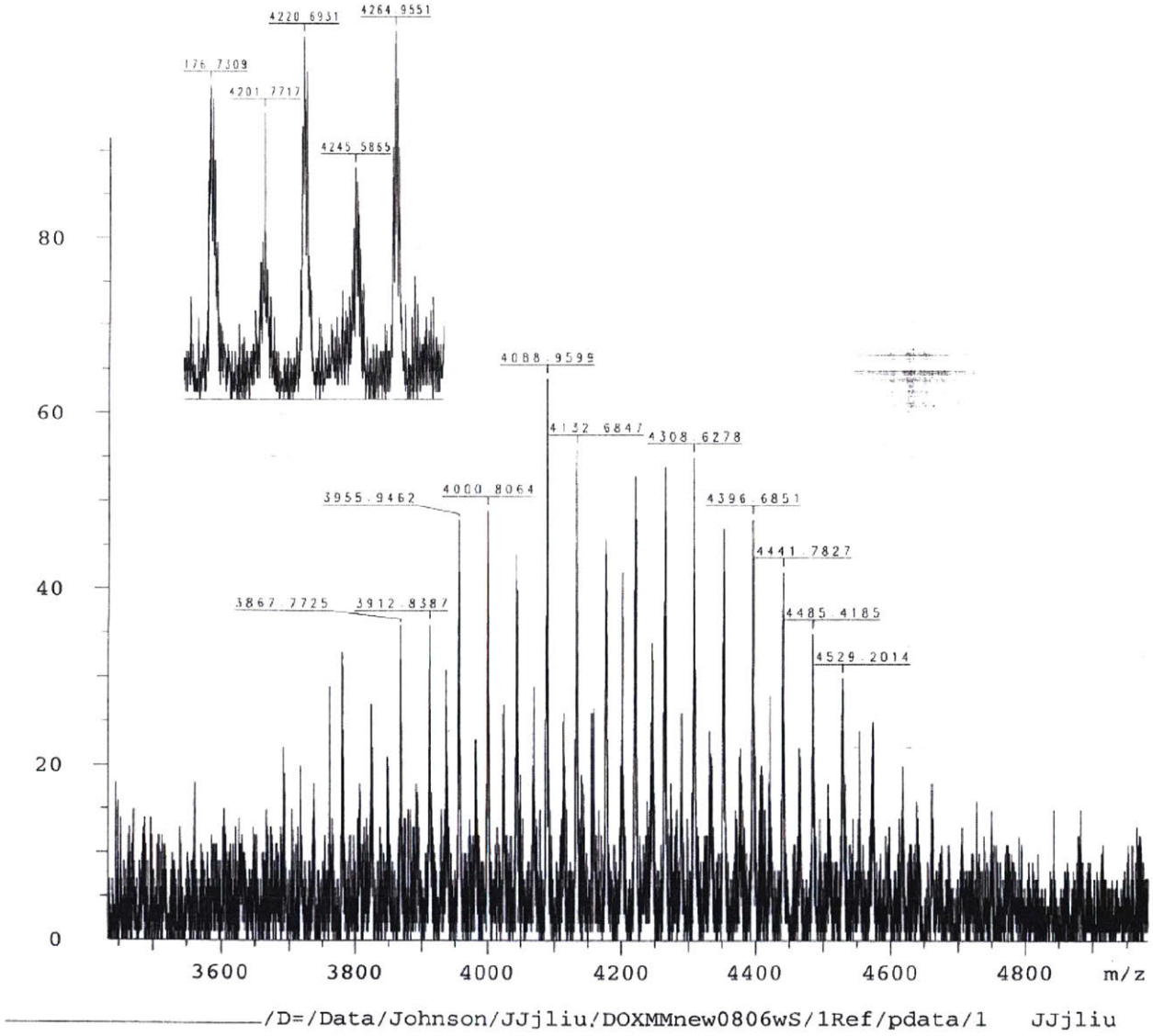

Chapter 3: Nano-FOLFIRINOX, a BASP combination therapy for advanced pancreatic cancer

3.1 Introduction

Brief Summary of Chapter and Respective Contributions

This chapter describes the synthesis and characterization of drug-conjugated macromonomers and BASPs that were designed for pancreatic cancer therapy. Results related to the application of these particles as a novel combination therapy are discussed. All work presented in the results section was that of the author, unless stated otherwise.

Introduction to Pancreatic Cancer

Pancreatic adenocarcinoma has one of the highest mortality rates among cancers with only a 6.0% 5-year survival rate.[1] It is one of the top 5 leading cancers for estimated deaths in the US.[1] There are two main forms of pancreatic cancer: (1) the more common exocrine cancer, or adenocarcinoma, which is cancer of the glandular tissue or pancreatic ducts that are responsible for producing digestive enzymes; and (2) endocrine caner, which is cancer of tissues responsible for producing hormones. Pancreatic adenocarcinoma, given its prevalence and low survival rates, is the subject of many research efforts aimed at more efficacious and safer treatments to extend and improve patient quality of life.

Limited therapeutic strategies and poor diagnostic tools are major causes of this high mortality rate. Regarding the latter, patients are often unaware that they have the disease until it has already metastasized to another organ, such as the liver, and symptoms of the metastasized cancer become apparent.[2-5] Pancreatic cancer is also known for its fast, aggressive growth; chemotherapies are rarely effective at inhibiting this growth and slowing spread of the disease. Additionally, pancreatic cancer often displays resistance to chemotherapeutics and poor drug accumulation due to a dense stroma and poorly developed vasculature, which limit drug accumulation in the tumor.[2,6] This "desmoplasia", which is the formation of a dense, fibrous stroma produced via tumor-associated myofibroblasts or pancreatic stellate cells that, in response to growth factors, lead to an increase in extracellular matrix (ECM) components such as hyaluronic acid and type I collagen and the build-up of inflammatory cells, such as macrophages, lymphocytes, and mass cells,[2,7,8] is a mechanical barrier that hinders drugs from reaching the tumor. Pancreatic cancer is also known for its hypovascular nature, which leads to high interstitial fluid pressures that further contribute to mechanical resistance of chemotherapy.[9] The

poor vasculature also impedes oxygen from reaching the tumor, and along with the already high consumption of oxygen from rapidly dividing cells, further contributes to hypoxia.[7] The hypoxic environment can affect the metabolism of tumor cells; for example, glycolysis to produce lactic acid can occur in lieu of oxidative phosphorylation, which in turn contributes to a decrease of pH in the tumor microenvironment.[10] Additionally, hypoxia in tumors is associated with increased malignant tumor progression, metastasis, and therapeutic resistance.[11,12] Thus, cancer therapeutics are being developed to treat hypoxia in order to slow progression of cancer.[13,14] The immune system and changes in immune system regulation also play an important role in tumor progression and drug resistance, thus pancreatic cancer tumor immunology is another area of research in combating and developing treatments against pancreatic cancer.[7,15-17] For the reasons listed above, pancreatic cancer is difficult to treat leading to high mortality rates; development of more efficacious treatments may address some of the issues in treating pancreatic cancer and improve patient outcome.

Combination Therapy for Pancreatic Cancer

The 4-drug combination therapy FOLFIRINOX is currently one of the most effective clinical treatment regimens; however, FOLFIRINOX has high associated toxicity that limits its use to a subset of healthier patients in advanced stage III or metastatic stage IV pancreatic cancer.[18,19] For typical patients, Abraxane (albumin-bound paclitaxel), Onivyde (liposomal irinotecan) or gemcitabine combinations are used, which feature fewer side effects, but are also less effective in increasing the median survival rate.[3,20] Also for a small percentage of patients with stage I or II pancreatic cancer, pancreaticoduodenectomy can help treat pancreatic cancer, but surgery is not effective in advanced stages.[7,21] The four drugs in FOLFIRINOX are irinotecan (IRT), oxaliplatin, 5-fluorouracil (5-FU), and leucovorin (**Scheme 3.1A**). Irinotecan is a prodrug of SN38; it is metabolized in the liver to SN38 (**Scheme 3.1B**).[22] SN38 is a camptothecin analog, which inhibits DNA topoisomerase type I, and prevents re-ligation of DNA after a single strand break by topoisomerase I.[23] In turn, the DNA damage can cause cell death by apoptosis. Oxaliplatin is also proposed to hinder DNA replication, and 5-fluorouracil is a nucleobase analog that can inhibit DNA synthesis.[24,25] 5-fluorouracil can be converted to a nucleotide by enzymes in the body and inhibit thymidylate synthase, thus preventing the synthesis of thymidine from uridine, or it can inhibit DNA synthesis directly by acting as a

nucleotide analog. Drugs of this type, which work by inhibiting DNA synthesis, are more effective against rapidly dividing cells, such as malignant tumor cells.

Table 3.1 shows the dosages of these four drugs used in a phase III clinical trial that compared the FOLFIRINOX combination therapy with a standard gemcitabine therapy.[18] The dose of 5-fluorouracil in FOLFIRINOX is quite high at 400 mg/m^2 bolus dose and a 2400 mg/m^2 46h continuous infusion. Furthermore, leucovorin is used not as a therapeutic agent itself but instead to help modulate the side effects of this large dose of 5-fluorouracil. Notably, the FOLFIRINOX regimen had a 1 -month survival rate at 18.6% compared to only 6% with the gemcitabine treatment. Thus, the combination therapy was shown to be more effective at extending life expectancy to those with pancreatic cancer. However, the adverse side effects, including neutropenia, vomiting, alopecia, and peripheral neuropathy, were much higher in FOLFIRINOX than with standard gemcitabine chemotherapy. We reasoned that a "nano-FOLFIRINOX" BASP could greatly improve upon the major toxicity concerns of FOLFIRINOX by enabling more selective drug accumulation, potentially with synchronized release of an optimized drug ratios, in the pancreas. There is some evidence in the literature that, despite the desmoplasia and tumor vasculature issues listed above, nanoparticles in the size range of ~30 nm or less can display enhanced uptake in orthotopic pancreatic cancer animal models.[26]

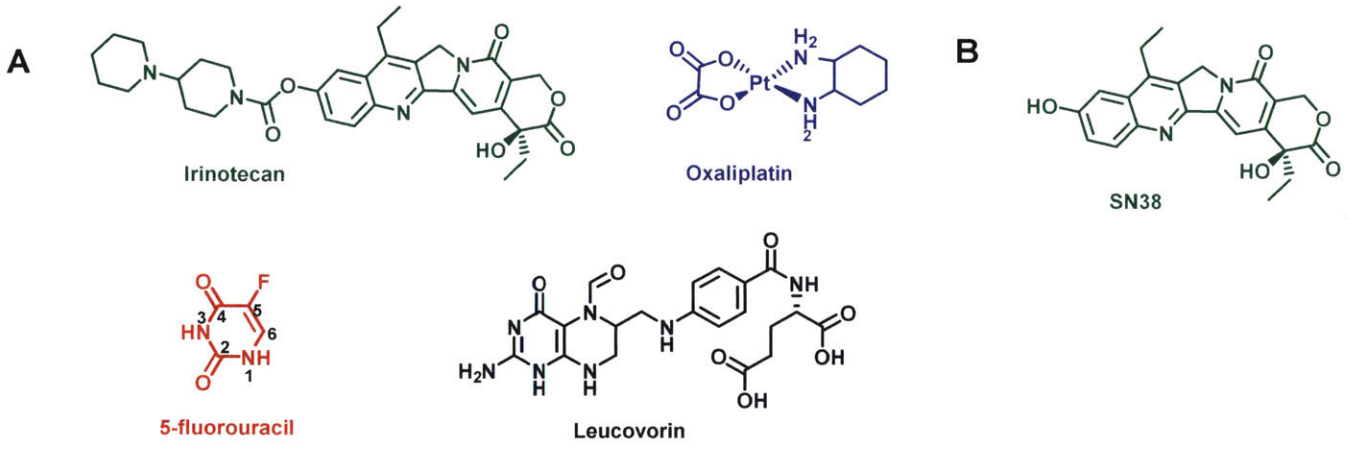

Scheme 3.1: A) Chemotherapeutic components of FOLFIRINOX. (Note: 5-fluorouracil atoms are labelled for reference.) B) Structure of SN38, the active metabolite of irinotecan.

Results from Phase III Clinical Trial	Folfirinox (n=171)	Gemcitabine (n=171)
Dosage	85 mg/m^2 Oxaliplatin 180 mg/m^2 Irinotecan 400 mg/m^2 Leucovorin 400 mg/m^2 5-Fluorouracil bolus 2400 mg/m^2 46h 5-Fluorouracil continuous infusion	1000 mg/m^2 IV weekly X7, 1 week rest, weekly X3
1-year survival rate	48.4%	20.6%
18-month survival rate	18.6%	6%
Adverse Effects	Neutropenia (45.7%) Vomiting (14.5%) Alopecia (11.5%) Peripheral neuropathy (9%)	Neutropenia (18.7%) Vomiting (4.7%) Alopecia (0.6%) Peripheral neuropathy (0%)

Table 3.1[18]**:** Results from a clinical trial comparing FOLFIRNOX combination therapy with standard gemcitabine treatment. Table compares the dosage of chemotherapeutics, survival rates, and some of the adverse effects, and shows better overall survival rates with FOLFIRINOX, but fewer adverse side effects with gemcitabine therapy.

Rationale for Nanoparticle Combination Therapy

There are now several literature precedents for nanoparticle-based approaches to pancreatic cancer therapy.[27,28] Most of these involve the use of single-drug therapies; however, a few multi-drug combination therapies have also been reported. Most relevant to this thesis is the work of Li et al., which involved the synthesis of layer-by-layer PEG-polylactide (PLA) lipid nanoparticle loaded with camptothecin, 5-fluorouracil, and oxaliplatin and tested its stability, efficacy, and side effects *in vivo*.[29] Due to the simultaneous drug release, serum stability, and long circulation times of the nanoparticle, their formulation had improved antitumor efficacy compared with an equivalent free drug combination in mice with subcutaneous xenograft pancreatic tumors. However a subcutaneous model may not be indicative of efficacy for poorly permeable tumors, such as pancreatic cancer. Thus, the efficacy of a FOLFIRINOX nanoparticle combination should be addressed in an orthotopic mouse model of pancreatic cancer, which is one of the key goals of this project.

Despite this example, there is also still great need for a flexible nanoparticle combination therapy for pancreatic cancer that combines the right ratio of chemotherapeutic agents with production scalability and modular functionality for the addition or removal of other

experimental agents. To address these challenges, we designed a Nano-FOLFIRINOX BASP for co-delivery of oxaliplatin, SN-38 or irinotecan, and 5-fluorouracil, as seen in **Figure 3.1**. Note: our design leaves out leucovoran, because, as stated above, this drug is given to ameliorate the side effects of 5FU, which we hope to accomplish through nanoparticle delivery (both by avoiding the need for such a large dose of 5FU and through enhanced tumor uptake). This design also provides a platform for studying the *in vivo* properties, such as pharmacokinetics, biodistribution, therapeutic index, and toxicity, of BASPs in a highly relevant application. With an improved understanding of these features, we can then potentially expand upon the BASP system and produce nanoparticle therapies for other diseases.

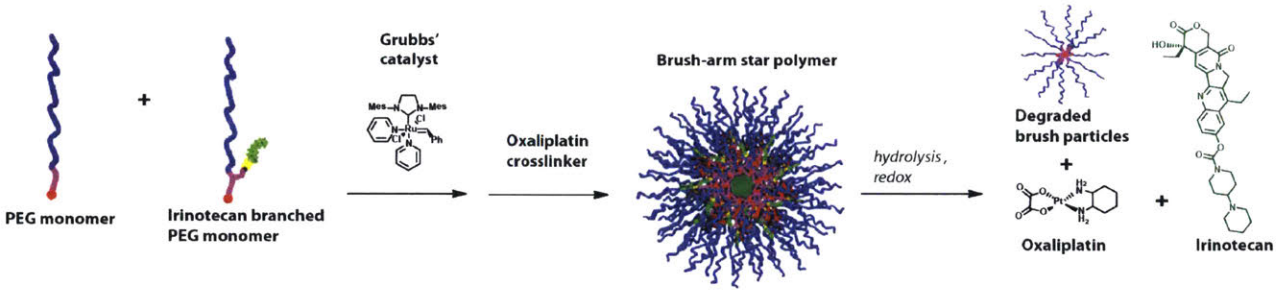

Figure 3.1: PEG-MM and an irinotecan-loaded MM can be polymerized with G3 to synthesize a living bottle-brush that can be subsequently crosslinked by an oxaliplatin prodrug crosslinker to make drug-loaded BASPs. The particle, MMs, and crosslinkers are designed to break the brush into smaller components and release free drug in response to the environment.

As alluded to in Chapter 2, a key advantage of the BASP synthesis strategy is that it provides control over the approximate ratiometric loading of multiple agents. Although the ratio in each individual particle cannot be absolutely precise, it can be controlled within a narrow distribution thanks to the excellent efficiency of ROMP. In order to identify the optimal ratio of oxaliplatin, 5FU, and SN38 for use in nano-FOLFIRINOX, we explored the possibility of using combination index studies to determine synergistic, additive, or antagonistic ratios of these drugs, with the plan of building these ratios into BASPs.[30-32] The basic definition of an additive effect is when the total effect of two or more drugs is equal to the sum of the individual drugs. However, predicting the additive contributions of two or more drugs can be complicated when considering factors such as same-target effects or drug-drug interactions. Synergism is defined as two more drugs working together to have a greater effect than the sum of the individual drugs. Antagonism is defined as two more drugs having a lesser effect than its individual components.[33]

In other words, synergistic chemotherapeutics will be more toxic than the predicted additive toxicity, whereas antagonistic drugs will be less toxic than the additive effect. Synergism is often desired because in principle one can use a smaller concentration of drugs to achieve the desired efficacy, which in turn may help lower unwanted side effects. Indeed, researchers have found that many drugs display synergism when administered in specific ratios,[34-36] and such synergism was recently exploited by Celator pharmaceuticals to produce the first FDA-approved 2-drug nanoparticles for treatment of AML.

Nonetheless, it is still very difficult to predict synergism between two or more drugs. For example, in the case of oxaliplatin and irinotecan, one could hypothesize that since oxaliplatin's disruption of DNA can be offset by repair from topoisomerase I, the combination of oxaliplatin with a topoisomerase I inhibitor, such as irinotecan, could potentiate the effect of oxaliplatin and lead to synergism between the two drugs.[36] Despite this potential biochemical rationale, one must conduct careful cell-based assays to validate synergism using an appropriate statistical model. A number of different methods have been developed to quantitatively evaluate drug synergism and mathematically define an additive effect, including the Chou-Talalay method and the Bliss independence model.[31,32] It must be noted that *in vitro* combination index studies must also ultimately be validated *in vivo*, and even then may not necessarily translate into human patients. Thus, though the Celator example cited above provides an example to the contrary, combination index studies may not always be able to provide a valid rationale for choosing therapeutic ratios in humans; nonetheless, we reasoned that it would be a good starting point for BASP design.

Importantly, in clinical combination therapy, free drugs with different properties are administered separately and thus they may not reach the tumor at a synergistic ratio. By appending a synergistic ratio of drugs to one BASP, in principle that synergistic ratio of drugs could delivered to the cell with all drug arriving at exactly the same time. With this concept in mind, this chapter focuses on the development of nano-FOLFIRINOX BASPs for applications in combination pancreatic cancer therapy.

3.2 Results and Discussion

At the outset, we needed to achieve two key goals: (1) the synthesis of suitable BASP components (macromonomers and crosslinkers) for nano-FOLFIRINOX, and (2) the identification of ratios of FOLFIRINOX drugs (oxaliplatin, irinotecan/SN38, and 5FU) that would be synergistic (if any). This section focuses on the synthesis first, and attempts to identify synergistic drug ratios are described below. Our synthesis is based on the drug-conjugated macromonomer approach outlined in Chapter 2 for doxorubicin. This approach utilizes copper-catalyzed azide-alkyne cycloaddition (CuAAC) click chemistry between PEG-alkyne-MM drug-azide derivatives.[37] To focus on biologically relevant linkers that cleave under physiological conditions, the camptothecin linker (azide-PEG4-acid) that was published previously from the Johnson lab was synthesized (**Scheme 3.2)** and scaled up to couple to irinotecan, a camptothecin analog.[38] This irinotecan-azide (IRT-Az) was coupled to PEG-alkyne-MM to provide IRT-MM (**Scheme 3.3**). It must be noted that irinotecan is a prodrug of the active compound SN38; it is metabolized by the liver to become active.[22,23] Indeed, *in vitro* cell viability assays show that SN38 is orders-of-magnitude more potent than irinotecan across different cell lines.[23] Thus, to avoid the need for an additional metabolism step after cleavage of the drug from the BASP nanoparticle, and to overcome solubility issues that hinder the use of free SN38, we synthesized an SN38 macromonomer for comparison to irinotecan (**Scheme 3.4**).

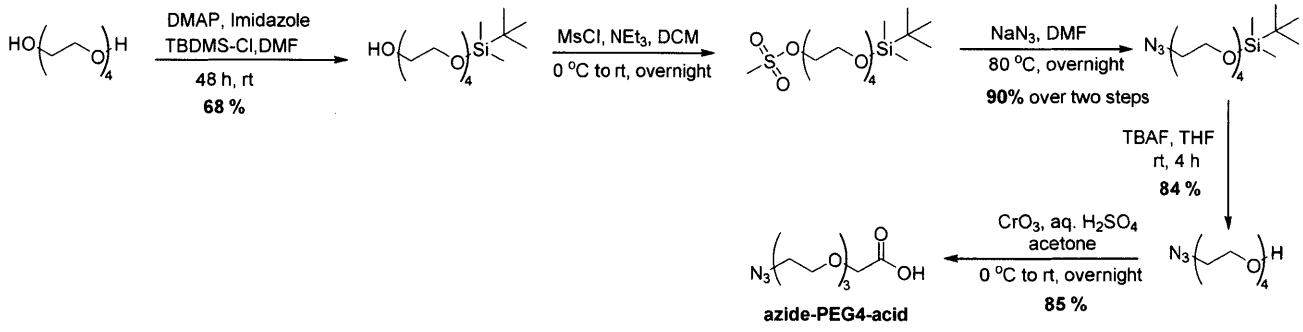

Scheme 3.2: Synthesis of azide-PEG4-acid.

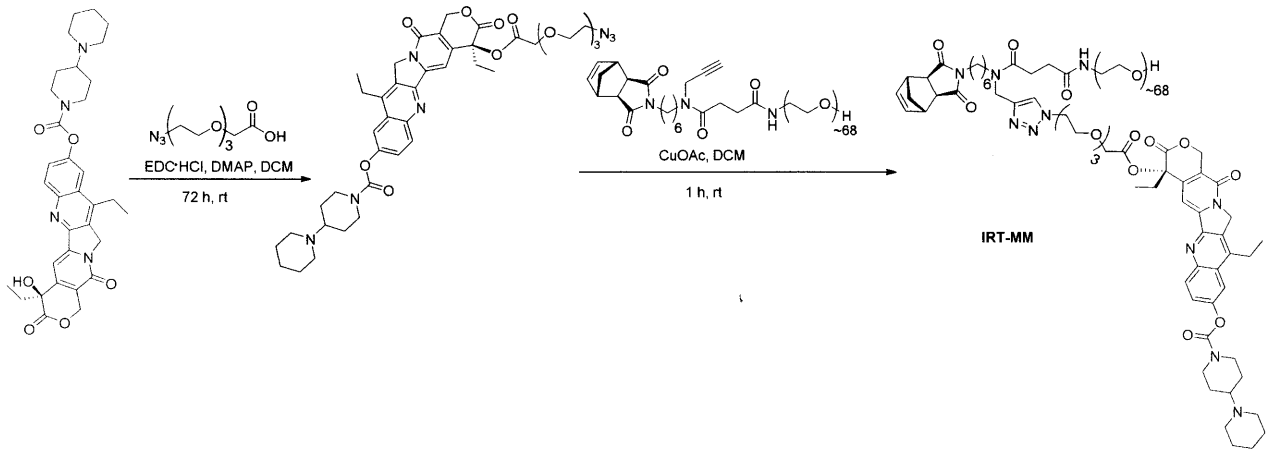

Scheme 3.3: Synthesis of IRT-MM from irinotecan and azide-PEG4-acid.

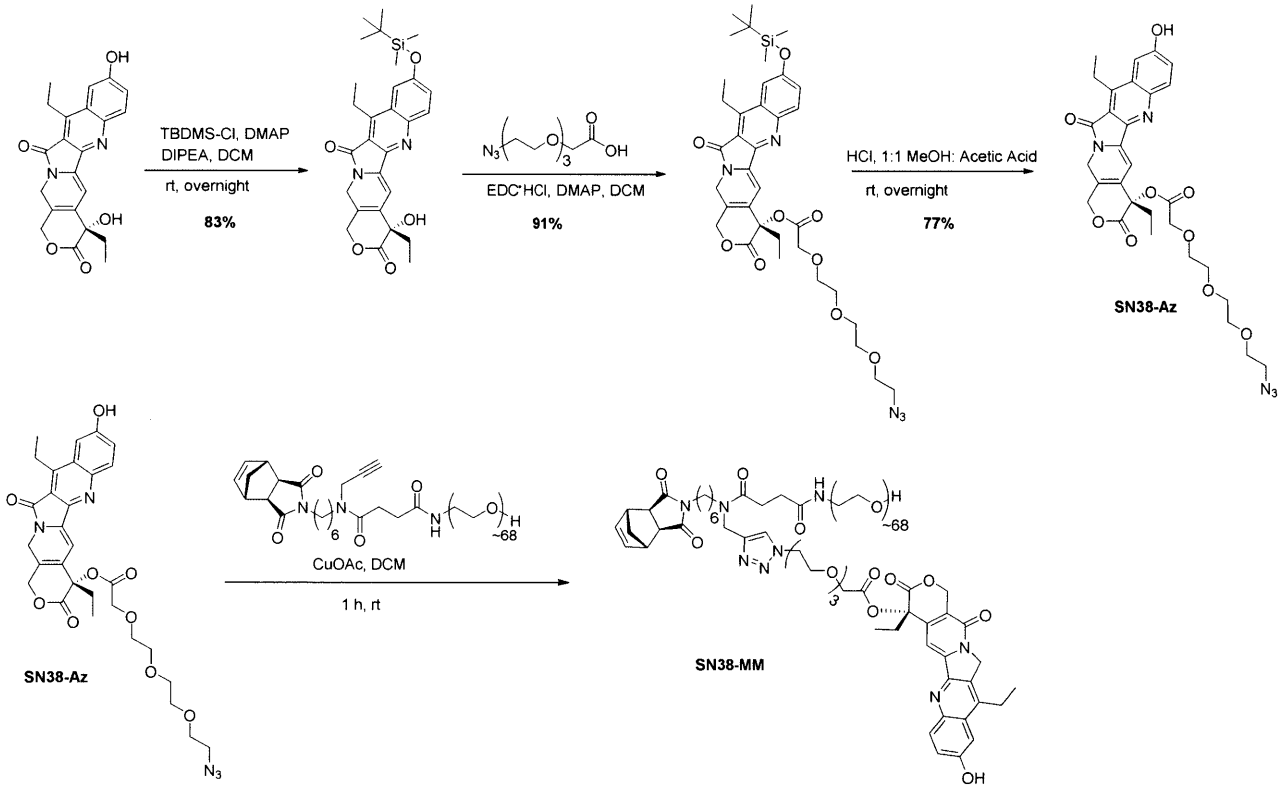

Scheme 3.4: Synthesis of SN38-MM from SN38 and azide-PEG4-acid.

Next, we turned to the synthesis of a 5-fluorouracil macromonomer, but after many failed attempts (discussed further later in this chapter) we decided instead to focus on the incorporation of oxaliplatin. Following from her work on the cisplatin crosslinker, Dr. Liao designed an oxaliplatin prodrug crosslinker, Oxali-XL (**Scheme 3.5**); this synthesis was scale up for this

project.[38] Oxali-XL is a platinum (IV) prodrug of oxaliplatin that releases free oxaliplatin upon intracellular reduction.[39] This release process also leads to BASP degradation, thereby potentially facilitating the clearance of the BASP byproducts. The previously reported acetal crosslinker, Acetal-XL (see Chapter 2), was also prepared as a "blank" crosslinker for use in the synthesis of BASPs that lack oxaliplatin (for comparison to BASPs that do have oxaliplatin) (**Scheme 3.6**).[40] Through screening of various macromonomer to oxaliplatin crosslinker ratios, we found that uniform BASPs formed most readily using 5 equivalents of crosslinker with 7-12 equivalents of macromonomer. With this fact in mind, it is possible to generate a wide range of SN38 or irinotecan to oxaliplatin ratios through the use of the non-drug conjugated PEG-MM described extensively in Chapter 1. For example, if a 3:5 ratio of SN38 to oxaliplatin is desired, then one could use 3 equivalents of SN38-MM plus 4 equivalents of PEG-MM to 5 equivalents of Oxali-XL to prepare BASPs.

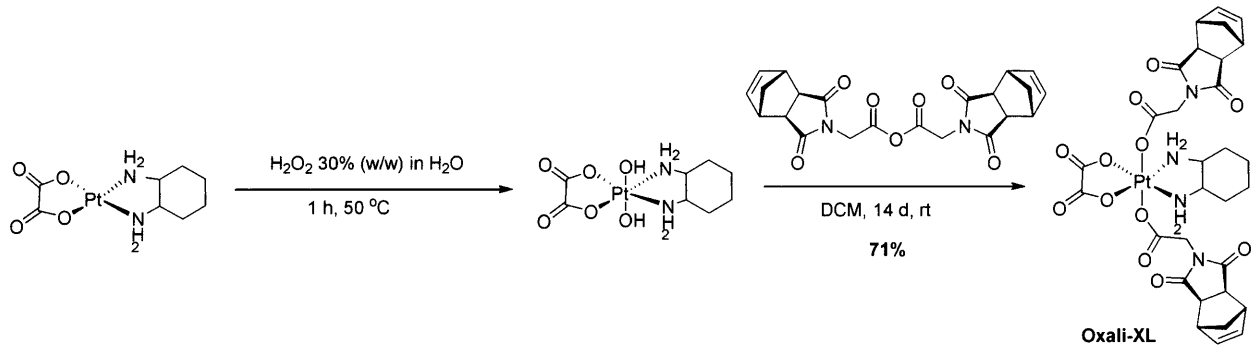

Scheme 3.5: Synthesis of Oxali-XL.

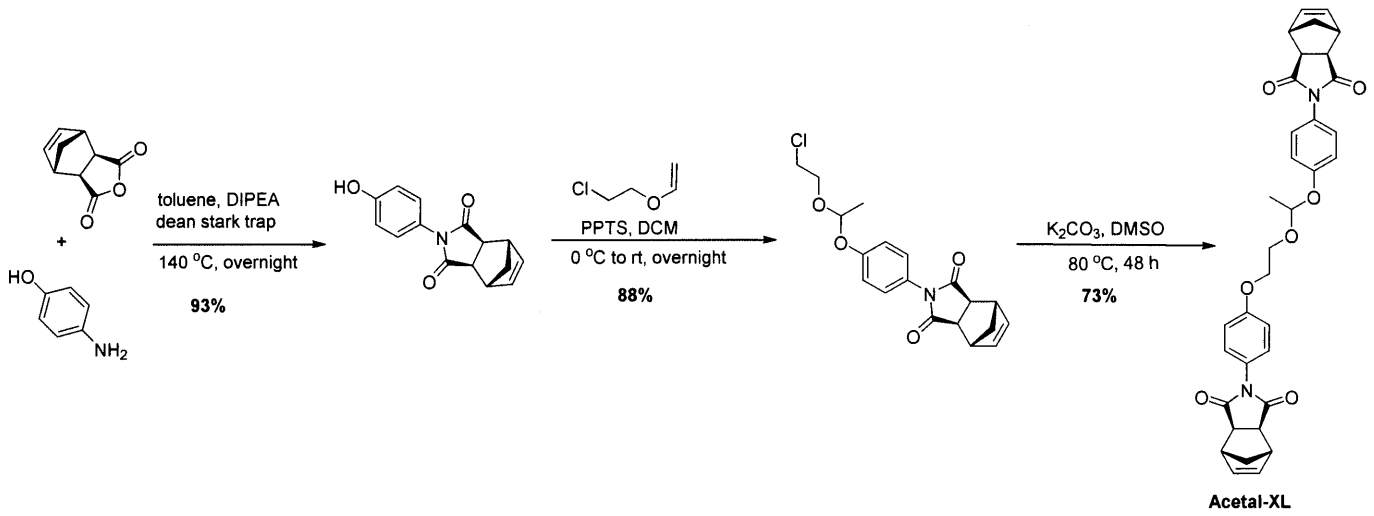

Scheme 3.6: Synthesis of Acetal-XL.

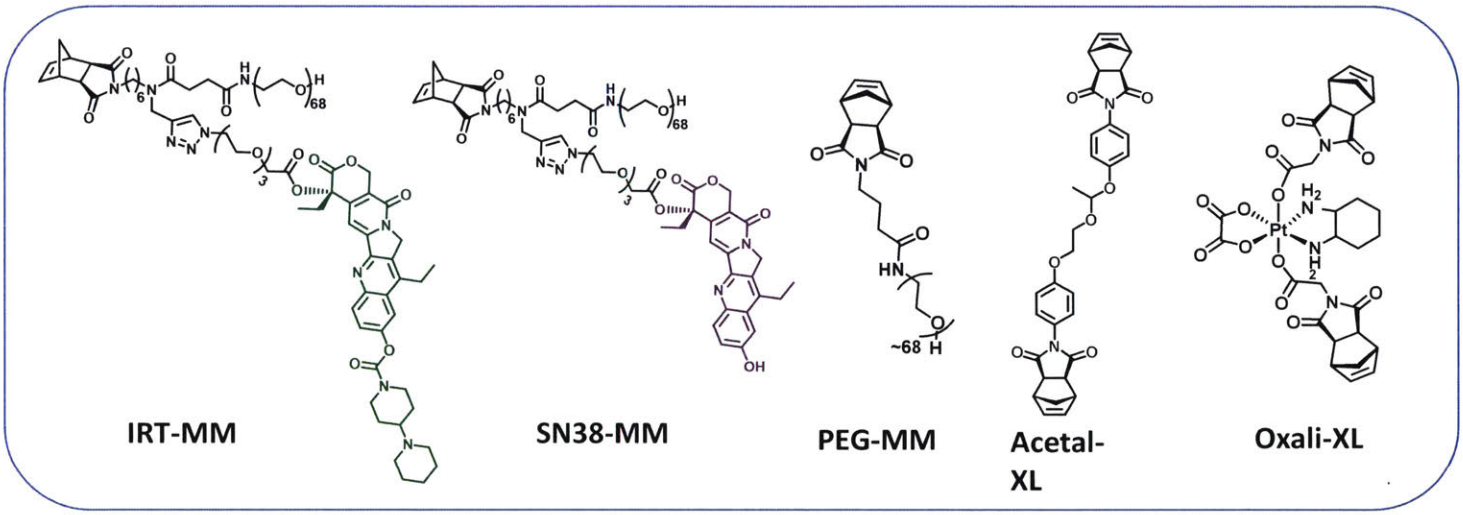

Figure 3.2: Structures of MMs and crosslinkers synthesized for use in BASPs.

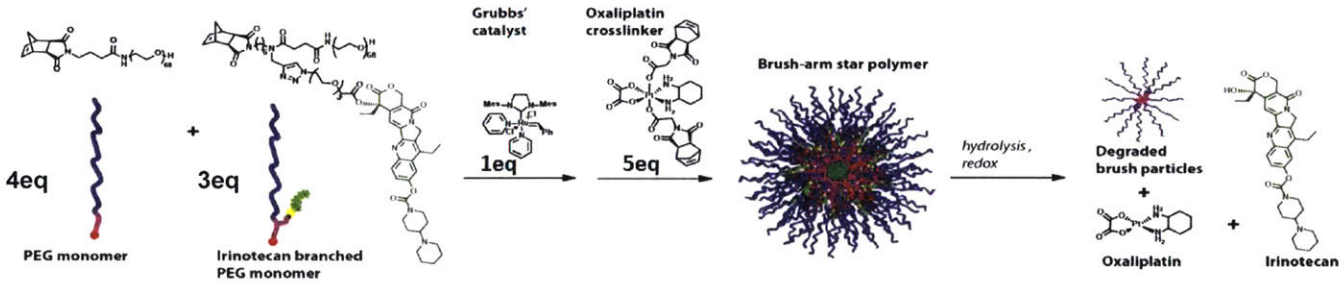

Figure 3.3: Sample synthesis of BASPs illustrating 4 units of PEG-MM with 3 units of IRT-MM polymerized to form a living brush initiator, which is then added to 5 equivalents of Oxali-XL to form irinotecan and oxaliplatin loaded BASPs. This multi-drug particle can respond to hydrolysis or reducing conditions to release free irinotecan and oxaliplatin, respectively, and break the particle apart into smaller components.

With the SN38 or irinotecan macromonomers and oxaliplatin crosslinker in hand, we prepared a series of one-drug and two-drug conjugated BASPs (**Figure 3.2**).[38] Following the general procedure outlined in previous chapters, the desired macromonomers were first polymerized to produce a living bottlebrush initiator, which was subsequently crosslinked using

N equivalents of crosslinker (**Figure 3.3**). Solvent screening studies revealed that THF gave the most reliable BASP formation reactions. Furthermore, it was noted that while BASP-forming reactions with Acetal-XL were complete in ~2 h, those with Oxali-XL required ~6 h to reach completion. Nonetheless, the BASP sizes were similar in both cases, which highlights the versatility of the BASP synthesis protocol. Furthermore, it is critical to note a key difference between these two crosslinkers in terms of their practical use: Acetal-XL is partially soluble in THF, and therefore it was added dropwise slowly to the living bottlebrush initiator; if it is added too quickly then the reaction will rapidly gel. In contrast, Oxali-XL is poorly soluble in THF, and it can be added directly to the living bottlebrush as a solid. Its poor solubility ensures that the crosslinker is slowly incorporated into the BASP, thereby avoiding gelation and producing narrowly dispersed nanoparticles.

In general, upon complete conversion, the reaction solutions were quenched with excess ethyl vinyl ether. The particles were then dialyzed in MilliQ water in two-to-three rounds at 2-3 hours per round with 1000 mL of water for every 1 mL of BASP solution. Note: dialysis for greater than 9 h has been avoided to limit any premature drug release due to hydrolysis. Finally the BASPs were lyophilized to provide a fluffy powder (**Figure 3.4**). It is critical to note that if at any point after quenching the ROMP reaction, the BASP solution is concentrated prior to lyophilization, the BASPs can aggregate, presumably due to PEG entanglement. When it occurs, this aggregation is generally difficult to reverse and the aggregated particles cannot re-disperse in water. In contrast, the lyophilized particles dissolved readily in water at concentrations of 40 mg/mL and below.

Figure 3.4: Sample photograph of lyophilized BASPs as a fluffy powder.

Table 3.2 shows a summary of five of the BASPs that were synthesized. A single drug-conjugated oxaliplatin BASP, **PEG_7Oxali_5**, was synthesized with 7 equivalents of PEG-MM, 5 equivalents of Oxali-XL, and 1 equivalent of G3. A single drug-conjugated irinotecan BASP, **$IRT_5PEG_5Acetal_{10}$**, was synthesized with 5 equivalent of IRT-MM, 5 equivalent of PEG-MM, 10 equivalent of Acetal-XL, and 1 equivalent of G3. A single drug-conjugated SN38 BASP, **$SN38_5PEG_5Acetal_{10}$**, was synthesized with 5 equivalent of SN38-MM, 5 equivalent of PEG-MM, 10 equivalent of Acetal-XL, and 1 equivalent of G3. A two drug-conjugated BASP was synthesized with 3 equivalent of IRT-MM and 4 equivalent of PEG-MM to 5 equivalent of Oxali-XL and 1 equivalent of G3 to provide the **$IRT_3PEG_4Oxali_5$**. Another two-drug conjugated BASP was synthesized with 3 equivalent of SN38-MM and 4 equivalent of PEG-MM to 5 equivalent of Oxali-XL and 1 equivalent of G3 to provide the **$SN38_3PEG_4Oxali_5$**.

Name	Composition	M_w (GPC-MALLS)	$Đ$ (GPC-MALLS)	D (TEM)	Approx. Average D_H (DLS)	Theoretical drug wt.% (actual wt.% by UV/vis)
PEG_7Oxali_5	PEG-MM 7eq Oxali-XL 5eq	3.723×10^5 g/mol	1.265	18.6 ± 2.6 nm	24.0 nm	Oxaliplatin: 7.5%
$SN38_5PEG_5Acetal_{10}$	SN38-MM 5eq PEG-MM 5eq Acetal-XL 10eq	4.549×10^5 g/mol	1.263	27.3 ± 7.9 nm	29.4 nm	SN-38: 4.7% (4.5%)
$IRT_5PEG_5Acetal_{10}$	IRT-MM 5eq PEG-MM 5eq Acetal-XL 10eq	4.680×10^5 g/mol	1.475	13.3 ± 2.9 nm	16.2 nm	Irinotecan: 7.0% (4.0%)
$SN38_3PEG_4Oxali_5$	SN38-MM 3eq PEG-MM 4eq Oxali-XL 5eq	3.087×10^5 g/mol	1.104	27.2 ± 5.5 nm	21.4 nm	SN-38: 4.1% (4.5%) Oxaliplatin: 6.9%
$IRT_3PEG_4Oxali_5$	IRT-MM 3eq PEG-MM 4eq Oxali-XL 5eq	2.189×10^5 g/mol	1.166	15.7 ± 3.8 nm	15.2 nm	Irinotecan: 6.1% (3.7%) Oxaliplatin: 6.9%

Table 3.2: Summary of some of the BASPs synthesized and their characterization data, including weight average molar mass (M_w) as determined by GPC-MALLS; dispersity index ($Đ$) as determined by GPC-MALLS; diameter (D) as determined by TEM; hydrodynamic diameter (D_H) as determined by DLS, theoretical calculated drug weight % assuming complete conversion; and the experimentally determined drug-loading in brackets when applicable.

The GPC, DLS, and TEM data for these BASPs are shown in **Supplemental Figures 3.S1-3.S5**. The GPC chromatograms were obtained pre-dialysis (immediately after quenching the ROMP reaction); these data were used to obtain M_w, M_n, and $Đ$. TEM images were obtained post-lyophilization; the samples were non-stained for BASPs containing platinum and positively stained with ruthenium tetroxide for BASPs without platinum. BASPs made with the Acetal-XL were ~27 nm in diameter, whereas particles made with the Oxali-XL were around ~13-19 nm in diameter by TEM, keeping in mind that the PEG corona is unlikely to be observed in the latter images of unstained particles. The hydrodynamic diameters observed by DLS agreed somewhat with the average diameters obtained by TEM. UV-vis was generally used to determine the drug loading in the irinotecan and SN38 particles.

Next, we characterized the properties of these BASP using *in vitro* assays and drug release studies. Originally, *in vitro* cytotoxicity assays were performed by Dr. Zhimin Tao of the Ghoroghchian group. The cytotoxicity assays were performed using 8988T pancreatic ductal adenocarcinoma (PDAC) cells seeded at 3000 cells/well and incubated with drug-conjugated BASP or free drug for 72 hours. All single-drug conjugated BASPs tested showed similar toxicity toward 8988T cells as the corresponding free drug (**Figure 3.5**). These cytotoxicity assays were repeated by myself with single-drug conjugated and dual drug-conjugated BASPs using 2980A PDAC cells (**Figure 3.6**, **Table 3.3**). In these cells, BASPs with oxaliplatin alone were the least toxic. Of the two drug-conjugated BASPs, the **IRT$_3$PEG$_4$Oxali$_5$** BASPs were less toxic than the **SN38$_5$PEG$_5$Acetal$_{10}$** BASPs, as expected. Also both dual-drug conjugated BASPs were more toxic than their single-drug conjugated counterparts when the x-axis is plotted with respect to the total concentration of either SN38 or irinotecan.

We also characterized the drug release of these systems in buffer solutions. BASPs were incubated in pH 7.5 PBS buffer at 37 °C and release of SN38 or irinotecan was monitored by LCMS over 7 or 8 d (**Figure 3.7**). The amount of drug released was determined by the area under the curve (A.U.C.) of free SN38 or irinotecan observed at 360 nm divided by the total A.U.C. of free drug plus bound drug at 360 nm, assuming only SN38 or irinotecan contribute to absorbance at 360 nm. **Supplemental Figure 3.S6** and **Figure 3.S7** show sample LCMS traces from these studies. In all cases, greater than 45% release of SN38 or irinotecan from its linker was observed after incubating in pH 7.5 PBS buffer for 8 days. The release of free oxaliplatin under physiologically relevant reducing conditions (e.g., low mM glutathione and other cellular

reducing agents) was not determined for these BASPs; however, using a dialysis experiment and ICP-AES, Dr. Liao characterized the release of free oxaliplatin from $PEG_{12}Oxali_5$ BASPs exposed to 10 mM glutathione in pH 7.4 PBS buffer (**Figure 3.8**). The results indicate that release of oxaliplatin is complete within ~2 d. Taken together, the studies above confirm that these BASPs (a) can be successfully synthesized with sizes desirable for drug delivery, (b) release their drug contents under different stimuli, and (c) are cytotoxic towards pancreatic cancer cells with multi-drug BASPs displaying superior toxicity to single-drug conjugated ones.

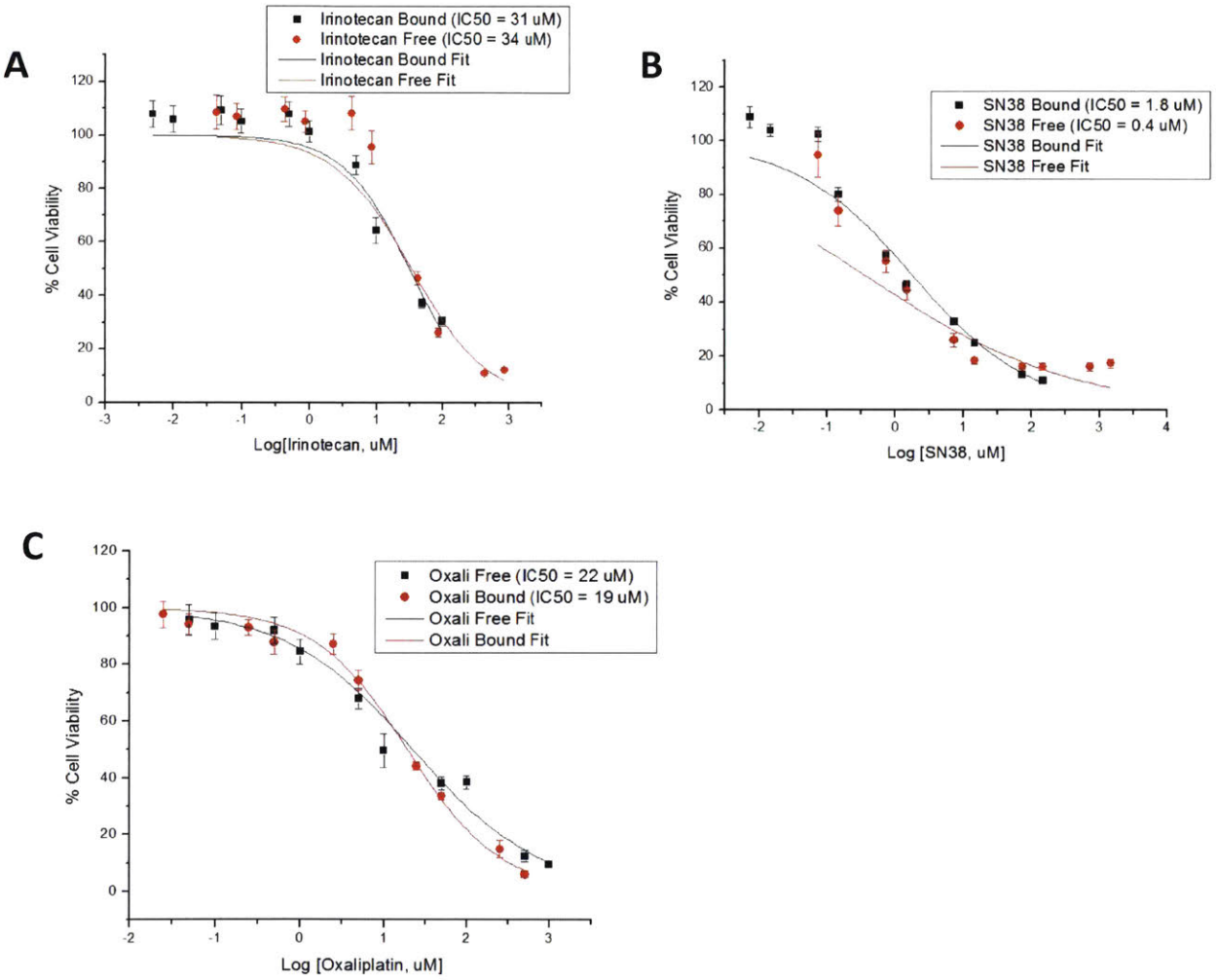

Figure 3.5: Cytotoxicity assays performed by Zhimin Tao from the Ghoroghchian lab on 8988T pancreatic cancer cells seeded at 3000 cells per well and incubated with BASP or drug for 72 h. A) Cytotoxicity assay comparing irinotecan bound BASPs (**$IRT_5PEG_5Acetal_{10}$**) with free irinotecan. B) Cytotoxicity assay comparing SN38 bound BASPs (**$SN38_5PEG_5Acetal_{10}$**) with free SN38. C) Cytotoxicity assay comparing oxaliplatin bound BASPs (**PEG_7Oxali_5**) with free oxaliplatin.

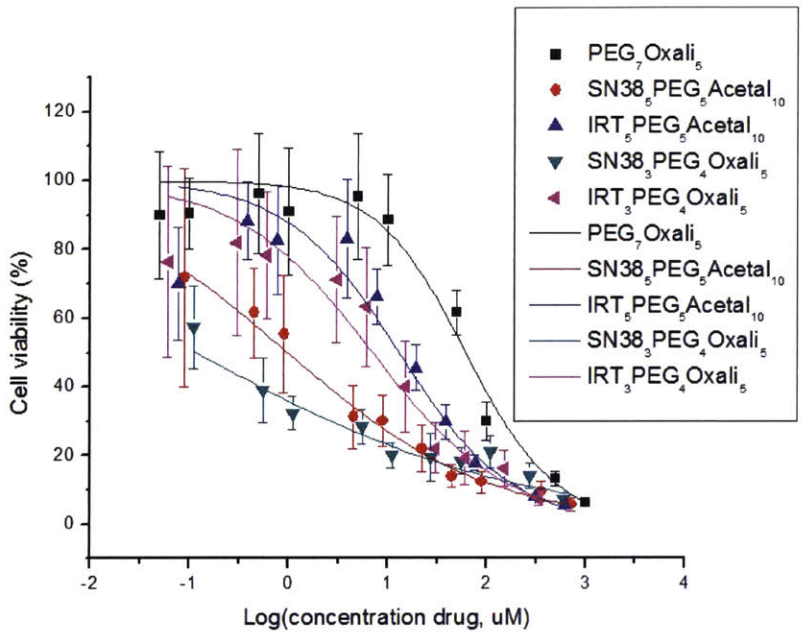

Figure 3.6: Cytotoxicity assays were performed on 2980A PDAC cells with incubation of the desired BASP for 72h. Cell viability was quantified by MTT assay. The concentration of drug (x-axis) refers to the concentration of SN-38 or irinotecan only, except for the Peg_7Oxali_5 particle, which uses the concentration of oxaliplatin. For the two-drug conjugated BASPs, the theoretical ratio of SN-38 or irinotecan to oxaliplatin is 0.6.

Nanoparticle	IC50	Theoretical drug wt.% (actual wt.%)
PEG_7Oxali_5	60 μM Oxali (0.3 mg/mL BASP)	Oxaliplatin: 7.5%
$SN38_5PEG_5Acetal_{10}$	1 μM SN38 (0.009 mg/mL BASP)	SN-38: 4.7% (4.5%)
$IRT_5PEG_5Acetal_{10}$	13 μM IRT (0.2 mg/mL BASP)	Irinotecan: 7.0% (4.0%)
$SN38_3PEG_4Oxali_5$	0.1 μM SN38 (0.0009 mg/mL BASP)	SN-38: 4.1% (4.5%) Oxaliplatin: 6.9%
$IRT_3PEG_4Oxali_5$	7 μM IRT (0.1 mg/mL BASP)	Irinotecan: 6.1% (3.7%) Oxaliplatin: 6.9%

Table 3.3: Summary of IC50s for BASP toxicity tested in 2980A PDAC cells. IC50 is respect to the concentration of SN38 or irinotecan, except for the PEG_7Oxali_5 BASPs, in which the IC50 is respect to the concentration of oxaliplatin. The IC50 listed in brackets is relative to the concentration of BASP, and the theoretical drug loading is given in the last column with the experimentally determined drug loading in brackets, when applicable.

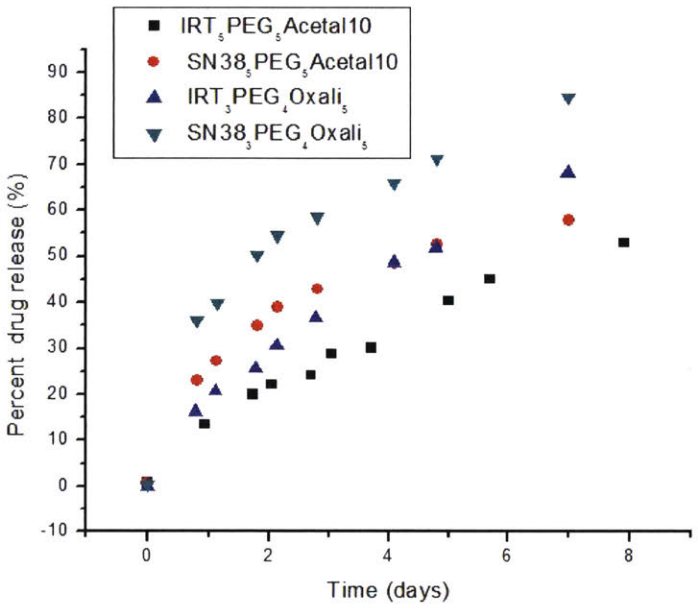

Figure 3.7: BASPs were incubated at 37 °C in pH 7.5 phosphate-buffered saline (PBS) buffer and drug release was monitored by liquid chromatography-mass spectrometry (LC-MS). Fractional drug release is calculated as AUC_{360} for free drug divided by AUC_{360} for bound + free drug (total drug in solution).

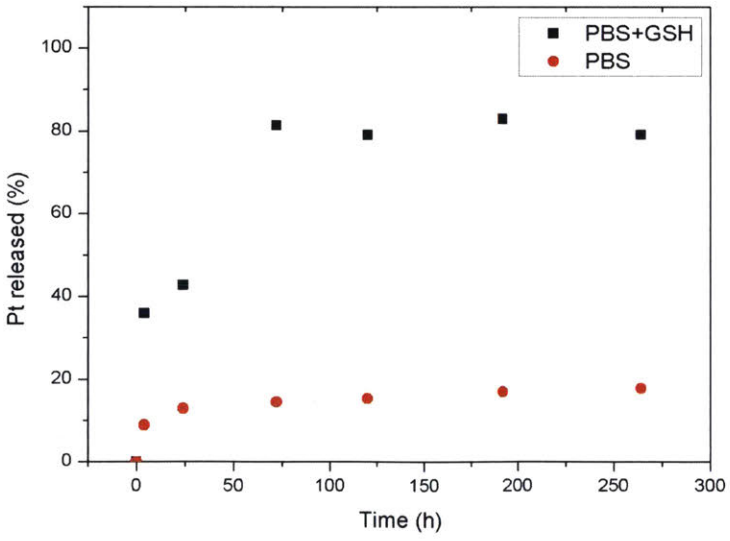

Figure 3.8: Dr. Liao incubated $PEG_{12}Oxali_5$ BASPs at 37 °C in pH 7.4 PBS buffer with or without 10 mM glutathione (GSH) and monitored the release of Pt by ICP-MS.

As stated at the outset of this chapter, our goal was to synthesize nano-FOLFIRINOX BASPs containing oxalipltain, irinotecan or SN38, and 5-fluorouracil. Unfortunately, our efforts to synthesize a 5-fluorouracil-linked macromonomer that could release free 5-fluorouracil under biologically relevant conditions proved difficult. Briefly, an ester based linker for 5-fluorouracil was developed, which we hoped would cleave by hydrolysis and release free drug following a 1,4-benzylic elimination to release free 5-fluorouracil and carbon dioxide (**Scheme 3.7**).[41] In our attempt to prepare the desired carbamate by deprotonation of 5-fluorouracil with sodium hydride followed by coupling with a 4-nitrophenol-carbonate activated benzyl-alcohol, we instead obtained benzyl-linked 5-fluorouracil azide, 5FU-Az, which results from attack of the 5-fluorouracil anion directly at the benzylic position rather than the nitrophenyl carbonate. Nonetheless, 5FU-MM and 5FU-BASP (**$5FU_7PEG_3Acetal_{10}$,** sample GPC trace shown in **Figure 3.9**) were synthesized with the benzyl-linked 5-FU. Unfortunately, both the 5-fluorouracil MM and BASP were orders of magnitude less cytotoxic than free 5-fluorouracil (**Figure 3.10**), likely due to the limited release of 5-fluorouracil.

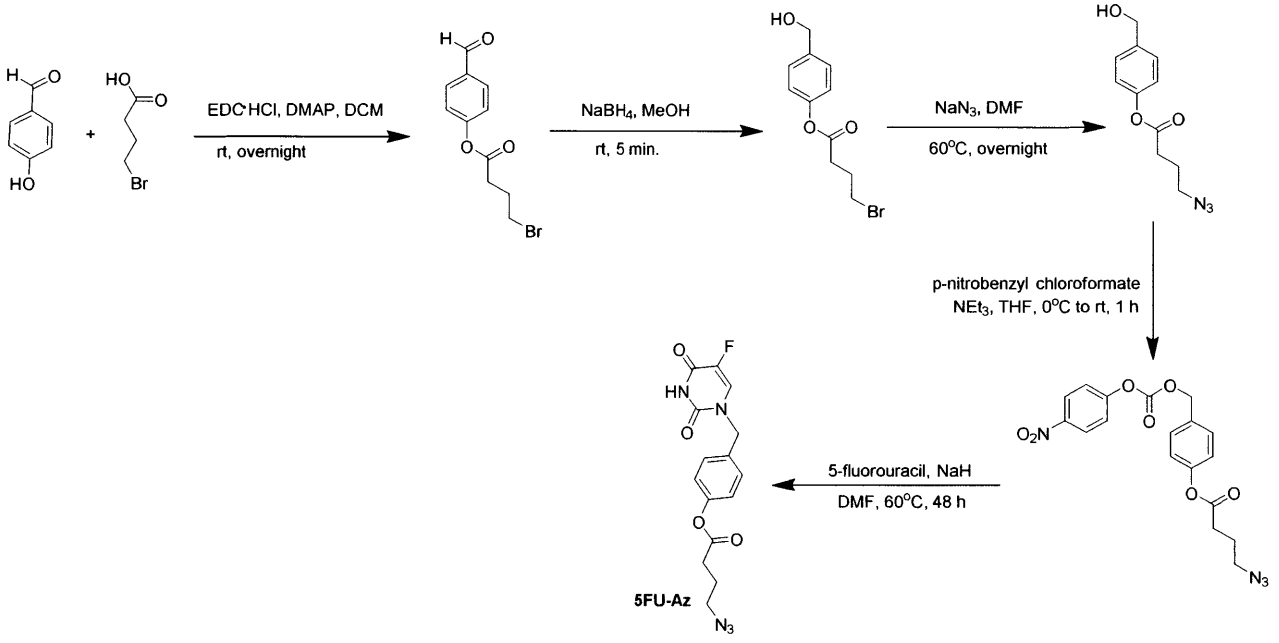

Scheme 3.7: Synthesis of 5FU-Az. A decarboxylation occurs during the coupling of 5-fluorouracil to the linker resulting in a poorly labile benzyl-linked 5FU-Az.

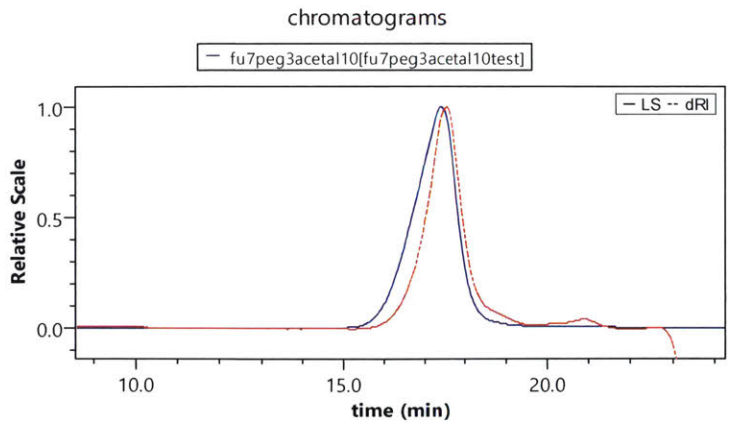

Figure 3.9: Sample GPC-MALLS chromatogram of **$5FU_7PEG_3Acetal_{10}$** with M_n = 437 000 g/mol, M_w = 548 000 g/mol, and $Đ$ = 1.25.

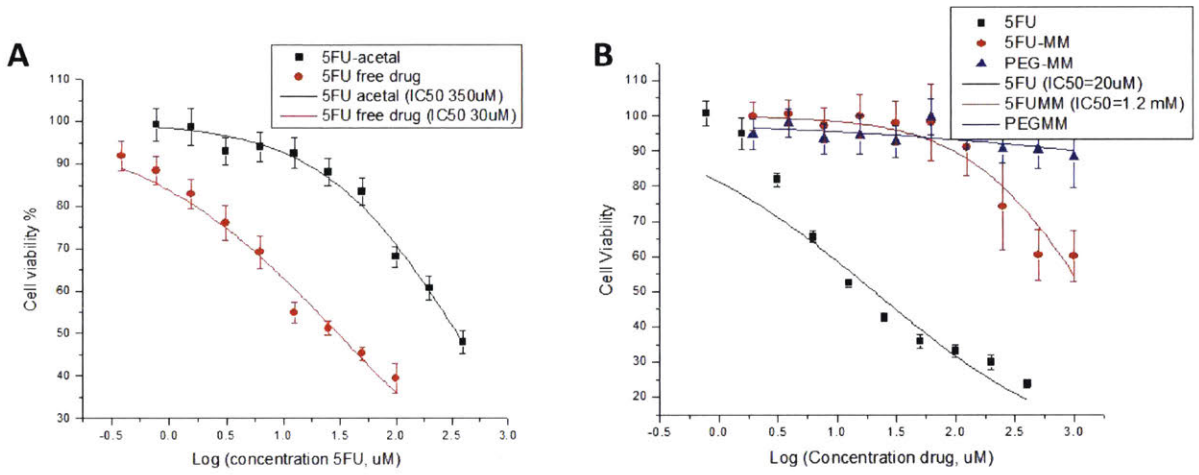

Figure 3.10: Cytotoxicity assay performed on 2980A PDAC cells incubated with 5FU BASP, MM, or drug for 72 hours. A) Cytotoxicity assay comparison between free 5-fluorouracil and **$5FU_7PEG_3Acetal_{10}$**. IC50 values are listed as an average of three trials. B) Cytotoxicity assay comparison among free 5-fluorouracil, PEG-MM, and 5FU-MM. IC50 values are listed as an average of three trials.

The discussion above focuses on BASP synthesis. Here, we describe studies aimed toward the identification of potential synergistic, additive, and antagonistic ratios of the three-drug combination in FOLFIRINOX. Our hope was to determine a synergistic and antagonistic ratio of 5-fluorouracil, SN-38, and oxaliplatin *in vitro*, and then test the efficacy of three-drug synergistic and antagonistic combination BASPs on mouse models of pancreatic cancer. Although combination index studies have been experimentally performed on two-drug systems, three-drug combination experiments are limited to few examples in literature.[42] However, both the Bliss and Chou-Talalay theoretical models of drug synergism/antagonism can be extended to

multi-drug systems.[31,32] The Bliss independence model assumes no drug-drug interactions, and non-overlapping drug targets. In the Bliss model, the theoretical additive drug effect is calculated by summing the fractional dose response of each individual drug, then subtracting the product of the drugs' dose responses. *In vitro* dose response is defined as the cell viability or % killing for a given dose (ie. concentration of drug). For a three drug system, an additive dose response would be defined by the equation: Bliss = (Ea+Eb+Ec)-(Ea*Eb)-(Ea*Ec)-(Eb*Ec) where E is the dose response.[32,42] The three-drug dose response *in vitro* is experimentally determined and compared to the Bliss model's theoretical additive dose response. If the cell killing of a drug ratio is greater than the expected additive result, then we conclude a synergistic drug ratio. On the other hand, if the cell killing is less than the predicted additive cell killing, then we conclude an antagonistic effect.

Though several combination index studies were conducted in these efforts, only one example is provided here (**Table 3.5**). In **Table 3.5A**, the concentrations of drugs used to treat cells in each well of a 96-well plate and their respective drug ratios are shown. For those respective drug ratios, the combination index is represented by the Bliss Excess % and given in **Table 3.5B**. Here, a more positive number indicates drug synergism at the corresponding drug ratios, and a more negative number suggests antagonism based on the Bliss Model.

A

	[5FU]		3.91E-09	7.81E-09	1.56E-08	3.13E-08	6.25E-08	1.25E-07	2.50E-07	5.00E-07	1.00E-06	
[Oxali]	A	B	C	D	E	F	G	H	I	J	K	L
			0.071 5FU	0.14 5FU	0.29 5FU	0.57 5FU	1.14 5FU	2.29 5FU	4.57 5FU	9.14 5FU	18.29 5FU	
		No	0.14 SN38	0.14 SN38	0.14 SN38	0.14 SN38	0.14 SN38	0.14 SN38	0.14 SN38	0.14 SN38	0.14 SN38	Pos.
5.47E-08	1	cells	1 Oxali	1 Oxali	1 Oxali	1 Oxali	1 Oxali	1 Oxali	1 Oxali	1 Oxali	1 Oxali	Con.
			0.036 5FU	0.071 5FU	0.14 5FU	0.29 5FU	0.57 5FU	1.14 5FU	2.29 5FU	4.57 5FU	9.14 5FU	
		No	0.07 SN38	0.07 SN38	0.07 SN38	0.07 SN38	0.07 SN38	0.07 SN38	0.07 SN38	0.07 SN38	0.07 SN38	Pos.
1.09E-07	2	cells	1 Oxali	1 Oxali	1 Oxali	1 Oxali	1 Oxali	1 Oxali	1 Oxali	1 Oxali	1 Oxali	Con.
			0.018 5FU	0.036 5FU	0.071 5FU	0.14 5FU	0.29 5FU	0.57 5FU	1.14 5FU	2.29 5FU	4.57 5FU	
		No	0.03 SN38	0.03 SN38	0.03 SN38	0.03 SN38	0.03 SN38	0.03 SN38	0.03 SN38	0.03 SN38	0.03 SN38	Pos.
2.19E-07	3	cells	1 Oxali	1 Oxali	1 Oxali	1 Oxali	1 Oxali	1 Oxali	1 Oxali	1 Oxali	1 Oxali	Con.
			0.009 5FU	0.018 5FU	0.036 5FU	0.071 5FU	0.14 5FU	0.29 5FU	0.57 5FU	1.14 5FU	2.29 5FU	
		No	0.02 SN38	0.02 SN38	0.02 SN38	0.02 SN38	0.02 SN38	0.02 SN38	0.02 SN38	0.02 SN38	0.02 SN38	Pos.
4.38E-07	4	cells	1 Oxali	1 Oxali	1 Oxali	1 Oxali	1 Oxali	1 Oxali	1 Oxali	1 Oxali	1 Oxali	Con.
			0.004 5FU	0.009 5FU	0.018 5FU	0.036 5FU	0.071 5FU	0.14 5FU	0.29 5FU	0.57 5FU	1.14 5FU	
		No	0.009 SN38	0.009 SN38	0.009 SN38	0.009 SN38	0.009 SN38	0.009 SN38	0.009 SN38	0.009 SN38	0.009 SN38	Pos.
8.75E-07	5	cells	1 Oxali	1 Oxali	1 Oxali	1 Oxali	1 Oxali	1 Oxali	1 Oxali	1 Oxali	1 Oxali	Con.
			0.002 5FU	0.004 5FU	0.009 5FU	0.018 5FU	0.036 5FU	0.071 5FU	0.14 5FU	0.29 5FU	0.57 5FU	
		No	0.004 SN38	0.004 SN38	0.004 SN38	0.004 SN38	0.004 SN38	0.004 SN38	0.004 SN38	0.004 SN38	0.004 SN38	Pos.
1.75E-06	6	cells	1 Oxali	1 Oxali	1 Oxali	1 Oxali	1 Oxali	1 Oxali	1 Oxali	1 Oxali	1 Oxali	Con.
			0.001 5FU	0.002 5FU	0.004 5FU	0.009 5FU	0.018 5FU	0.036 5FU	0.071 5FU	0.14 5FU	0.29 5FU	
		No	0.002 SN38	0.002 SN38	0.002 SN38	0.002 SN38	0.002 SN38	0.002 SN38	0.002 SN38	0.002 SN38	0.002 SN38	Pos.
3.50E-06	7	cells	1 Oxali	1 Oxali	1 Oxali	1 Oxali	1 Oxali	1 Oxali	1 Oxali	1 Oxali	1 Oxali	Con.
			0.001 5FU	0.001 5FU	0.002 5FU	0.004 5FU	0.009 5FU	0.018 5FU	0.036 5FU	0.071 5FU	0.14 5FU	
		No	0.001 SN38	0.001 SN38	0.001 SN38	0.001 SN38	0.001 SN38	0.001 SN38	0.001 SN38	0.001 SN38	0.001 SN38	Pos.
7.00E-06	8	cells	1 Oxali	1 Oxali	1 Oxali	1 Oxali	1 Oxali	1 Oxali	1 Oxali	1 Oxali	1 Oxali	Con.

[SN38] = 7.5E-09 M

B

BLISS EXCESS %									
	C	D	E	F	G	H	I	J	K
1	-13.7	-23.8	-28.8	-19.1	-21.6	-28.1	-31.2	-21.5	-14.5
2	-23.0	-26.1	-26.2	-28.2	-9.7	-25.2	-28.1	-13.0	-8.2
3	-26.0	-46.8	-45.9	-36.0	-13.6	-41.2	-28.7	-21.2	-23.0
4	-30.3	-45.8	-34.4	-22.2	-13.2	-32.2	-20.4	-9.5	-17.2
5	-26.6	-32.9	-25.1	-27.4	-18.0	-23.4	-11.0	-6.8	-10.4
6	-16.6	-31.0	-18.2	-8.6	-7.9	-24.9	-13.9	-13.3	-15.9
7	-15.7	-18.1	-12.7	4.7	6.8	-15.5	-16.4	-29.9	-26.7
8	-12.4	-6.9	-17.5	-12.1	-10.8	-18.9	-20.8	-30.8	-35.1

Table 3.5: A) This table shows the concentration of drugs used to treat the cells in a 96-well plate. The top row displays concentration of 5-fluorouracil across the wells with each vertical column having the same concentration of 5-fluorouracil. The concentration of oxaliplatin changes down the well with each horizontal row having the same concentration of oxaliplatin. The concentration of SN38 is held constant at 7.5 nM. The wells show the ratio of [5FU]:[SN38]:[Oxali]. Thus, D1 would have a ratio of 0.14: 0.14: 1 ratio of [5FU]:[SN38]:[Oxali] corresponding to a concentration of 7.8 nM, 7.5 nM, and 55 nM of 5FU, SN38, and oxaliplatin, respectively. All concentrations listed in the table have units of M. Any value in the well listed in blue font correspond to synthetically feasible ratios where ([5FU]+[SN38] < 1.4). Also the value in green font is the closest one to the IC50 ratio, where the single drug IC50s of 5FU, SN38, and oxaliplatin are 4.8μM, 0.02μM, and 12.4μM, respectively.
B) The Bliss Excess %, shown in this table, is representation of results from a combination index study applying the Bliss Model. A positive number (more red in color) indicates more %killing than expected and synergism. A negative number indicates less %killing than expected and antagonism. The well in white is negligible.

Despite carrying out several combination index assays, the results were not reproducible across assays. Furthermore, given the very different toxicities of these drugs, we could not identify concentrations of each drug that would be both synthetically tractable in BASPs and near the inflection point of the sigmoidal IC50 curves for the individual drug, which is required to avoid going beyond 100% cell killing. Complicating matters further, how conjugation to the PEG-based BASP may affect synergism and antagonism is unknown ways, and any synergistic and antagonistic ratios predicted *in vitro* may not extend or be applicable to complex systems *in vivo.* Therefore, these combination index studies were abandoned, and we decided to move forward with preliminary *in vivo* studies using the ratios of SN-38 and oxaliplatin described above.

The biodistribution and maximum tolerated dose (MTD) of fluorescently-labeled BASPs were explored in an orthotopic mouse model of PDAC. The BASPs were synthesized by the author, and then transferred to Dr. Q. Chen in the Johnson group to perform animal studies. Mice

that had developed orthotopic pancreatic cancer tumors were treated with blank BASP (**$PEG_{10}Acetal_{10}$**) containing approximately 1.5 wt.% Cy7.5-MM. *In vivo* optical imaging (IVIS) indicated that, as expected, the BASP distributed to various organs including the liver, lung, kidney, and tumor, suggesting that the BASP can circulate and accumulate in the pancreatic cancer tumor (**Figure 3.12**). Using control mice without tumors, Dr. Chen ran MTD studies of single drug-conjugated BASPs in mice. The theoretical wt.% of drug in the SN38-loaded BASP was 4.7%, the oxaliplatin-loaded BASP was 7.4%, and the non-labile 5-fluorouracil linked BASP was 2.1% of which the GPCs and formulations are given in **Supplemental Figure 3.S9**. The mice were able to tolerate at least 6.4 mg/kg of each BASP, which was the highest dose studied (**Figure 3.13**). We briefly looked into the MTDs of two three-drug loaded particles (**Figure 3.14**). Sample A had a ratio of 0.2 eq SN38-MM, 4.8 eq PEG-MM, 2 eq 5FU-MM to 5 eq Oxali-XL, whereas sample B had a ratio of 5 eq SN38-MM, 1.5 eq PEG-MM, 0.5 eq 5FU-MM to 5 eq Oxali-XL (GPC-MALS and DLS characterization in **Supplemental Figure 3.S10**). Mice treated with these particles at 3.2 mg/kg did not see any loss in body weight after three days suggesting that the MTD is higher than 3.2 mg/kg. Further studies treating mice with a larger amount of BASP/kg should be performed to determine the MTD, which can help guide us in designing efficacy and survival experiments. Due to issues with synthesizing a labile 5-fluorouracil linker, further *in vivo* studies of biodistribution, efficacy, and survival on orthotopic mouse models treated with FOLFIRINOX BASPs have not yet been performed, but will hopefully be an area of investigation in the future.

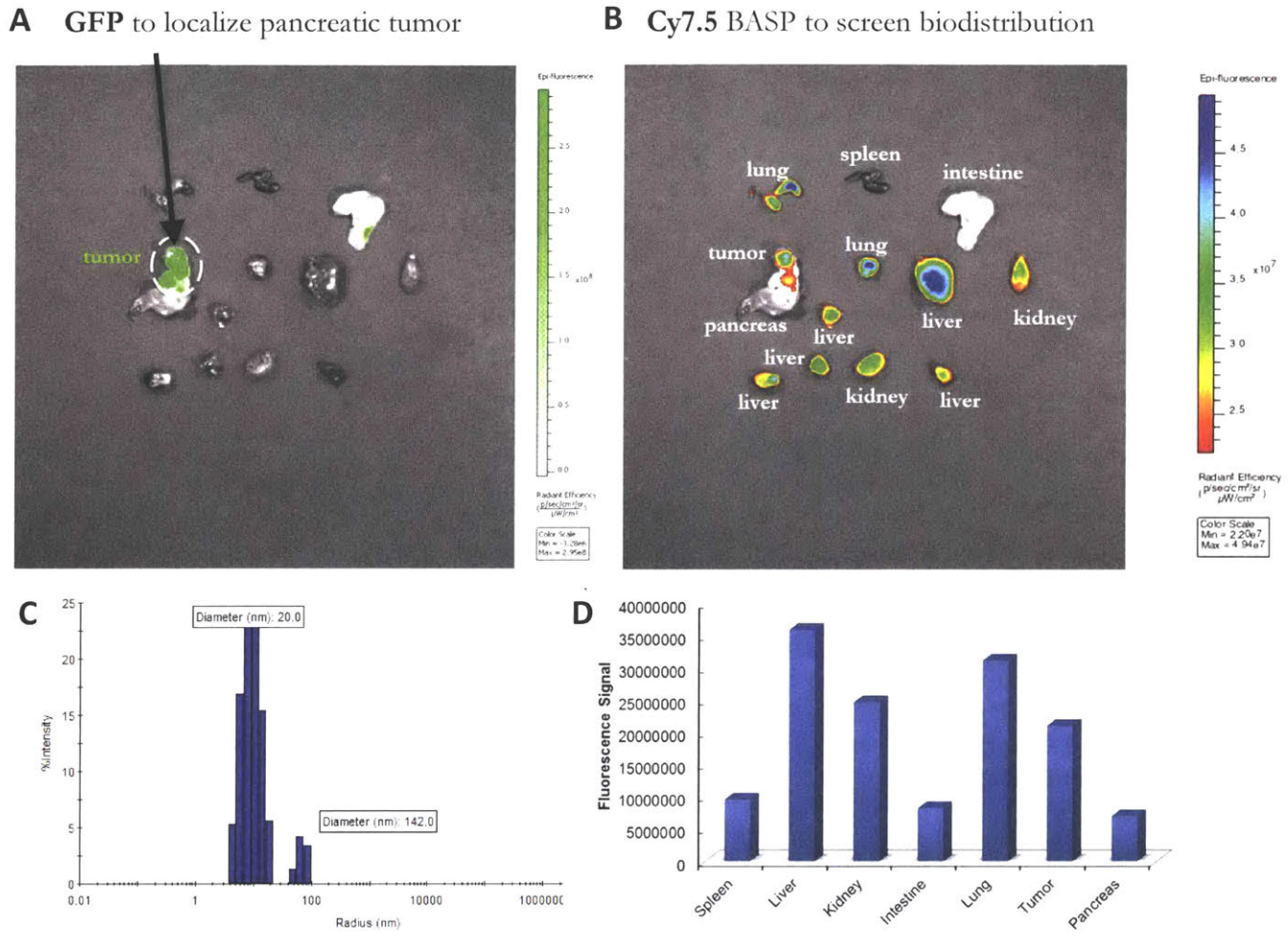

Figure 3.12: A) Green fluorescent protein (GFP) expression shows where the tumor is localized in the mouse model of PDAC. B) Mice with PDAC were also treated with a $\mathbf{PEG_{10}Acetal_{10}}$ BASP containing about 1.5 wt.% Cy7.5-MM. IVIS shows the biodistribution of these particles in mouse tissues. C) The approximate hydrodynamic diameter of the fluorescent $\mathbf{PEG_{10}Acetal_{10}}$ particles by DLS. D) Quantification of the fluorescent signal from Cy7.5 in each organ. Mouse studies were performed by Qixian Chen in the Johnson Lab.

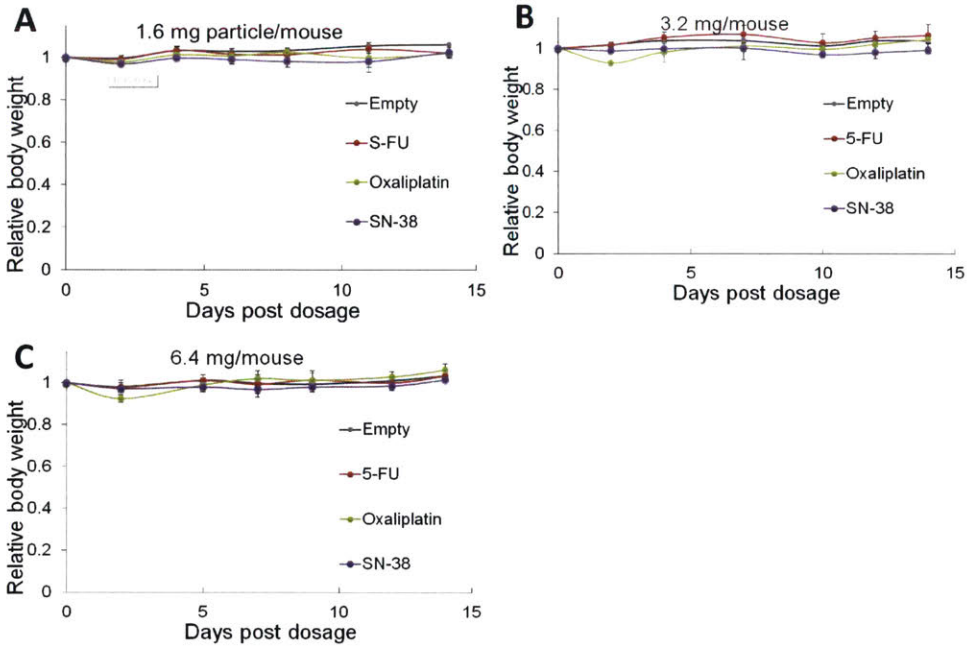

Figure 3.13: MTD studies at A) 1.6 mg particles/mouse, B) 3.2 mg/mouse, and C) 6.4 mg/mouse shows no toxicity at the dosages tested. The empty BASP follows a 10 eq PEG-MM, 10 eq Acetal-XL formulation. The 5-FU BASP consists of 7 eq 5FU-MM, 3 eq PEG-MM, and 10 eq Acetal-XL. The oxaliplatin BASP consists of 7 eq PEG-MM, and 5 eq Oxali-XL. The SN38 BASP consists of a 5 eq SN38-MM, 5 eq PEG-MM, and 10 eq Acetal-XL. GPC characterization of these particles is located in **Supplemental Figure 3.S9**.

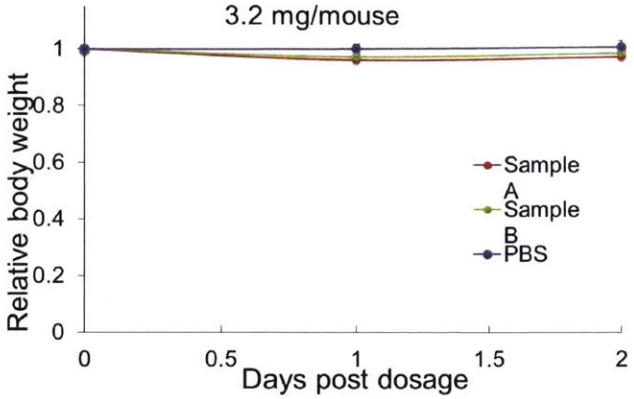

Figure 3.14: MTD study on three-drug loaded BASPs treated at 3.2 mg/mouse. BASP Sample A is a 0.2eq SN38-MM, 2eq 5FU-MM, 4.8eq PEG-MM, 5eq Oxali-XL; and 1.1 wt.% Cy7.5-MM formulation. BASP Sample B is a 5eq SN38-MM; 0.5eq 5FU-MM; 1.5eq PEG-MM; 5eq Oxali-XL; and 1.3 wt.% Cy7.5-MM formulation. GPC-MALLS and DLS characterization can be found in **Supplemental Figure 3.S10**.

3.3 Conclusion

In previous chapters, a method for synthesizing BASPs via ROMP was illustrated. This method is amenable to the formation of multifunctional BASPs through a convergent synthetic strategy. By preparing drug-conjugated macromonomers and crosslinkers, multifunctional nanoparticles conjugated with various drugs can be synthesized with ratiometric control. Due to the success of combination therapy FOLFIRINOX in clinic, polymeric nanoparticles with the components of FOLFIRINOX were synthesized containing the therapeutics: oxaliplatin, 5-fluorouracil, and/or SN38- the pharmacologically active form of irinotecan. Drug combination index assays were used to determine the synergistic, additive, or antagonistic ratios of free SN38, oxaliplatin, and 5-fluorouracil *in vitro*. Once an ideal synergistic ratio is found, BASPs can be synthesized with a synergistic ratio of the three drugs and compared to BASPs loaded with the clinical ratio or an antagonistic ratio. However, the combination index assay proved to be irreproducible because of measurement errors and limitations to the ratios that could be tested. Also, ratios determined *in vitro* may not be applicable with the BASP vehicle nor be relevant *in vivo*. Next, we initiated *in vivo* studies with BASPs and observed promising biodistribution in an orthotopic mouse model of pancreatic cancer and high MTDs suggesting delivery of chemotherapeutics with BASPs may result in fewer off-target effects. In the future, we hope to pursue other applications of BASPs for drug delivery because of the flexibility and potential of the BASP platform to be applied to different types of cancer or diseases.

3.4 Experimental

General Considerations

Unless otherwise noted, all reagents and solvents were purchased from Sigma Aldrich or Alfa Aesar and used as supplied. Grubbs' 2nd generation catalyst was obtained from Materia and converted to G3 using the procedure in chapter one of this thesis. SN38 (as known as 7-ethyl-10-hydroxycamptothecin) was purchased from TCI America. Cyanine7.5-azide was purchased from Lumiprobe. Silica gel used in column chromatography was ZEOprep 60 HYD, 40-63 μm. Compounds purified by flash chromatography were purified on a Biotage Isolera One.

GPC-MALLS characterization was performed on an Agilent 1260 LC system equipped with a Wyatt T-rEX refractive index detector and Wyatt DAWN EOS 18 angle light scattering detector. Samples were run on two Shodex KD-806M GPC columns in series at a temperature of 60 °C, flow rate of 1 ml/min, and dimethyl formamide (DMF) containing 0.025 M LiBr as the eluent.

^{1}H nuclear magnetic resonance (^{1}H-NMR) and ^{13}C nuclear magnetic resonance (^{13}C-NMR) spectra were recorded on Bruker AVANCE-400 MHz NMR spectrometer, VARIAN Inova-500 MHz NMR spectrometer, or a JEOL 500 MHz NMR spectrometer. Spectra were analyzed on MestReNova NMR software. Chemical shifts are expressed in parts per million (ppm); splitting patterns are designated as s (singlet), d (doublet), t (triplet), m (multiplet), and br (broad); and coupling constants, J, are reported in Hertz (Hz).

Samples submitted to the MIT Department of Chemistry Instrumentation Facility (DCIF) for high-resolution mass spectrometry (HRMS) were obtained on a Bruker Daltonics APEXIV 4.7 Tesla Fourier Transform Ion Cyclotron Resonance Mass Spectrometer (FT-ICR-MS).

Matrix-assisted laser desorption ionization time-of-flight (MALDI-TOF) mass spectrometry was analyzed for macromonomers on a Bruker Omniflex MALDI-TOF with a Reflectron accessory. For MALDI-TOF, sample was prepared by dissolving 1 mg of MM in 200 μL MeCN, and matrix was prepared by dissolving approximately 20 mg of α-cyano-4-hydroxycinnamic acid (CHCA) in 500 uL of 1:1 MeCN:water + 0.1% TFA solution to make a saturated solution. 3 μL of sample solution was mixed with 50 μL of matrix solution, then about 0.7 μL of this mixture was spotted onto the MALDI target. Some samples were submitted to the

Koch Institute Biopolymers and Proteomics Core Facility for MALDI-TOF using CHCA as the matrix.

Liquid chromatography-mass spectrometry (LC-MS) was performed on an Agilent 1260 LC system equipped with an Agilent 6130 single quadrupole mass spectrometer. Samples were obtained on an Advanced Materials Technology Halo C18 or an Agilent ZORBAX 300SB-C18 analytical column in a gradient eluent of 0.1% acetic acid in purified water from a MilliQ Biocel A10 water purification system to 100% MeCN.

UV-vis was performed on a 50 Cary spectrophotometer. Dynamic light scattering (DLS) was performed on a Wyatt Technologies Möbiuζ instrument equipped with 660 nm laser. Analysis was performed using Wyatt's Dynamics software.

High-pressure liquid chromatography (HPLC) was performed on an Agilent 1260 LC system equipped with an Agilent ZORBAX 300SB-C18 PrepHT (21.2 x 150 mm) preparative column and using a gradient eluent of 0.1% acetic acid in MilliQ purified water to 100% MeCN.

In vitro cell experiments were performed in a biological safety cabinet belonging to the Essigmann Lab at MIT. A Labconco lyophilizer was used for lyophilization.

Synthesis of 5FU-MM:

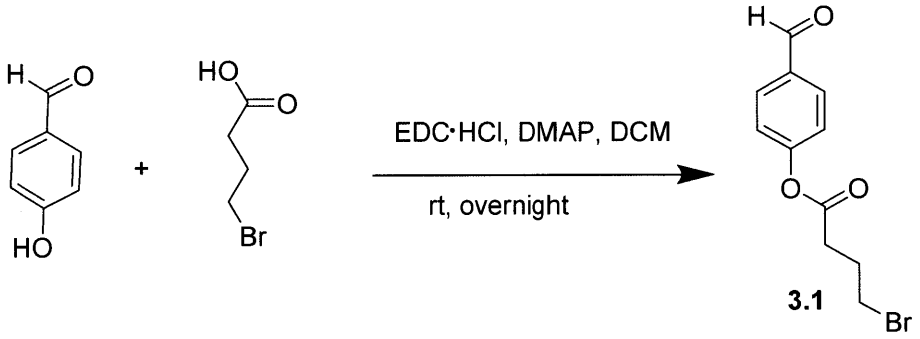

4-formylphenyl 4-bromobutanoate, compound 3.1: 1-bromobutanoic acid (9.5g, 0.057 mol, 3 eq), EDC·HCl (10.9g, 0.057 mol, 3 eq), and DMAP (1g, 0.0082 mol, 0.43 eq) were dissolved in dichloromethane (200 mL) in a dry 500-mL flask equipped with a stirbar. After stirring for 30 min, 4-hydroxybenzoic acid (2.3 g, 0.019 mol, 1eq) was added and the reaction stirred at room temperature overnight. The reaction was washed with 200 mL of water twice and brine once, then dried over magnesium sulfate. After concentration by rotary evaporation, the organic layer was loaded onto a silica cartridge and purified by flash chromatography (0% EtOAc/Hexanes to 50% EtOAc/Hexanes) to afford 4-formylphenyl 4-bromobutanoate (7g crude yield*). ^{1}H NMR

(400 MHz, $CDCl_3$) δ 10.00 (s, 1H), 7.93 (d, J = 8.7 Hz, 2H), 7.29 (d, J = 8.7 Hz, 2H), 3.55 (t, J=6.4 Hz, 2H), 2.82 (t, J=7.2 Hz, 2H), 2.31 (p, J=6.8 Hz, 2H). HRMS: calcd. for $C_{11}H_{11}BrO_3$ $[M+H]^+$, 270.9964; found, 270.9965. *Trace impurities observed in NMR, but does not interfere with next step: ^{1}H NMR (400 MHz, $CDCl_3$) δ 3.69 (t, J=6.1 Hz, 0.41 H), 2.23 (p, J=6.7 Hz, 0.35H) ^{13}C-NMR of product + impurities (100 MHz, CD_2Cl_2) δ 190.86, 170.45, 155.19, 134.08, 131.24, 122.30, 43.82, 32.56, 32.33, 31.33, 27.42, 27.36.

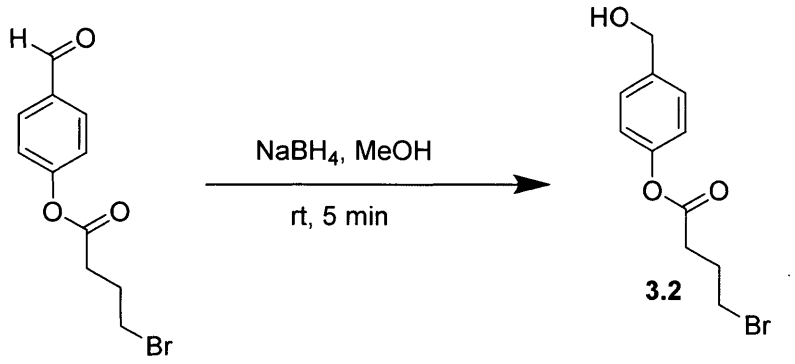

4-(hydroxymethyl)phenyl 4-bromobutanoate, compound 3.2: Sodium borohydride (1g, 0.026 mol, 1 eq) was added to 4-formylphenyl 4-bromobutanoate (7g crude, ~1 eq) dissolved in methanol (100 mL) in a dry 250 mL flask, and stirred for 5 min at room temperature. The reaction was quenched with slow addition of water (150 mL), and product was extracted with 100 mL of dichloromethane three times, then dried over sodium sulfate. After concentration by rotary evaporation, the organic layer was loaded onto a silica cartridge and purified by flash chromatography (0% EtOAc/Hexanes to 70% EtOAc/Hexanes) to afford 4-(hydroxymethyl)phenyl 4-bromobutanoate (3.5 g crude yield*) as a viscous oil. ^{1}H NMR (400 MHz, $CDCl_3$) δ 7.38 (d, J = 8.6 Hz, 2H), 7.08 (d, J = 8.6 Hz, 2H), 4.69 (s, 2H), 3.54 (t, J=6.4 Hz, 2H), 2.78 (t, J=7.1 Hz, 2H), 2.29 (p, J=6.8 Hz, 2H). ^{13}C-NMR (100 MHz, $CDCl_3$) δ 171.17, 149.94, 138.59, 128.09, 121.60, 64.75, 32.54, 32.50, 27.59. HRMS: calcd. for $C_{11}H_{13}BrO_3$ $[M+NH_4]^+$, 290.0386; found, 290.0389 . *Trace impurities observed in NMR, but does not interfere with next step: ^{1}H NMR (400 MHz, $CDCl_3$) δ 4.35 (t, J=7.1 Hz, 0.08H), 3.68 (t, J=6.3 Hz, 0.37H), 2.49 (t, J=8.2 Hz, 0.09 H), 2.22 (p, J=6.7 Hz, 0.35H) ^{13}C-NMR (100 MHz, CD_2Cl_2) δ 31.31, 27.52.

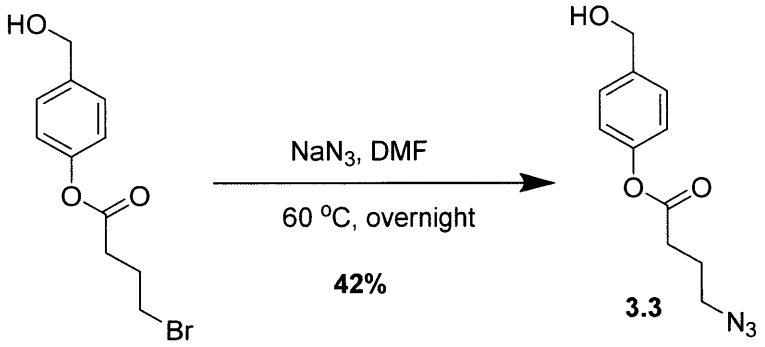

4-(hydroxymethyl)phenyl 4-azidobutanoate, compound 3.3: In a 100 mL round bottom flask equipped with a stirbar, sodium azide (885 mg, 0.014 mol, 1.5 eq) was added to solution of 4-(hydroxymethyl)phenyl 4-bromobutanoate (2.48g, 0.0091 mol, 1 eq) in DMF, then stirred overnight at 60 °C. The reaction was diluted in ethyl acetate (100mL) and washed twice with water, once with brine, then dried over magnesium sulfate. After concentration by rotary evaporation, the organic layer was loaded onto a silica cartridge and purified by flash chromatography (0% EtOAc/Hexanes to 50% EtOAc/Hexanes) to afford 4-(hydroxymethyl)phenyl 4-azidobutanoate (890 mg, 42% yield) as a viscous oil. ^{1}H NMR (500 MHz, $CDCl_3$) δ 7.38 (d, J = 8.5 Hz, 2H), 7.08 (d, J = 8.5 Hz, 2H), 4.69 (s, 2H), 3.45 (t, J=6.6 Hz, 2H), 2.68 (t, J=7.1 Hz, 2H), 2.03 (p, J=6.9 Hz, 2H). ^{13}C-NMR (100 MHz, $CDCl_3$) δ 171.32, 149.95, 138.59, 128.10, 121.59, 64.74, 50.57, 31.27, 24.23. HRMS: calcd. for $C_{11}H_{13}N_3O_3$ $[M+NH_4]^+$, 253.1295; found, 253.1290.

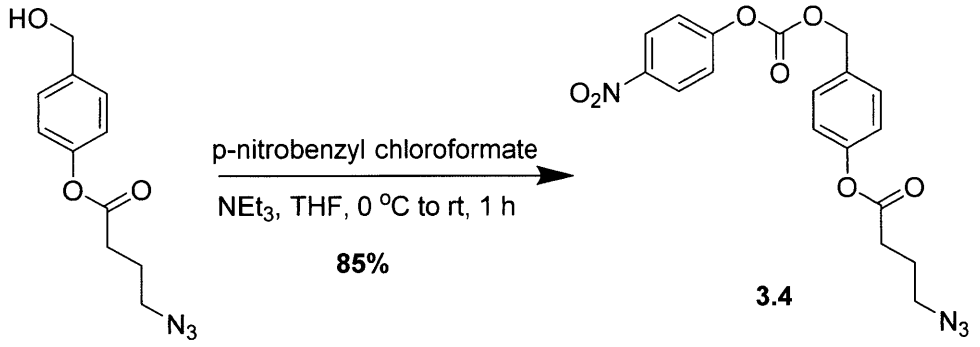

Compound 3.4: 4-(hydroxymethyl)phenyl 4-azidobutanoate (410 mg, 1.7 mmol, 1 eq), and triethylamine (0.45 mL, 3.2 mmol, 1.9 eq) dissolved in THF (10 mL) were added dropwise to a solution of 4-nitrophenyl chloroformate (635 mg, 3.2 mmol, 1.8 eq) stirring in THF (10 mL) in a dry 50 mL round bottom flask at 0 °C under nitrogen. The ice bath was removed and the solution was stirred for 1 h, and then the THF was removed under rotary evaporation. The reaction

mixture was re-dissolved in a small amount of dichloromethane, then loaded onto a silica cartridge and purified by flash chromatography (0% EtOAc/Hexanes to 50% EtOAc/Hexanes) to afford compound 3.4 (0.8 g, 2.0 mmole, 85% yield). ^{1}H NMR (400 MHz, $CDCl_3$) δ 8.28 (d, J = 9.2 Hz, 2H), 7.47 (d, J = 8.5 Hz, 2H), 7.38 (d, J = 9.2 Hz, 2H), 7.14 (d, J = 8.5 Hz, 2H), 5.29 (s, 2H), 3.46 (t, J=6.6 Hz, 2H), 2.70 (t, J=7.2 Hz, 2H), 2.04 (p, J=6.8 Hz, 2H). ^{13}C-NMR (100 MHz, $CDCl_3$) δ 171.15, 155.47, 152.42, 151.06, 145.45, 131.90, 130.10, 125.33, 121.96, 121.79, 70.24, 50.55, 31.28, 24.19. HRMS: calcd. for $C_{18}H_{16}N_4O_7$ $[M+NH_4]^+$, 418.1357; found, 418.1352. *Trace impurities observed in NMR, but does not interfere with next step: ^{1}H NMR (400 MHz, $CDCl_3$) δ 8.17 (d, J = 9.1 Hz, 0.20H), 6.89 (d, J = 9.3 Hz, 0.23H).

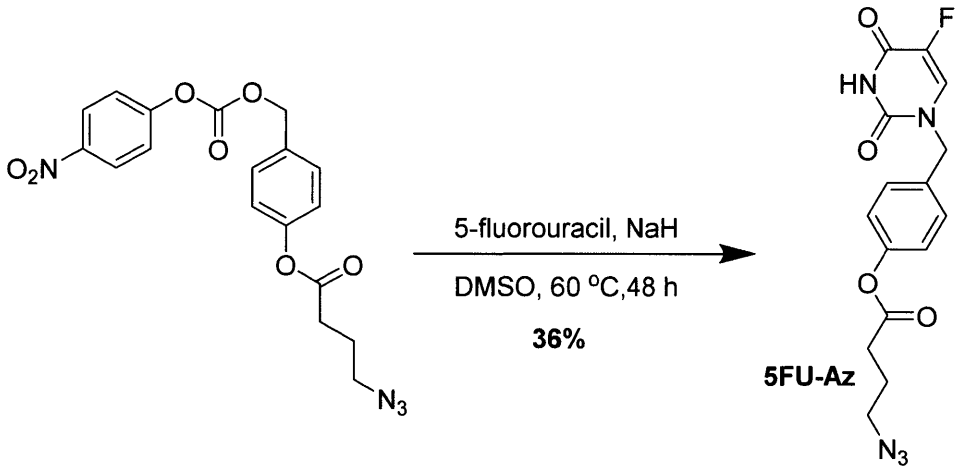

5FU-Azide: Sodium hydride (54 mg, 2.2 mmol, 1.5 eq) was dissolved in DMSO (3 mL) and added dropwise as a slurry to a solution of 5-fluorouracil (390 mg, 3 mmol, 2 eq) stirring in DMSO (5 mL) in a 50 mL round bottom flask under nitrogen. Compound 3.4 (0.6 g, 1.5 mmol, 1 eq) was dissolved in DMSO (5 mL) and added dropwise to the sodium hydride and 5-fluorouracil solution. The reaction was heated to 60 °C and stirred until completed as monitored by LCMS (~48 h). The solution was dissolved in dichloromethane (100 mL) and washed with water (100mL) twice, brine (100 mL) once, then dried over magnesium sulfate. After concentration by rotary evaporation, the reaction mixture was loaded onto a silica cartridge and purified by flash chromatography (0% EtOAc/Hexanes to 100% EtOAc/Hexanes) to afford 5FU-Az (186 mg, 36% yield*) as a white solid. ^{1}H NMR (500 MHz, $CDCl_3$) δ 9.30 (s, 1H), 7.33 (d, J = 8.3 Hz, 2H), 7.21 (d, J = 5.3 Hz, 1H), 7.13 (d, J = 8.3 Hz, 2H), 4.87 (s, 2H), 3.45 (t, J=6.6 Hz, 2H), 2.69 (t, J=7.1 Hz, 2H), 2.02 (p, J=6.8 Hz, 2H). ^{13}C-NMR (125 MHz, $CDCl_3$) δ 171.13, 157.27 (**C**-CF, d, J=26.1 Hz), 150.42 (**C**F, d, J=120.3 Hz), 141.69, 139.79, 132.31, 129.60,

128.01 (CF-**C**, d, J=32.6 Hz), 122.50 , 51.06, 50.60, 31.33, 24.23. HRMS: calcd. for $C_{15}H_{14}FN_5O_4$ $[M+NH_4]^+$, 365.1368; found, 365.1380 . *Trace impurities observed likely isomer: ^{1}H NMR (400 MHz, $CDCl_3$) δ 9.45 (s, 0.09H), 7.57(d, J = 8.5 Hz, 0.13H), 7.02 (d, J = 8.5 Hz, 0.15H), 5.11 (s, 0.13H). ^{13}C-NMR (125 MHz, CD_2Cl_2) δ 131.07, 121.58.

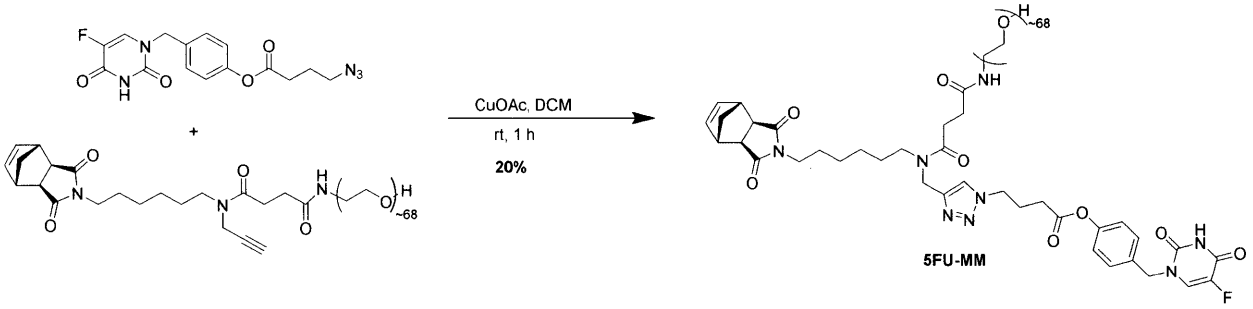

5FU-MM: A 20-mL scintillation vial was charged with 5FU-Az (74.5mg, 0.45 mmol, 1.05 eq), PEG-alkyne-MM (616 mg, 0.43 mmol, 1eq), and a stirbar, and then brought into the glovebox. The reagents were dissolved in dichloromethane (5 mL), followed by addition of approximately 3 eq of copper (I) acetate, and stirred outside the glovebox until complete consumption of PEG-alkyne-MM by LCMS (1 hour). The 5FU-MM was purified by HPLC (10% MeCN and 0.1% acetic acid in MilliQ deionized water to 100% MeCN) twice to remove all unreacted 5FU-azide. Once water was removed by rotary evaporation, the 5FU-MM was redissolved in dichloromethane and dried over sodium sulfate. After concentration by rotary evaporation, the 5FU-MM solid was washed with diethyl ether by centrifugation of solids in ether and decantation of ether. This wash step was repeated three times to afford the 5FU-MM (320 mg, 20% yield) as a powder. ^{1}H-NMR and MALDI-TOF are given in **Supplemental Figure 3.S21** and **3.S22**, respectively.

Synthesis of Az-PEG4-Acid linker:

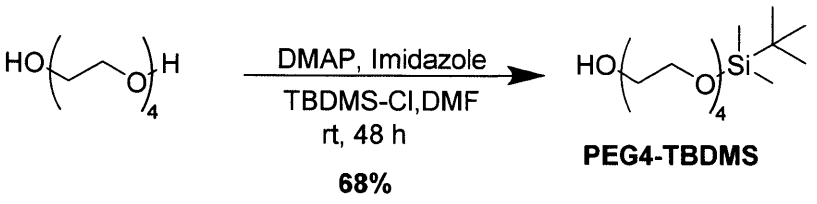

PEG4-TBDMS: Tetraethylene glycol (14 mL, 0.081 mol, 1 eq), imidazole (5.5 g, 0.081 mol, 1 eq), and DMAP (0.99 g, 0.0081 mol, 0.1 eq) were dissolved in 80 mL of anhydrous DMF in a dry flask under nitrogen equipped with an addition funnel and stir-bar. TBDMS-Cl (7.9 g, 0.052 mmol, 0.65 eq) was dissolved in DMF (30 mL) and added via addition funnel slowly to the tetraethylene glycol solution. The reaction was allowed to proceed at room temperature for 48 h, then the solution was concentrated by rotary evaporation. The solution was diluted in water (75 mL), and extracted with ethyl acetate three times (100 mL each). The organic layer was dried over magnesium sulfate, which was removed by filtration. After concentration of the organic layer by rotary evaporation, the reaction mixture was purified by column chromatography (30% EtOAc/Hexanes to remove impurities, 70% EtOAc/Hexanes to 100% EtOAc/Hexanes to elute product) to yield PEG4-TBDMS (11 g, 68% yield with respect to TBDMS-Cl as the limiting reagent) as a clear viscous oil. ^{1}H-NMR, ^{13}C-NMR, and HRMS are as reported in literature.[43]

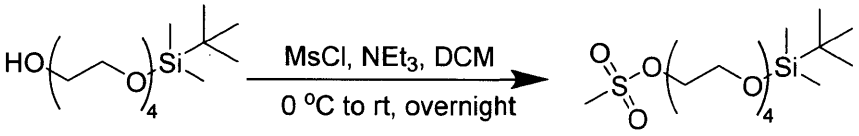

Ms-PEG4-TBDMS: PEG4-TBDMS (11 g, 0.036 mol, 1 eq) was dissolved in 500 mL of anhydrous DCM (250 mL) under nitrogen. The flask was cooled to 0 °C on an ice bath and triethylamine (7.5 mL, 0.054 mol, 1.5 eq) and methanesulfonyl chloride (4.2 mL, 0.054 mol, 1.5 eq) were added sequentially dropwise. The ice bath was removed and reaction was stirred overnight at room temperature. The reaction was washed with water (200 mL) twice and brine (200 mL) once, then dried over magnesium sulfate. The organic layer was concentrated by rotary evaporation, then re-diluted in ethyl acetate (100 mL) and purified by a silica plug to yield Ms-

PEG4-TBDMS as a viscous oil; product was immediately carried over to the next step. ^{1}H-NMR, ^{13}C-NMR, and HRMS are as reported in literature.[43]

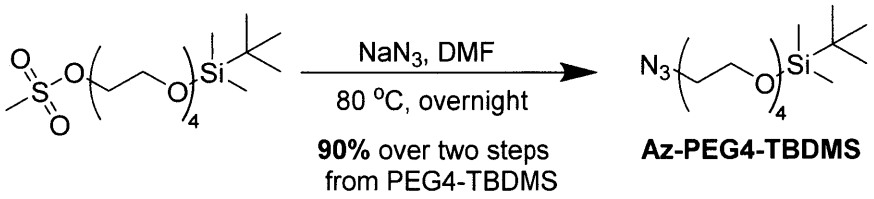

Az-PEG4-TBDMS: Ms-PEG4-TBDMS (from previous step, 0.036 mol of PEG-TBDMS, 1 eq) was dissolved in anhydrous DMF (150 mL) in a dry flask under N_2. Sodium azide (3.5 g, 0.054 mol, 1.5 eq) was added and the reaction was stirred at 80 °C overnight. The solution was carefully concentrated by rotary evaporation, then diluted with ethyl acetate (100 mL) and washed with water twice (100 mL each) and brine once (100 mL), then dried over magnesium sulfate. After concentration of the organic layer by rotary evaporation, the reaction mixture was purified by column chromatography (0% EtOAc/Hexanes to 70% EtOAc/Hexanes) to yield Az-PEG4-TBDMS (10.7 g, 90% yield over two steps with respect to PEG4-TBDMS as the limiting reagent) as a clear viscous oil. ^{1}H-NMR, ^{13}C-NMR, and HRMS are as reported in literature.[43]

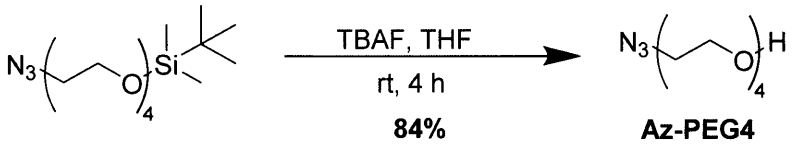

Az-PEG4: TBAF (71.3 mL of a 1 M solution, 0.0713 mol, 1.2 eq) was added to Az-PEG4-TBDMS (19.8 g, 0.059 mol, 1 eq) in anhydrous THF (300 mL), and the reaction was stirred at room temperature for four hours or until complete. The solution was concentrated and directly loaded onto a silica column, then purified by column chromatography (50% EtOAc/Hexanes to 100% EtOAc/Hexanes) to yield Az-PEG4 (10.8 g, 84% yield) as a clear viscous oil. ^{1}H-NMR, ^{13}C-NMR, and HRMS are as reported in literature.[43]

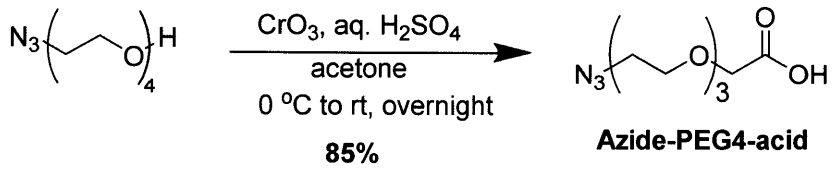

Azide-PEG4-acid

Azide-PEG4-acid: Az-PEG4 (5.2 g, 0.024 mol, 1 eq) was dissolved in acetone (240 mL) and the reaction flask was cooled to 0 °C over an ice bath. Chromium trioxide (7.1 g, 0.071 mol, 3 eq) was dissolved in 1.5 M sulfuric acid solution (142 mL) and added to the reaction via slow dropwise addition from an addition funnel. The ice bath was removed and the reaction was stirred at room temperature overnight. Isopropanol (100 mL) was added slowly to quench the reaction, followed by addition of water (100 mL), and the solution was extracted with dichloromethane twice (100 mL each). The organic layer was dried over magnesium sulfate, which was filtered out; then the solution was concentrated to yield Azide-PEG4-acid (4.7 g, 85% yield). ^{1}H-NMR, ^{13}C-NMR, and HRMS are as reported in literature.[38]

Synthesis of SN38-MM:

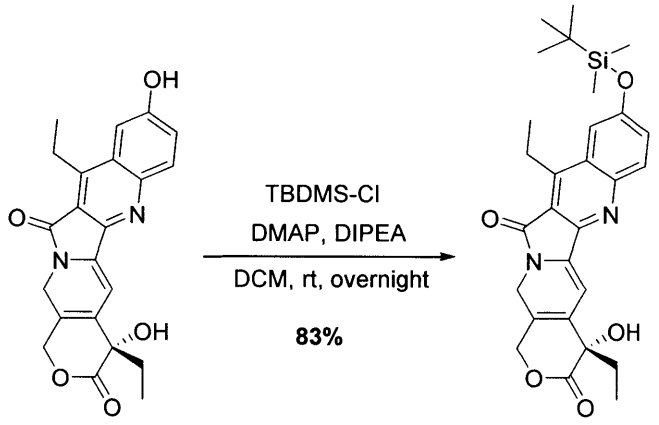

SN38-TBDMS

SN38-TBDMS: In a dry 20-mL scintillation vial, SN38 (150 mg, 0.38 mmol, 1 eq) and DMAP (23.4 mg, 0.19 mmol, 0.5 eq) were dissolved in dichloromethane (5 mL) under N_2, followed by addition of DIPEA (0.066 mL, 0.38 mmol, 1 eq). Next, TBDMS-Cl (69 mg, 0.46 mmol, 1.2 eq) dissolved in dichloromethane (2 mL) was added dropwise to the reaction, and stirred overnight at room temperature. The reaction mixture was loaded directly on a silica cartridge and purified by flash column chromatography (0% EtOAc/Hexanes to 100% EtOAc/Hexanes) to afford SN38-TBDMS (160 mg, 83% yield) as a yellow solid. ^{1}H NMR (400 MHz, $CDCl_3$) δ 8.13 (d, J = 9.5

Hz, 1H), 7.64 (s, 1H), 7.39-7.36 (m, *2*H), 5.52 (dd, *J* = 178, 16 Hz, 2H), 5.23 (s, 2H), 3.90 (s, 1H), 3.11 (q, J=7.7 Hz, 2H), 1.95-1.84 (m, 2H), 1.39 (t, J=7.7 Hz, 3H), 1.04-1.00 (m, 12H), 0.3 (s, 6H). ^{13}C-NMR (100 MHz, $CDCl_3$) δ 174.01, 157.72, 155.24, 150.23, 149.83, 147.20, 145.31, 143.89, 131.96, 128.26, 127.01, 126.14, 117.98, 110.51, 97.70, 72.85, 66.37, 49.44, 31.59, 25.65, 23.20, 18.38, 13.76, 7.86, -4.22 HRMS: calcd. for $C_{28}H_{34}N_2O_5Si$ $[M+H]^+$, 507.2310; found, 507.2317.

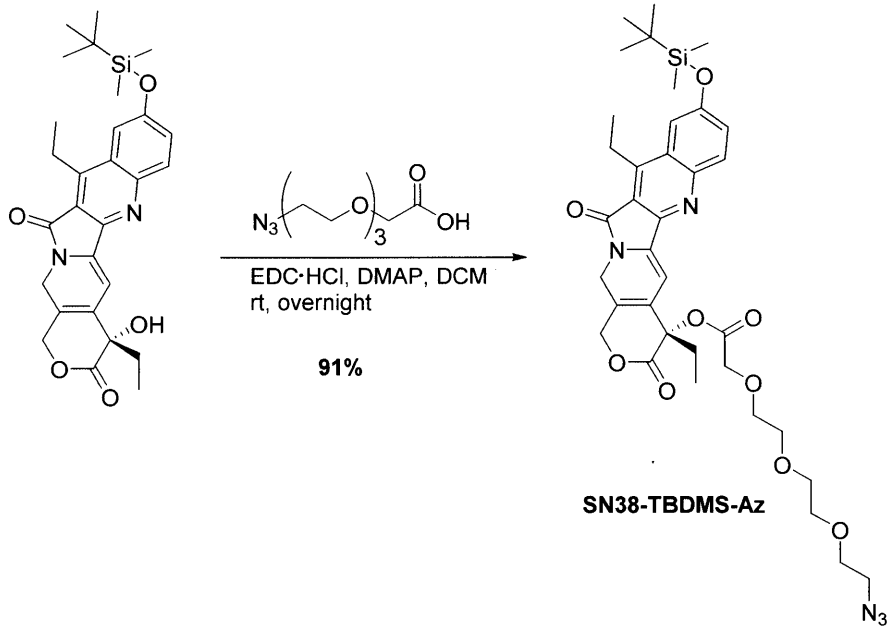

SN38-TBDMS-Az: To a dry 20-mL scintillation vial equipped with a stirbar, azide-PEG4-acid (55 mg, 0.24 mmol, 2 eq), EDC·HCl (45.6 mg, 0.24 mmol, 2 eq), and DMAP (7.3 mg, 0.06 mmol, 0.5 eq) were dissolved in dichloromethane (5 mL). Then SN38-TBDMS (60.2 mg, 0.12 mmol, 1 eq) was added, and the reaction was stirred at room temperature under nitrogen overnight or until complete as monitored by TLC or LCMS. Next, the reaction mixture was loaded directly onto a silica column and purified by flash chromatography (0% EtOAc/Hexanes to 100% EtOAc/Hexanes) to afford SN38-TBDMS-Az (78 mg, 91% yield) as a yellow solid. ^{1}H NMR (400 MHz, $CDCl_3$) δ 8.10 (d, *J* = 9.4 Hz, 1H), 7.4-7.37 (m, *2*H), 7.14 (s, 1H), 5.55 (dd, *J* = 109, 17 Hz, 2H), 5.21 (s, 2H), 4.34 (m, 2H), 3.77-3.63 (m, 10H), 3.36 (t, J = 4.9 Hz, 2H), 3.11 (q, J=7.5 Hz, 2H), 2.33-2.12 (m, 2H), 1.38 (t, J = 7.6 Hz, 3H), 1.04 (s, 9 H), 0.96 (t, J = 7.4 Hz, 3H), 0.31 (s, 6H). ^{13}C-NMR (125 MHz, $CDCl_3$) δ 169.73, 167.44, 157.47, 155.39, 149.67, 147.19, 145.53, 145.25, 144.29, 131.76, 128.43, 126.99, 126.38, 119.76, 110.68, 95.60, 76.47,

71.09, 70.73, 70.08, 68.20, 67.30, 50.73, 49.41, 31.86, 25.76, 23.30, 18.43, 13.84, 7.64, -4.16. HRMS: calcd. for $C_{36}H_{47}N_5O_9Si$ $[M+H]^+$, 722.3216; found, 722.3204.

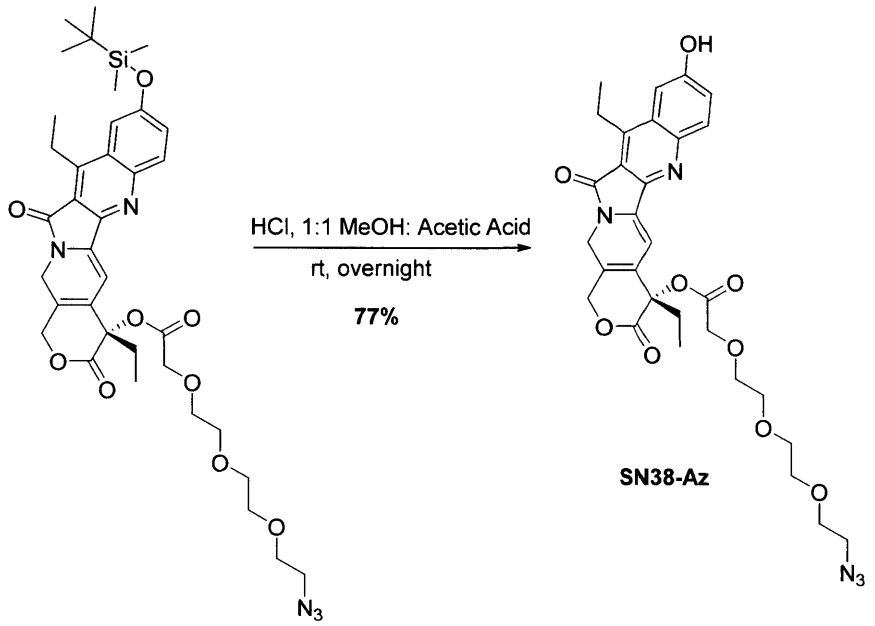

SN38-Az: of Two drops of concentrated HCl from a glass pipette was added to SN38-TBDMS-Az (155 mg, 0.21 mmol, 1 eq) dissolved in a mixture of 1 mL: 1 mL MeOH: acetic acid. The reaction was stirred at room temperature overnight, then diluted with DCM (50 mL). The organic layer was washed with water twice (50 mL), and brine once (50 mL), then dried over magnesium sulfate. After concentration by rotary evaporation, the reaction mixture was loaded onto a silica cartridge and purified by flash chromatography (0% MeOH/DCM to 5% MeOH/DCM) to afford SN38-Az (100 mg, 77% yield) as a yellow solid. ^{1}H NMR (400 MHz, $CDCl_3$) δ 7.97 (d, J = 9.7 Hz, 1H), 7.43-7.39 (m, 1H), 7.27 (m, 1H), 7.12 (s, 1H), 5.56 (dd, J = 62, 17 Hz, 2H), 4.97 (m, 2H), 4.41 (q, 17.4 Hz), 3.84-3.60 (m, 10H), 3.33 (t, J = 5.0 Hz, 2H), 3.00-2.85 (m, 2H), 2.30-2.09 (m, 2H), 1.27 (t, J = 7.4 Hz, 3H), 0.99 (t, J = 7.4 Hz, 3H). ^{13}C-NMR (125 MHz, $CDCl_3$) δ 170.07, 167.37, 157.47, 156.32, 148.58, 147.14, 146.00, 144.33, 143.72, 131.60, 128.49, 126.76, 122.85, 119.23, 105.33, 95.62, 76.79, 71.16, 70.65, 70.05, 68.12, 67.15, 50.68, 49.33, 31.72, 23.12, 13.59, 7.86. HRMS: calcd. for $C_{30}H_{33}N_5O_9Si$ $[M+H]^+$, 608.2351; found, 608.2352.

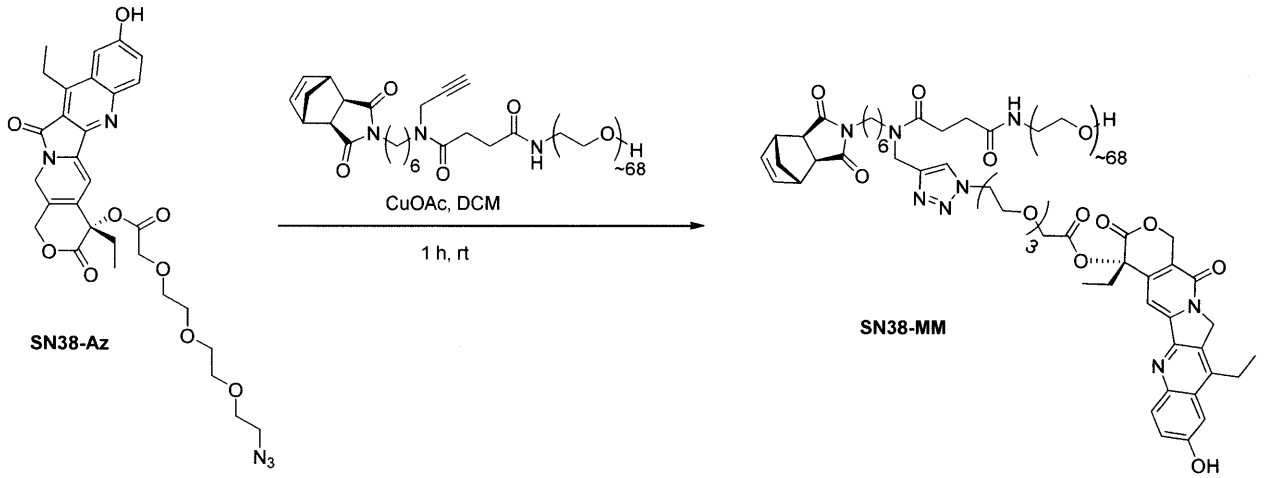

SN38-MM: A 20-mL scintillation vial was charged with SN38-Az (75.8 mg, 0.13 mmol, 1.05 eq), PEG-alkyne-MM (404 mg, 0.12 mmol, 1 eq), and a stirbar, then brought into the glovebox. The reagents were dissolved in dichloromethane (5 mL), followed by addition of approximately 3 eq of copper (I) acetate, and allowed to stir outside the glovebox until complete consumption of PEG-Alkyne-MM by LCMS (1 h). The SN38-MM was purified by HPLC (10% MeCN and 0.1% acetic acid in MilliQ deionized water to 100% MeCN) twice to remove all unreacted SN38-Az. Once water was removed by rotary evaporation, the SN38-MM was redissolved in dichloromethane and dried over sodium sulfate. After concentration by rotary evaporation, the SN38-MM solid was washed with diethyl ether by centrifugation of solids in ether and decantation of ether. This wash step was repeated three times to afford SN38-MM as a yellow powder. ^{1}H-NMR and MALDI-TOF are given in **Supplemental Figure 3.S29** and **3.S30**, respectively.

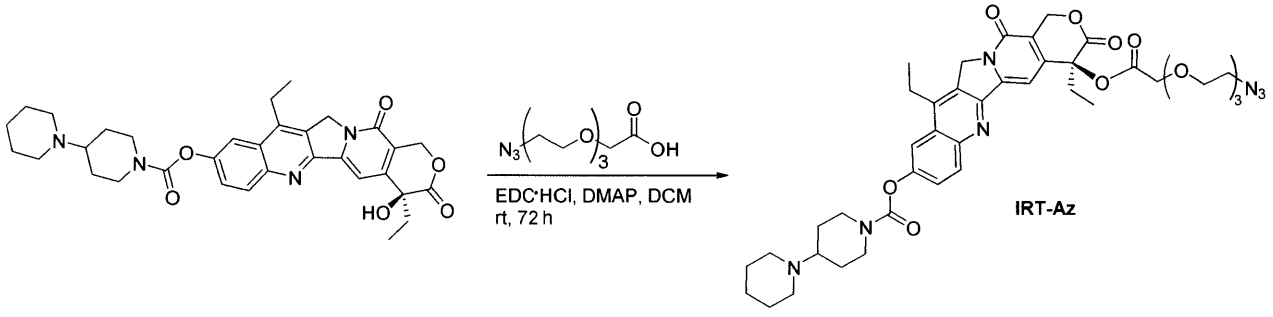

IRT-Az: To a dry 20-mL scintillation vial equipped with a stirbar, azide-PEG4-acid (150 mg, 0.64 mmol, 2 eq), EDC·HCl (1.84 g, 9.6 mmol, 30 eq), and DMAP (312 mg, 2.6 mmol, 8 eq) were dissolved in dichloromethane (5 mL). Then irinotecan trihydrate hydrochloride (218 mg,

0.32 mmol, 1 eq) and triethylamine (0.04 mL, 0.32 mmol, 1 eq) was added, and the reaction was stirred under nitrogen until complete as monitored by TLC or LCMS (~72 h). Next, the reaction mixture was loaded directly onto a silica column and purified by flash chromatography (0% EtOAc/Hexanes to 100% EtOAc/Hexanes) to afford IRT-Az as a pale yellow solid. ^{1}H-NMR is given in **Supplemental Figure 3.S31**.

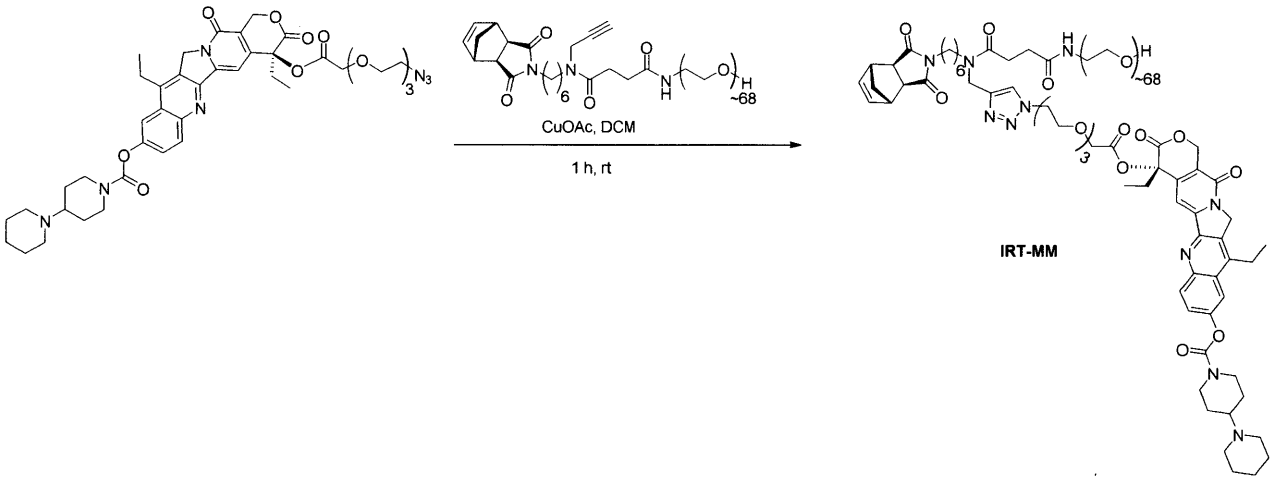

IRT-MM: A 20-mL scintillation vial was charged with IRT-Az (61.8 mg, 0.077 mmol, 1.05 eq), PEG-alkyne-MM (247 mg, 0.073 mmol, 1 eq), and a stirbar, then brought into the glovebox. The reagents were dissolved in dichloromethane (5 mL), followed by addition of approximately 3 eq of copper (I) acetate, and allowed to stir outside the glovebox until complete consumption of PEG-alkyne-MM by LCMS (1 h). The IRT-MM was purified by HPLC (10% MeCN and 0.1% acetic acid in MilliQ deionized water to 100% MeCN) twice to remove all unreacted IRT-Az. Once water was removed by rotary evaporation, the IRT-MM was redissolved in dichloromethane and dried over sodium sulfate. After concentration by rotary evaporation, the IRT-MM solid was washed with diethyl ether by centrifugation of solids in ether and decantation of ether. This wash step was repeated three times to afford the IRT-MM as a yellow powder. ^{1}H-NMR and MALDI-TOF are given in **Supplemental Figure 3.S32** and **3.S33**, respectively.

Synthesis of Oxali-XL:

Synthesis of Norb-glycine is reported in Chapter 1 of this thesis. Oxidized oxaliplatin was prepared by Longyan Liao in the Johnson group in a procedure similar to that of oxidized cisplatin.[38,44]

Norb-glycine-anhydride

Norb-glycine-anhydride: Norb-glycine (1g, 4.5 mmol, 2 eq) and DCC (0.474g, 2.3 mmol, 1 eq) was stirred in anhydrous dichloromethane (70 mL) over two days under nitrogen. Solids that formed in solution were filtered out, then the filtrate was dried *in vacuo* and placed under high vacuum to afford norb-glycine-anhydride as a white solid. ^{1}H-NMR, ^{13}C-NMR, and HRMS are as reported in literature.[38]

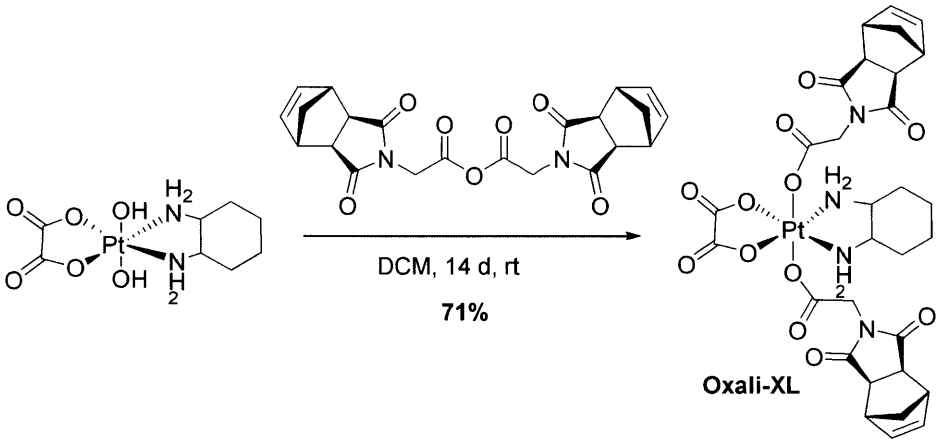

Oxali-XL

Oxali-XL: Oxidized oxaliplatin (50 mg, 0.126 mmol, 1 eq) and norbornene-glycine-anhydride (275 mg, 0.648 mmol, 5.14 eq) were stirred in anhydrous dichloromethane under nitrogen over two weeks or until oxidized oxaliplatin was consumed as monitored by crude ^{1}H-NMR. Dichloromethane was removed in vacuo, and the solids were washed in EtOAc by centrifugation of solids in EtOAc, followed by decantation of EtOAc. The centrifugation and decantation steps were repeated 6 times or until all norbornene glycine based impurities were removed to afford Oxali-XL (75 mg, 0.0895 mmol, 71% yield) as a white solid. ^{1}H NMR (500 MHz, DMSO-d_6) δ 8.27 (s, 2H), 7.77 (s, 2H), 6.31 (s, 4H), 4.17 (s, 4H), 3.10 (1, 4H), 2.71 (s, 4H), 2.54 (br, 2H), 2.09 (br, 2H), 1.54-1.11 (m, 10H).

Synthesis of Acetal-XL:

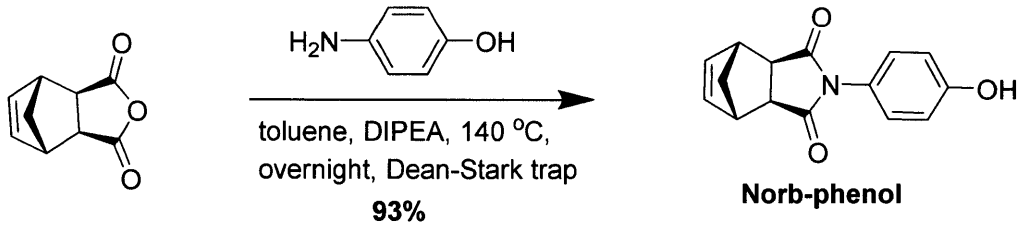

Norb-phenol

Norb-phenol: *Exo*-norbornene anhydride (8.0 g, 0.049 mol, 1 eq), 4-aminophenol (5.3g, 0.049 mol, 1.05 eq), and DIPEA (8.5 mL, 0.049 mol, 1 eq) was dissolved in 100 mL of toluene in a 250 mL round bottom flask equipped with stirbar, Dean-Stark trap, and reflux condenser. The oil bath was heated to 140 °C or until solvent was refluxing, and stirred overnight. The heat was turned off and the reaction was allowed to reach room temperature, then placed in a -20 °C freezer. If necessary, the inside of the glassware was scratched to induce the product to precipitate out of solution. The solid product was filtered and washed with small amounts of toluene, then dried on high vacuum overnight to yield Norb-phenol (11.6 g, 93%). ^{1}H-NMR, ^{13}C-NMR, and HRMS are as reported in literature. ^{1}H-NMR, ^{13}C-NMR, and HRMS are as reported in literature.[40]

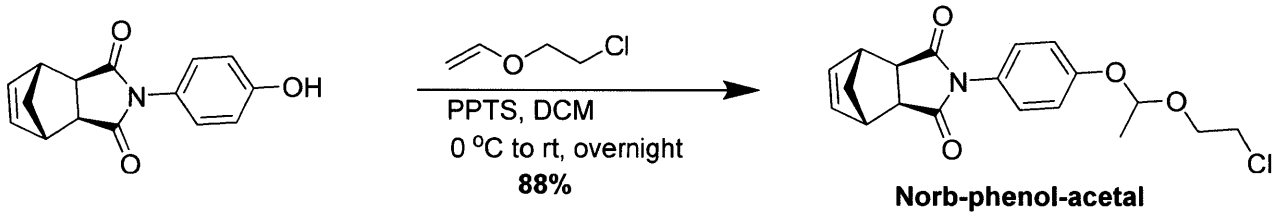

Norb-phenol-acetal

Norb-phenol-acetal: Norb-phenol (1.0 g, 3.9 mmol, 1 eq) and pyridinium p-toluenesulfonate (0.098 g, 0.39 mmol, 0.1 eq) were dissolved in anhydrous DCM (100 mL) in a dry flask under N_2. The reagents were chilled to 0 °C in an ice bath and 2-chloroethyl vinyl ether (2.0 mL, 19.7 mmol, 5 eq) was added dropwise. The ice bath was removed and the reaction was stirred at room temperature overnight. The reaction was washed with saturated sodium bicarbonate solution (100 mL), water (100 mL), and brine (100 mL), and then the organic layer was dried over sodium sulfate. After concentration of the organic layer by rotary evaporation, the reaction mixture was loaded onto a silica cartridge and purified by flash chromatography (0% EtOAc/Hexanes to 30% EtOAc/Hexanes) to afford Norb-phenol-acetal (1.24 g, 88% yield) as a solid. ^{1}H-NMR, ^{13}C-NMR, and HRMS are as reported in literature.[40]

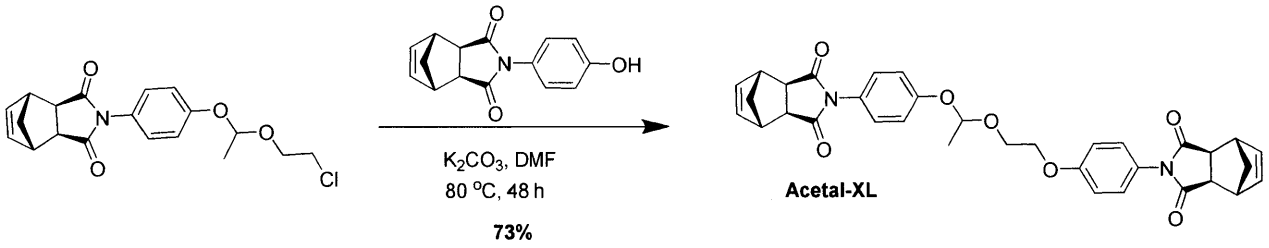

Acetal-XL: Norb-phenol-acetal (250 mg, 0.69 mmol, 1 eq), norb-phenol (350 mg, 1.4 mmol, 2 eq), and potassium carbonate (192 mg, 1.4 mmol, 2 eq) were dissolved in anhydrous DMF (15 mL) in a dry flask under N_2. The reaction was heated to 80 °C and stirred for 48 h or until complete as monitored by LCMS. The reaction was diluted with DCM (100 mL) and washed with saturated sodium bicarbonate solution (100 mL), water (100 mL), and brine (100 mL), and then the organic layer was dried over sodium sulfate. After concentration of the organic layer by rotary evaporation, the reaction mixture was loaded onto a silica cartridge and purified by flash chromatography (slow gradient of 0% EtOAc/Hexanes to 50% EtOAc/Hexanes). If necessary, the solid product was washed with diethyl ether to remove DMF to yield Acetal-XL (292 mg, 73% yield). ^{1}H-NMR, ^{13}C-NMR, and HRMS are as reported in literature.[40]

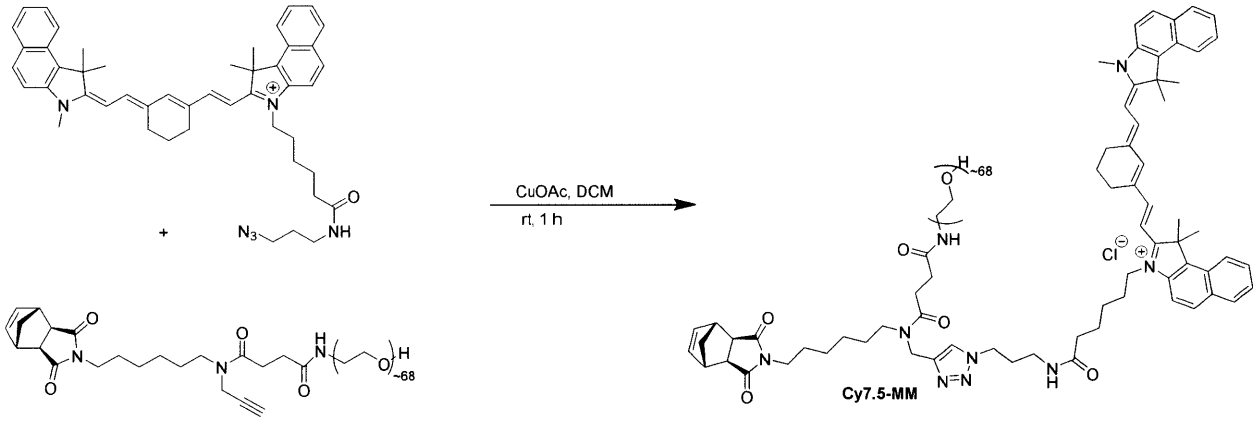

Cy7.5-MM: A 20-mL scintillation vial was charged with Cy7.5-Az (25.4 mg, 0.034 mmol, 1.03 eq), PEG-alkyne-MM (111 mg, 0.033 mmol, 1.0 eq), and a stirbar, then brought into the glovebox. The reagents were dissolved in dichloromethane (2 mL), followed by addition of approximately 3 eq of copper (I) acetate, and allowed to stir outside the glovebox until complete consumption of PEG-Alkyne-MM as monitored by LCMS (1 h). The Cy7.5-MM was purified by HPLC (10% MeCN and 0.1% acetic acid in MilliQ deionized water to 100% MeCN) to

remove all unreacted Cy7.5-Az. Once water was removed by rotary evaporation, the Cy7.5-MM was redissolved in dichloromethane and dried over sodium sulfate. After concentration by rotary evaporation, the solid was washed with diethyl ether by centrifugation of solids in ether and decantation of ether. This wash step was repeated three times to afford Cy7.5-MM as a dark green powder. ^{1}H-NMR and MALDI provided in **Supplemental Figure 3.S35** and **3.S36**, respectively.

General Procedure for synthesis of BASPs by ROMP:

All ROMP reactions were performed in a glovebox. The published JOVE video can be used as a visual reference.[45]

1. ROMP using Oxali-XL

a. Living brush initiator solution: Drug-loaded MM (m_1 eq) and PEG-MM ($7 - m_1$ eq) was added to a 4 or 2 mL vial containing a stirbar (the total MM equivalents, m, is equal to 7 eq), then dissolved in THF. The volume of THF to use is calculated as the volume required for a 0.05 M solution of MM minus the volume of G3 solution to add in the next step. G3 was dissolved in THF to make a 0.02 g/mL solution, then G3 (1 eq) was added to the solution of MMs. The final concentration of MMs in solution should be 0.05 M. ROMP of MMs was allowed to proceed for 15 min to make a living brush solution, which was used immediately in formation of BASPs.

b. BASP formation: From this stock solution, living brush initiator (1 eq) was aliquoted into pre-weighed vials containing Oxali-XL (N= 5 eq). After ROMP had proceeded for 6 h, the reaction was quenched with ethyl vinyl ether (approximately 50 eq).

c. BASP workup: For general workup, the BASP solution is diluted with approximately one volume equivalent of MilliQ purified water, and then dialyzed against MilliQ purified water (1000 mL water per 1 mL of BASP solution). After three rounds of dialysis for 2-3 h each, the BASP solution was carefully added to scintillation vial(s). The

solution was frozen over liquid nitrogen and placed on a lyophilizer for 2-3 d to yield the BASP as a fluffy powder.

Example: SN38-MM (89.3 mg, 0.022 mmol, 5 eq), 5FU-MM (8.5 mg, 0.0022 mmol, 0.5 eq), and PEG-MM (21.4 mg, 0.0067 mmol, 1.5 eq) were weighed into a 4 mL vial. Also, a 0.02 g/mL stock solution of G3 in THF was prepared. For a 0.05 M solution of MMs, we would need 625 μL total volume of THF, and we would also need 162.3 μL of G3 from a 0.02 g/mL stock (0.0045 mmol, 1 eq). Thus, we dissolved MMs in 625 μL – 162.3 μL = 463 μL of THF and stirred until MMs were dissolved. Next we added the 162.3 μL of G3 from a 0.02 g/mL G3 stock solution. ROMP of MMs was allowed to proceed for 15 min to make a living brush solution. We added 568 μL of this living brush solution (0.0040 mmol) directly to a separate vial containing Oxali-XL (17 mg, 0.020 mmol), such that the crosslinker is in 5 eq to the brush. The leftover brush solution is quenched with a few drops of ethyl vinyl ether, and analyzed on GPC. The BASP reaction is allowed to stir for 6 h before quenching with a few drops of ethyl vinyl ether, followed by analysis by GPC and workup. For workup, the BASP solution is diluted with approximately one volume equivalent of water (500 μL), then dialyzed against MilliQ purified water (1000 mL water per 1 mL of BASP solution). After three rounds of dialysis for 2-3 h each, the BASP solution was carefully added to a scintillation vial. The solution was frozen over liquid nitrogen and placed on a lyophilizer for 2-3 d to yield the BASP as a fluffy powder.

2. *ROMP using Acetal-XL*

a. **Living brush initiator solution:** Drug-loaded MM (m_1 eq) and PEG-MM ($10 - m_1$ eq) was added to a 4 or 2 mL vial containing a stirbar (the total MM equivalents, m, is equal to 10 eq), then dissolved in THF. The volume of THF to use is calculated as the volume required for a 0.1 M solution of MM minus the volume of G3 solution to add in the next step. G3 was dissolved in THF to make a 0.02 g/mL solution, then G3 (1 eq) was added to the solution of MMs. The final concentration of MMs in solution should be 0.1 M. ROMP of MMs was allowed to proceed for 15 min to make a living brush solution, which was used immediately in formation of BASPs.

b. **BASP formation:** Acetal-XL is dissolved in THF to make a 0.1 M stock solution. The solution of acetal-XL (10 eq) is added dropwise slowly to living brush initiator (1 eq) solution. After ROMP had proceeded for 2 h, the reaction was quenched with ethyl vinyl ether (approximately 50 eq).

c. **BASP workup:** For general workup, the BASP solution is diluted with approximately one volume equivalent of MilliQ purified water, and then dialyzed against MilliQ purified water (1000 mL water per 1 mL of BASP solution). After three rounds of dialysis for 2-3 h each, the BASP solution was carefully added to scintillation vial(s). The solution was frozen over liquid nitrogen and placed on a lyophilizer for 2-3 d to yield the BASP as a fluffy powder.

Example: SN38-MM (18.6 mg, 0.0048 mmol, 5 eq) and PEG-MM (15.3 mg, 0.0048 mmol, 5 eq) were weighed into a 4 mL vial. Also, a 0.02 g/mL stock solution of G3 in THF was prepared, as well as a 0.1 M stock solution of Acetal-XL in THF. For a 0.1 M solution of MMs, we would need 95.4 μL total volume of THF, and we would also need 34.6 μL of G3 from a 0.02 g/mL stock (0.00095 mmol, 1 eq). Thus, we dissolved MMs in 95.4 – 34.6 μL = 60.8 μL of THF and stirred until MMs were dissolved. Next we added the 34.6 μL of G3 from the 0.02 g/mL G3 stock solution. ROMP of MMs was allowed to proceed for 15 min to make a living brush solution. Acetal-XL (95.4 μL of the 0.1M stock, 0.0095 mmol, 10 eq) is added dropwise slowly to the living brush solution. The BASP reaction is allowed to stir for 1-2 h before quenching with a few drops of ethyl vinyl ether, followed by analysis by GPC and workup. For workup, the BASP solution is diluted with approximately one volume equivalent of water (100 μL), then dialyzed against MilliQ purified water (1000 mL water per 1 mL of BASP solution). After three rounds of dialysis for 2-3 h each, the BASP solution was carefully added to a scintillation vial. The solution was frozen over liquid nitrogen and placed on a lyophilizer for 2-3 d to yield the BASP as a fluffy powder.

UV-vis drug loading calculation for SN38 and irinotecan:

Free SN38 or irinotecan was weighed out in triplicate on a high precision balance (~1 mg) and dissolved in solvent to make a 1.00 mg/mL. The drugs were diluted in solvent 20-fold or until necessary to be just within the UV-vis maximum absorbance range. From this concentration, a two-fold serial dilution was performed to prepare 5-6 standards. A UV-vis absorbance reading at 359 nm was taken of all standards, and $Abs_{359} - Abs_{800}$ was plotted against the concentration. The slope of the curve was used to determine the extinction coefficient. Path-length of the UV-vis cuvette was 1 cm. A sample of drug-loaded BASP was weighed out in triplicate on a high precision balance (~1 mg), and dissolved in the same solvent used for the extinction coefficient determination. If necessary, dilutions were made and the absorbance at 359 nm was obtained. Using Beer's law, the concentration of drug in solution was calculated, converted to a mass value, and divided against the mass of BASP in solution, in order to determine drug loading.

LCMS drug release assay for SN38 or irinotecan:

BASP was dissolved in PBS buffered at pH 7.5 at a concentration of 1 mg/mL in a sealed vial. The BASP was incubated in a 37 °C incubator, and solution was taken out at different time points for LCMS, then returned to the vial. LCMS was performed on an Agilent ZORBAX 300SB-C18 analytical column running at a 0.5 mL/min flowrate using a gradient eluent of solvent A: MilliQ purified water with 0.1% acetic acid to solvent B: 100% acetonitrile. The absorbance was monitored at 360 nm, and the AUC at 360 nm was determined for the free drug and BASP peak. The % drug release was calculated as $AUC_{free}/(AUC_{free} + AUC_{bound}) \times 100\%$. A plot of % drug release vs. time over 8 d was determined for each BASP sample.

In vitro cytotoxicity assays on 2980A PDAC cells:

2980A PDAC cells were obtained from the Ghoroghchian lab, and grown in media containing Dulbecco's Modification of Eagle's Medium (DMEM) with 4.5 g/L glucose, L-glutamine, and sodium pyruvate, 10% fetal bovine serum, and 1% penicillin-streptomycin (10

000 U/mL) antibiotic solution. All cells were incubated in a humidity controlled cell incubator at 37 °C and 5% CO_2. All cell work was performed in the Essigmann Lab cell culture room and biological safety cabinets. These cells were grown in tissue-culture treated 75 cm^2 culture flasks and passaged at least once before use in assays. A solution of 0.25% Trypsin with 2.21 mM EDTA was used for cell detachment. Proper sterilization technique and sterile procedures were used with cells.

When cells were between 70% to 90% confluent, the cells were seeded at 500-5000 cells/ well in a 96-well plate using a hemocytometer to count the cells, leaving one or two columns blank. The cells were left overnight, then cell media was removed and replaced with cell media containing BASPs or free drug with concentration of drug increasing across the plate. Also, one column of the 96-well plate was reserved for media with no drug as the negative control, and another column had media with MG-132 (10 μM) as the positive control. Generally BASPs and free drugs containing only oxaliplatin or 5-fluorouracil had an upper concentration in the 100s of μM and we used a two-fold serial dilutions with each adjacent vertical column. BASPs and free drugs with SN38 or irinotecan had an upper concentration in the low uM and we used a two-fold serial dilution with each adjacent vertical column. After 72 h of incubation with BASP or free drug, either a CellTiter-Glo (CTG) luminescent cytotoxicity assay or a standard MTT assay was performed and a plate reader was used at the Koch Institute to take measurements. For the MTT assay, the absorbance signal of 570 nm – 650 nm for each well was calculated, and then the average signal at each drug concentration was divided by the average signal from the negative control×100% to determine the % cell viability, which was plotted against log of drug concentration. For the CTG assay, all measurements were blank corrected, and then the average luminescent signal at each drug concentration was divided by the average luminescent signal from the negative control ×100% to determine the % cell viability, which was plotted against log of drug concentration. Using OriginPro8 software, the plot was fit to a Sigmoidal curve (**Equation 3.1**) with an upper bound of 100 and lower bound of 0, and used to calculate the IC50.

$$y = A1 + \frac{A2-A1}{1+1^{(Log(x0)-x)p}}$$

where $A2 = 100$
$A1 = 0$
$x0$ = IC50 concentration
p = hill slope

Equation 3.1

Also, cell density cytotoxicity assays were performed by seeding 2980A cells at an upper range of 10 000s of cells/well then a two-fold serial dilution in each adjacent column. The cells were incubated in media for a total of 24+ 72 h to reflect experimental conditions to be used. Then a CTG assay was performed and % viability was plotted against cell seeding density to determine an optimal seeding density for future experiments. We determined that 500 cells/well will be an optimal seeding density for 2980A pancreatic adenocarcinoma cells given our experimental conditions (**Supplemental Figure 3.S8**).

3-Drug Combination Index assay:

2980A PDAC cells were obtained from the Ghoroghchian lab, and grown in media containing Dulbecco's Modification of Eagle's Medium (DMEM) with 4.5 g/L glucose, L-glutamine, and sodium pyruvate, 10% fetal bovine serum, and 1% penicillin-streptomycin (10 000 U/mL) antibiotic solution. All cells were incubated in a humidity controlled cell incubator at 37 °C and 5% CO_2. All cell work was performed in the Essigmann Lab cell culture room and biological safety cabinets. These cells were grown in tissue-culture (TC) treated 75 cm^2 culture flasks and passaged at least once before use in assays. A solution of 0.25% Trypsin with 2.21 mM EDTA was used for cell detachment. Proper sterilization technique and sterile procedures were used with cells. Single-drug cytotoxicity assays for oxaliplatin, SN38, and 5-fluorouracil was performed prior to the CI assays, and the hill slope and IC50 values were recorded. The results of the cytotoxicity assays are shown in **Figure 3.15**.

In advance of the CI study, we prepared and chose concentrations to use in each well as shown in **Table 3.6**. 2980A cells were seeded at 500 cells/ well in triplicate and incubated in cell media for 24 h. Using a 96-well plate, we prepared the 3-drug concentration gradients in advance. First we set up a serial dilution of 5-fluorouracil in media starting at 4 μM in the last vertical column, which is at 4x the desired concentration (of 1 μM), and diluting by a factor of 2

from right to left of the deep well plate. The final volume in each well is 100 μL. Next we prepared serial dilutions of oxaliplatin in 2-mL Eppendorf tubes starting at 28 μM, which is at 4x the desired concentration (of 7 μM), and serial diluting by a factor of 2 in labeled Eppendorf tubes. We add 100 μL of oxaliplatin solution horizontally in each row of the well plate, such that the highest concentration of oxaliplatin is added to the first bottom row and each subsequent dilution is in the row above. Given the dilution, the final concentration of oxaliplatin and 5-fluorouracil is 14 μM and 2 μM, respectively, in each well and is at 2x the desired concentration. Next, in a falcon tube we prepared a 2x stock solution of SN38 at 15 nM, which is at 2x the desired concentration (of 7.5 nM). After removing the media from the plated cells, we added 50 μL of oxali/5FU solution and 50 μL of the SN38 solution to each of the replicates, such that the cells are now incubated with 1x the desired concentration. **Table 3.7** lists the final concentrations of each of the three drugs in each well. Note that one column of cells should be treated with blank media to use as a negative control. After incubation for 72 h, a CTG assay was performed on the plates to determine viability in each well and the data was analyzed.

For data analysis the % cell killing is calculated as 100% – % cell viability. To calculate the Bliss expectation % killing based on an additive effect (**Table 3.8**), we first find the single drug dose response, y, by using **Equation 3.1**. We plug-in hill slope, p, and $\log(x0)$, as determined by the single drug cytotoxicity assay obtained prior to the CI study, and input the single drug concentration, x, used for the CI study to calculate y. The value, y, determined as % cell viability is subtracted from 100% to get a dose response value for % cell killing. We do this for each of the three drugs to determine a % cell killing dose response at a given concentration of single drug, then for the concentrations of drug in a given well, we plug each dose response into the Bliss equation: Bliss expectation % = $(E_a+E_b+E_c)-(E_a*E_b)-(E_a*E_c)-(E_b*E_c)$ where E_x is the dose response for drugs x = a,b, and c. Next for each well, we subtract the Bliss expectation % killing from the experimental % cell killing (**Table 3.9**) to get the Bliss excess% (**Table 3.10**), where a more positive value indicates synergistic ratio and a more negative value indicates an antagonistic ratio.

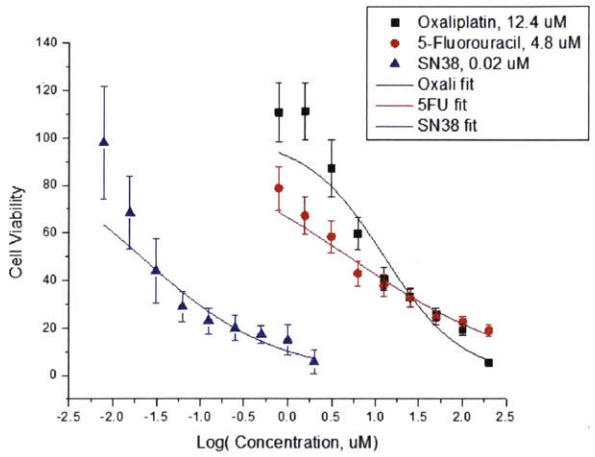

Figure 3.15: Cytotoxicity assays on 2980A PDAC cells seeded at 500 cells/well and incubated with drug for 72 h. The IC50 is shown in the legend, next to the drug name.

		[5FU]		3.91E-09	7.81E-09	1.56E-08	3.13E-08	6.25E-08	1.25E-07	2.50E-07	5.00E-07	1.00E-06	
[Oxali]		A	B	C	D	E	F	G	H	I	J	K	L
				0.071 5FU	0.14 5FU	0.29 5FU	0.57 5FU	1.14 5FU	2.29 5FU	4.57 5FU	9.14 5FU	18.29 5FU	
		No	Neg	0.14 SN38	0.14 SN38	0.14 SN38	0.14 SN38	0.14 SN38	0.14 SN38	0.14 SN38	0.14 SN38	0.14 SN38	Pos.
5.47E-08	1	cells	Con.	1 Oxali	1 Oxali	1 Oxali	1 Oxali	1 Oxali	1 Oxali	1 Oxali	1 Oxali	1 Oxali	Con.
				0.036 5FU	0.071 5FU	0.14 5FU	0.29 5FU	0.57 5FU	1.14 5FU	2.29 5FU	4.57 5FU	9.14 5FU	
		No	Neg	0.07 SN38	0.07 SN38	0.07 SN38	0.07 SN38	0.07 SN38	0.07 SN38	0.07 SN38	0.07 SN38	0.07 SN38	Pos.
1.09E-07	2	cells	Con.	1 Oxali	1 Oxali	1 Oxali	1 Oxali	1 Oxali	1 Oxali	1 Oxali	1 Oxali	1 Oxali	Con.
				0.018 5FU	0.036 5FU	0.071 5FU	0.14 5FU	0.29 5FU	0.57 5FU	1.14 5FU	2.29 5FU	4.57 5FU	
		No	Neg	0.03 SN38	0.03 SN38	0.03 SN38	0.03 SN38	0.03 SN38	0.03 SN38	0.03 SN38	0.03 SN38	0.03 SN38	Pos.
2.19E-07	3	cells	Con.	1 Oxali	1 Oxali	1 Oxali	1 Oxali	1 Oxali	1 Oxali	1 Oxali	1 Oxali	1 Oxali	Con.
				0.009 5FU	0.018 5FU	0.036 5FU	0.071 5FU	0.14 5FU	0.29 5FU	0.57 5FU	1.14 5FU	2.29 5FU	
		No	Neg	0.02 SN38	0.02 SN38	0.02 SN38	0.02 SN38	0.02 SN38	0.02 SN38	0.02 SN38	0.02 SN38	0.02 SN38	Pos.
4.38E-07	4	cells	Con.	1 Oxali	1 Oxali	1 Oxali	1 Oxali	1 Oxali	1 Oxali	1 Oxali	1 Oxali	1 Oxali	Con.
				0.004 5FU	0.009 5FU	0.018 5FU	0.036 5FU	0.071 5FU	0.14 5FU	0.29 5FU	0.57 5FU	1.14 5FU	
		No	Neg	0.009 SN38	0.009 SN38	0.009 SN38	0.009 SN38	0.009 SN38	0.009 SN38	0.009 SN38	0.009 SN38	0.009 SN38	Pos.
8.75E-07	5	cells	Con.	1 Oxali	1 Oxali	1 Oxali	1 Oxali	1 Oxali	1 Oxali	1 Oxali	1 Oxali	1 Oxali	Con.
				0.002 5FU	0.004 5FU	0.009 5FU	0.018 5FU	0.036 5FU	0.071 5FU	0.14 5FU	0.29 5FU	0.57 5FU	
		No	Neg	0.004 SN38	0.004 SN38	0.004 SN38	0.004 SN38	0.004 SN38	0.004 SN38	0.004 SN38	0.004 SN38	0.004 SN38	Pos.
1.75E-06	6	cells	Con.	1 Oxali	1 Oxali	1 Oxali	1 Oxali	1 Oxali	1 Oxali	1 Oxali	1 Oxali	1 Oxali	Con.
				0.001 5FU	0.002 5FU	0.004 5FU	0.009 5FU	0.018 5FU	0.036 5FU	0.071 5FU	0.14 5FU	0.29 5FU	
		No	Neg	0.002 SN38	0.002 SN38	0.002 SN38	0.002 SN38	0.002 SN38	0.002 SN38	0.002 SN38	0.002 SN38	0.002 SN38	Pos.
3.50E-06	7	cells	Con.	1 Oxali	1 Oxali	1 Oxali	1 Oxali	1 Oxali	1 Oxali	1 Oxali	1 Oxali	1 Oxali	Con.
				0.001 5FU	0.001 5FU	0.002 5FU	0.004 5FU	0.009 5FU	0.018 5FU	0.036 5FU	0.071 5FU	0.14 5FU	
		No	Neg	0.001 SN38	0.001 SN38	0.001 SN38	0.001 SN38	0.001 SN38	0.001 SN38	0.001 SN38	0.001 SN38	0.001 SN38	Pos.
7.00E-06	8	cells	Con.	1 Oxali	1 Oxali	1 Oxali	1 Oxali	1 Oxali	1 Oxali	1 Oxali	1 Oxali	1 Oxali	Con.

[SN38] = 7.5E-09 M

Table 3.6: This table shows the concentration of drugs used to treat the cells in a 96-well plate, and is the same Table as shown in **Table 3.5A** of the main text. The top row displays concentration of 5-fluorouracil across the wells with each vertical column having the same concentration of 5-fluorouracil. The concentration of oxaliplatin changes down the well with each horizontal row having the same concentration of oxaliplatin. The concentration of SN38 is held constant at 7.5 nM. The wells show the ratio of [5FU]:[SN38]:[Oxali]. Thus, D1 would have a ratio of 0.14: 0.14: 1 ratio of [5FU]:[SN38]:[Oxali] corresponding to a concentration of 7.8 nM, 7.5 nM, and 55 nM of 5FU, SN38, and oxaliplatin, respectively. All concentrations listed in the table have units of M. Any value in the well listed in blue font correspond to synthetically feasible ratios where ([5FU]+[SN38] < 1.4). Also the value in green font is the closest one to the IC50 ratio, where the single drug IC50s of 5FU, SN38, and oxaliplatin are 4.8μM, 0.02μM, and 12.4μM, respectively.

5FU, [M]											
		3.9E-09	7.8E-09	1.6E-08	3.1E-08	6.3E-08	1.3E-07	2.5E-07	5.0E-07	1.0E-06	
		3.9E-09	7.8E-09	1.6E-08	3.1E-08	6.3E-08	1.3E-07	2.5E-07	5.0E-07	1.0E-06	
		3.9E-09	7.8E-09	1.6E-08	3.1E-08	6.3E-08	1.3E-07	2.5E-07	5.0E-07	1.0E-06	
		3.9E-09	7.8E-09	1.6E-08	3.1E-08	6.3E-08	1.3E-07	2.5E-07	5.0E-07	1.0E-06	
		3.9E-09	7.8E-09	1.6E-08	3.1E-08	6.3E-08	1.3E-07	2.5E-07	5.0E-07	1.0E-06	
		3.9E-09	7.8E-09	1.6E-08	3.1E-08	6.3E-08	1.3E-07	2.5E-07	5.0E-07	1.0E-06	
		3.9E-09	7.8E-09	1.6E-08	3.1E-08	6.3E-08	1.3E-07	2.5E-07	5.0E-07	1.0E-06	
		3.9E-09	7.8E-09	1.6E-08	3.1E-08	6.3E-08	1.3E-07	2.5E-07	5.0E-07	1.0E-06	

Oxali, [M]											
		5.47E-08	5.47E-08	5.47E-08	5.47E-08	5.47E-08	5.47E-08	5.47E-08	5.47E-08	5.47E-08	
		1.09E-07	1.09E-07	1.09E-07	1.09E-07	1.09E-07	1.09E-07	1.09E-07	1.09E-07	1.09E-07	
		2.19E-07	2.19E-07	2.19E-07	2.19E-07	2.19E-07	2.19E-07	2.19E-07	2.19E-07	2.19E-07	
		4.38E-07	4.38E-07	4.38E-07	4.38E-07	4.38E-07	4.38E-07	4.38E-07	4.38E-07	4.38E-07	
		8.75E-07	8.75E-07	8.75E-07	8.75E-07	8.75E-07	8.75E-07	8.75E-07	8.75E-07	8.75E-07	
		1.75E-06	1.75E-06	1.75E-06	1.75E-06	1.75E-06	1.75E-06	1.75E-06	1.75E-06	1.75E-06	
		3.50E-06	3.50E-06	3.50E-06	3.50E-06	3.50E-06	3.50E-06	3.50E-06	3.50E-06	3.50E-06	
		7.00E-06	7.00E-06	7.00E-06	7.00E-06	7.00E-06	7.00E-06	7.00E-06	7.00E-06	7.00E-06	

Table 3.7: These tables list the final concentrations of each individual drug in each well of the 3-drug CI assay. [SN38] was constant in each well at 7.5 nM.

5FU+oxali+SN38, BLISS expectation % killing									
	C	D	E	F	G	H	I	J	K
1	41.0	42.5	44.4	46.8	49.9	53.7	58.4	63.9	70.1
2	41.5	43.0	44.9	47.3	50.4	54.2	58.9	64.3	70.6
3	42.4	43.9	45.8	48.3	51.3	55.2	59.8	65.3	71.5
4	44.2	45.7	47.6	50.0	53.1	57.0	61.6	67.1	73.3
5	47.6	49.0	50.9	53.4	56.4	60.3	64.9	70.4	76.6
6	53.4	54.9	56.8	59.2	62.3	66.1	70.8	76.2	82.5
7	63.0	64.5	66.4	68.8	71.9	75.7	80.4	85.8	92.0
8	76.8	78.2	80.1	82.6	85.6	89.4	94.1	99.5	105.7

Table 3.8: Theoretical Bliss expectation % killing for the concentrations of drugs in each well based on an additive effect, calculated by the Bliss Model.

A % Cell killing (experimental)

	C	D	E	F	G	H	I	J	K
1	27.4	18.7	15.6	27.7	28.3	25.7	27.1	42.4	55.6
2	18.5	16.9	18.6	19.2	40.7	29.0	30.8	51.4	62.4
3	16.5	-2.9	-0.1	12.2	37.7	14.0	31.1	44.1	48.5
4	13.9	-0.1	13.2	27.8	39.9	24.8	41.2	57.6	56.1
5	21.0	16.1	25.8	25.9	38.5	36.9	53.9	63.6	66.2
6	36.9	23.9	38.6	50.7	54.4	41.3	56.9	62.9	66.6
7	47.3	46.3	53.7	73.6	78.7	60.3	64.0	55.9	65.3
8	64.4	71.4	62.7	70.4	74.8	70.5	73.3	68.8	70.6

B Standard deviation of % cell killing

	C	D	E	F	G	H	I	J	K
1	11.1	5.5	10.5	28.2	34.5	23.3	18.6	18.6	11.6
2	31.0	34.4	28.8	37.7	22.8	25.6	9.8	11.1	11.5
3	25.4	7.2	10.1	30.6	25.3	24.1	19.1	13.0	18.5
4	24.5	24.5	27.1	29.1	22.3	35.0	13.5	10.8	12.3
5	27.1	13.0	27.5	35.7	8.4	13.4	11.5	9.5	2.5
6	35.8	25.0	24.3	18.8	21.4	25.7	9.0	2.2	4.7
7	9.7	6.3	21.3	2.7	5.6	12.2	11.3	2.5	6.8
8	14.8	13.2	16.8	1.5	0.4	7.0	1.6	7.5	2.7

Table 3.9: The experimentally determined % cell killing based on drug concentrations given in **Table 3.4**. A) shows an average of three trials with the standard deviation shown in B). In A), wells colored more green are at lower values of %killing, whereas wells colored more orange are at high values of % killing. In B), more red in color signifies higher error, whereas more white signifies lower error.

BLISS EXCESS %									
	C	D	E	F	G	H	I	J	K
1	-13.7	-23.8	-28.8	-19.1	-21.6	-28.1	-31.2	-21.5	-14.5
2	-23.0	-26.1	-26.2	-28.2	-9.7	-25.2	-28.1	-13.0	-8.2
3	-26.0	-46.8	-45.9	-36.0	-13.6	-41.2	-28.7	-21.2	-23.0
4	-30.3	-45.8	-34.4	-22.2	-13.2	-32.2	-20.4	-9.5	-17.2
5	-26.6	-32.9	-25.1	-27.4	-18.0	-23.4	-11.0	-6.8	-10.4
6	-16.6	-31.0	-18.2	-8.6	-7.9	-24.9	-13.9	-13.3	-15.9
7	-15.7	-18.1	-12.7	4.7	6.8	-15.5	-16.4	-29.9	-26.7
8	-12.4	-6.9	-17.5	-12.1	-10.8	-18.9	-20.8	-30.8	-35.1

Table 3.10: The Bliss Excess % shown in this chart is calculated from subtracting the Bliss Expectation % killing (**Table 3.8**) from the experimental % Cell Killing (**Table 3.9A**). A positive number (more red in color) indicates more %killing than expected and synergism. A negative number indicates less %killing than expected and antagonism. The well in white is negligible since the Bliss Expectation % killing for that well was greater than 100%.

3.5 References

1 Siegel, R. L., Miller, K. D. & Jemal, A. Cancer statistics, 2015. *CA: A Cancer Journal for Clinicians* **65**, 5-29 (2015).

2 Hidalgo, M. Pancreatic cancer. *New England Journal of Medicine* **362**, 1605-1617 (2010).

3 Li, D., Xie, K., Wolff, R. & Abbruzzese, J. L. Pancreatic cancer. *The Lancet* **363**, 1049-1057 (2004).

4 Montet, X., Weissleder, R. & Josephson, L. Imaging pancreatic cancer with a peptide-nanoparticle conjugate targeted to normal pancreas. *Bioconjugate Chemistry* **17**, 905-911 (2006).

5 Yang, L. *et al.* Molecular imaging of pancreatic cancer in an animal model using targeted multifunctional nanoparticles. *Gastroenterology* **136**, 1514-1525 (2009).

6 Li, C. *et al.* Identification of pancreatic cancer stem cells. *Cancer Research* **67**, 1030-1037 (2007).

7 Ryan, D. P., Hong, T. S. & Bardeesy, N. Pancreatic adenocarcinoma. *New England Journal of Medicine* **371**, 1039-1049 (2014).

8 Apte, M. *et al.* Desmoplastic reaction in pancreatic cancer: role of pancreatic stellate cells. *Pancreas* **29**, 179-187 (2004).

9 Provenzano, P. & Hingorani, S. Hyaluronan, fluid pressure, and stromal resistance in pancreas cancer. *British Journal of Cancer* **108**, 1-8 (2013).

10 Trédan, O., Galmarini, C. M., Patel, K. & Tannock, I. F. Drug resistance and the solid tumor microenvironment. *Journal of the National Cancer Institute* **99**, 1441-1454 (2007).

11 Höckel, M. & Vaupel, P. Tumor hypoxia: definitions and current clinical, biologic, and molecular aspects. *Journal of the National Cancer Institute* **93**, 266-276 (2001).

12 Harris, A. L. Hypoxia—a key regulatory factor in tumour growth. *Nature Reviews Cancer* **2**, 38-47 (2002).

13 Wilson, W. R. & Hay, M. P. Targeting hypoxia in cancer therapy. *Nature Reviews Cancer* **11**, 393-410 (2011).

14 Brown, J. M. & Wilson, W. R. Exploiting tumour hypoxia in cancer treatment. *Nature Reviews Cancer* **4**, 437-447 (2004).

15 Sideras, K. *et al.* Role of the immune system in pancreatic cancer progression and immune modulating treatment strategies. *Cancer Treatment Reviews* **40**, 513-522 (2014).

16 Coussens, L. M. & Werb, Z. Inflammation and cancer. *Nature* **420**, 860-867 (2002).

17 Mantovani, A., Allavena, P., Sica, A. & Balkwill, F. Cancer-related inflammation. *Nature* **454**, 436-444 (2008).

18 Conroy, T. *et al.* FOLFIRINOX versus gemcitabine for metastatic pancreatic cancer. *New England Journal of Medicine* **364**, 1817-1825 (2011).

19 Kim, R. FOLFIRINOX: a new standard treatment for advanced pancreatic cancer? *The lancet Oncology* **12**, 8-9 (2011).

20 Von Hoff, D. D. *et al.* Increased survival in pancreatic cancer with nab-paclitaxel plus gemcitabine. *New England Journal of Medicine* **369**, 1691-1703 (2013).

21 Wolfgang, C. L. *et al.* Recent progress in pancreatic cancer. *CA: A Cancer Journal for Clinicians* **63**, 318-348 (2013).

22 Rivory, L. P., Bowles, M. R., Robert, J. & Pond, S. M. Conversion of irinotecan (CPT-11) to its active metabolite, 7-ethyl-10-hydroxycamptothecin (SN-38), by human liver carboxylesterase. *Biochemical Pharmacology* **52**, 1103-1111 (1996).

23 Kawato, Y., Aonuma, M., Hirota, Y., Kuga, H. & Sato, K. Intracellular roles of SN-38, a metabolite of the camptothecin derivative CPT-11, in the antitumor effect of CPT-11. *Cancer Research* **51**, 4187-4191 (1991).

24 Raymond, E., Faivre, S., Woynarowski, J. M. & Chaney, S. G. Oxaliplatin: mechanism of action and antineoplastic activity. *Seminars in Oncology* **25**, 4-12 (1998).

25 Longley, D. B., Harkin, D. P. & Johnston, P. G. 5-fluorouracil: mechanisms of action and clinical strategies. *Nature Reviews Cancer* **3**, 330-338 (2003).

26 Cabral, H. *et al.* Accumulation of sub-100 nm polymeric micelles in poorly permeable tumours depends on size. *Nature Nanotechnology* **6**, 815-823 (2011).

27 Patra, C. R., Bhattacharya, R., Mukhopadhyay, D. & Mukherjee, P. Fabrication of gold nanoparticles for targeted therapy in pancreatic cancer. *Advanced Drug Delivery Reviews* **62**, 346-361 (2010).

28 Meng, H. *et al.* Use of a lipid-coated mesoporous silica nanoparticle platform for synergistic gemcitabine and paclitaxel delivery to human pancreatic cancer in mice. *ACS Nano* **9**, 3540-3557 (2015).

29 Li, F. *et al.* Multiple layer-by-layer lipid-polymer hybrid nanoparticles for improved FOLFIRINOX chemotherapy in pancreatic tumor models. *Advanced Functional Materials* **25**, 788-798 (2015).

30 Chou, T.-C. Drug combination studies and their synergy quantification using the Chou-Talalay method. *Cancer Research* **70**, 440-446 (2010).

31 Chou, T.-C. Theoretical basis, experimental design, and computerized simulation of synergism and antagonism in drug combination studies. *Pharmacological Reviews* **58**, 621-681 (2006).

32 Greco, W. R., Bravo, G. & Parsons, J. C. The search for synergy: a critical review from a response surface perspective. *Pharmacological Reviews* **47**, 331-385 (1995).

33 Tallarida, R. J. Drug synergism: its detection and applications. *Journal of Pharmacology and Experimental Therapeutics* **298**, 865-872 (2001).

34 Goldin, A. & Mantel, N. The employment of combinations of drugs in the chemotherapy of neoplasia: a review. *Cancer Research* **17**, 635-654 (1957).

35 Mayer, L. D. & Janoff, A. S. Optimizing combination chemotherapy by controlling drug ratios. *Molecular Interventions* **7**, 216 (2007).

36 Jia, J. *et al.* Mechanisms of drug combinations: interaction and network perspectives. *Nature Reviews Drug discovery* **8**, 111-128 (2009).

37 Johnson, J. A. *et al.* Drug-loaded, bivalent-bottle-brush polymers by graft-through ROMP. *Macromolecules* **43**, 10326-10335 (2010).

38 Liao, L. *et al.* A convergent synthetic platform for single-nanoparticle combination cancer therapy: ratiometric loading and controlled release of cisplatin, doxorubicin, and camptothecin. *Journal of the American Chemical Society* **136**, 5896-5899 (2014).

39 Barnes, J. C. et al. Using an RNAi signature assay to guide the design of three-drug-conjugated nanoparticles with validated mechanisms, *in vivo* efficacy, and low toxicity. *Journal of the American Chemical Society* **138**, 12494-12501 (2016).

40 Gao, A. X., Liao, L. & Johnson, J. A. Synthesis of acid-labile PEG and PEG-doxorubicin-conjugate nanoparticles via brush-first ROMP. *ACS Macro Letters* **3**, 854-857 (2014).

41 Greenwald, R. B. et al. Drug delivery systems employing 1,4-or 1,6-elimination: poly(ethylene glycol) prodrugs of amine-containing compounds. *Journal of Medicinal Chemistry* **42**, 3657-3667 (1999).

42 Stergiopoulou, T. *et al.* Synergistic interaction of the triple combination of amphotericin B, ciprofloxacin, and polymorphonuclear neutrophils against Aspergillus fumigatus. *Antimicrobial Agents and Chemotherapy* **55**, 5923-5929 (2011).

43 Bertozzi, C. R. & Bednarski, M. D. The synthesis of heterobifunctional linkers for the conjugation of ligands to molecular probes. *The Journal of Organic Chemistry* **56**, 4326-4329 (1991).

44 Hall, M. D. *et al.* The cellular distribution and oxidation state of platinum (II) and platinum (IV) antitumour complexes in cancer cells. *Journal of Biological Inorganic Chemistry* **8**, 726-732 (2003).

45 Liu, J., Gao, A. X. & Johnson, J. A. Particles without a box: brush-first synthesis of photodegradable PEG star polymers under ambient conditions. *Journal of Visualized Experiments* **80** (2013).

3.6 Supplemental Figures and Spectra

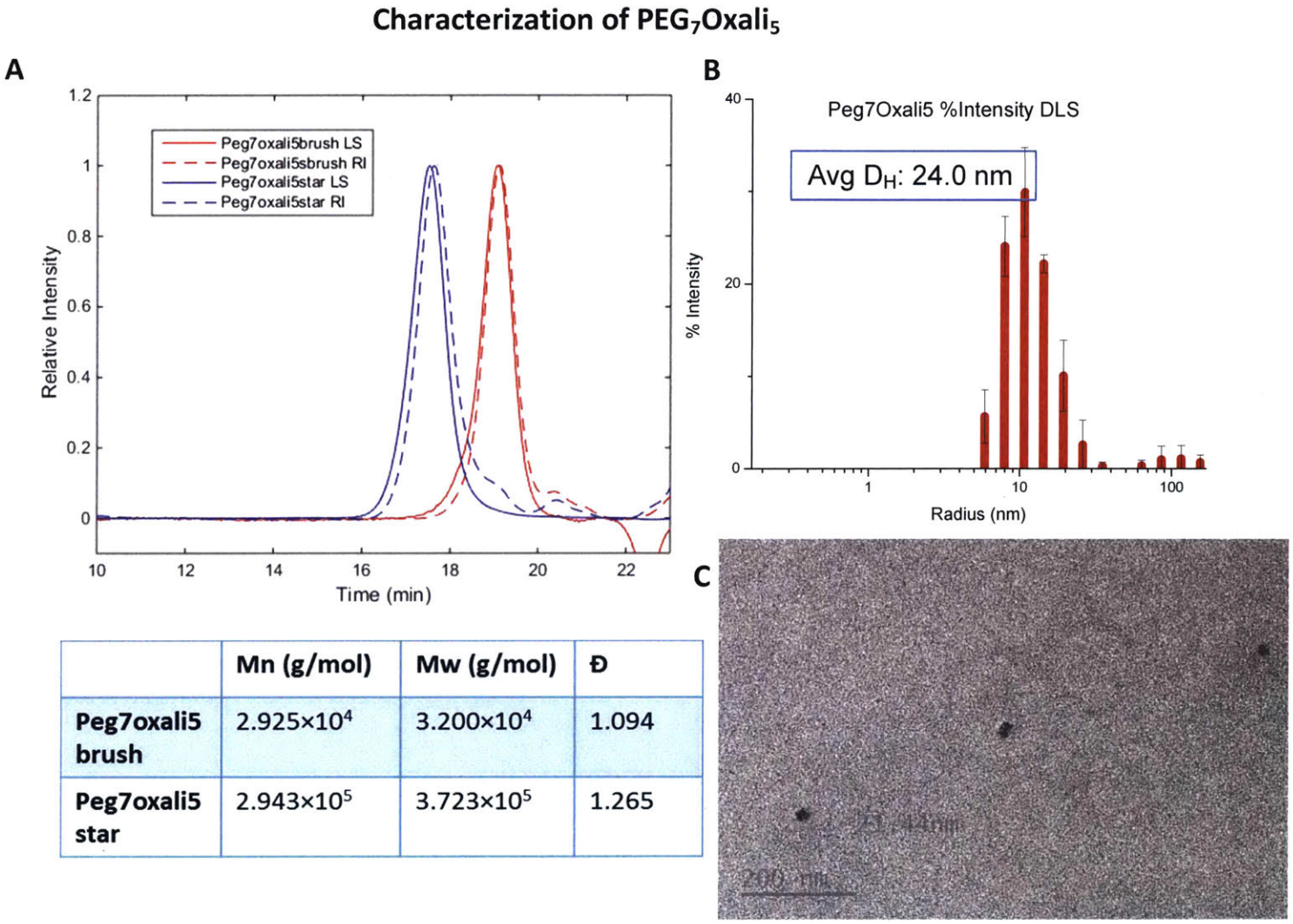

	Mn (g/mol)	Mw (g/mol)	Đ
Peg7oxali5 brush	2.925×10^4	3.200×10^4	1.094
Peg7oxali5 star	2.943×10^5	3.723×10^5	1.265

Figure 3.S1: A) GPC-MALLS characterization of the PEG_7Oxali_5 brush and BASP from **Table 3.2** with M_n, M_w, and $Đ$ given in the table below. B) Intensity average D_H from DLS. C) Sample TEM image of particles, unstained for PEG_7Oxali_5.

Characterization of $IRT_5PEG_5Acetal_{10}$

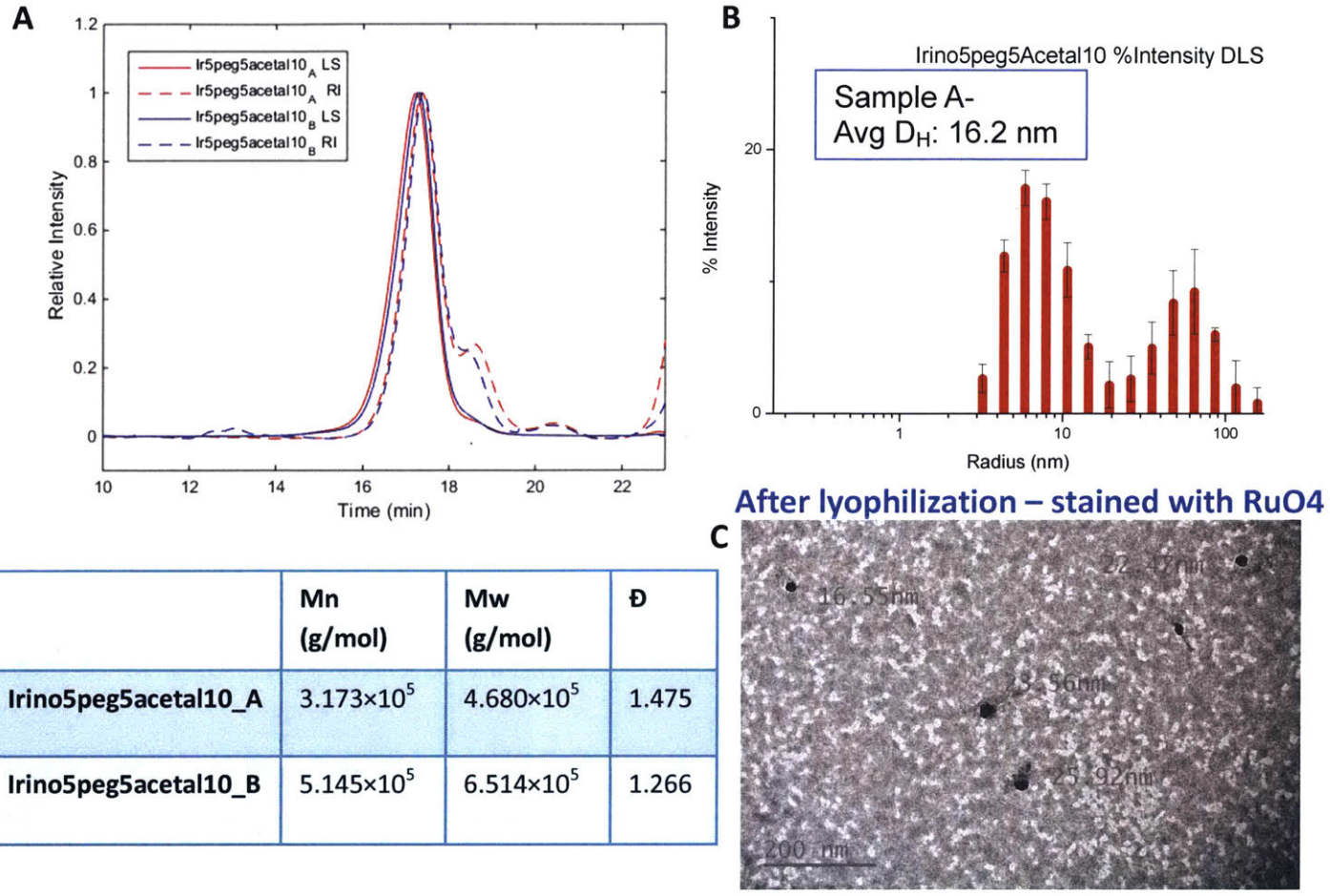

	Mn (g/mol)	Mw (g/mol)	Đ
Irino5peg5acetal10_A	3.173×10^5	4.680×10^5	1.475
Irino5peg5acetal10_B	5.145×10^5	6.514×10^5	1.266

Figure 3.S2: A) GPC-MALLS characterization of the $IRT_5PEG_5Acetal_{10}$ (Batch A) BASP as seen in **Table 3.2** and $IRT_5PEG_5Acetal_{10}$_B, another batch not in **Table 3.2**, with M_n, M_w, and $Đ$ given in the table below. B) Intensity average D_H of $IRT_5PEG_5Acetal_{10}$ BASP as seen in **Table 3.2**. C) Sample TEM image of $IRT_5PEG_5Acetal_{10}$ BASP from **Table 3.2**, stained with RuO_4.

Characterization of $SN38_5PEG_5Acetal_{10}$

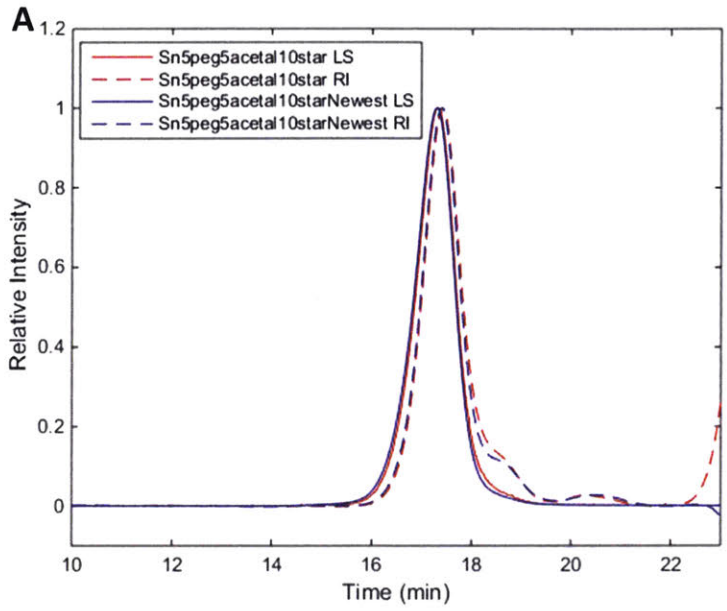

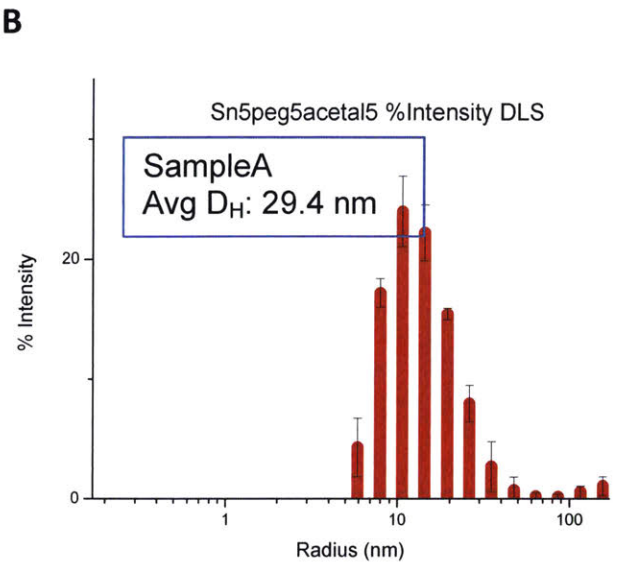

C **After lyophilization – stained with RuO4**

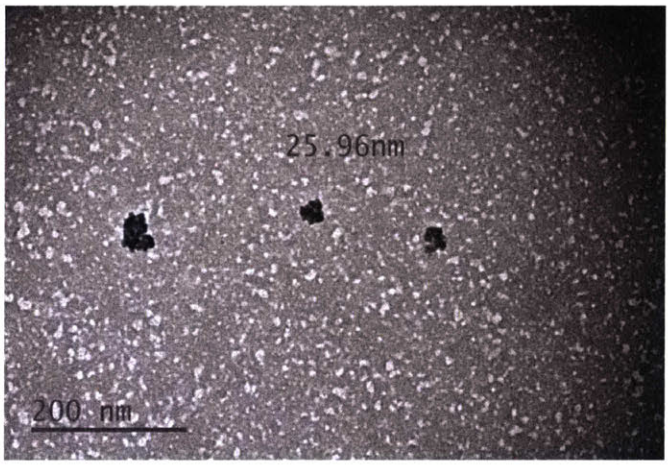

	Mn (g/mol)	Mw (g/mol)	Đ
Sn5peg5acetal10_A	3.602×10^5	4.549×10^5	1.263
Sn5peg5acetal10_B	3.792×10^5	5.021×10^5	1.342

Figure 3.S3: A) GPC-MALLS characterization of the $SN38_5PEG_5Acetal_{10}$ (Batch A) BASP as seen in **Table 3.2** and $SN38_5PEG_5Acetal_{10}$_B, another batch not in **Table 3.2**, with M_n, M_w, and $Đ$ given in the table below. B) Intensity average D_H of $SN38_5PEG_5Acetal_{10}$ BASP as seen in **Table 3.2**. C) Sample TEM image of $SN38_5PEG_5Acetal_{10}$ BASP from **Table 3.2**, stained with RuO_4.

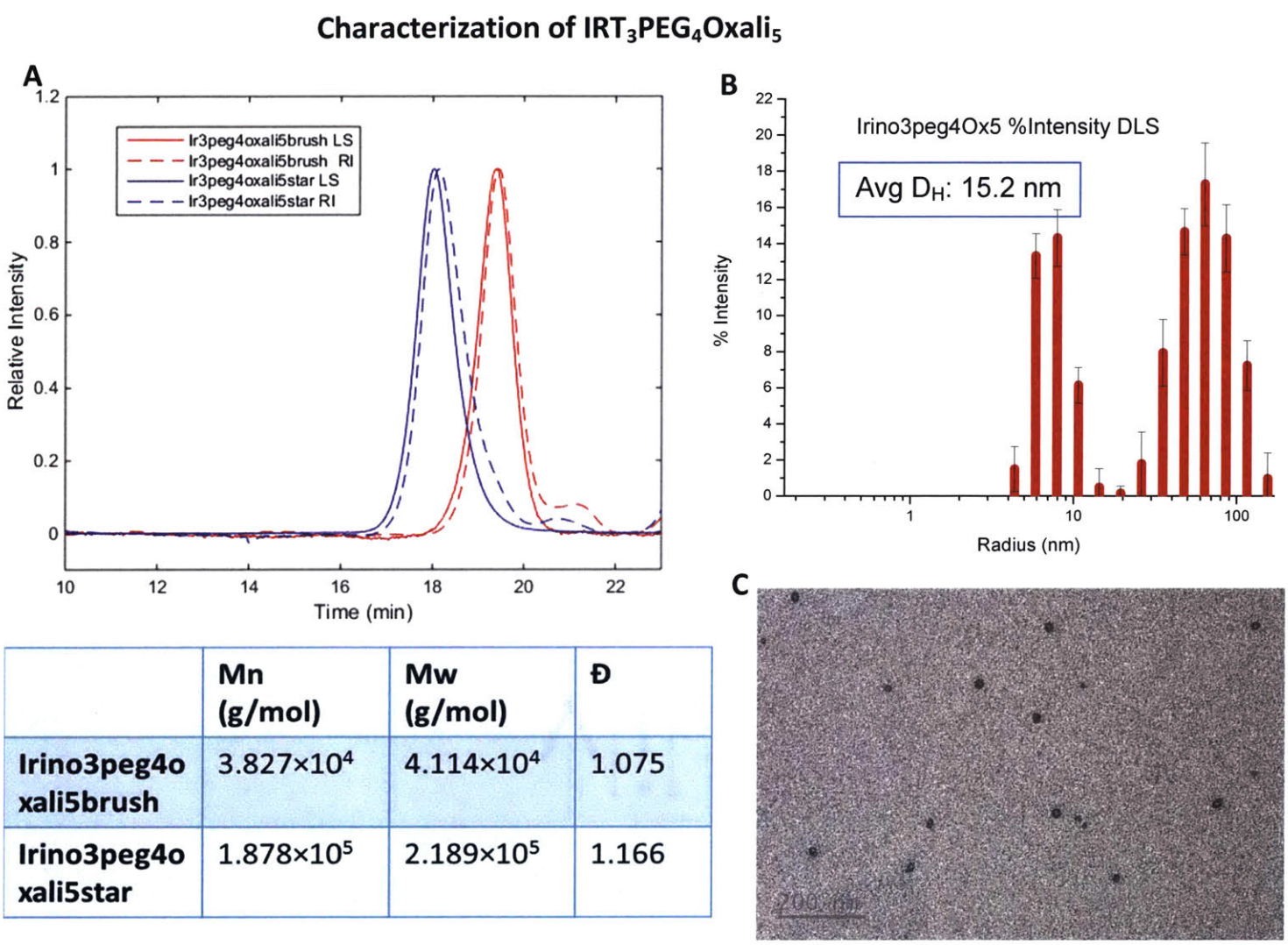

	Mn (g/mol)	Mw (g/mol)	Đ
Irino3peg4oxali5brush	3.827×10^4	4.114×10^4	1.075
Irino3peg4oxali5star	1.878×10^5	2.189×10^5	1.166

Figure 3.S4: A) GPC-MALLS characterization of the $IRT_3PEG_4Oxali_5$ brush and BASP from **Table 3.2** with M_n, M_w, and $Đ$ given in the table below. B) Intensity average D_H from DLS. C) Sample TEM image of particles, unstained for $IRT_3PEG_4Oxali_5$.

Characterization of $SN38_3PEG_4Oxali_5$

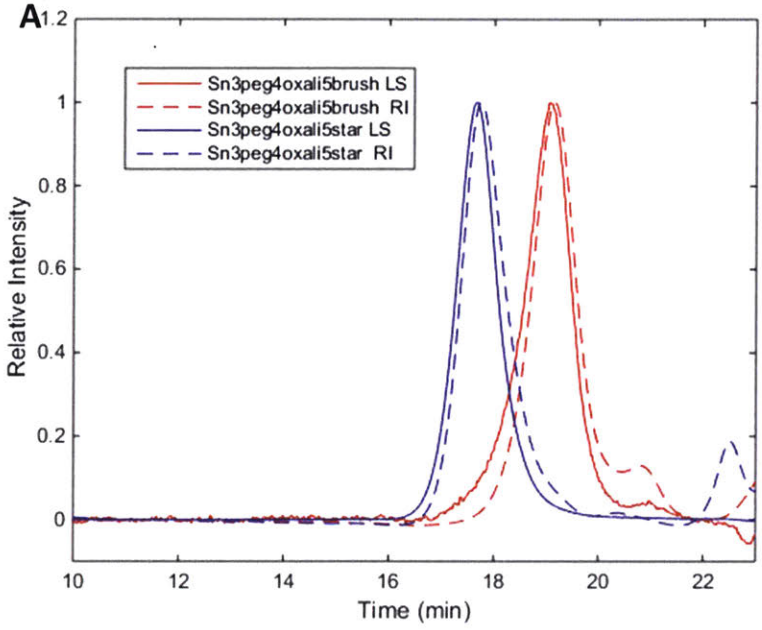

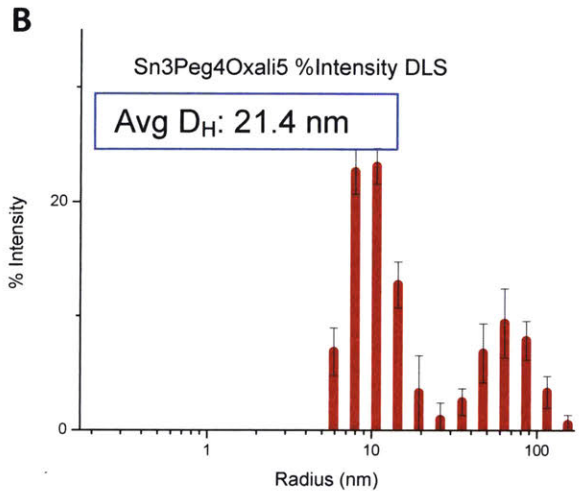

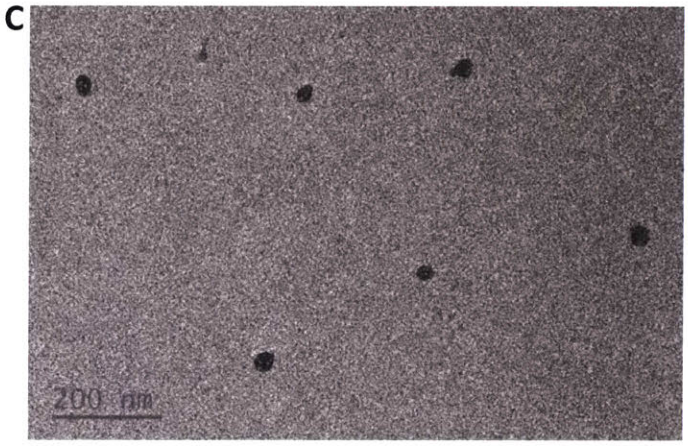

	Mn (g/mol)	Mw (g/mol)	Đ
Sn3peg4oxali5brush	4.257×10^4	4.747×10^4	1.115
Sn3peg4oxali5star	2.795×10^5	3.087×10^5	1.104

Figure 3.S5: A) GPC-MALLS characterization of the $SN38_3PEG_4Oxali_5$ brush and BASP from **Table 3.2** with M_n, M_w, and $Đ$ given in the table below. B) Intensity average D_H from DLS. C) Sample TEM image of particles, unstained for $SN38_3PEG_4Oxali_5$.

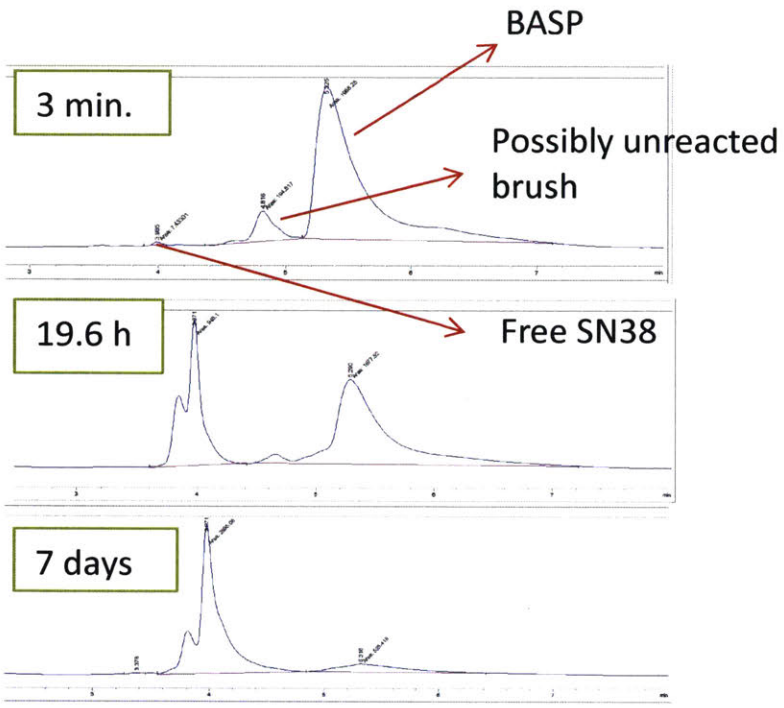

Figure 3.S6: Sample LCMS trace of the SN38 release from **$SN38_3PEG_4Oxali_5$**. Free drug can be observed as both the closed and open lactone forms.

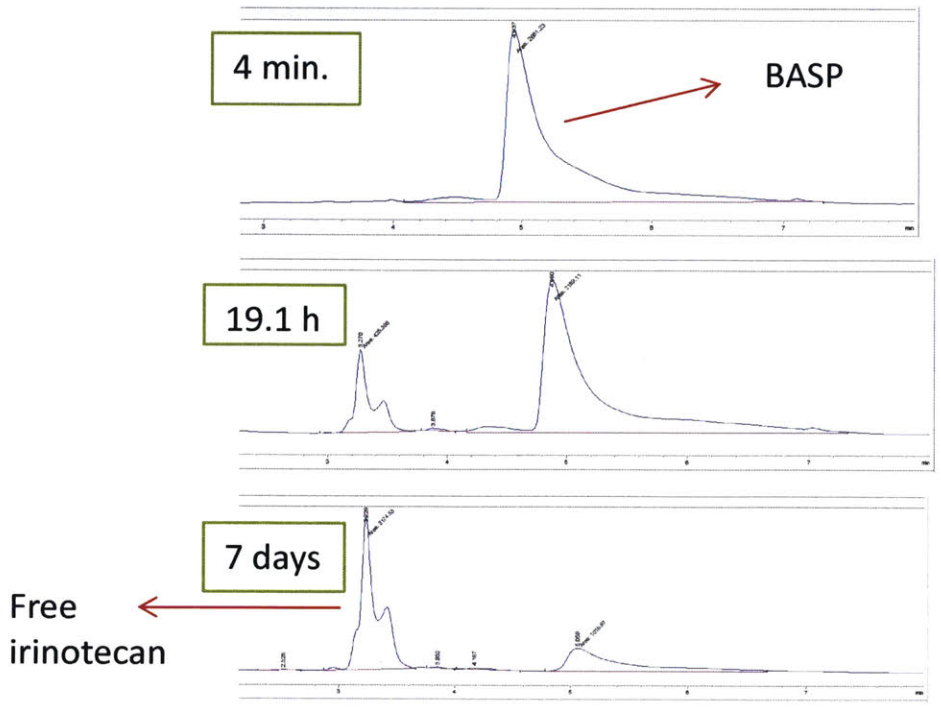

Figure 3.S7: Sample LCMS trace of the irinotecan release from **$IRT_3PEG_4Oxali_5$**. Free drug can be observed as both the closed and open lactone forms.

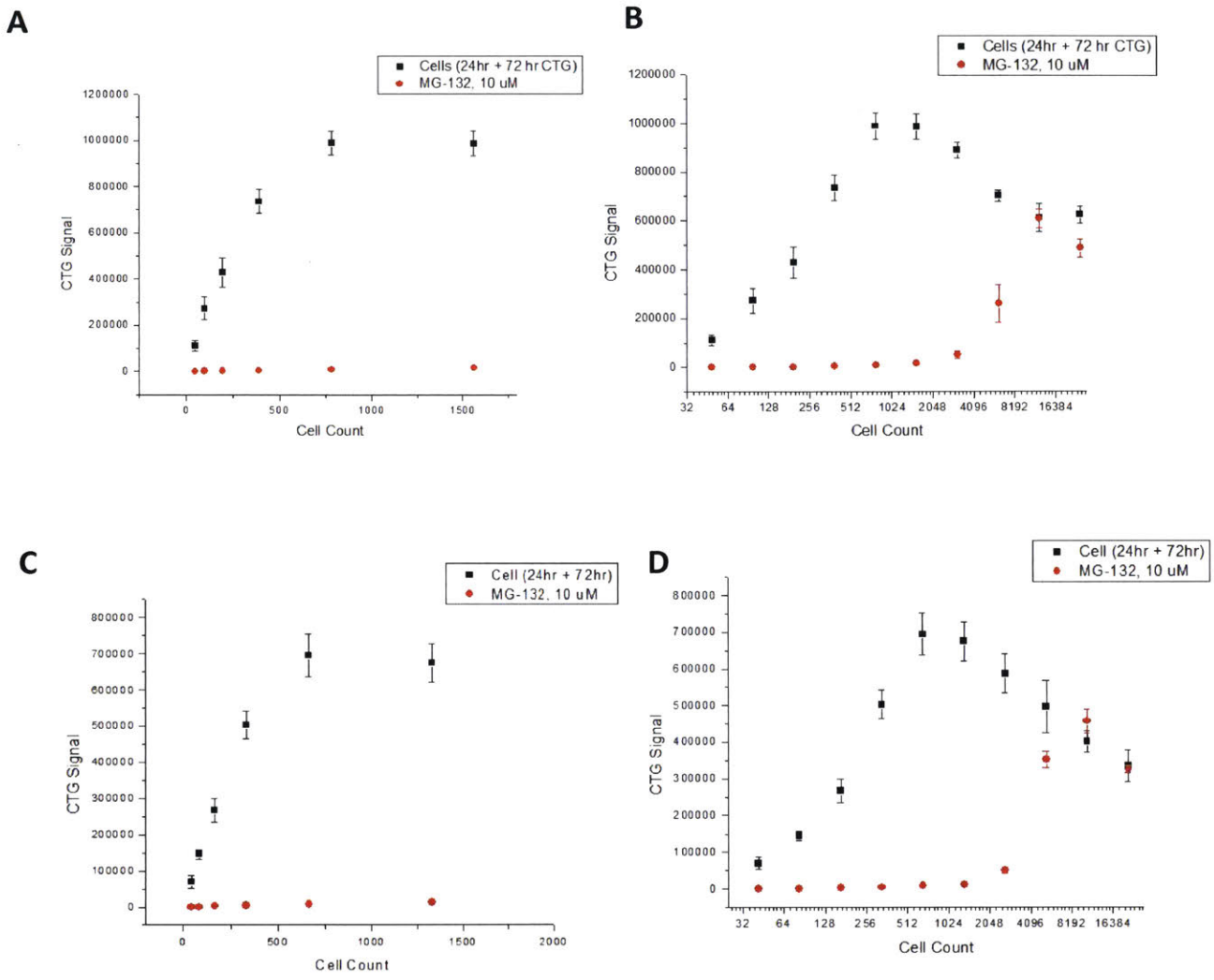

Figure 3.S8: 2980A cell density assays plotting cell seeding count vs. CTG assay cell viability signal after 24+ 72 h of incubation time, which is representative of incubation period for the CI studies. Trial 1 is shown in A) zoom-in with x-axis plotted linearly, and B) full plot with x-axis plotted on log 2 scale. Trial 2 is shown in C) zoom-in with x-axis plotted linearly, and D) full plot with x-axis plotted on log 2 scale. We chose to seed cells at 500 cells/well, which is in the linear region of seeding densities.

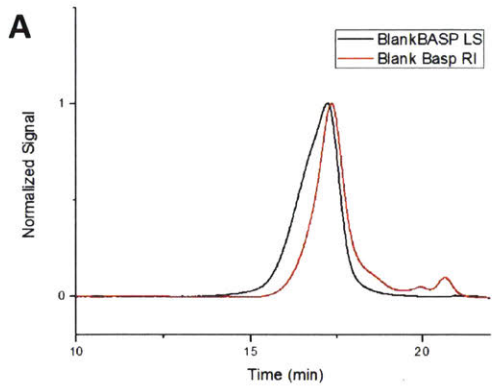

Blank BASP (10 eq PEG-MM, 10 eq Acetal-XL,1 eq G3)	
M_w (g/mol)	456 000
M_n (g/mol)	315 000
Đ	1.45

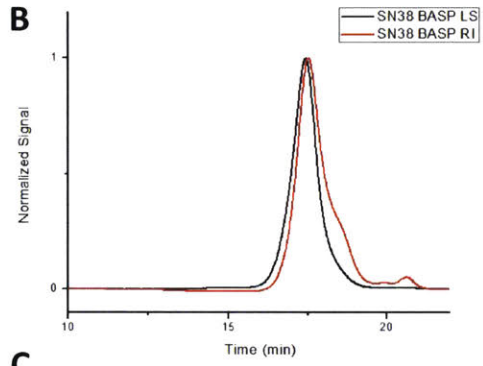

SN38 BASP (5 eq SN38-MM, 5 eq PEG-MM, 10 eq Acetal-XL, 1 eq G3)	
M_w (g/mol)	263 000
M_n (g/mol)	197 000
Đ	1.34

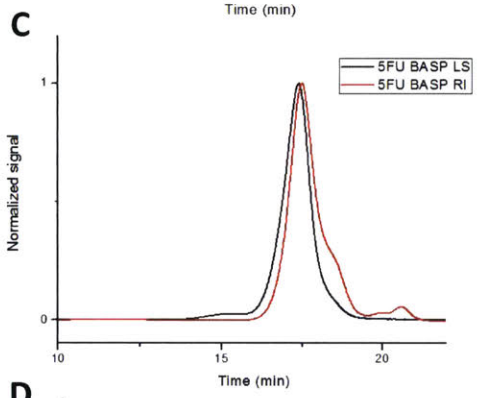

5FU BASP (7 eq 5FU-MM, 3 eq PEG-MM, 10 eq Acetal-XL, 1 eq G3)	
M_w (g/mol)	282 000
M_n (g/mol)	207 000
Đ	1.36

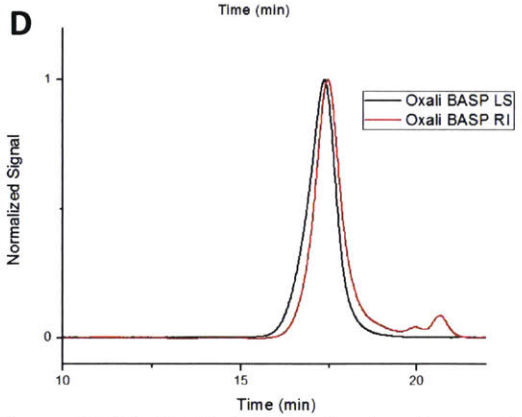

Oxali BASP (7 eq PEG-MM, 5 eq Oxali-XL, 1 eq G3)	
M_w (g/mol)	336 000
M_n (g/mol)	271 000
Đ	1.24

Figure 3.S9: GPC characterization for particles used in the single drug MTD studies in **Figure 3.18** including A) blank BASP, B) SN38 loaded BASP, C) 5-fluorouracil loaded BASP, and D) oxaliplatin loaded BASPs.

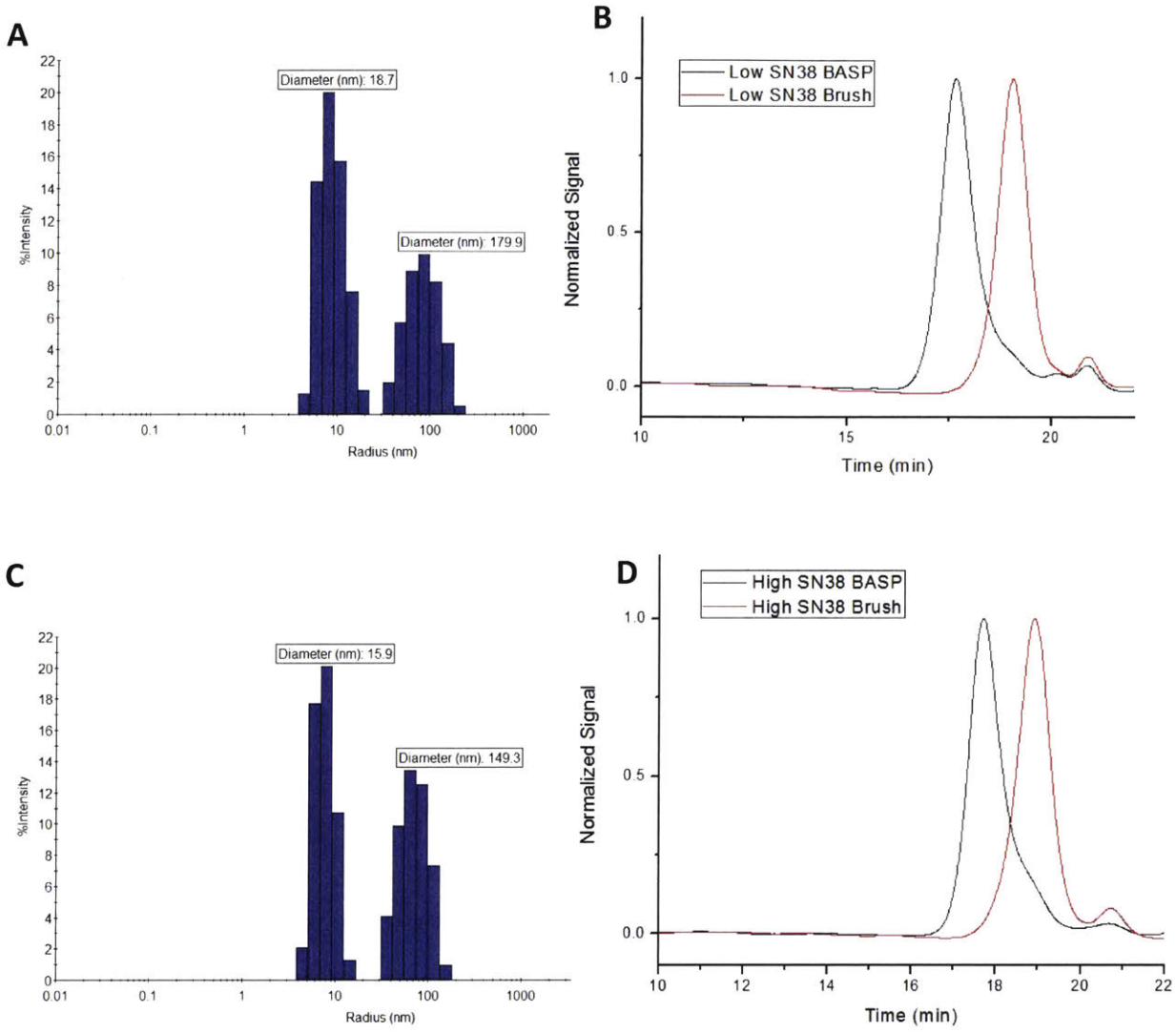

Figure 3.S10: Characterization of three drug-conjugated BASPs used in the MTD study in **Figure 3.19**. A) DLS showing intensity average D_H of 18.7 nm, and B) GPC-MALLS chromatograph of brush and BASP Sample A: 0.2 eq SN38-MM, 2 eq 5FU-MM, 4.8 eq PEG-MM, 5 eq Oxali-XL, and 1.1 wt.% Cy7.5-MM formulation. C) DLS showing intensity average D_H of 15.9 nm, and D) GPC-MALLS chromatograph of brush and BASP Sample B: 5 eq SN38-MM, 0.5 eq 5FU-MM; 1.5 eq PEG-MM; 5 eq Oxali-XL, and 1.3 wt.% Cy7.5-MM formulation.

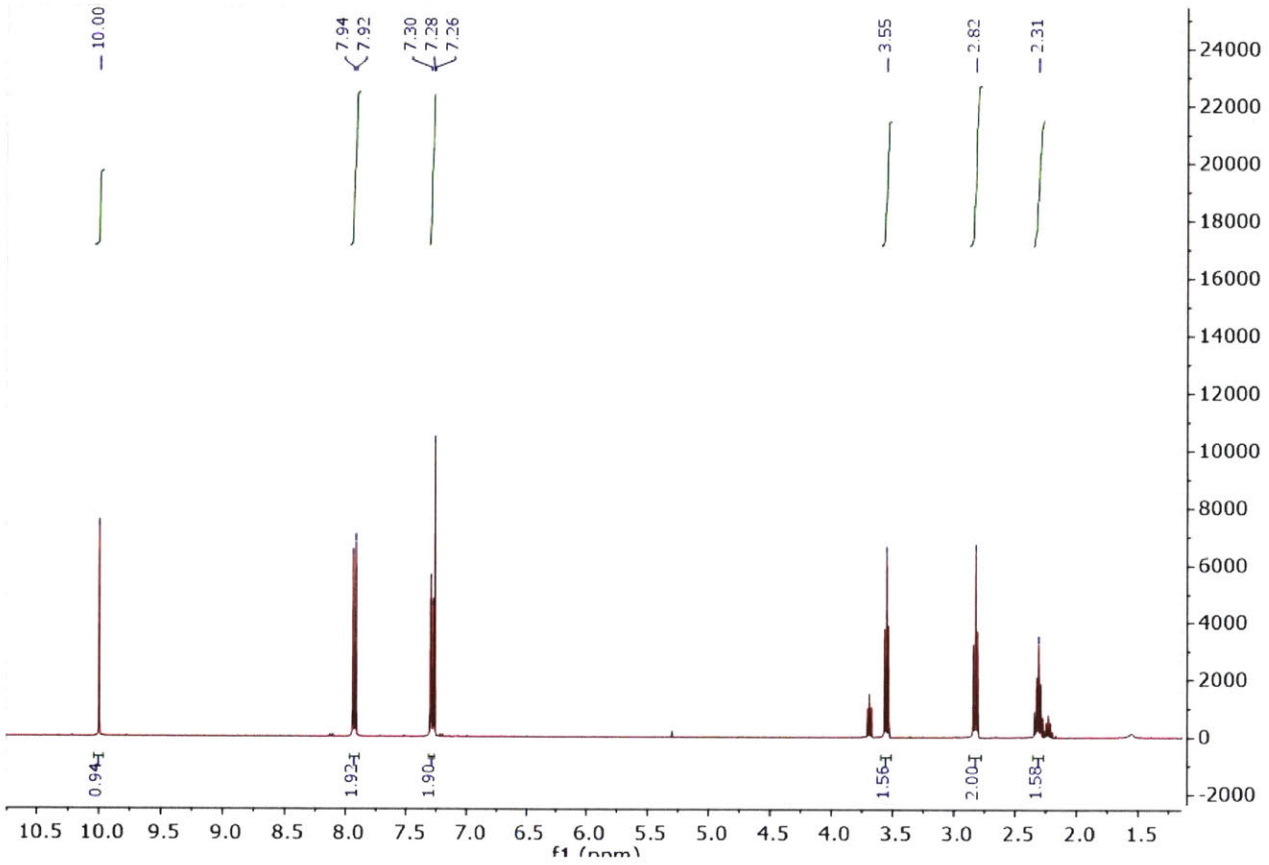

Figure 3.S11. ^{1}H-NMR spectrum of **4-formylphenyl 4-bromobutanoate, compound 3.1** in $CDCl_3$.

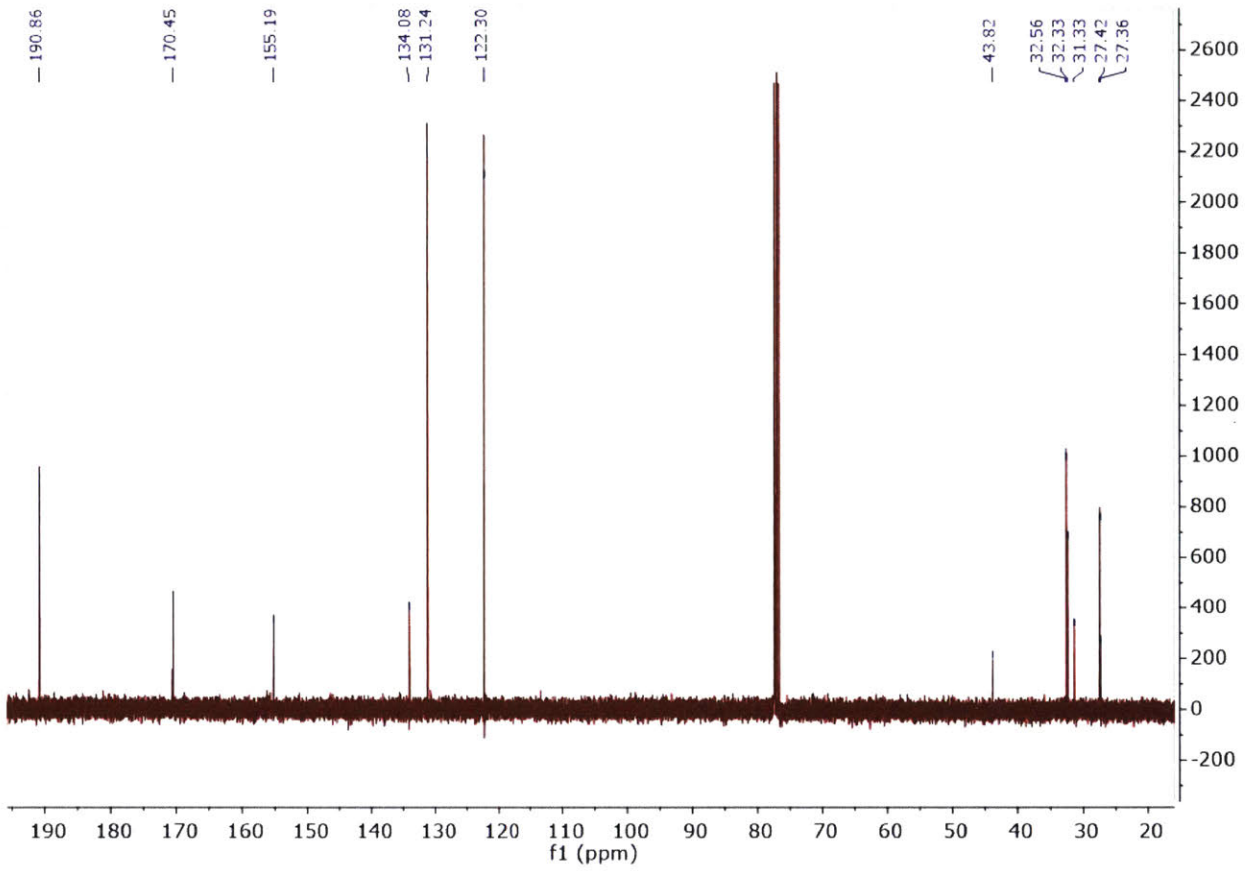

Figure 3.S12. ^{13}C-NMR spectrum of **4-formylphenyl 4-bromobutanoate, compound 3.1** in $CDCl_3$.

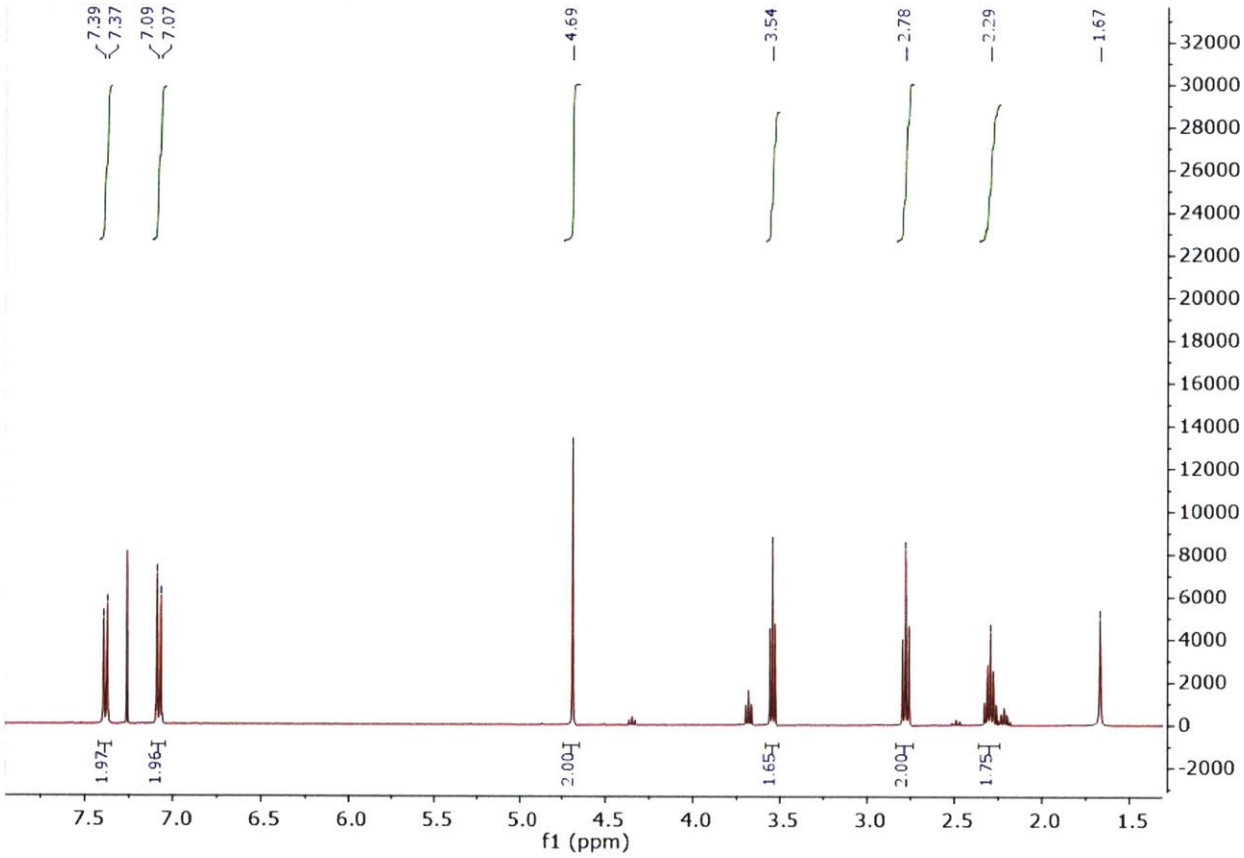

Figure 3.S13. ^{1}H-NMR spectrum of **4-(hydroxymethyl)phenyl 4-bromobutanoate, compound 3.2** in $CDCl_3$.

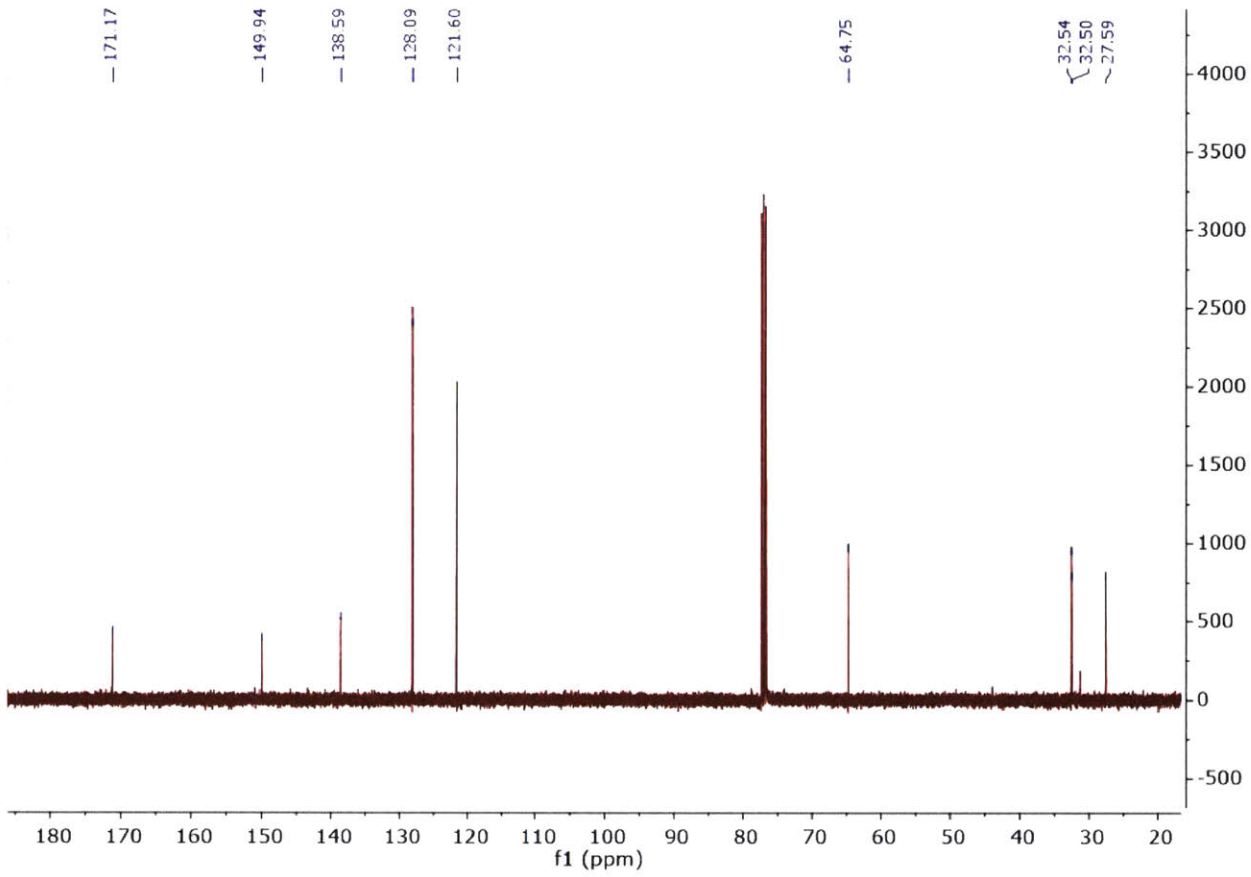

Figure 3.S14. ^{13}C-NMR spectrum of **4-(hydroxymethyl)phenyl 4-bromobutanoate, compound 3.2** in $CDCl_3$.

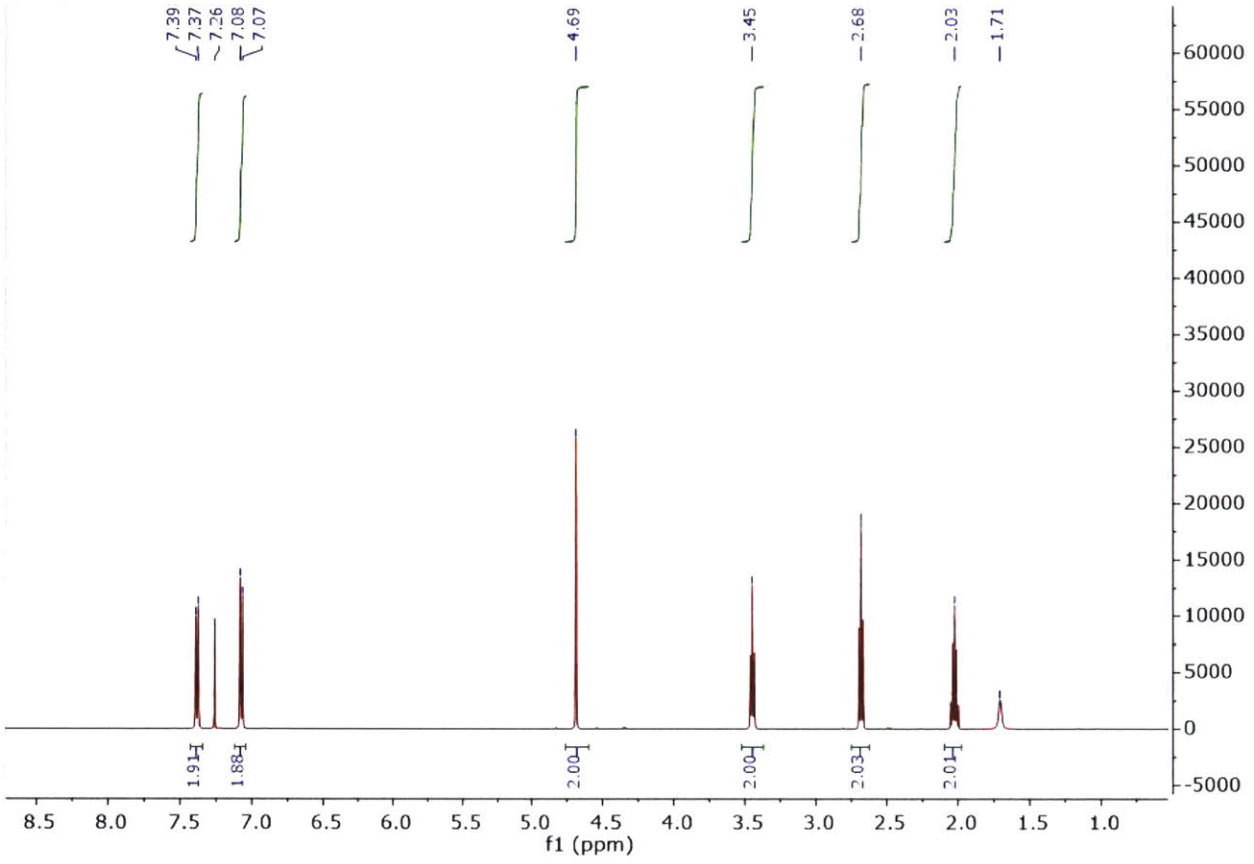

Figure 3.S15. ^{1}H-NMR spectrum of **4-(hydroxymethyl)phenyl 4-azidobutanoate, compound 3.3** in $CDCl_3$.

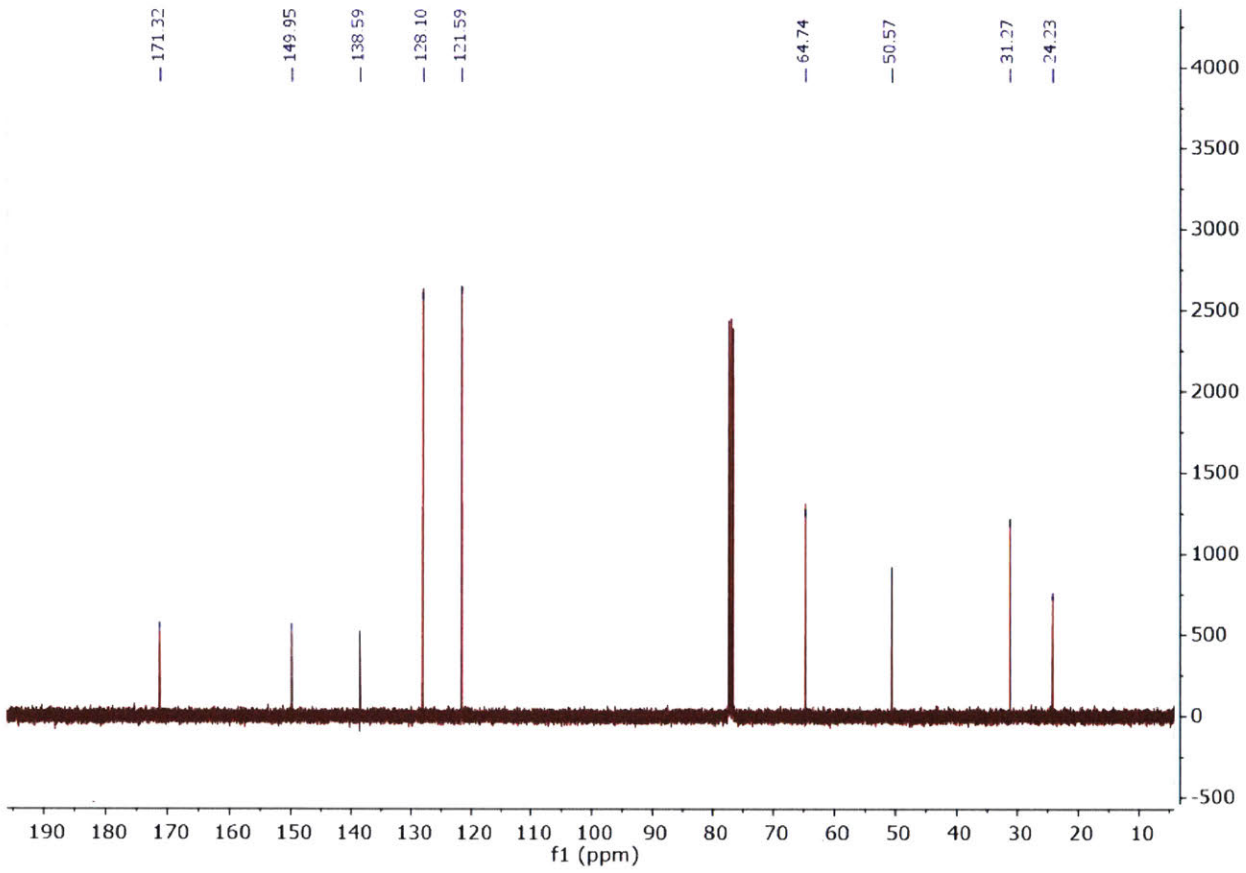

Figure 3.S16. ^{13}C-NMR spectrum of **4-(hydroxymethyl)phenyl 4-azidobutanoate, compound 3.3** in $CDCl_3$.

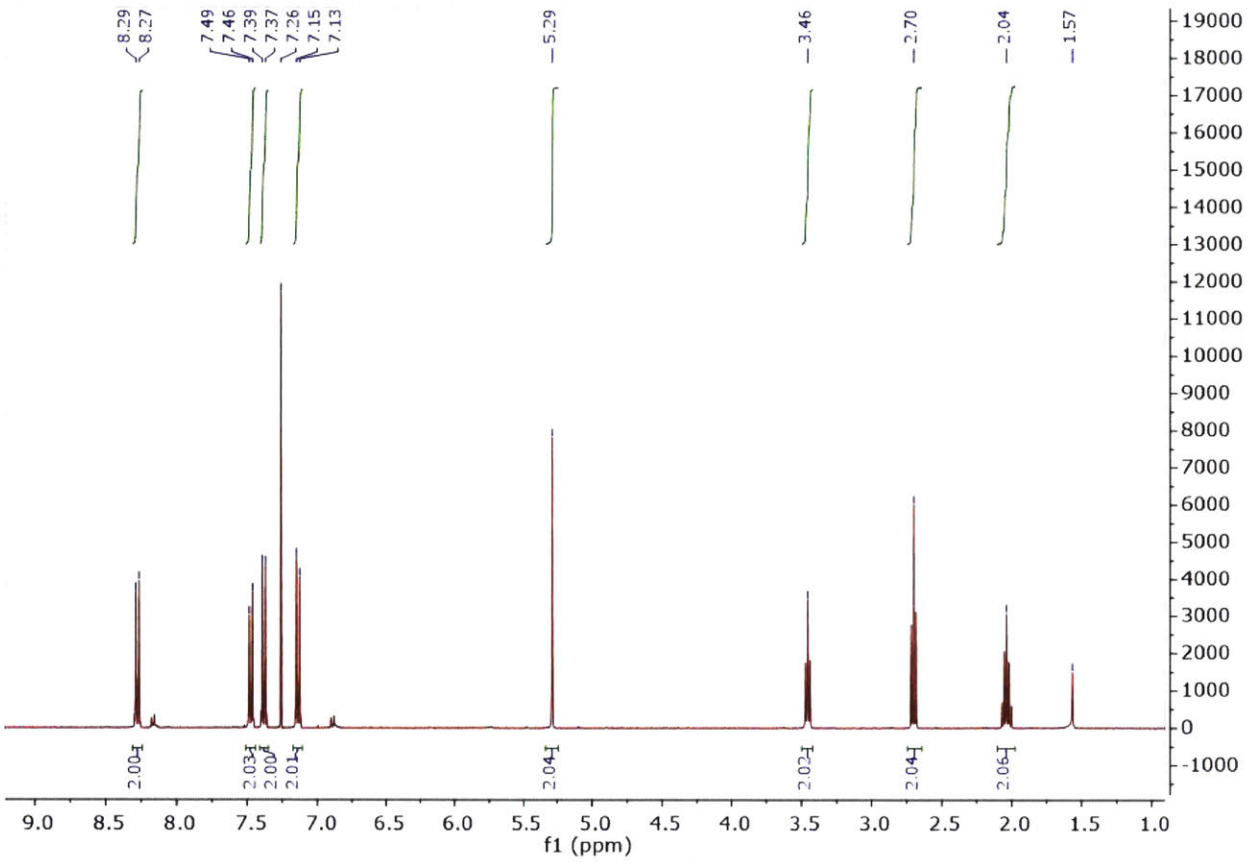

Figure 3.S17. ^{1}H-NMR spectrum of **compound 3.4** in $CDCl_3$.

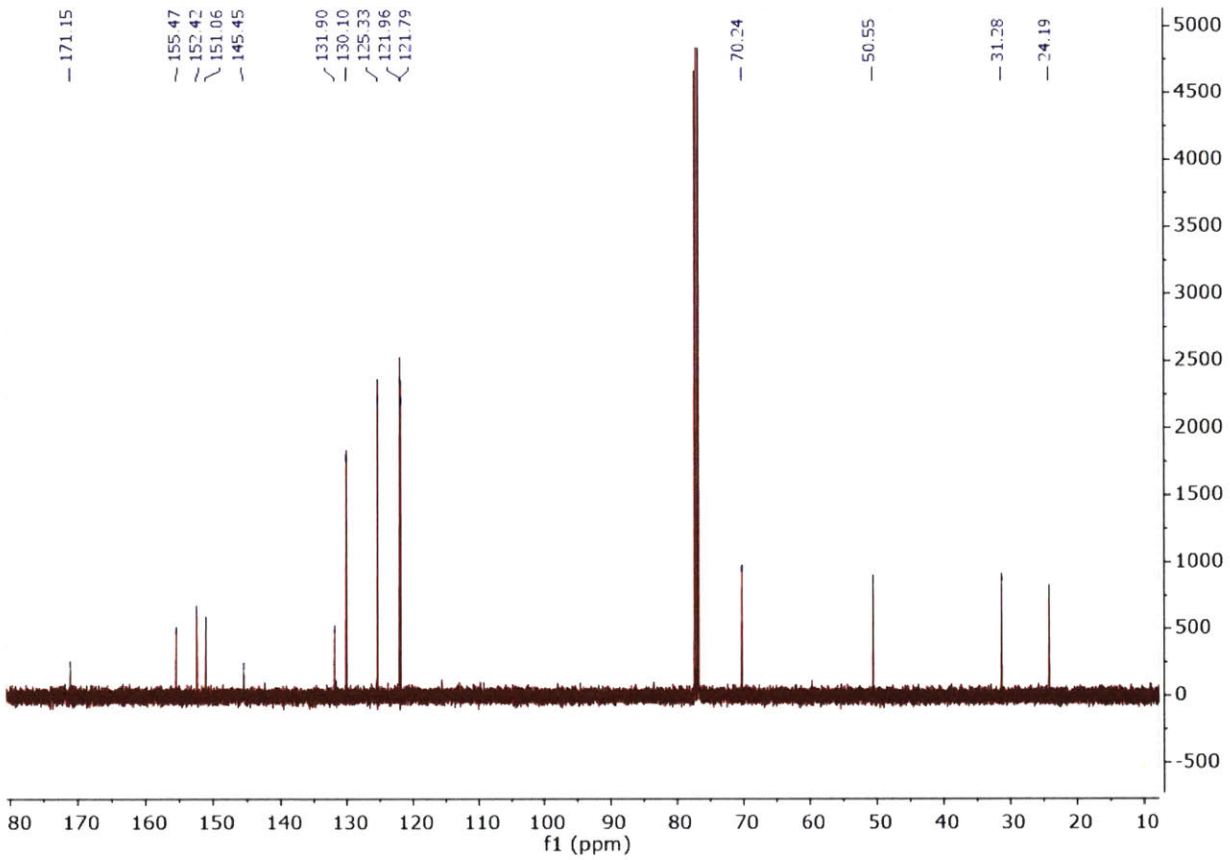

Figure 3.S18. ^{13}C-NMR spectrum of **compound 3.4** in $CDCl_3$.

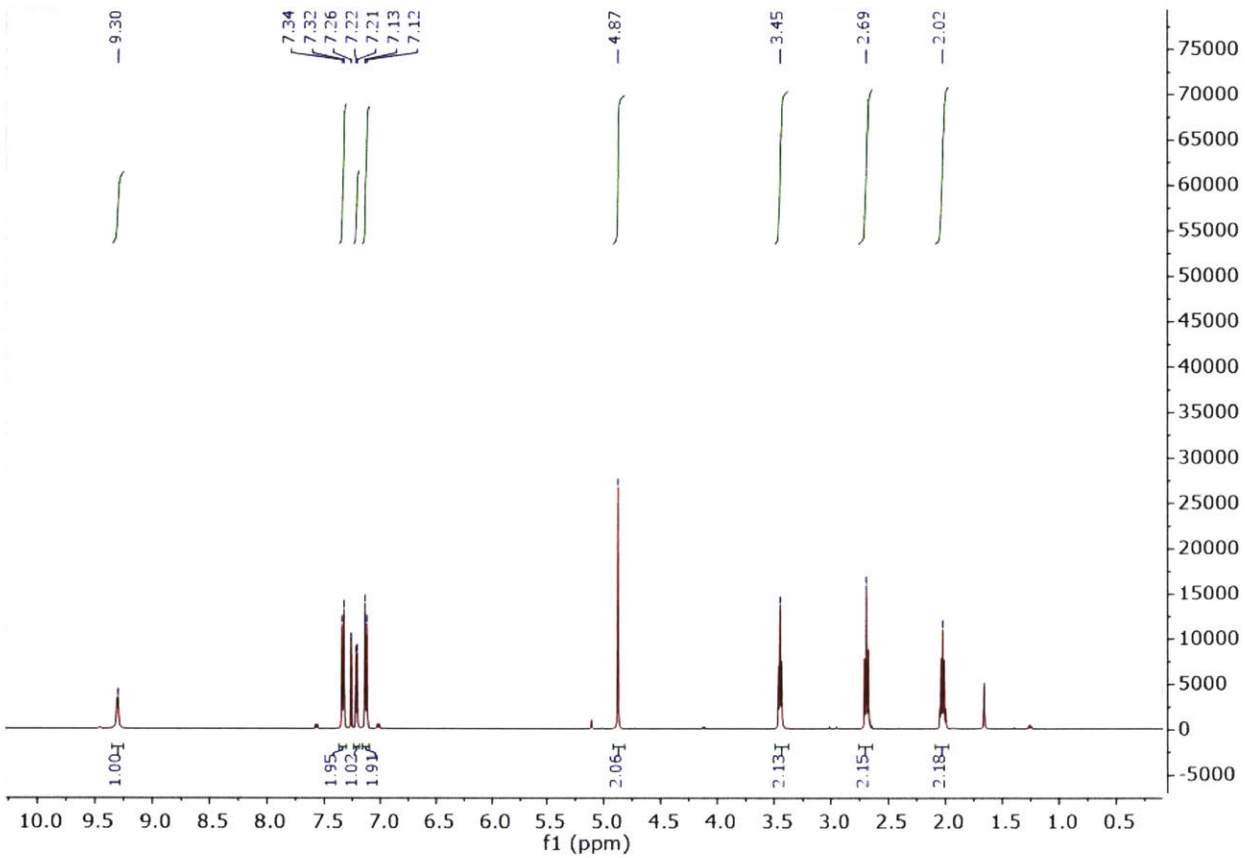

Figure 3.S19. ^{1}H-NMR spectrum of **5FU-Az** in $CDCl_3$.

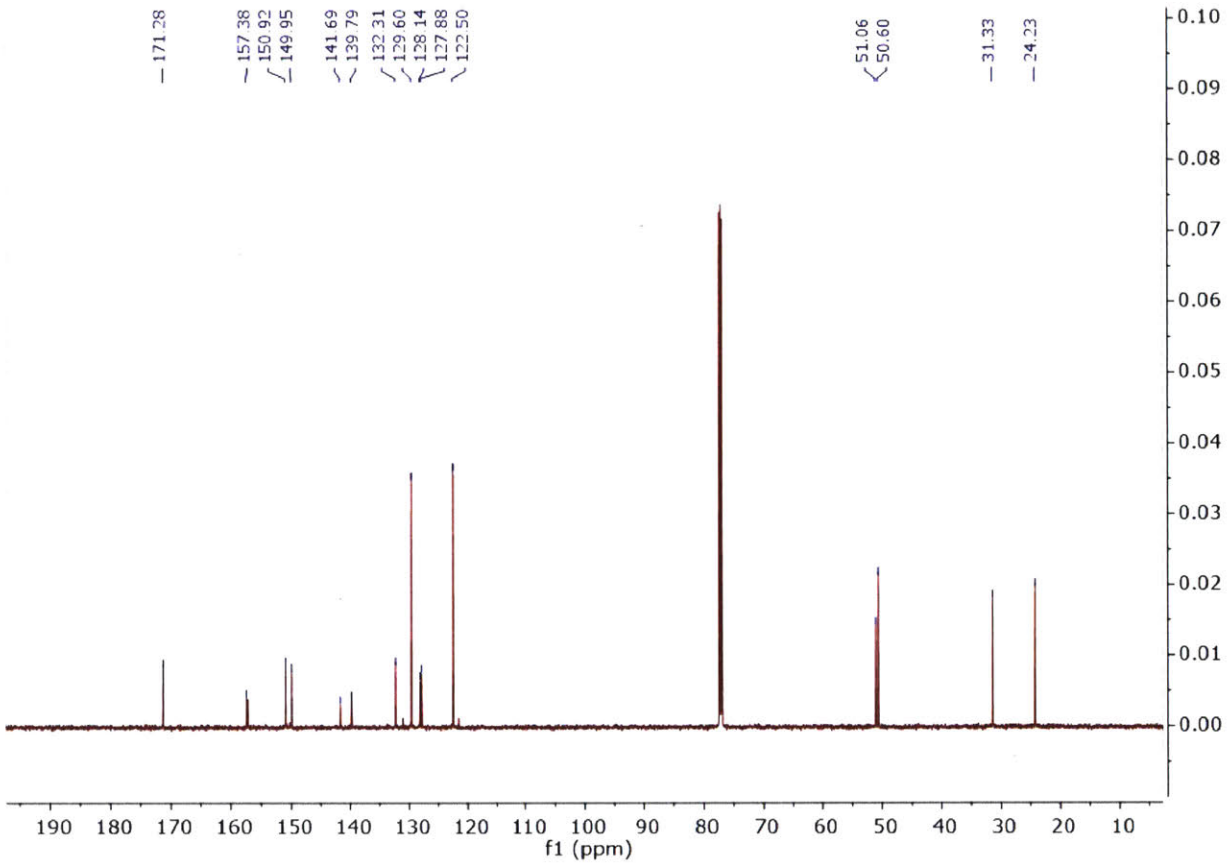

Figure 3.S20. ^{13}C-NMR spectrum of **5FU-Az** in $CDCl_3$.

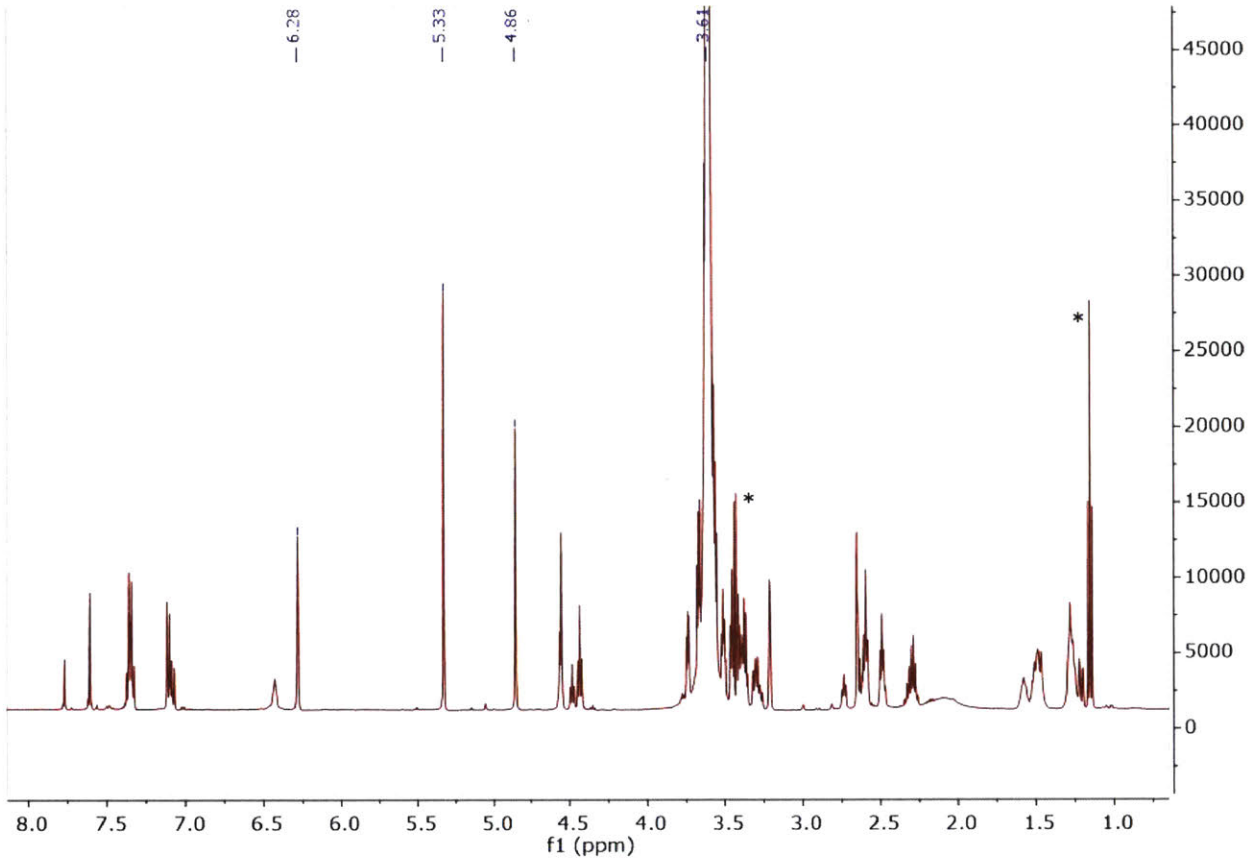

Figure 3.S21: ^{1}H-NMR of 5FU-MM taken on a 500 MHz NMR spectrometer in CD_2Cl_2. Some diethyl ether contaminant present as indicated by the *.

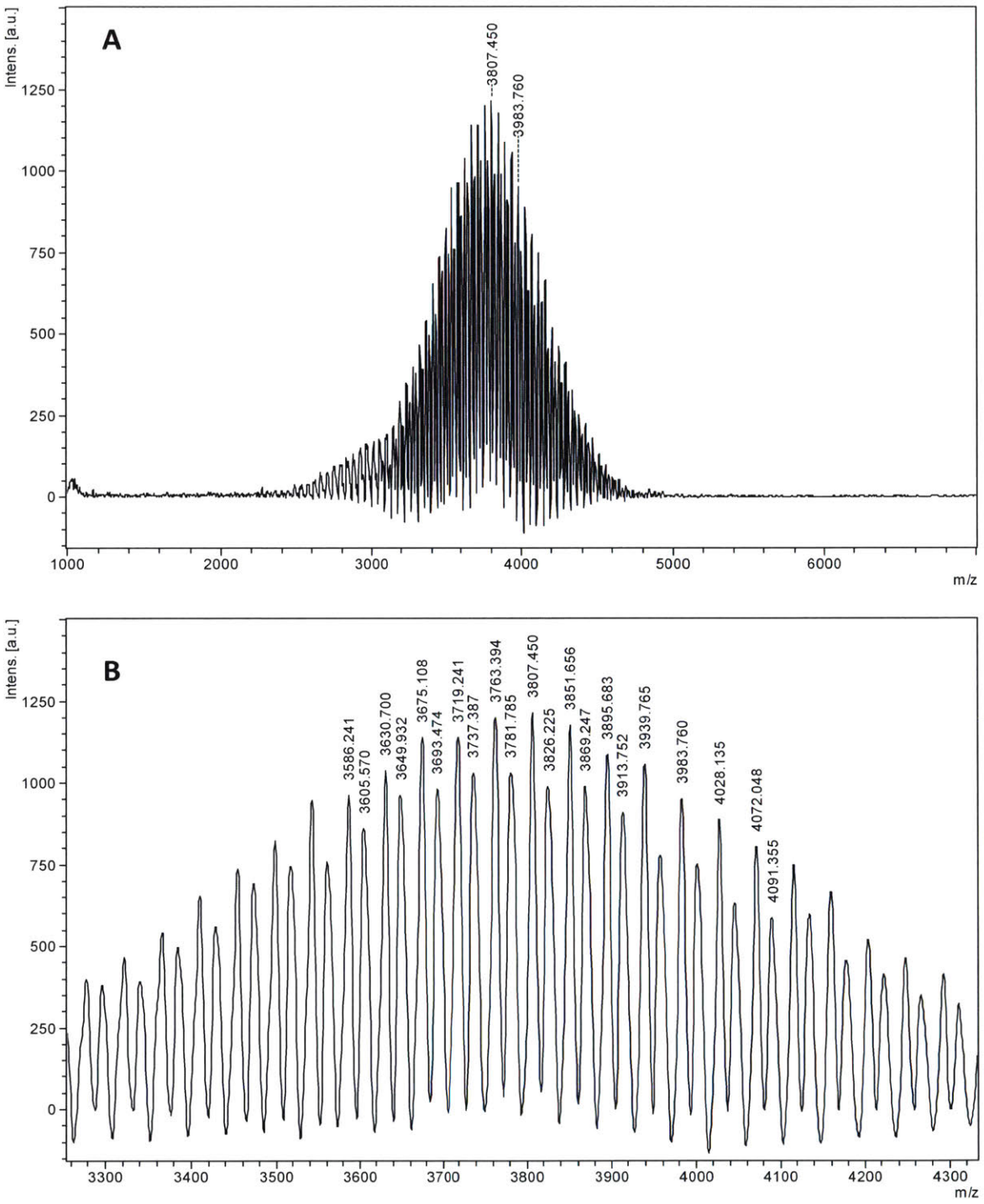

Figure 3.S22: MALDI-TOF of 5FU-MM. A) Full spectra. B) Expanded. (M+Na)+ calcd. for $C_{173}H_{315}FN_8O_{76}Na^+$: 3764.1, Observed: 3763.4; (M+K)+ calcd. for $C_{173}H_{315}FN_8O_{76}K^+$: 3780.1, Observed: 3781.8.

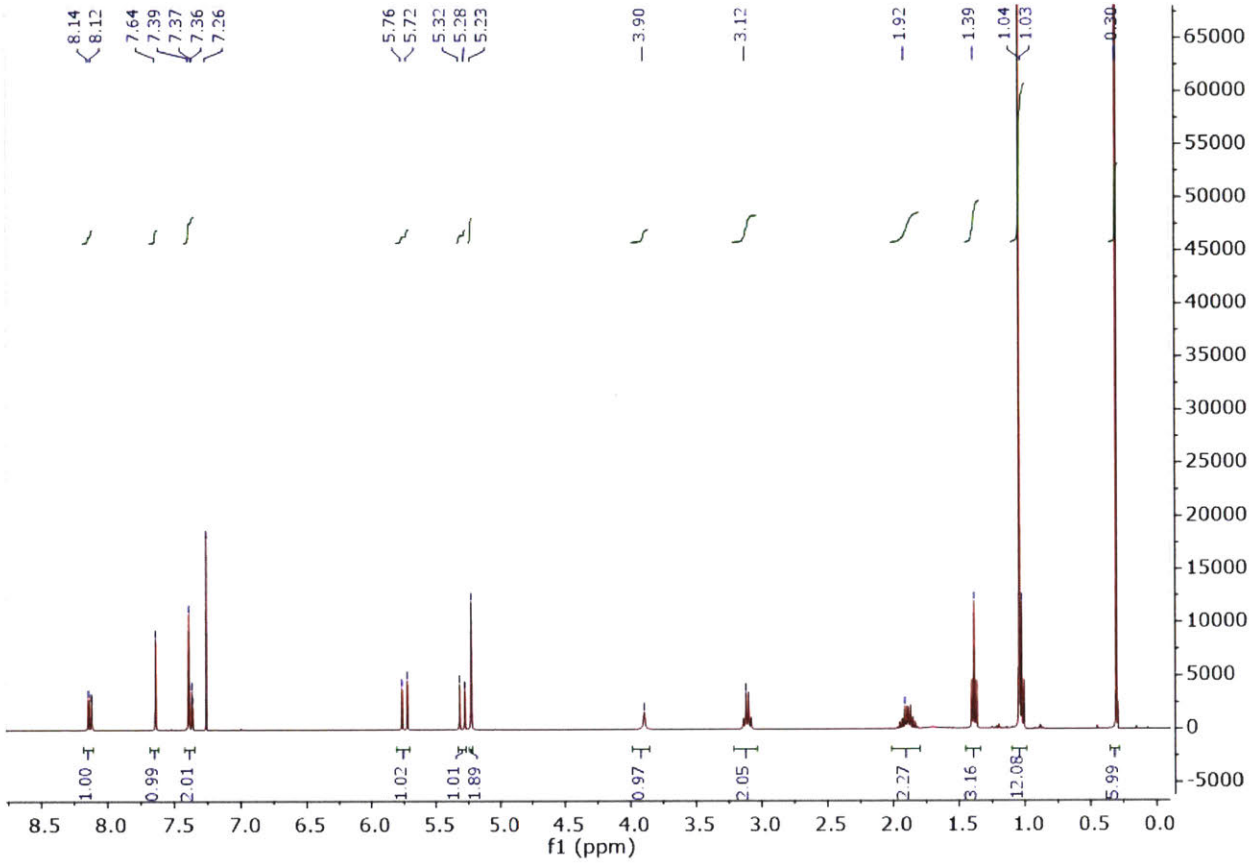

Figure 3.S23. ^{1}H-NMR spectrum of **SN38-TBDMS** in $CDCl_3$.

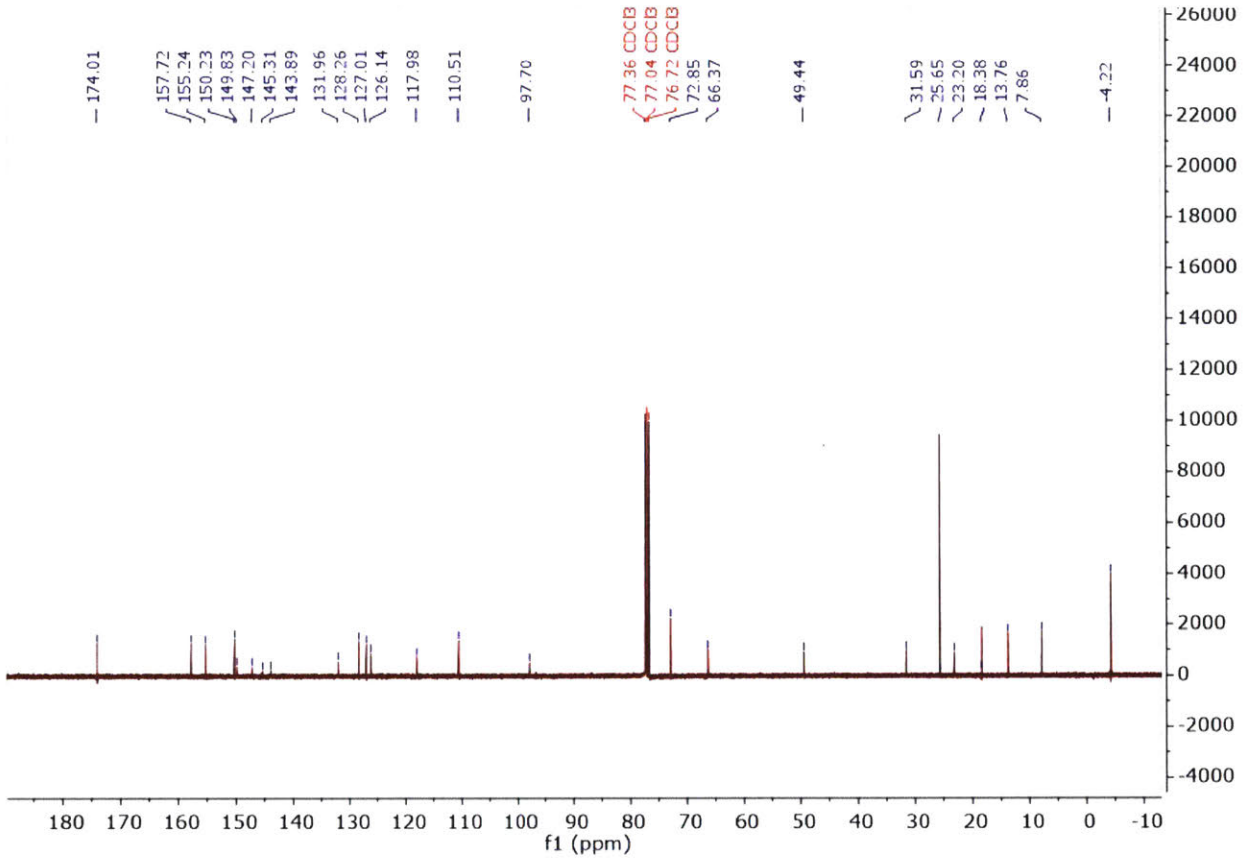

Figure 3.S24. ^{13}C-NMR spectrum of **SN38-TBDMS** in $CDCl_3$.

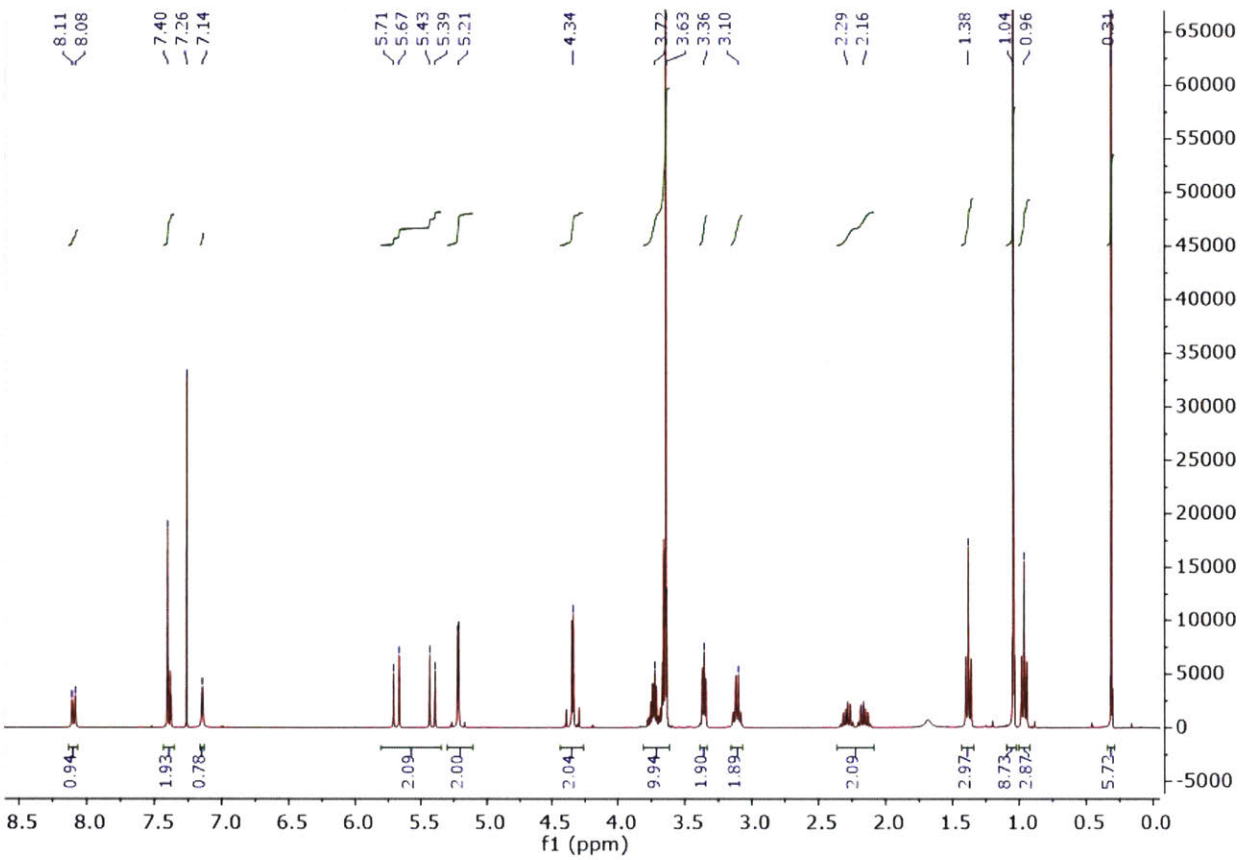

Figure 3.S25. ^{1}H-NMR spectrum of **SN38-TBDMS-Az** in $CDCl_3$.

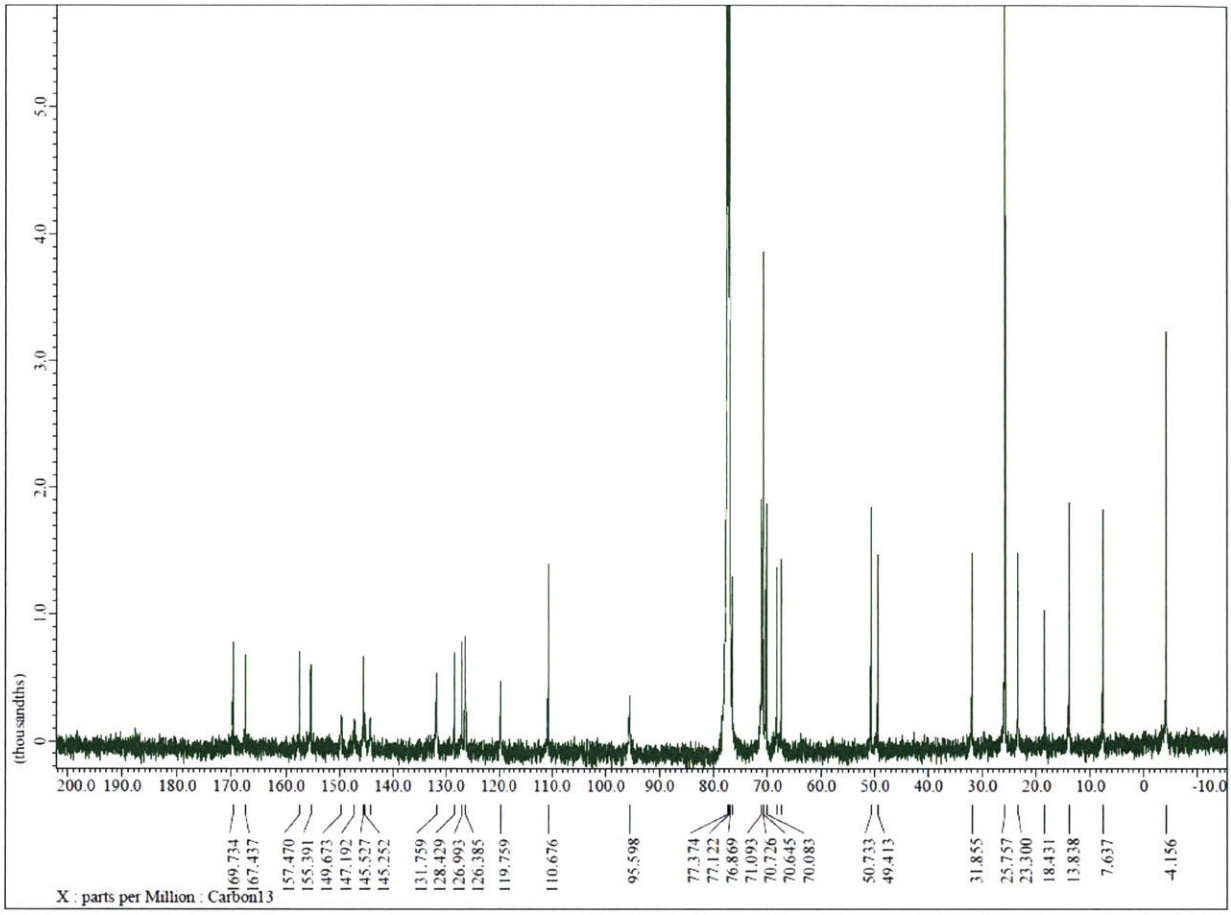

Figure 3.S26. ^{13}C-NMR spectrum of **SN38-TBDMS-Az** in $CDCl_3$.

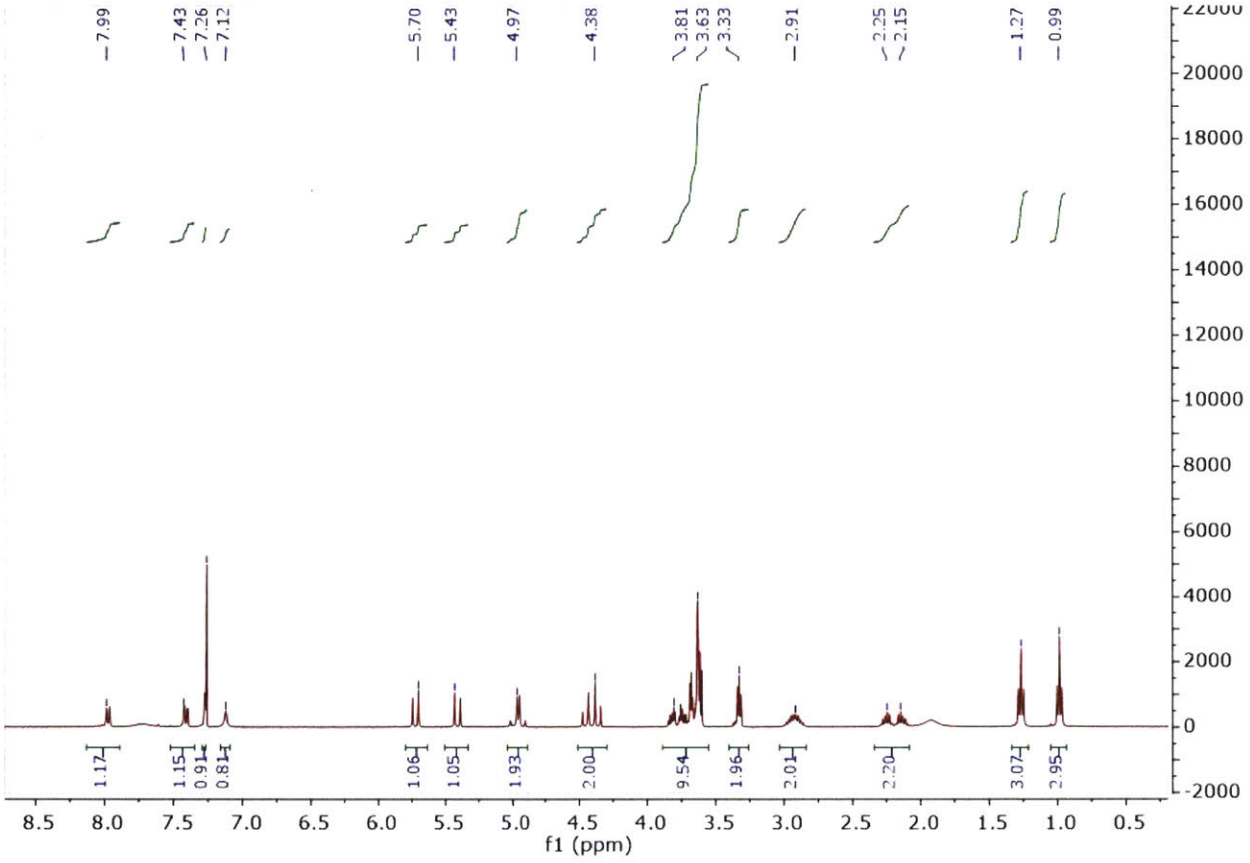

Figure 3.S27. ^{1}H-NMR spectrum of **SN38-Az** in $CDCl_3$.

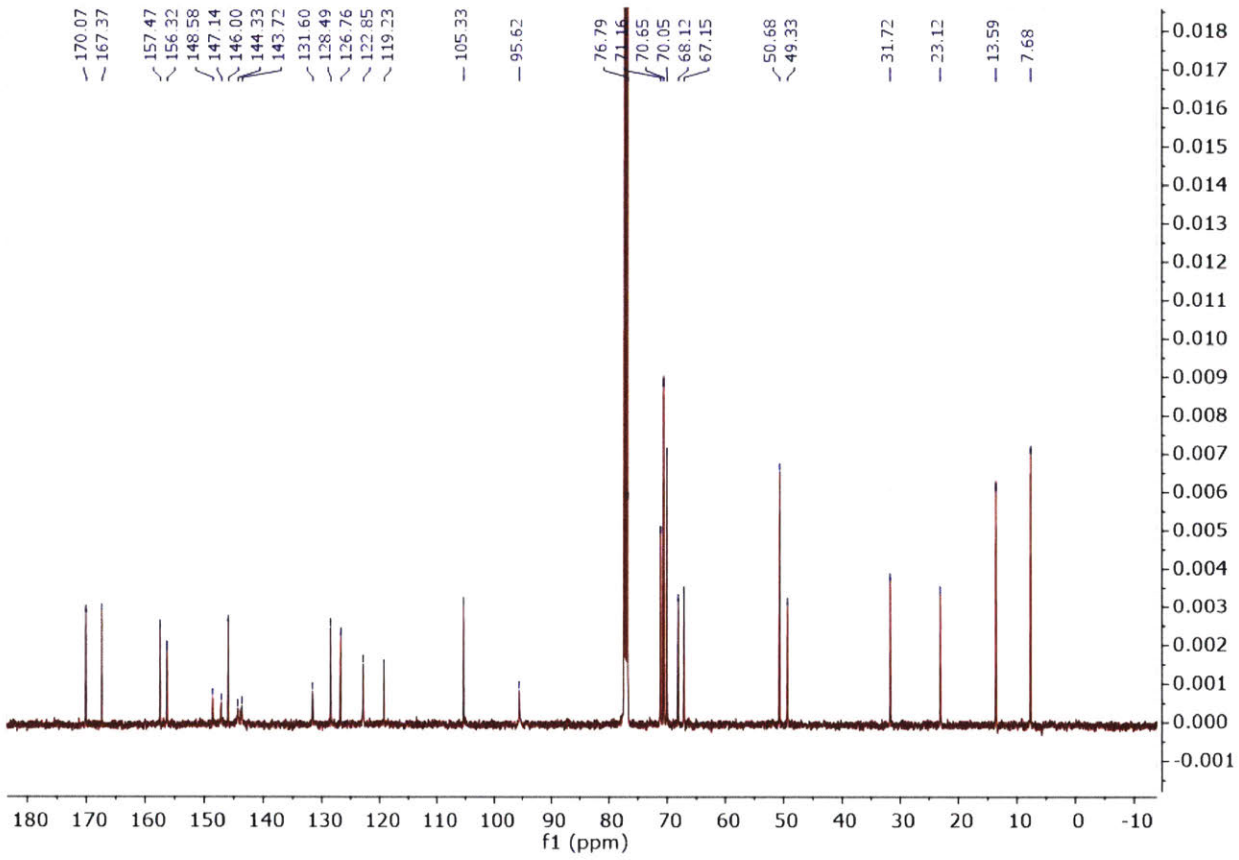

Figure 3.S28. ^{13}C-NMR spectrum of **SN38-Az** in $CDCl_3$.

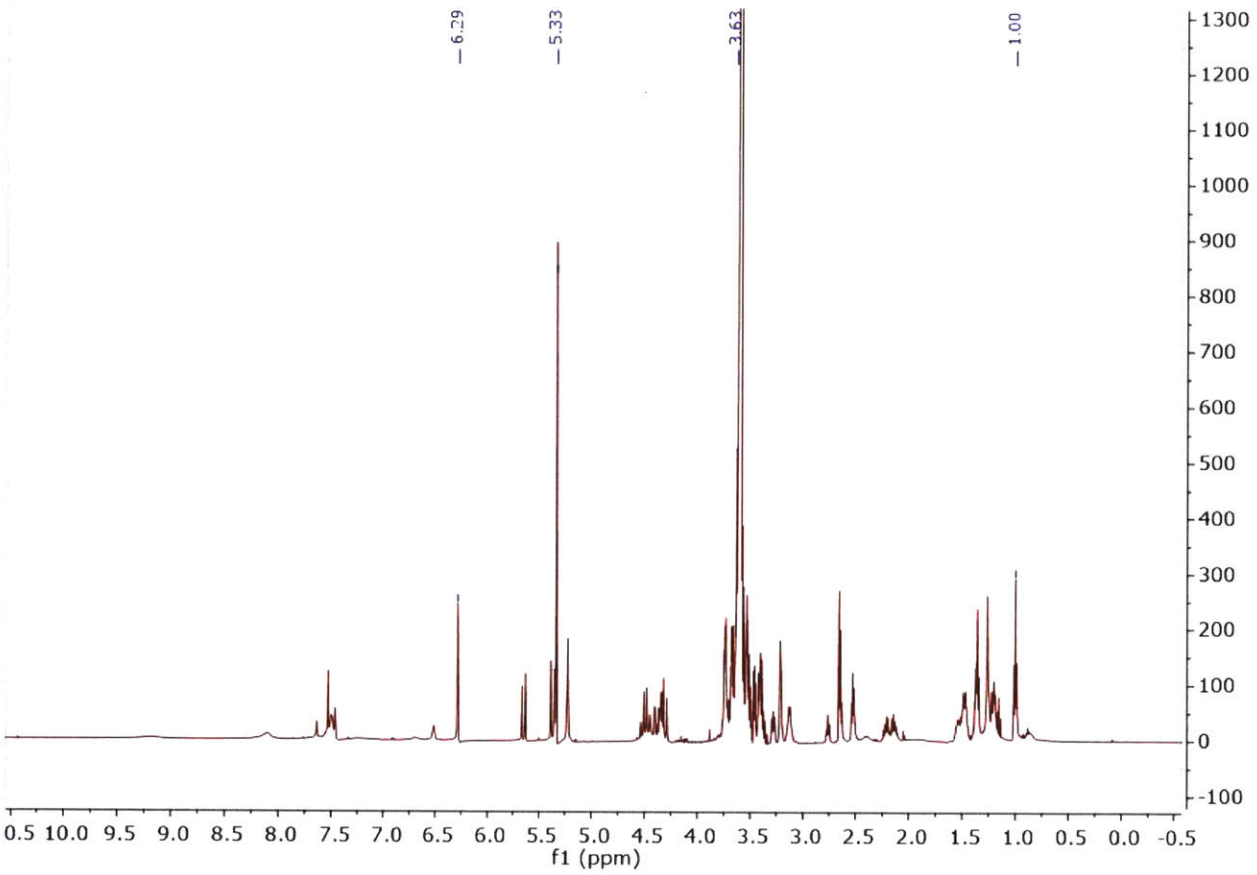

Figure 3.S29: ^{1}H-NMR of SN38-MM taken on a 500 MHz NMR spectrometer in CD_2Cl_2.

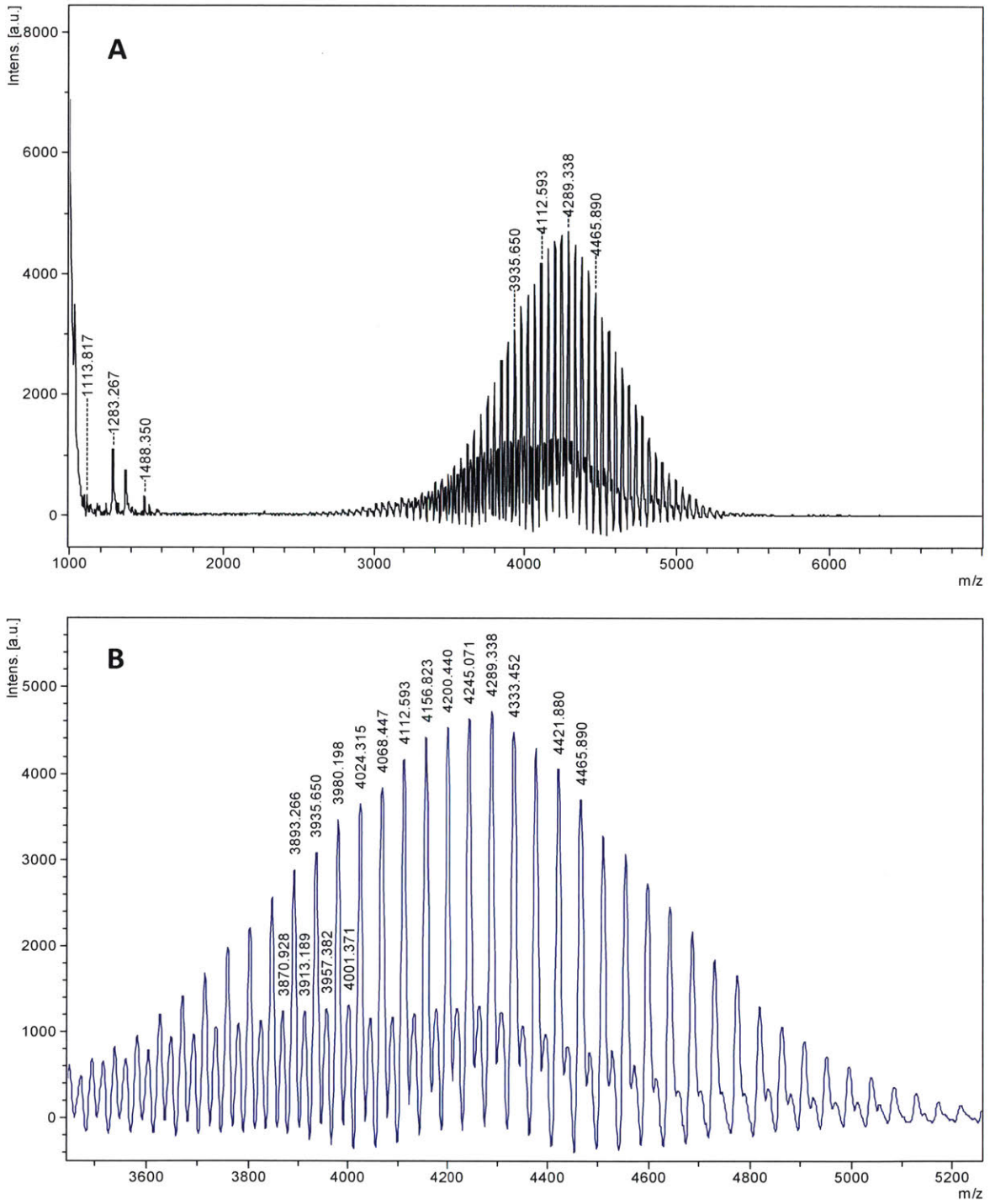

Figure 3.S30: MALDI-TOF of SN38-MM. A) Full spectra. B) Expanded. (M+Na)+ calcd. for $C_{188}H_{334}N_8O_{81}Na^+$: 4025.2, Observed: 4024.3; (M+H)+ calcd. for $C_{188}H_{335}N_8O_{81}^+$: 4003.2, Observed: 4001.4.

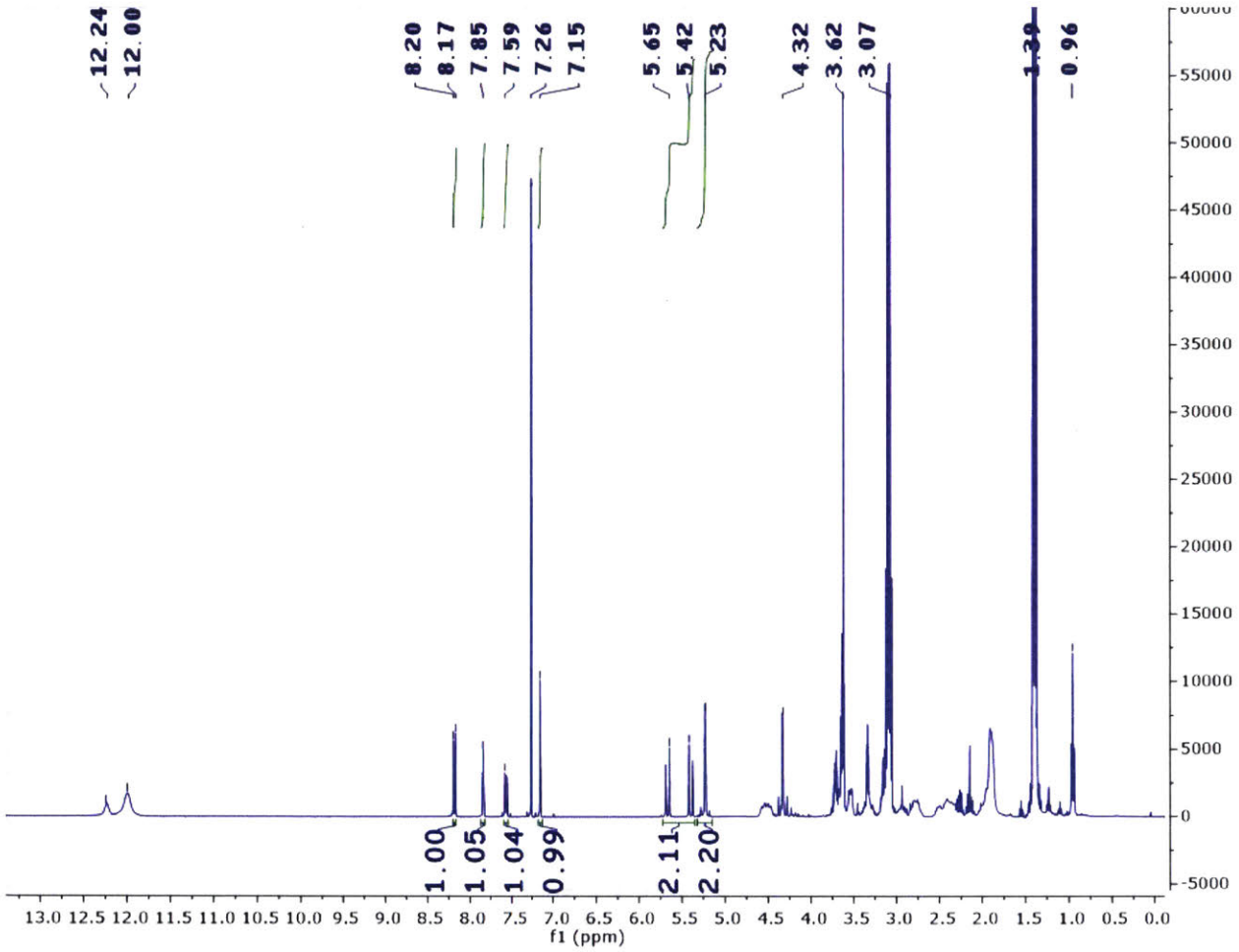

Figure 3.S31: ^{1}H-NMR of IRT-Az taken on a 400 MHz NMR spectrometer in $CDCl_3$ by Leila Terrab, a MIT Summer Research Program undergraduate.

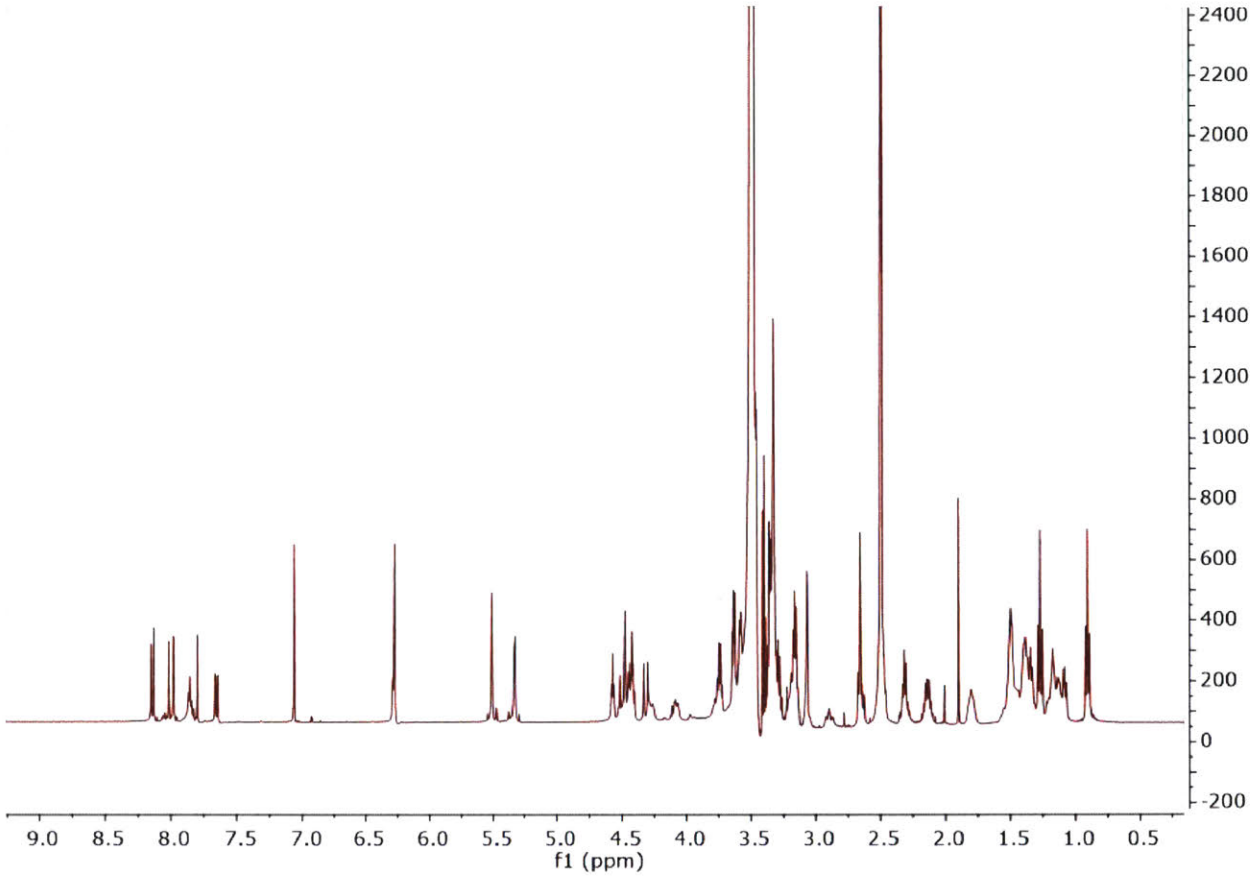

Figure 3.S32: ^{1}H-NMR of IRT-MM taken on a 500 MHz NMR spectrometer.

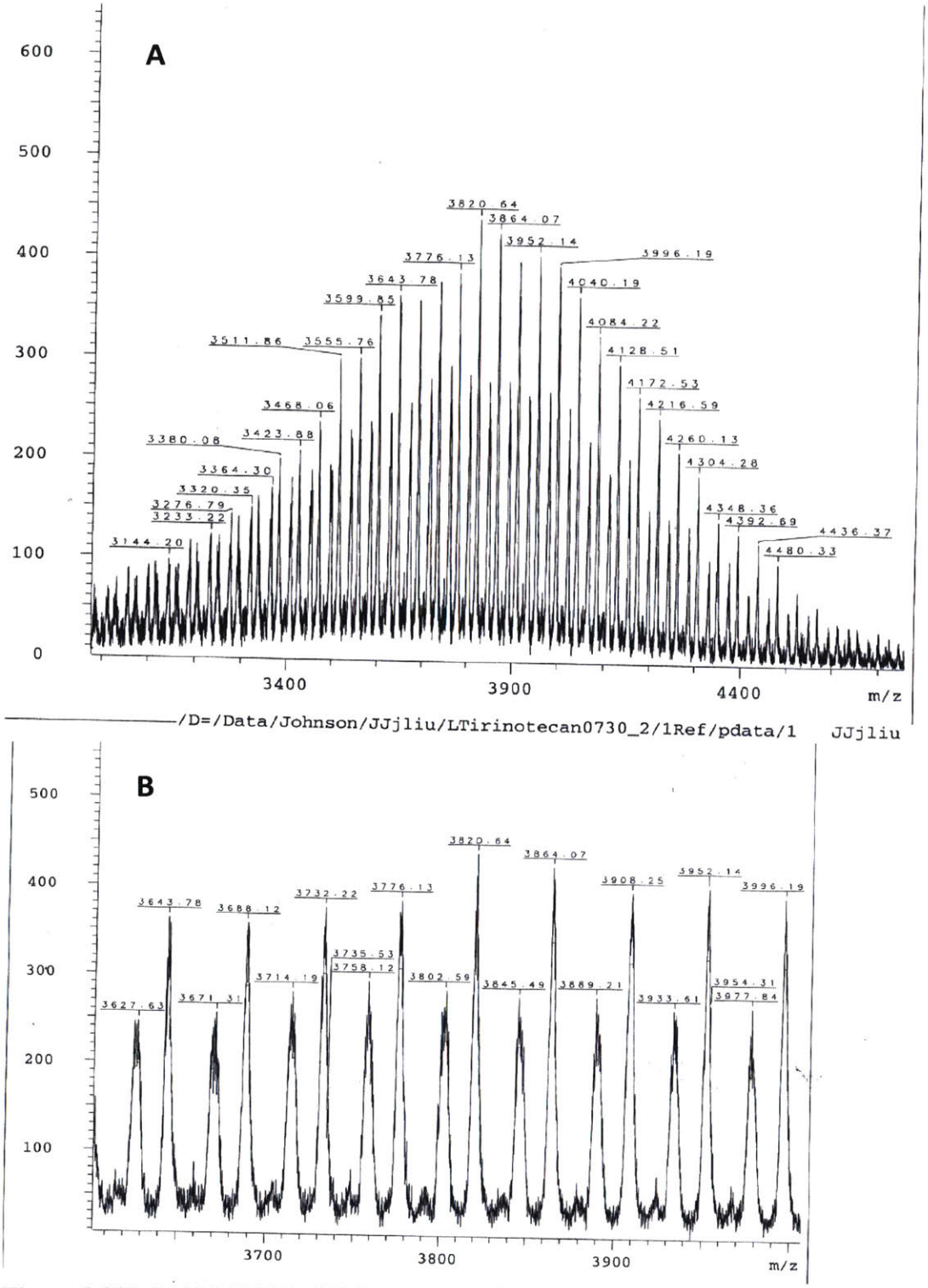

Figure 3.S33: MALDI-TOF of IRT-MM. A) Full spectra. B) Expanded. (M+Na)+ calcd. for $C_{183}H_{320}N_{10}O_{74}Na^+$: 3866.1, Observed: 3864.1; (M+H)+ calcd. for $C_{183}H_{321}N_{10}O_{74}^+$: 3844.2, Observed: 3845.5.

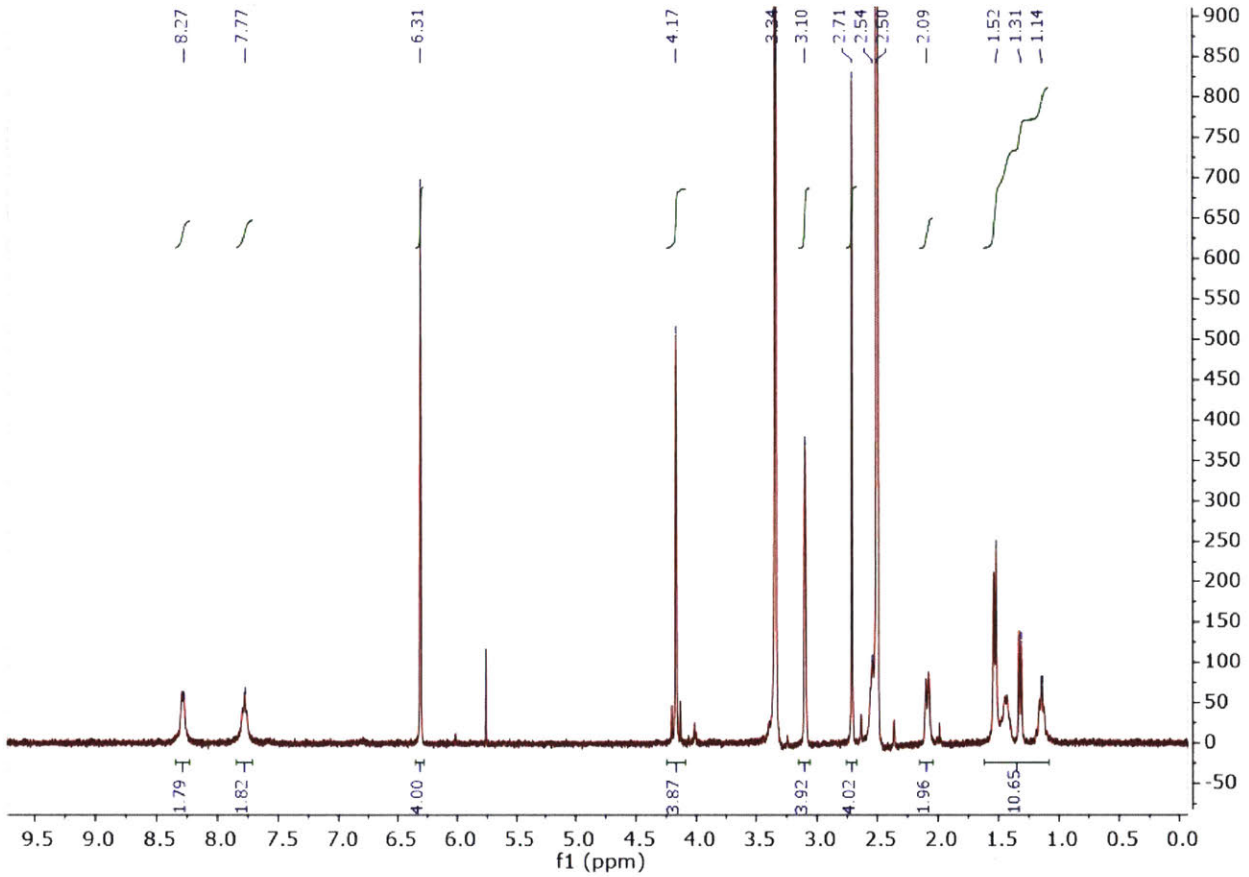

Figure 3.S34: ^{1}H-NMR of Oxali-XL taken on a 500 MHz NMR spectrometer in DMSO-d_6 (2.50 ppm); water is evident in spectra at 3.34 ppm.

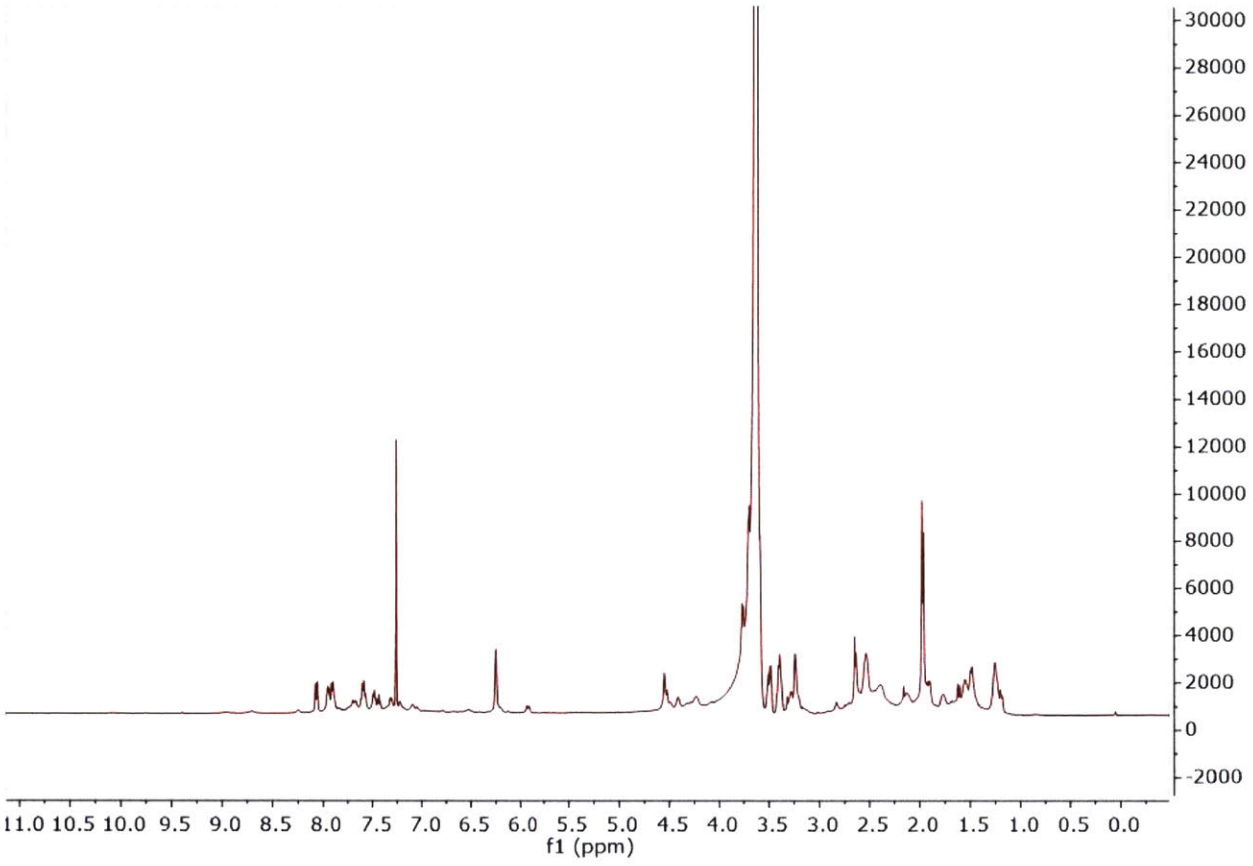

Figure 3.S35: ^{1}H-NMR of Cy7.5-MM in $CDCl_3$ taken on a 500 MHz NMR spectrometer.

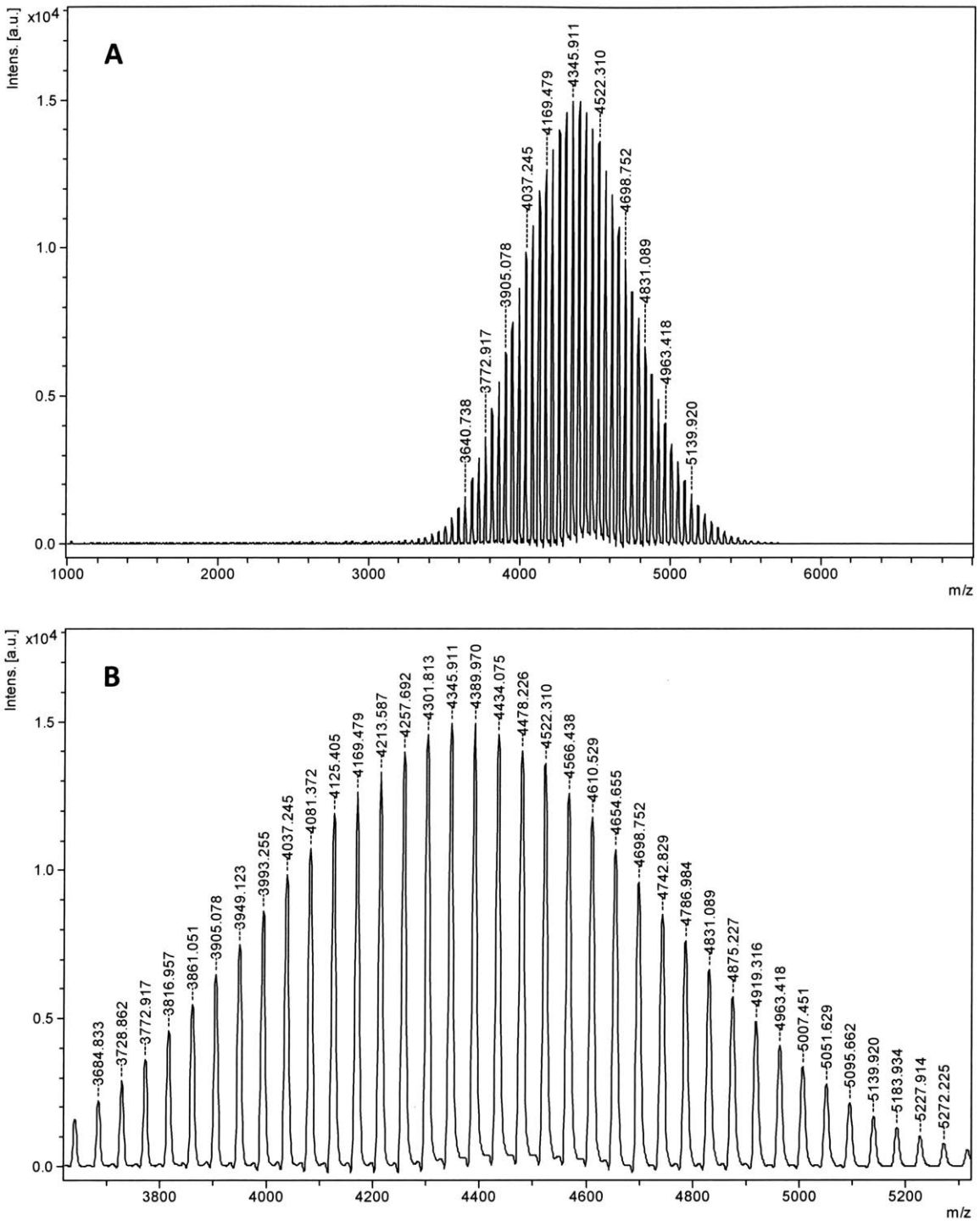

Figure 3.S36: MALDI-TOF of Cy7.5-MM. A) Full spectra. B) Expanded. [M]+ calcd. for $C_{206}H_{356}N_9O_{73}^+$: 4126.4, Observed: 4125.4.

Appendix I, Chapter 4: Developing a DNA barcoding system for bottle-brush polymers

4.1 Introduction

Brief Summary of Chapter and Respective Contributions

This chapter explores the conjugation of nucleic acids to polymers synthesized by ROMP and the possible use of these nucleic acid sequences as barcodes for polymers. No papers have been produced from this project and all work presented in the results section was that of the author.

Introduction to Nanoparticle Delivery of Nucleic Acids

Appending nucleic acids to nanoparticles has become an area of interest due to the potential of gene delivery, such as siRNA therapy and more recently, CRISPR-based gene editing. Delivery of nucleic acids without enzymatic degradation and metabolism can be a difficult challenge, but nanoparticles may provide key advantages if polymer layers or shells could protect sensitive nucleic acid cargos from nucleases and enable delivery into cells.[1-5] In the Johnson group, DNA conjugation to polymer brushes was explored not necessarily for therapeutic purposes, but instead to facilitate barcoding of the polymers. In this approach, each particle would be labeled with its own DNA barcode making identification and quantification of the components in a mixture possible.[6] The Weissleder group has shown the DNA barcodes could be appended to different antibodies and used as a high-throughput detection assay for antigens displayed on cell surfaces.[7] Once cells are treated with the DNA-antibody conjugates, thorough washing of these cells removes any unbound or weakly bound antibodies. Photocleavage of the DNA, followed by PCR amplification and gel electrophoresis was used to determine the antigens present on the cell's surface.

In the future, labeling BASPs with DNA may provide easy identification of BASPs in a mixture (e.g., tissue samples from an *in vivo* drug delivery experiment). Given a library of monomers, the convergent synthesis of BASPs and tunable sizes could potentially lend itself to a mix-and-match approach to create multifunctional, ratiometric particles. If studies of multiple BASPs are required, individually running experiments on each BASP would be tedious, require large numbers of animals, and potentially lead to errors from human and environmental variations between experiments. With DNA barcodes, experiments can be conducted with a mixture of particles, followed by DNA extraction, amplification, and sequencing to identify target BASPs (**Figure 4.1**).

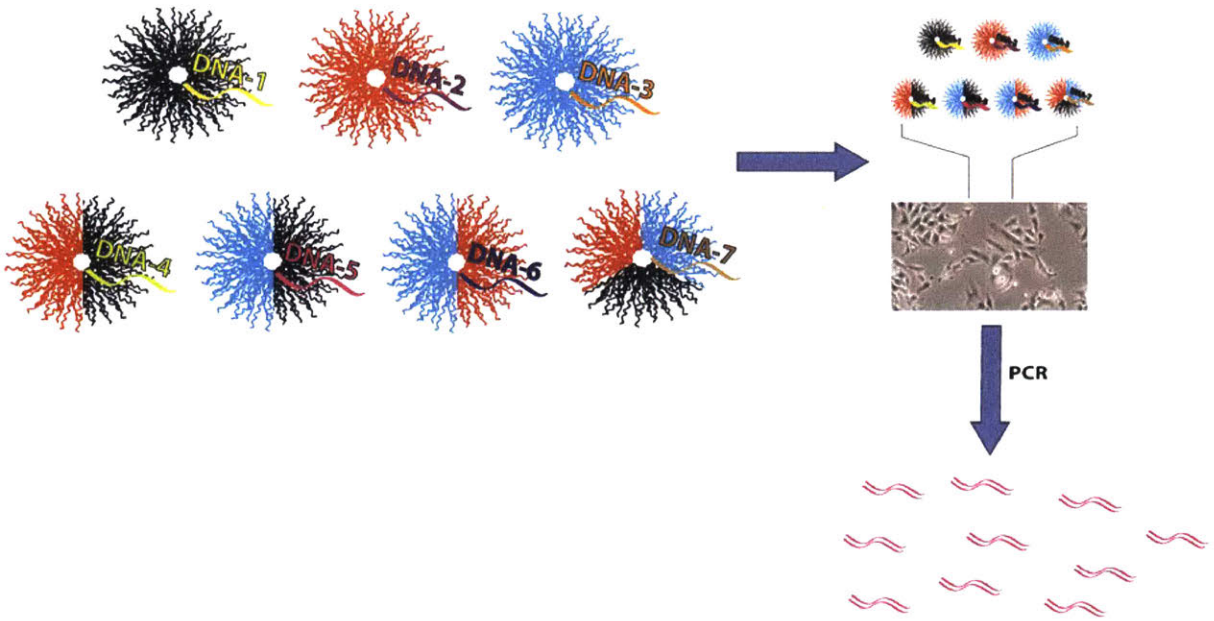

Figure 4.1: BASPs with different properties could each be labelled with its own individual barcode. Properties, such as cellular uptake dependence on BASP size, can be tested by treating cells with the mixture of labeled BAPS. DNA is then extracted and analyzed to determine which particles were preferentially taken up into cells.

To simplify this study, DNA conjugation was tested initially on simple bottle-brush polymers. ROMP can be used to synthesize bottle-brush polymers of different average molecular weight and sizes. PEG-based brush particles of different sizes can then be delivered to cells to determine the optimal sizes for cellular internalization. Although a number of chemistries for the DNA conjugation were tested, a thiol-maleimide Michael addition between polymer brushes functionalized with maleimides and DNA terminated thiol was the most efficient conjugation chemistry tested. A 55 nucleotide sequence with a poly-T spacer and a thiol functional group (DNA1) was chosen as the DNA sequence for conjugation to maleimides on PEG bottle-brushes (**Figure 4.2**). PCR amplification of DNA directly from the bottle-brush was challenging, especially for the larger particles. Therefore, the synthesis of photocleavable DNA conjugated polymer brushes was attempted. However, the linker chemistry would hydrolyze and prematurely release DNA into solution. Further research will be needed for this project, especially in the design of a DNA conjugated system that can chemically or physically release DNA from a particle without other side reactions. Pursuing this project could be promising due

to the opportunities DNA labels can provide for identification of nanoparticles and to optimize experimental protocols involving a large number of options to test.

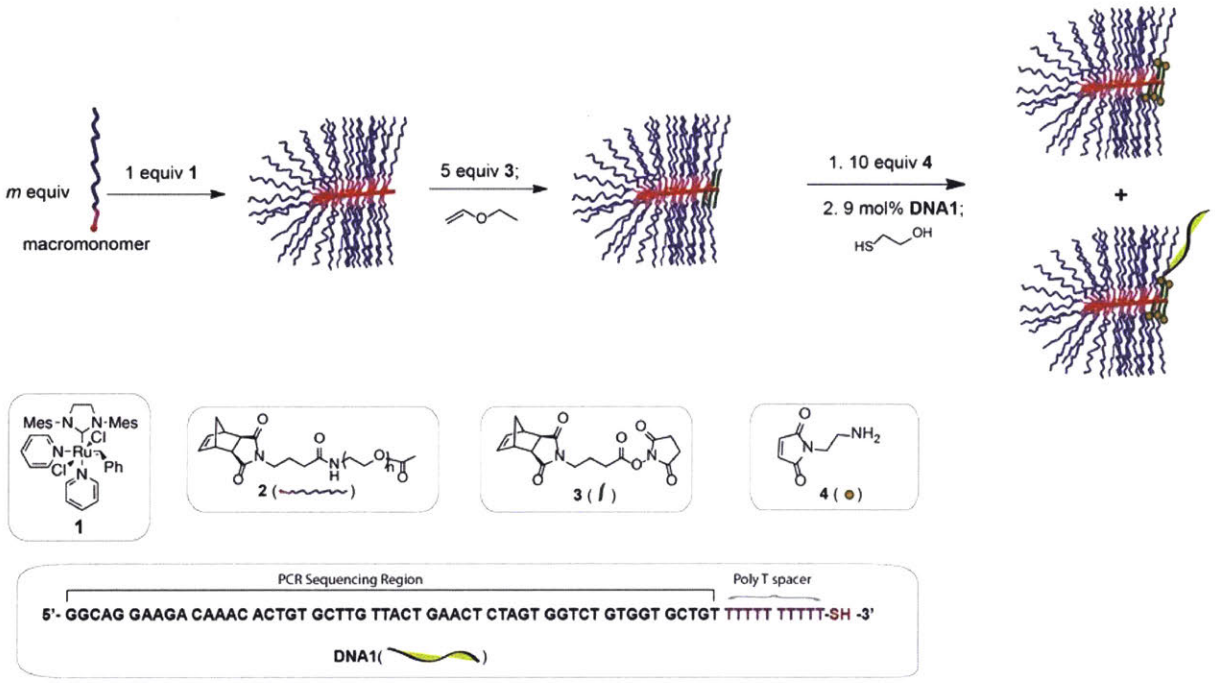

Figure 4.2: Synthesis of DNA-loaded bottle-brush polymers. A diblock bottle-brush polymer of Acetyl-PEG-MM (**2**) and Norb-NHS (**3**) is synthesized. Maleimide-amine (**4**) is added to react with the NHS-ester, followed by DNA terminated thiol (**DNA1**) to react with the maleimide.

4.2 Results and Discussion

This chapter focuses on appending ssDNA to bottle-brush polymers instead of BASPs to first optimize the DNA conjugation on a simpler architecture. The chemistry of DNA conjugation to bottle-brush polymers was investigated, followed by optimization of the PCR amplification of DNA from bottle-brush polymers to improve signal-to-noise when sequencing the DNA. Without DNA barcodes or labels, testing polymers one-by-one can be tedious and introduce errors between experiments. By testing a mixture of labelled polymers in a batch and streamlining a convenient method to extract and quantify the DNA from cells, factors, such as cellular uptake, can be studied in a high throughput fashion with all particles at once and keeping any environmental variables constant.

For initial proof-of-concept experiments, an oligonucleotide similar to those used by Weissleder with 55 nucleotides, a 10 nucleotide poly-T spacer, and a thiol functional group for attachment chemistry (DNA1) was chosen for conjugation. CuAAC to append ssDNA terminated with an alkyne to an azide moiety on bottle-brush polymers did not achieve high conversion. Thus, conjugation of DNA terminated with an amine to a polymer brush containing a small amount of NHS-ester was attempted; however, due to hydrolysis of the NHS-ester, the amide bond formation did not achieve high conversion in water. Next, maleimide-thiol chemistry was explored, which led to the most promising results. In this approach (**Figure 4.2**), *m* equivalents of acetyl-PEG-MM (**2**) was polymerized with 1 equivalent of G3 (**1**) in THF, followed by addition of 5 units of a norb-NHS ester (**3**) and quenching with ethyl vinyl ether to produce a diblock polymer brush. Acetyl-PEG-MM was used instead of PEG-MM to prevent reaction of the terminal PEG alcohols with NHS esters. In the case of unprotected PEG-MM, crosslinking and a tailing large MW aggregate peak were visible on the GPC-MALLS chromatogram. Next, the bottle-brush polymer in THF was incubated with 10 equivalents of N-(2-aminoethyl)maleimide (**4**), and the excess maleimide was removed using repeated dilution and concentration cycles with concentrators or on a Sephadex G-25 gel permeation column. The brush maleimides were reacted with a substoichiometric amount of thiol-functionalized ssDNA (DNA1), followed by capping of unreacted maleimide groups with β-mercaptoethanol.

A 60 kDa bottle-brush particle was synthesized and conjugated to DNA1 (DNA1-brush1). On DNA gel electrophoresis (**Figure 4.3**), the free ssDNA moves readily through the native PAGE gel as shown in lane 2. The lane containing DNA1-brush1 (lane 1) had ssDNA present close to the top of the gel, suggesting it was conjugated to polymer and not existing as free oligomers. PCR on DNA1-brush1 directly was attempted and an increase of free DNA was observed (lane 4). However, also barely noticeable was a faint band for unconjugated free ssDNA in lane 1, so the increase of free DNA in lane 4 may have resulted more from PCR of the free ssDNA than from the ssDNA-bound polymer. The GPC of this brush after DNA conjugation shows an extra higher molecular weight species (**Figure 4.4**), which could correspond to DNA1-brush1 and agrees qualitatively with the use of conjugating only a substoichiometric amount of DNA. This experiment was repeated with a 300 kDa bottle-brush polymer (DNA1-brush2), but to ensure removal of unconjugated DNA, an extra PAGE purification step of DNA1-brush2 was performed. Lane 5 and 6 show the results of before and after PAGE purification, respectively

(**Figure 4.5**). PCR directly of this purified bottle-brush polymer did not lead to any observed amplified ssDNA (lane 3) at concentrations tested, which may suggest direct PCR of larger bottle-brush polymers could be hindered.

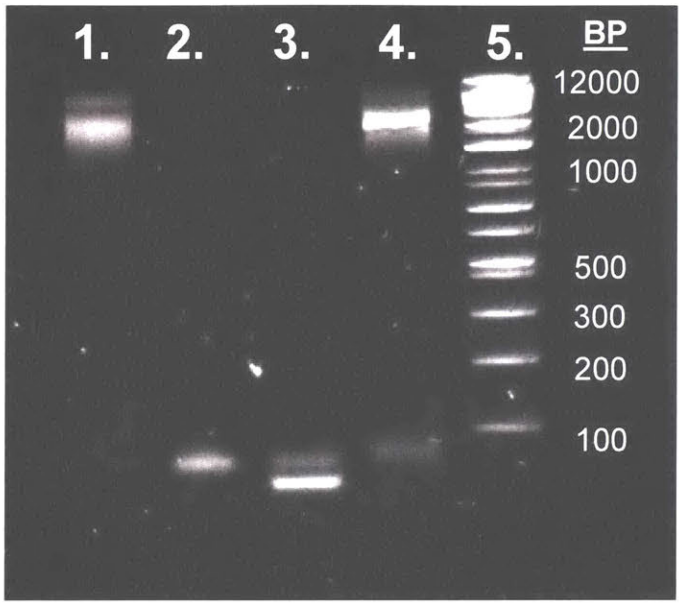

1. **DNA1-Brush1**
2. Control DNA1 (same sequence, but not thiol terminated)
3. PCR of Control DNA1 (same sequence, but not thiol terminated)
4. PCR of **DNA1-Brush1**
5. MW ladder

Figure 4.3: Native PAGE gel of DNA1 and DNA1-Brush1, before and after PCR amplification.

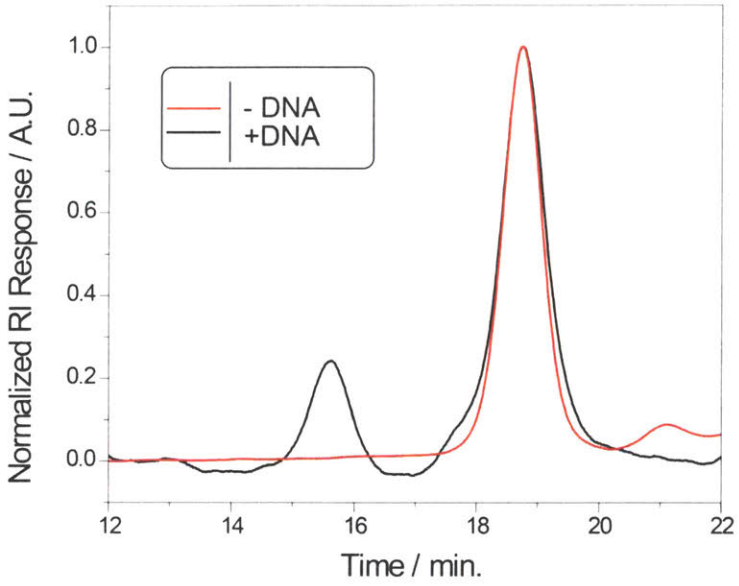

Figure 4.4: GPC refractive index trace of DNA1-brush1 before and after conjugation with substoichiometric amounts of DNA1 relative to polymer.

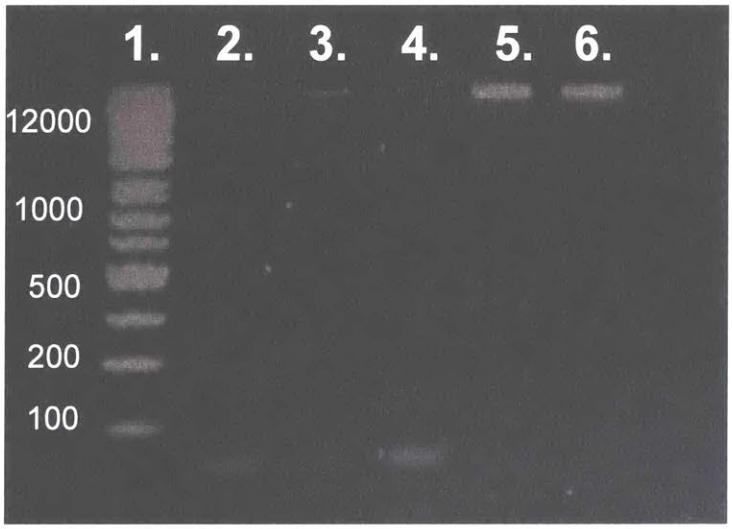

1. MW ladder
2. PCR of free DNA1, no polymer
3. PCR of **DNA1-Brush2** (~300 kDa brush)
4. Free DNA1, no polymer
5. **DNA1-Brush2**, before PAGE purification
6. **DNA1-Brush2**, after PAGE purification

Figure 4.5: Native PAGE gel of DNA1 and DNA1-Brush2, before and after PCR amplification, and before and after PAGE purification.

Since PCR directly from the polymer brushes proved too difficult, photo-releasable DNA polymer conjugates were explored. Briefly, photocleavable linkers for the DNA were designed, in which a norbornene-NHS ester with a photocleavable NBOC group (**Scheme 4.1,** compound C) would replace norb-NHS in the protocol displayed in **Figure 4.2**. However, the ester in compound C was sensitive to hydrolysis leading to premature DNA release prior to PCR amplification. More work went into developing a less hydrolysable photocleavable linker (**Scheme 4.1**, Compound A and B), but given that linker synthesis was lengthy and low yielding, we decided to postpone working on this project. Future studies to continue this project should focus on designing a DNA-linked particle that can cleanly release the DNA barcodes upon a chemical, biological, or physical stimulus without premature hydrolysis.

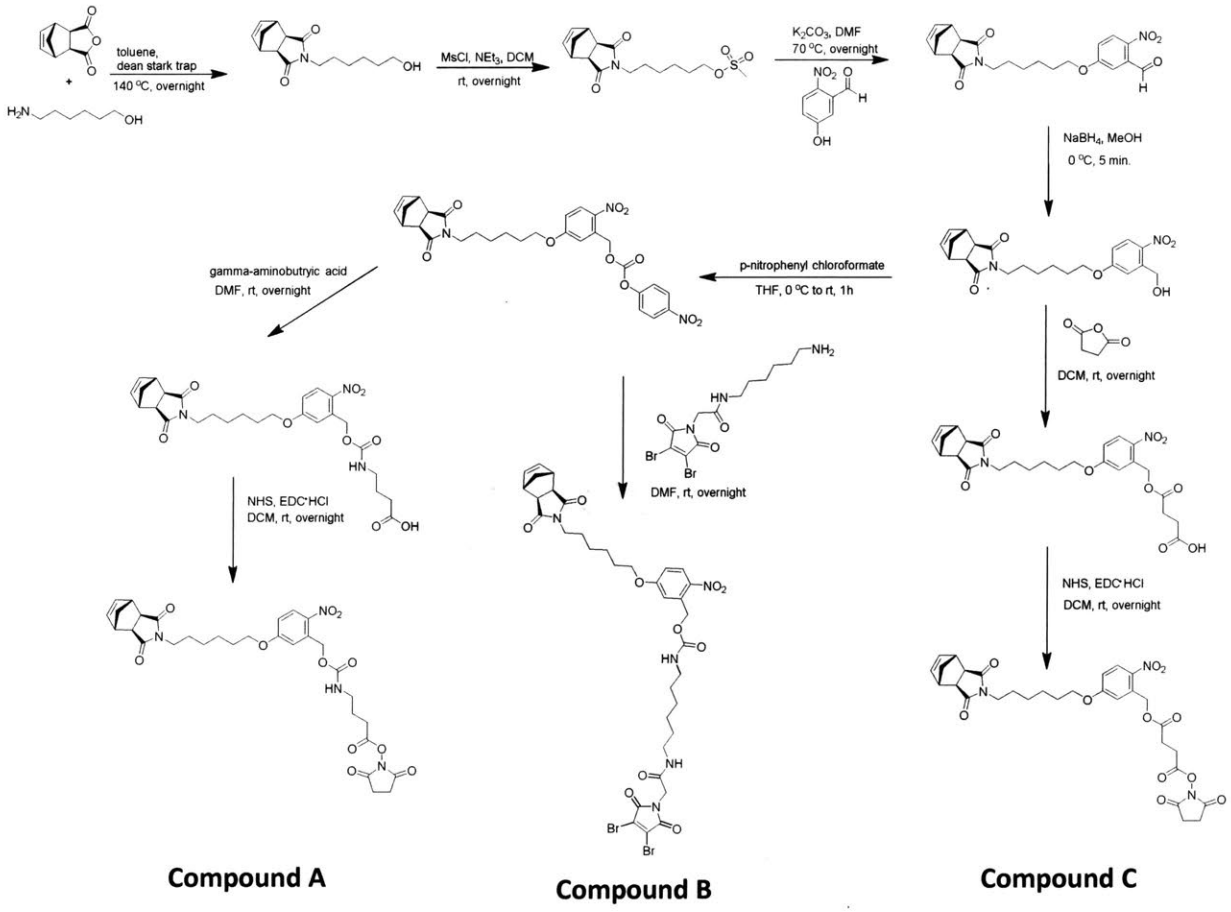

Scheme 4.1: Some of the syntheses that were explored for developing new photoreleasable DNA linkers. DNA would hydrolyze readily from compound C during the PAGE purification step, so we looked into constructs, such as compound A. Also, compound B is a photo-releasable norbornene monomer functionalized with a 2,3-dibromomaleimide group, and could allow for simplification of post-polymerization modification steps to make synthesis and purification easier.

4.3 Conclusion

The synthesis and design of DNA barcoded polymers was explored for use as polymer identifiers in biological experiments. In this chapter, PEG-based bottle-brush polymers were conjugated to thiol-terminated ssDNA by maleimide-thiol Michael addition. Attempts to PCR directly from larger bottle-brush polymers proved difficult, thus photo-releasable DNA conjugated polymers were designed. The DNA could then be cleaved using light irradiation and PCR could be performed on the cleaved DNA; however, the linker chemistry also hydrolyzed slowly to release free DNA prior to PCR amplification. Future experiments will have to address the design of a cleavable linker for DNA that cannot hydrolyze. DNA barcoding for polymer identification is useful in cellular studies that require a large number of polymers all at once instead of individually, thus reducing the overall time to run experiments and removing error due to environmental variations between studies. Successful implementation of these ideas could also enable delivery of nucleic acid therapeutics using advanced polymer architectures.

4.4 Experimental

General Considerations

Unless otherwise noted, all reagents and solvents were purchased from Sigma Aldrich or Alfa Aesar and used as supplied. Grubbs' 2nd generation catalyst was obtained from Materia and converted to G3 using the procedure given in Chapter 1. Silica gel used in column chromatography was the ZEOprep 60 HYD, 40-63 μm. Compounds purified by flash chromatography were purified on a Biotage Isolera One. MilliQ water was purified on a Millipore MilliQ Biocel A10 water purification system. DNA sequences and primers were purchased from Integrated DNA Technologies (IDT). Phusion high-fidelity DNA polymerase kit was purchased from New England Biolabs.

^{1}H nuclear magnetic resonance (^{1}H-NMR) and ^{13}C nuclear magnetic resonance (^{13}C-NMR) spectra were recorded on Bruker AVANCE-400 MHz NMR spectrometer, or a VARIAN Inova-500 MHz NMR spectrometer. Spectra were analyzed on MestReNova NMR software. Chemical shifts are expressed in parts per million (ppm); splitting patterns are designated as s

(singlet), d (doublet), t (triplet), m (multiplet), and br (broad); and coupling constants, J, are reported in Hertz (Hz).

Samples submitted to the MIT Department of Chemistry Instrumentation Facility (DCIF) for high-resolution mass spectrometry (HRMS) were obtained on a Bruker Daltonics APEXIV 4.7 Tesla Fourier Transform Ion Cyclotron Resonance Mass Spectrometer (FT-ICR-MS).

Liquid chromatography-mass spectrometry (LC-MS) was performed on an Agilent 1260 LC system equipped with an Agilent 6130 single quadrupole mass spectrometer. Samples were obtained on an Advanced Materials Technology Halo C18 or an Agilent ZORBAX 300SB-C18 analytical column in a gradient eluent of 0.1% acetic acid in MilliQ purified water to 100% MeCN.

PAGE gel electrophoresis equipment was purchased from Bio-Rad and power/voltage supply was purchased from Fisher-Scientific. PCR thermal cycler was used at the Stubbe Lab in the Department of Chemistry at MIT.

GPC-MALLS characterization was performed on an Agilent 1260 LC system equipped with a Wyatt T-rEX refractive index detector and Wyatt DAWN EOS 18 angle laser light scattering detector. Samples were run on two Shodex KD-806M GPC columns in series at a temperature of 60 °C, flow rate of 1 ml/min, and dimethylformamide with 0.025 M LiBr as the eluent.

Synthesis procedures:

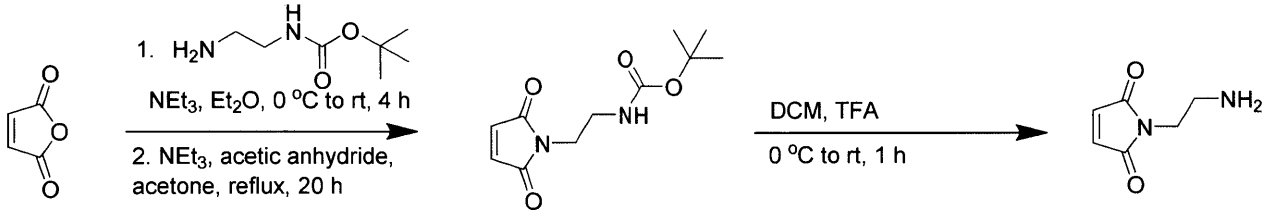

N-(2-aminoethyl)maleimide: N-Boc-ethylenediamine (1g, 6.24 mmol, 1 eq) and triethylamine (1.3 mL, 9.32 mmol, 1.5 eq) were dissolved in diethyl ether (11.8 mL), and the reaction flask was cooled to 0 °C in an ice bath. Maleic anhydride (0.61 g, 6.22 mmol, 1 eq) dissolved in diethyl ether (11.8 mL) was added dropwise to the amine to react with and open the maleic anhydride. The ice bath was removed and the reaction was stirred for 4 h at room temperature.

The solution was concentrated by rotary evaporation. To form the maleimide, the concentrated mixture was redissolved in acetone (30 mL), and then triethylamine (1.7 mL, 12.4 mmol, 2 eq) and acetic anhydride (0.88 mL, 9.3 mmol, 1.5 eq) were added. The reaction was stirred at reflux for 20 h, and then the solvent was removed *in vacuo*. The product was purified by column chromatography (0% EtOAc/Hexanes to 50% EtOAc/Hexanes) and the solids washed with diethyl ether to yield boc-protected N-(2-aminoethyl)maleimide as a white solid. ^{1}H-NMR, ^{13}C-NMR, and HRMS are as reported in literature.[8] Next, boc-protected maleimide-amine was dissolved in 2 mL of DCM and the reaction was cooled to 0 °C over an ice bath. TFA (1.5 mL) was slowly added, ice bath removed, and the reaction stirred at room temperature for 1 h. The mixture was concentrated and precipitated into cold diethyl ether. The solids were washed with diethyl ether to yield N-(2-aminoethyl)maleimide as a white solid. ^{1}H-NMR, ^{13}C-NMR, and HRMS are as reported in literature.[8]

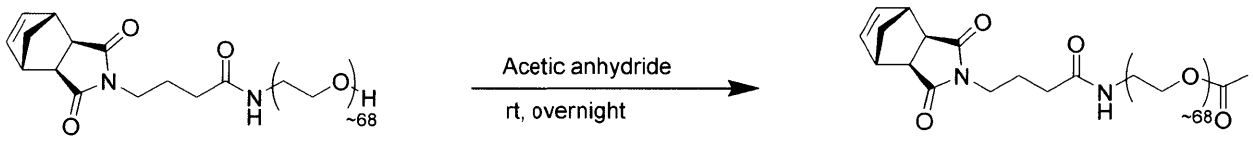

Acetyl-PEG-MM: PEG-MM (300 mg, 0.09 mmol, 1eq) was stirred in acetic anhydride (3 mL) overnight. The solution was diluted in dichloromethane (50 mL) then washed with water twice (50 mL each) and brine once (50 mL). The organic layer was dried over sodium sulfate, and the dichloromethane was removed in vacuo. The solids were triturated in diethyl ether, then centrifuged followed by decantation of diethyl ether. The centrifugation and decantation was repeated five times to yield acetyl-PEG-MM as a white solid.

General procedure for ROMP of bottle-brushes, conjugation of DNA to bottle-brushes, and PCR of DNA (**Figure 4.2**):

Acetyl-PEG-MM (*m* eq) was dissolved in THF, followed by addition of G3 (1 eq) from a stock solution. The total volume of THF used was such that acetyl-PEG-MM would be at 0.05 M (eg. volume of THF to dissolve acetyl-PEG-MM is total volume required for a 0.05 M stock solution minus volume to be added from the G3 stock solution). After stirring for *m* minutes (eg.

if m=30, stir for 30 minutes), Norb-NHS (5 eq) was added and the solution was stirred for an additional ten minutes, then quenched with a few drops of ethyl vinyl ether. Next, N-(2-aminoethyl)maleimide (10 eq) was added, and the solution was stirred at room temperature overnight. N-(2-aminoethyl)maleimide was purified out by using concentrators (Amicon Ultra Centrifugal Filters 3000 MWCO) and repeated dilution and concentration cycles, or by using a pre-packed Sephadex G-25 column (PD-10 columns, Sephadex G-25, GE Healthcare).

DNA1, as purchased from IDT, was prepared by incubating in a 0.18 M sodium phosphate and 0.1 mM DTT buffer for 1 h. Then the DNA was purified from the reducing agent on a Sephadex G-5 Column (GE Healthcare illustra NAP-5 Sephadex G-25 DNA-grade columns) with PBS pH 8.0 as the eluting buffer. The purified maleimide bottle-brush is added to the DNA solution (at 9 mol% of DNA relative to moles of bottle-brush) and stirred at room temperature overnight. Then, β-mercaptoethanol is added to solution to react with any unreacted maleimide groups, and the reaction is stirred at room temperature overnight. A 10-12% native PAGE gel is run in TBE buffer (0.5X TBE Buffer: 45 mM Tris-borate, 1 mM EDTA) to separate out the polymer-DNA conjugate from free, unreacted DNA. The polymer-DNA conjugated is excised from the gel and extracted into MilliQ water.

PCR was set up in PCR 8-well tube strips (VWR) with primers purchased from IDT and the Phusion high-fidelity DNA polymerase kit (New England Biolabs, contains nucleotides, DMSO, and buffer with $MgCl_2$). Initial denaturation step was set to 30 s at 98 °C in a PCR thermal cycler. Then the thermos cycler was set to perform 25 cycles of the following steps: 1) denaturation for 10 s at 98 °C, 2) annealing at 54 °C for 15 s, and 3) elongation at 72 °C for 35 s. The final extension occurred at 72 °C for 5 min, and then the PCR product were analyzed on a 10-12% PAGE gel.

4.5 References

1 Rush, A. M., Thompson, M. P., Tatro, E. T. & Gianneschi, N. C. Nuclease-resistant DNA via high-density packing in polymeric micellar nanoparticle coronas. *ACS Nano* **7**, 1379-1387 (2013).

2 Panyam, J. & Labhasetwar, V. Biodegradable nanoparticles for drug and gene delivery to cells and tissue. *Advanced Drug Delivery Reviews* **55**, 329-347 (2003).

3 Ghosh, P., Han, G., De, M., Kim, C. K. & Rotello, V. M. Gold nanoparticles in delivery applications. *Advanced Drug Delivery Reviews* **60**, 1307-1315 (2008).

4 Tian, H., Chen, J. & Chen, X. Nanoparticles for gene delivery. *Small* **9**, 2034-2044 (2013).

5 Vijayanathan, V., Thomas, T. & Thomas, T. DNA nanoparticles and development of DNA delivery vehicles for gene therapy. *Biochemistry* **41**, 14085-14094 (2002).

6 Nam, J.-M., Park, S.-J. & Mirkin, C. A. Bio-barcodes based on oligonucleotide-modified nanoparticles. *Journal of the American Chemical Society* **124**, 3820-3821 (2002).

7 Agasti, S. S., Liong, M., Peterson, V. M., Lee, H. & Weissleder, R. Photocleavable DNA barcode–antibody conjugates allow sensitive and multiplexed protein analysis in single cells. *Journal of the American Chemical Society* **134**, 18499-18502 (2012).

8 Richter, M. *et al.* Multivalent design of apoptosis-inducing Bid-BH3 peptide–oligosaccharides boosts the intracellular activity at identical overall peptide concentrations. *Chemistry–A European Journal* **18**, 16708-16715 (2012).

Appendix II, Chapter 5: Analyzing molecular network defects in protein or peptide hydrogels

5.1 Introduction

Brief Summary of Chapter and Respective Contributions

In this chapter, the synthesis of hydrogels from artificial proteins or peptide-PEG conjugates is explored. Although no main papers have been prepared from this project, some of the small peptide synthesis has contributed to a paper by K. Kawamoto *et al.*[1] All work presented in the results section was that of the author.

Introduction to Hydrogels as Extracellular Matrix Mimics

As substrates for cell growth and encapsulation, hydrogels have potential applications in tissue regeneration, wound healing, and stem cell differentiation.[2-5] Hydrogel networks are also viable platforms for studying cell growth, cell migration, and cell interactions in an environment that mimics the extracellular matrix (ECM). The ECM is complex and plays a number of functional roles, such as providing structural support, filling up interstitial space between cells and tissues, and playing a role in intercellular communication and cell growth.[6,7] It consists of polysaccharides and fibrous proteins, such as collagen and elastin, plus many other biomolecules, such as growth factors, that respond to surrounding cells. Artificial hydrogels that mimic the ECM are an important research tool to simplify the complexity of the ECM so that researchers can study cell-matrix interactions in a laboratory setting. The physical properties of hydrogels impact cell behavior and can be designed and optimized for cell growth.[3,8-10] For example, molecular network defects, such as dangling chain ends and elastically inactive primary loops, may impact the behavior of cells in currently unknown ways; correlation between these defects and cell migration would provide new molecular insights into cell/biomaterial interactions, and define the shortest critical length scales for hydrogel design.

The Hubbell group has studied the factors that affect cell growth and behavior in hydrogels. Cell adhesion domains, such as RGD or RGDS groups that bind to integrins on cells;[11] and cell protease sensitive degradation sites, such as plasmin,[12] collagenase,[13] or matrix metalloproteinase degradable peptide sequences,[14-17] can be incorporated into PEG-based hydrogels to promote cell-dependent spreading, growth, and migration. These studies show that cells thrive when they are able to re-shape and interact with the environment around them. The Anseth group has worked on 3D encapsulation of cells in modifiable hydrogels with cell adhesion and cleavage domains, and photodegradable 3D gels for real-time, dynamic

modification of hydrogels encapsulated with cells.[18-20] These studies illustrate the benefits of 3D encapsulation and dynamic modification of the extracellular environment.[21,22] The physical properties of hydrogels, including chemical composition and stiffness, can also play a role in how stem cells differentiate.[23] Cell-matrix interactions are complex, but it is clear that cells interact with and modify the environment and substrates around them.[24] Understanding cellular interactions with topological defects, such as primary loops and dangling chains, may give us more insight and understanding into cell-matrix interactions on the molecular scale.

Studying the Molecular Network Defects of Protein or Peptide-Based Hydrogels

A goal in the Johnson Lab is to study the impact of molecular network defects, such as primary loops, on cell behavior in hydrogels. The fraction of primary loops in an artificial protein network can be quantified using a technique called network disassembly spectrometry (NDS) as previously published for non-protein networks by the Johnson group.[25] In this chapter, an artificial random coil protein macromer is recombinantly expressed, purified, and chemically crosslinked to form hydrogels. Proteins offer a key advantage in the control over amino acid sequences that can be optimized for cell growth and migration. Amino acid sequences are designed at key positions within the protein macromer to encode enzymatically degradable domains and cell adhesion sites. The bulk of the protein macromer consisted of AGAGAGPEG amino acid repeats, originally developed by the Tirrell group, which exist as random coils making soft hydrogel formation from a protein possible due to the lack of tertiary structure.[26-29] Enzymatic degradation of the hydrogel, followed by NDS analysis by LCMS, will allow for determination of the fraction of primary loops and dangling chains in the protein hydrogel (**Figure 5.1**).

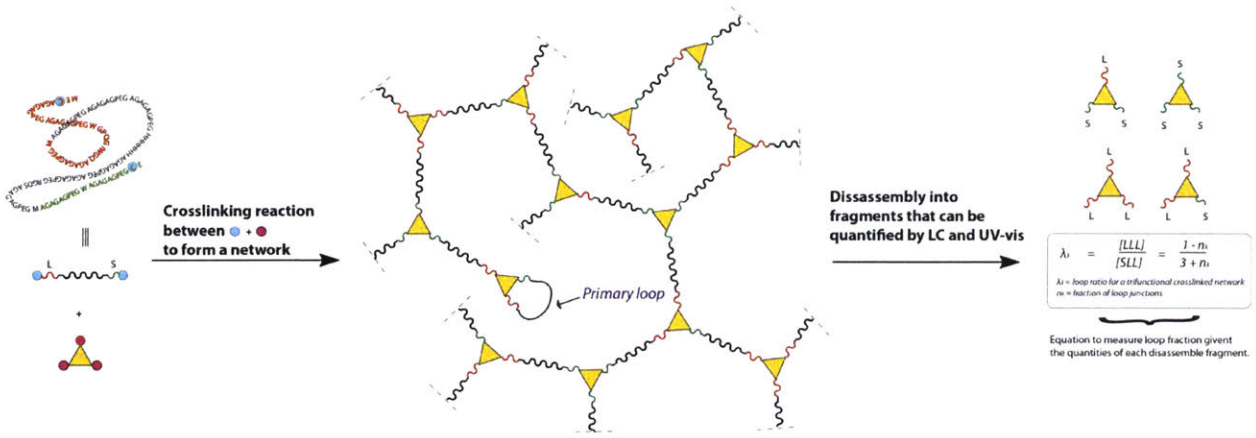

Figure 5.1: Model protein hydrogels are prepared via end-linking of a bifunctional protein macromer and a trifunctional monomer. NDS analysis provides the fraction of dangling chain and primary loop network defects.

In addition to the recombinant protein model, the synthesis of hydrogels from polymer-peptide conjugates was explored for analysis by the SILDaS method to determine primary loop fractions, as previously reported for other networks.[30] In this project, enzymatically degradable short peptide sequences are designed containing either an isoleucine or a valine amino acid as a mass label for MS that differs by one methyl group (**Figure 5.2**). The peptides are coupled to a PEG chain and crosslinked to make hydrogels. After enzymatic degradation, these gels can be analyzed by mass spectrometry (MS) to determine the fraction of primary loops using the SILDaS method (**Figure 5.3**).

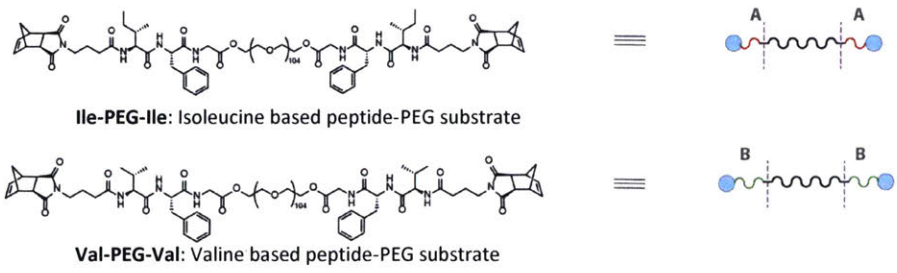

Figure 5.2: The peptide-PEG substrates used in hydrogel formation and SILDaS analysis of primary loop fractions.

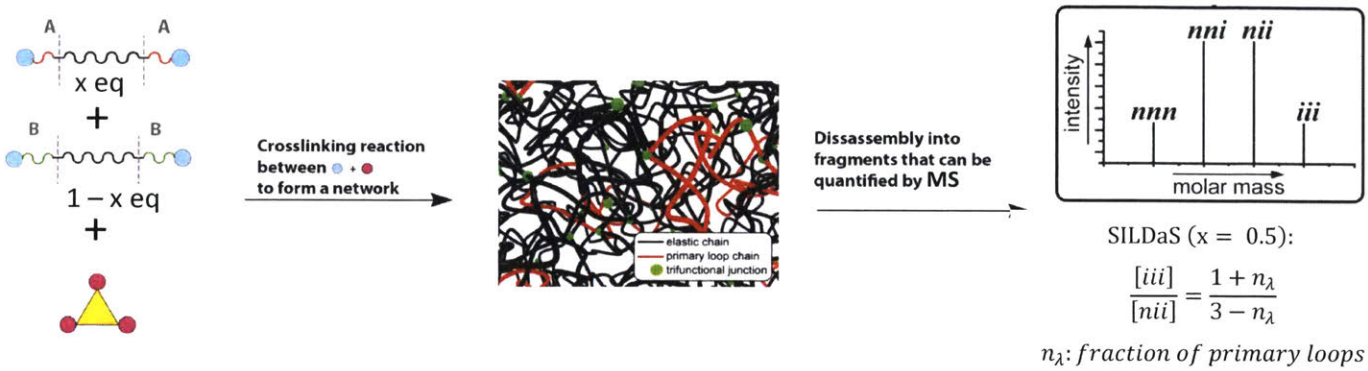

Figure 5.3: Peptide-PEG substrates are crosslinked with a trifunctional crosslinker to form a model network. The network is degraded and the degradation components are analyzed by MS to determine the fraction of primary loops using SILDaS.

Both approaches illustrate two different ways to potentially build biocompatible hydrogels as ECM mimics wherein the numbers of topological defects could be quantified for the first time. These hydrogel models were designed to study primary loop fractions and the impact of molecular network defects on cell behavior, growth, and migration on a substrate.

5.2 Results and discussion

5.2.1 Protein-based hydrogels

In this chapter, hydrogels as ECM mimics were synthesized as substrates for cells to grow and migrate on. Key components for successful growth and migration of cells on a substrate include biocompatibility, cell adhesion sites (e.g., RGD peptide groups), and cellular degradation domains (e.g., protease cleavage sites). The method of primary loop counting, published by Dr. H. Zhou,[25,30] can be used to study whether the number of primary loops can hinder or support cellular migration and growth. Developing new substrates can help us understand cell growth in the ECM, which has implications in tumor growth and metastasis, tissue engineering, wound healing, and stem cell differentiation.

Initially, protein-based hydrogels were produced through recombinant protein expression in *E. coli* based on work by Petka et al. that showed that AGAGAGPEG repeats exist as random coils with no tertiary structure.[26] Thus, this sequence can be used to synthesize soft hydrogels for

use as ECM mimics. The synthetic gene design included RGDS domains for cell adhesion, a His-Tag for purification by a nickel-NTA (Ni-NTA) column, and a phenylalanine amino acid for degradation by chymotrypsin (**Figure 5.4**). The chymotrypsin degradation was designed to be used for loop counting by the NDS method.[25] Briefly, the protein would be end-linked with a trifunctional molecule, and the resulting hydrogel would be degraded with chymotrypsin. The chymotrypsin should cut the protein after the phenylalanine group creating asymmetric fragments, one short (S) and one longer (L) amino acid chain. When crosslinked to a three-arm crosslinker, degradation gives us molecules with three peptide chains composing of SSS, SSL, SLL, and LLL, which can be separated and analyzed on LCMS as summarized in **Figure 5.1**. Primary loops can only occur in the case of SSL and SLL, and determining the excess ratio of SSS/LLL to SSL or SSS/LLL to SLL can be used to calculate a primary loop ratio by **Equation 5.1** derived in previously published work.[25]

M E HHHHHH AGAGAGPEG RGDS AGAGAGPEG F AGAGAGPEG AGAGAGPEG AGAGAGPEG AGAGAGPEG AGAGAGPEG F AGAGAGPEG AGAGAGPEG RGDS AGAGAGPEG HHHHHH E M

HHHHHH – His-tag
RGDS – RGDS integrin cell binding domain
F – phenylalanine chymotrypsin cleaving domain
M – Methionine can be exchanged for AHA in methionine auxotrophs

Figure 5.4: Protein sequence (AHA-P) used initially for our model hydrogel studies that include a His-Tag for purification, RGDS for cell binding, MET for exchange with AHA to use in our crosslinking chemistry, and a phenylalanine for chymotrypsin cleavage. Degradation by chymotrypsin would lead to two asymmetric fragments, one short (S) and one long (L) that can be used in loop counting.

$$\frac{[LLL]}{[SLL]} = \frac{1 - n_\lambda}{3 + n_\lambda}$$

$$n_\lambda = fraction\ of\ primary\ loops$$

Equation 5.1: General loop counting equation. Ratio of LLL or SSS to SLL or SSL can give us the fraction of primary loops at a network junction.

For the hydrogel crosslinking chemistry, we sought to use a non-canonical amino acid, in particular L-azidohomoalanine (AHA), on the ends of the protein macromer.[31,32] **Table 5.1** shows a list of other possible protein end-groups and compatible, bio-orthogonal crosslinking chemistries. AHA can be used to replace methionine in methionine auxotrophic bacterial cells (e.g., M15MA cells) when in methionine depleted media (**Scheme 5.1**). MET to AHA media exchange occurs at time of induction with IPTG, so protein expression will occur with AHA in place of MET. **Supplemental Figure 5.S1** shows the sequence we designed and ordered as a gene. The translated protein (called AHA-P) should have 10 AGAGAGPEG repeats separated by RGDS cell adhesion sites, His-tag, and two MET units for AHA exchange (**Figure 5.4**). The AHA-P gene was cloned into a pQE60 plasmid and transformed into M15MA cells for expression. Due to the unexpected toxicity of the expressed protein, any basal level expression from activation of the lac operon before induction needed to be repressed. Thus, transformation of an additional plasmid, pREP4, was performed. This additional plasmid contains a lac repressor gene that expresses a lac repressor to inhibit any basal level protein expression from the lac operon. Likewise plasmid replication was accomplished with XL1-Blue cells, which contains a lac repressor gene and can repress basal level expression of AHA-P. However, yields of the AHA-P were too low to justify using it in the protein hydrogels.

Protein End-Groups	Possible Crosslinking Chemistries		
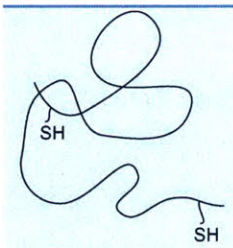	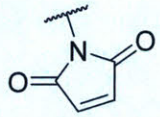		
	Maleimide	Pentafluorophenyl	Thiol-ene
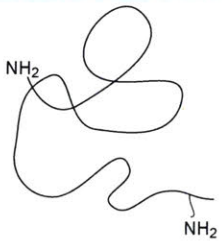	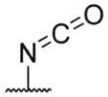	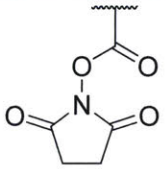	
	Isocyanate	N-hydroxysuccinimide	
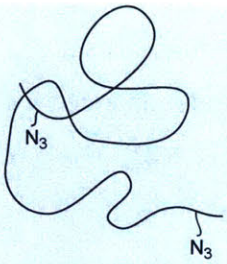		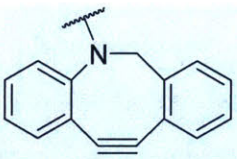	
	Alkyne	Dibenzylcyclooctyne	

Table 5.1: List of possible protein end-groups and crosslinking chemistries.

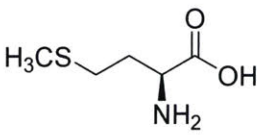

MET

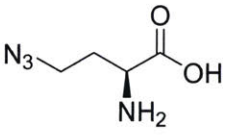

AHA

Scheme 5.1: Media exchange with azidohomoalanine (AHA), a methionine (MET) analogue, can be used to incorporate AHA in place of MET in methionine auxotrophic cells.

Thus, new protein designs were explored including the use of amines from lysine and the protein's N-terminus or thiols from cysteines for the crosslinking end-group. **Figure 5.5** shows an optimized amino acid sequence of the final recombinant protein design, CYS-P, which

contains two cysteines for crosslinking, AGAGAGAPEG repeats, RGDS domains for cell adhesion, a his-tag for protein purification, GPQGIWGQ as a matrix metalloprotease cell degradation domain, and tryptophan residues for chymotrypsin degradation and loop counting. The gene sequence (**Supplementary Figure 5.S2**) was optimized for protein expression by choosing codons with high codon usage in *E. coli* and avoiding nucleotide sequences with undesirable mRNA structure. Traditional cloning methods created a recombinant plasmid with the desired CYS-P gene in a pET28a plasmid. These were transformed into *E. coli* BL21(DE3) cells for protein expression, and IPTG was used once OD_{600} was 0.9-1.1 to induce the lac operon for protein production. Cells were harvested and lysed, then centrifuged to remove cell debris. The protein was collected through a Ni-NTA column and further purified on HPLC (**Figure 5.6**). However, yields for a 4 L culture were low, and attempts to make hydrogels from reacting the cysteines with a three-armed crosslinker proved to be unsuccessful, thus this project was suspended.

MECI AGAGAGPEG GPQGIWGQ AGAGAGPEG M AGAGAGPEG RGDS AGAGAGPEG AGAGAGPEG AGAGAGPEG AGAGAGPEG AGAGAGPEG RGDS AGAGAGPEG AGAGAGPEG MW AGAGAGPEG ICEMW HHHHHH Stop

HHHHHH – His-tag

RGDS – RGDS integrin cell binding domain

W – tryptophan chymotrypsin cleaving domain

C – cysteines for crosslinking chemistry

GPQGIWGQ – Matrix metalloprotease (MMP) cell degradation domain

Figure 5.5: Updated protein sequence (CYS-P) used for our model hydrogel studies that includes a His-Tag for purification, RGDS for cell binding, cysteines to use in our crosslinking chemistry, tryptophan residues for chymotrypsin cleavage, and a matrix metalloprotease cell degradation domain. Degradation by chymotrypsin will lead to two asymmetric fragments, one short (S) and one long (L) that can be used in loop counting. Some cells express MMP to degrade the ECM for growth and migration, so having this domain will help support cell growth and can be used to study cell behavior on hydrogels.

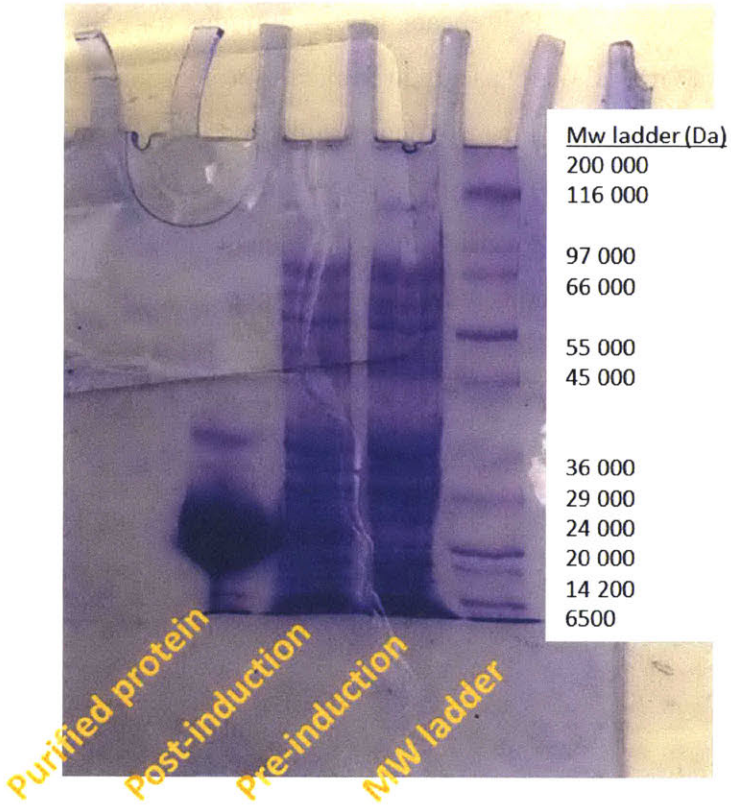

Figure 5.6: SDS-PAGE gel showing purified protein, CYS-P, in comparison to the lysed pre-induction and post-induction samples and the MW ladder.

5.2.2 Peptide-PEG conjugates for hydrogel formation

In addition to protein hydrogels as cellular substrates, synthesis of hydrogels from polymer-peptide hybrids was explored. In this approach, a peptide by solid-phase peptide synthesis was synthesized and coupled to a 4.6 kDa PEG chain. Next, the peptide-PEG conjugate can be crosslinked and degraded to study loop counting (**Figure 5.3**) by the SILDaS method, developed by the Johnson group.[30] The peptide sequences consisted of norb-acid, isoleucine, phenylalanine, and glycine (Norb-Ile-Phe-Gly) and norb-acid, valine, phenylalanine, and glycine (Norb-Val-Phe-Gly). Instead of using deuterium and hydrogen labels as was done previously in the Johnson group, the extra methyl group on isoleucine vs. valine was used as the mass difference label. These peptides were coupled to the ends of a PEG 4.6 kDa chain resulting in a symmetrically labeled macromers: Val-PEG-Val and Ile-PEG-Ile (**Figure 5.2**). The synthesis of a three-arm tetrazine crosslinker is also shown in **Scheme 5.2**.[25] With tetrazine-norbornene inverse-electron demand Diels-Alder ligation chemistry, the terminal norbornene groups on the

peptide-PEG conjugates react with the tetrazine groups to form gels with trifunctional network junctions. Chymotrypsin was used to digest the crosslinked peptides of the hydrogel at the phenylalanine positions and mass spectrometry was performed to determine the ratios of degradation fragments: VVV, VVI, VII, and III (chemical structures are shown in **Scheme 5.4**). Using **Equation 5.2** derived previously, the primary loop ratios can be calculated.[30]

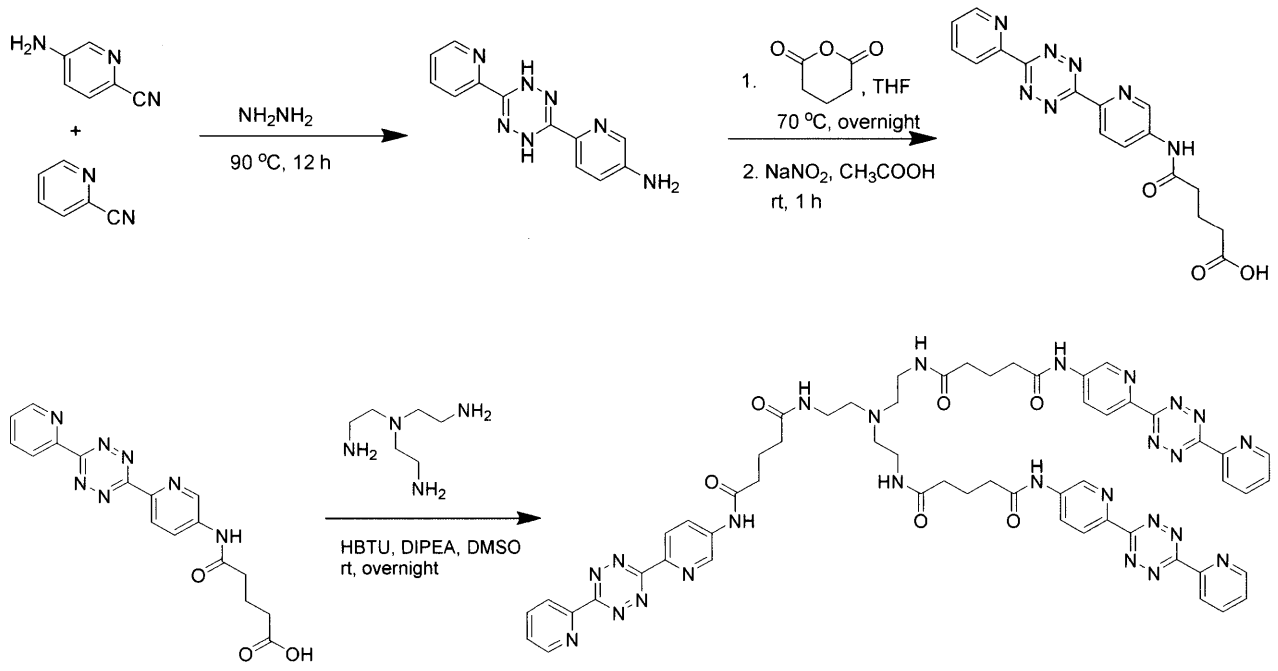

Scheme 5.2: Synthesis of a tri-tetrazine crosslinker.

$$\frac{[VVV]}{[VII]} = \frac{1 + n_\lambda}{3 - n_\lambda} \; for \; x = 0.5$$

$$n_\lambda = fraction \; of \; primary \; loop$$
$$x = fraction \; of \; chain \; 1$$

Equation 5.2: SILDaS loop counting equation. Ratio of VVV or III to VII or VVI can give us the fraction of primary loops at a junction. The fraction of chain 1 is x, whereas chain 2 is $1 - x$. The above equation only applies to $x = 0.5$; for determining loop fractions at other values of x, refer to literature.[30]

Gels were synthesized by reacting the tri-tetrazine crosslinker with various concentrations of Val-PEG-Val and Ile-PEG-Ile at a fraction of $x = 0.5$ (**Scheme 5.3**). Gels formed at a total concentration of PEG chains at 15.8 and 13 mM, but not at 8 or 10 mM. The tetrazine-norbornene ligation product, a dihydropyridazine, can exist as isomers, so after adding a small molecule norb-acid to quench any free tetrazines, the hydrogels were treated with DDQ to oxidize the dihydropyridazines to pyridazines (**Figure 5.7**). After washing out the DDQ with DMSO, chunks of gel were digested in a solution of chymotrypsin in pH 7.8 Tris buffer (38 mM Tris, 53 mM calcium chloride, pH 7.8). Mass spectrometry shows peaks corresponding to VVV, VVI, VII, and III fragments (**Scheme 5.4**), as well as extra MS peaks that occurred from hydrolysis at ester-bonds connecting the glycine to PEG (**Figure 5.8A**). Base digest was also performed by incubating the gels with 2 M LiOH and, as expected, observed only one set of peaks for the digestion of the PEG-peptide ester bond (**Figure 5.8B**) The peptide fragments were coupled to PEG-4.6kDa-diamine to avoid premature hydrolysis at the PEG-glycine ester bond during chymotrypsin digest (**Scheme 5.5**). Any premature hydrolysis would not be ideal for kinetic analysis of loop formation because the enzymatic digest with peptide-PEG chains might occur at a different rate than the hydrolyzed peptide substrate. Also for any kinetic analysis of primary loop formation, the kinetic constants of valine vs. isoleucine peptide substrates should be determined, in order to make necessary adjustments to loop parameter kinetics in the case that the two peptides do not degrade at equal rates. For the mass spectrometry analysis to be valid, the ionization propensities of the VVV, VVI, VII, and III fragments need to be determined to make necessary adjustments in the case ionizations are not equal. These studies and controls have not been completed at this point of time, but would be an area of future work if this study on primary loop counting of biologically relevant hydrogels were to continue.

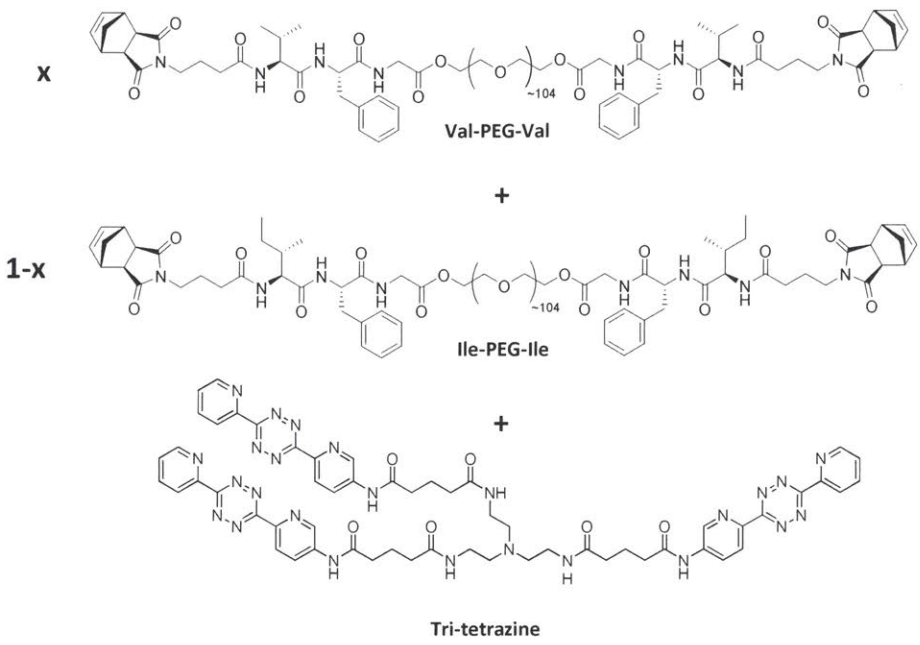

Scheme 5.3: These three components are mixed to form model network hydrogels for loop analysis. The mixture is reacted for 2 days to allow for full conversion.

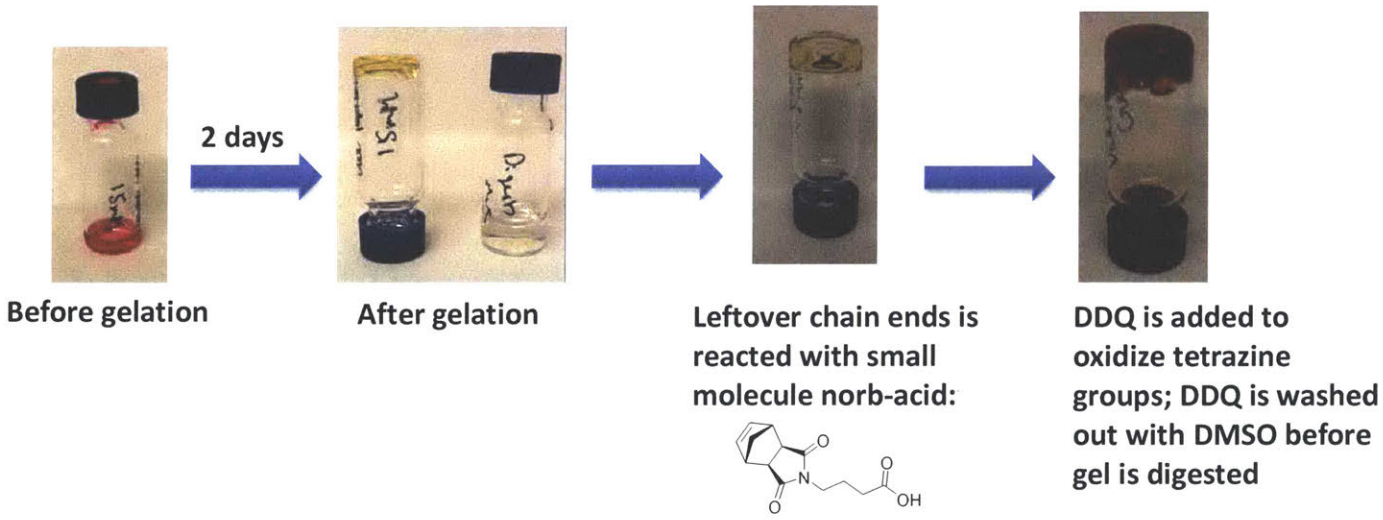

Figure 5.7: Pictorial representation of gelation and workup, including reacting any unreacted tetrazines with a small molecule, norb-acid, and using DDQ to oxidize the gels.

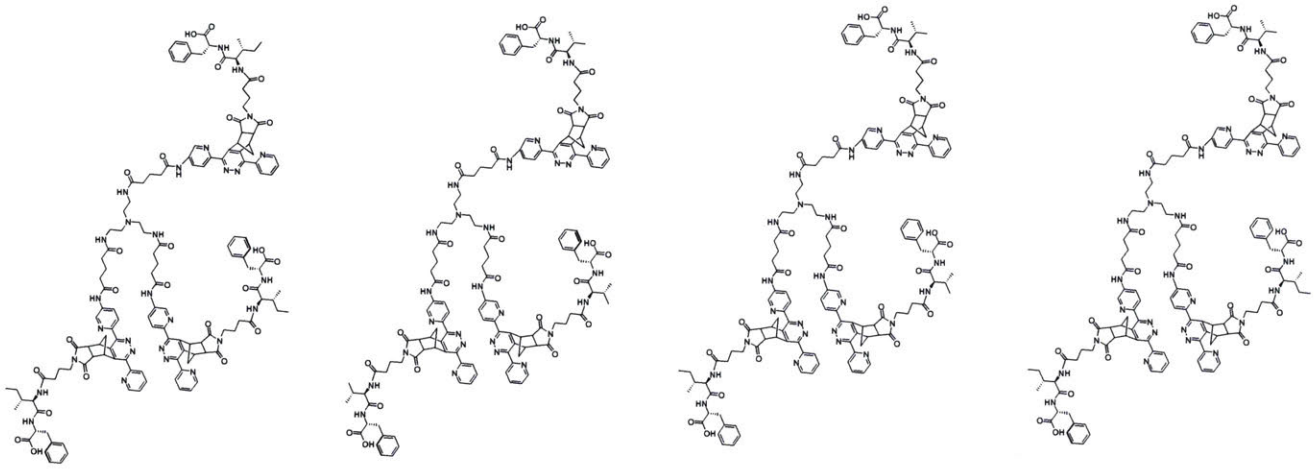

III **VVV** **VVI** **VII**

Scheme 5.4: Portions of the gels were incubated with chymotrypsin in buffer until the gel had dissolved. Digestion by chymotrypsin can lead to trifunctional fragments of VVV, VVI, VII, and III (structures shown above), which are analyzed on the MS.

A

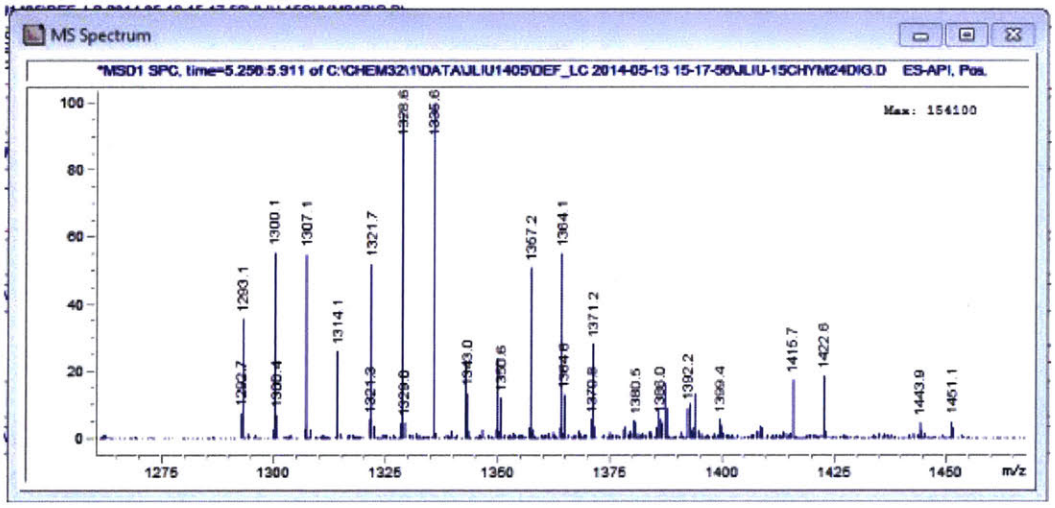

Ions Observed (m/z)	Chymotrypsin digest fragment
1293.1, 1300.1, 1307.1, 1314.1	VVV, VVI, VII, III (+2 ion charge), as observed in **Scheme 5.4**
1321.7, 1328.6, 1335.6, 1343.0	VVV+gly, VII+gly, VII+gly, III+gly (+2 ion charge); Each fragment has an extra glycine residue that was not fully digested by chymotrypsin.
1350.6, 1357.2, 1364.1,1371.2	VVV+2gly, VII+2gly, VII+2glyc, III+2gly (+2 ion charge); Each fragment has two extra glycine residues that were not fully digested by chymotrypsin.

B

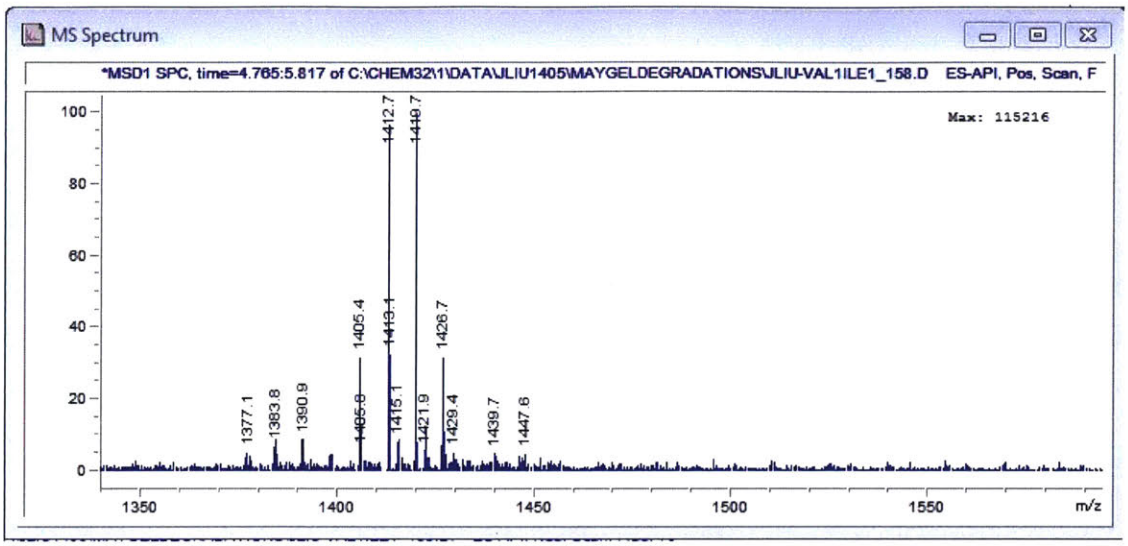

Ions Observed (m/z)	Base digest fragment
1405.4, 1412.7, 1419.7,1426.7	VVV, VVI, VII, and III with glycine residues (+2 charge) from base cleavage at the ester bond. Due to strong basic conditions, the fragments exist as the norbornene imide hydrolyzed form (see **Figure 5.8C**).

C

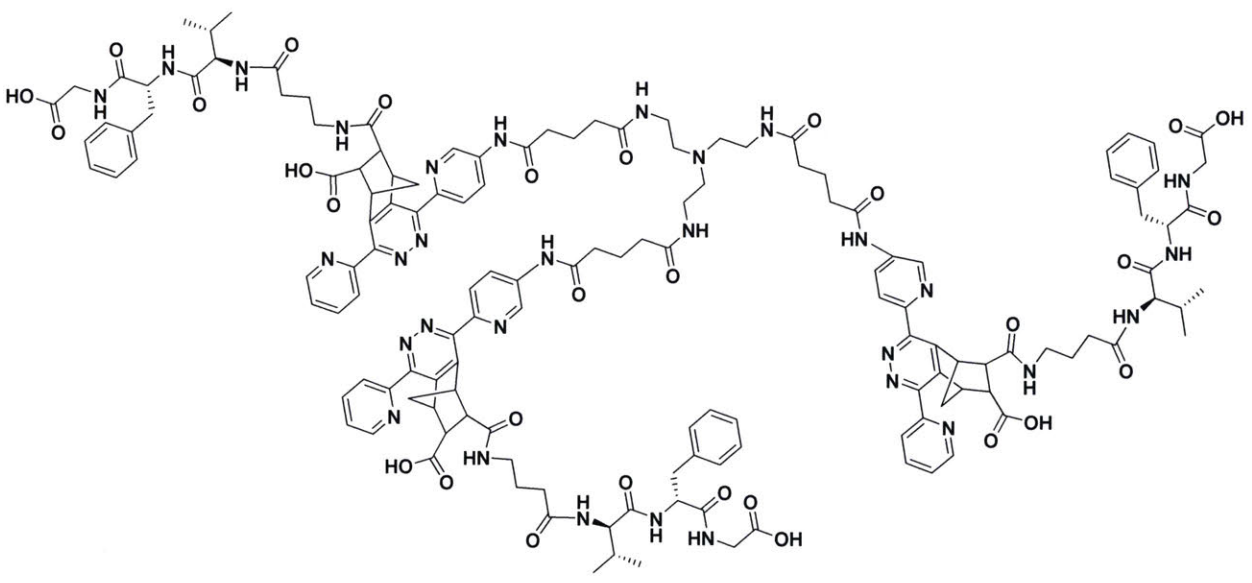

Figure 5.8: Sample analysis of products from MS (includes table of ions and fragments). A) Chymotrypsin digest MS fragments. B) Base digest MS fragments. C) Structure of the VVV base digest fragment, which is cleaved at the ester bond between glycine and PEG and exists in its hydrolyzed norbornene imide form.

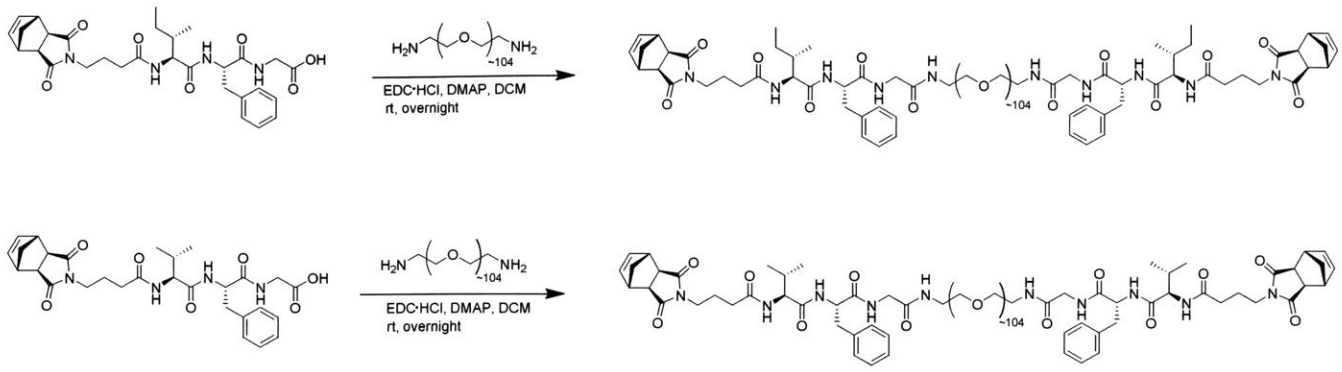

Scheme 5.5: Hydrolysis of the ester bond between PEG and peptide can be avoided by instead using an amide bond between PEG and peptide.

5.3 Conclusion

This project's aim is to develop bioactive hydrogels as ECM mimics and study primary loop fractions of these hydrogels. Primary loops are a molecular network defect that could impact the behavior, growth, and migration of cells interacting with the hydrogel. Two types of biocompatible hydrogels were studied: one based on protein recombinant expression and another based on polymer-peptide conjugates. Of the two, the polymer-peptide conjugates successfully formed gels using tetrazine-olefin coupling chemistry and the gels were responsive to chymotrypsin degradation. Further experiments will be required to determine the primary loop fractions of these gels, and use these gels for cell growth. These gels can help us study the impact of molecular network defects on cell growth and migration for the first time, which could be an important factor in designing hydrogels for tissue engineering.

5.4 Experimental

5.4.1 Protein hydrogels

General considerations:

Salts and antibiotics were purchased from Sigma Aldrich and Thermo Fisher Scientific, and used as purchased. The AHA-P custom gene was purchased from GenScript, and the CYS-P custom gene was purchased from Integrated DNA Technologies (IDT). Primers were also purchased from Integrated DNA Technologies (IDT). XL1-Blue and DH5-α competent cells were purchased from Thermo Fisher Scientific, and BL21(DE3) cells were purchased from Sigma Aldrich. M15MA cells were generously provided by the Brad Olsen lab at MIT. The empty PET28A vector was generously provided by the Stubbe Lab at MIT. PQE60 vector was purchased from Qiagen. Restriction enzymes, T4 DNA ligase, and buffers for restriction digest and ligation were purchased from New England Biolabs. MilliQ water was obtained from a Millipore Biocel A10 water purification system.

Miniprep kit for purification of plasmid DNA was purchased from Qiagen (QiaPrep Spin Miniprep Kit), and used as directed. DNA gel extraction kit was also purchased from Qiagen (QiaQuick Gel Extraction Kit), and used as directed. SDS-PAGE gel electrophoresis equipment was purchased from Bio-Rad and power/voltage supply was purchased from Fisher-Scientific.

Sterile procedures were used for any solution coming into contact with cells. Solutions were either autoclaved or sterilized through a 0.2 μm filter. Glassware was pre-sterilized by using an autoclave. Opening any sterile bottles or handling cells was done in the presence of a flame on a workplace sprayed with ethanol and wiped down.

LB agar plates consist of 25 g/L LB powder, 15 g/L Agar powder, and if necessary, 100 μg/mL ampicillin or 50 μg/mL kanamycin. LB broth (Miller) was made from 25 g of LB powder (Miller) per 1 L of water and autoclaved. Antibiotic, IPTG, and DTT stock solutions were prepared in MilliQ purified water at the following 1000x stock concentrations: 100 mg/mL ampicillin (AMP), 50 mg/mL kanamycin (KAN), 1M isopropyl β-D-1-thiogalactopyranoside (IPTG), and 1 M 1,4-dithiothreitol (DTT). All other buffers and salt formulas are listed in the procedures as they appear.

Concentration of DNA in solution was monitored on UV-vis at 260 nm, with the approximation of 50 ng/μL dsDNA per 1 AU. AHA was synthesized from commercial available *N*-Boc-*O*-Bn-L-aspartic acid using literature protocol.[32]

Preparing Chemically Competent *E. coli* Cells:

For any cells that were not already purchased as chemically competent (eg. M15MA cells), this procedure was used to prepare the cells for transformation of a plasmid by heat shock. Under sterile procedures, cells were plated in LB agar plate with antibiotic, if necessary, and incubated overnight at 37 °C. One colony was inoculated from the LB plate into 2 mL LB medium, and cells were shaken at 37 °C overnight. 1 mL of overnight cell culture was added to 100 mL LB medium (in a 500 mL flask), and shaken vigorously until OD_{600} ~0.25-0.30. The culture was chilled on ice for 15 min, and a 0.1 M $CaCl_2$ solution and 0.1 M $CaCl_2$ plus 15% glycerol solution were also chilled on ice. Cells were centrifuged for 10 min at 3300g (4000 rpm) at 4 °C. Medium was discarded and cell pellet was resuspended in 30-40 mL cold 0.1M $CaCl_2$. The cells were kept on ice for 30 min, and then centrifuged for 10 min at 3300g (4000 rpm) at 4 °C. The supernatant was removed and the cell pellet was resuspended in 6 mL of cold 0.1 M $CaCl_2$ solution + 15% glycerol. Cell suspension was pipetted at 0.4-0.5 mL volumes into sterile 1.5 mL tubes. Competent cells were frozen on a dry ice, acetone bath and transferred to a -70 °C freezer.

Transformation and plasmid preparation:

Plasmids for transformation, chemically competent *E. coli* cells, and any necessary antibiotics were thawed on ice. Plasmid (1 μL, at approximately 100 ng/μL) was added to 50 μL of cells (from competent cell stocks), and solution was stirred gently with a pipette tip. The cells were left on ice for 10 min, then heat shocked in a 42 °C water bath for 45-60 s and immediately placed on ice after to reduce damage to cells. LB media (450 μL) with antibiotic is added to the cells, and the cells are incubated at 37 °C with slow shaking for 45 to 60 min. Then, 50 uL (dilute) and 200 uL (concentrated) of cells are plated onto LB agar plates with antibiotic and incubated overnight at 37 °C. Ten colonies are chosen, and part of each colony is inoculated into 8-10 mL of LB media with antibiotic. The cells are incubated on a shaker for 12-16 h at 37 °C. Then, the cells are pelleted down at 5000xg for ten minutes and a miniprep protocol is followed to purify out plasmid. Plasmid is submitted with primers purchased from IDT for DNA

sequencing at the Koch Institute at MIT. Colonies with the correct plasmid can be re-inoculated into media and plated or stored as glycerol stock.

Cloning Procedures:

To prepare *E. coli* cells for protein expression, the custom gene of interest was cloned into an appropriate vector, as follows:

- AHA-P gene was purchased from GenScript in a pUC57 plasmid with cohesive (sticky-end) restriction sites: NcoI and HindIII. This gene was cloned into a PQE60 vector for expression in M15MA cells.
- CYS-P gene was purchased from IDT as a gBlock gene fragment with cohesive (sticky-end) restriction sites: NcoI and HindIII. This gene was cloned into a PET28a vector for expression in BL21(DE3) cells.

Restriction digest was performed on each plasmid or gene fragment by adding the following components to a 1.5 mL Eppendorf microcentrifuge tube: MilliQ water such that the total volume will be 50 μL, 5 μL of NE Buffer 4 (New England Biolabs, 10x digestion buffer solution), plasmid/gene fragment to be digested (*x* μL, containing usually 1-3 μg of plasmid), and restriction enzymes (0.5 μL of each enzyme for every 1 μg of plasmid). The solution was incubated at 37 °C for 1-2 h. For DNA purification, DNA agarose gel electrophoresis (1% agarose gel, TAE electrophoresis buffer: 40 mM Tris, 20 mM acetic acid, 1 mM EDTA, pH 8.3) was performed to separate out the DNA, and a Qiagen gel extraction kit was used to purify out the necessary digested gene or plasmid.

Using purified gene and vector, gene was ligated into vector using T4 DNA ligase (New England Biolabs) by adding the following components to a 1.5 mL Eppendorf tube: MilliQ water such that the total volume will be 20 μL, 2 μL of T4 DNA ligase buffer (New England Biolabs, 10x digestion buffer solution), ~50ng of purified gene insert DNA, ~50ng of digested vector DNA, and T4 DNA ligase (1 μL). The reaction is mixed by pipetting up and down gently, and quick micro-centrifugation. It is incubated at room temperature for at least one hour before chilling on ice and transforming 1-5 μL of cloned plasmid into 50 μL of competent cells following the procedure for transformation and using relevant antibiotics for the plasmid. Sequence of DNA was verified by DNA sequencing performed at Koch Institute.

AHA-P protein expression (based on literature protocols[26,33,34]):

M15MA cells were transformed with both pREP4 plasmid (Olsen Lab, pREP4 contains LacI repressor gene and kanamycin resistance) and PQE60-AHA-P plasmid (pQE60 is ampicillin resistant). The M15MA [pREP4/PQE60-AHA-P] cells were plated onto LB agar plates and incubated overnight. A single colony was inoculated into a small culture (50 mL LB broth plus antibiotics: KAN at 50 μg/mL and AMP at 100 μg/mL) and incubated on a shaker overnight at 37 °C. Four large cultures of 1 L LB broth plus antibiotics were prepared and inoculated with 10 mL each of the small culture. Cells were grown to OD_{600} of 0.9-1.1 and then centrifuged. The LB media was removed and the cells were resuspended in M9AA minimal media (M9 salts – 6.8 g/L Na_2HPO_4, 3 g/L KH_2PO_4, 1 g/L NH_4Cl, 0.5 g/L NaCl; 0.4% glucose, 0.1 mM $CaCl_2$, 1.0 mM $MgSO_4$, 35 ug/mL thiamine, 20 amino acids at 40 mg/L each and replacing MET with AHA, antibiotics), and protein expression was induced with 1 mM IPTG.

After 5 h, the cells were harvested by centrifugation and lysed with B-PER (4 mL per 1 g of cell pellet, Thermo-Fisher Scientific: B-PER bacterial protein extraction reagent, containing lysozyme and DNase I,) and PMSF (10 μL of 100 mM PMSF per 1 mL of BPER used). The solution was pipetted up and down until homogeneous. Guanidine hydrochloride was also added to the solution, such that the total concentration of guanidine hydrochloride was 6 M. The lysate was incubated at 10-15 min at room temperature, and then centrifuged down at 15000xg for 5 min. Any centrifuged cell debris was discarded, and the protein extract in the supernatant was purified by nickel affinity chromatography.

HisPur Nickel NTA resin (Thermo-Fisher Scientific) was packed in 3 mL plastic spin columns (VWR). 1 mL of Ni-NTA resin was added to the column, followed by addition of two resin volumes of Equilibriation Buffer (20 mM NaH_2PO_4, 300 mM NaCl, 10 mM imidazole, pH 7.4). The resin is mixed until suspended and column is centrifuged for 2 min at 700xg. The flow-through is removed and discarded. Protein extract is added to the spin column, which is centrifuged for 2 min at 700xg, and any flow-through is discarded. This step is repeated until all protein extract has gone through the column. Two resin volumes of Wash Buffer (20 mM NaH_2PO_4, 300 mM NaCl, 25 mM imidazole, pH 7.4) is added to the column, which is mixed and centrifuged for 2 min at 700xg. Flow through is discarded and this wash step is repeated a second time. Spin columns are placed in two new falcon tubes, and one resin volume of Elution Buffer (20 mM NaH_2PO_4, 300 mM NaCl, 250 mM imidazole, pH 7.4) is added to the resin. The

suspension is mixed and centrifuged for 2 min at 700xg, and the flow-through is collected and transferred to a 1.5 mL Eppendorf tube. This elution step is repeated 4 times. For regeneration, the resin is washed with 10 resin-bed volumes of MES Buffer (20 mM 2-(N-morpholine)-ethanesulfonic acid, 0.1 M NaCl, pH 5.0) and then 10 resin-bed volumes of MilliQ water, followed by storage of resin in one resin volume of 20% ethanol. Purified protein can be further desalted using a desalting column or by HPLC purification. Samples throughout the protein expression and purification were collected and run on SDS PAGE gel (10% acylamide). **Supplemental Figure 5.S3** shows a sample MALDI-TOF of the AHA-P protein with AHA in place of MET in comparison to an AHA-P control with MET instead of AHA.

CYS-P protein expression (based on literature protocol[26]):

BL21(DE3) cells are transformed with PET28a-CYS-P plasmid (Kanamycin resistant, contains LacI repressor gene) and plated onto LB-agar plates, then incubated overnight. A single colony was inoculated into a small culture (50 mL LB broth plus KAN at 50 μg/L), and incubated on a shaker overnight at 37 °C. Four large cultures of 1 L LB broth plus antibiotics were prepared and inoculated with 10 mL each of the small culture. Cells were grown to OD_{600} of 0.9-1.1 and protein expression was induced with 1 mM IPTG. After 5 h, the cells were harvested and protein was purified following the same procedure listed above for AHA-P purification, except 1 mM of DTT is added to buffers that contain protein.

5.4.2 Peptide-PEG hydrogels

General Considerations

Unless otherwise noted, all reagents and solvents were purchased from Sigma Aldrich or Alfa Aesar and used as supplied. PEG-4.6kDa and PEG-4kDa-diamine were purchased from Sigma Aldrich and JenKem Technology USA, respectively. Silica gel used in column chromatography was the ZEOprep 60 HYD, 40-63 μm. Compounds purified by flash chromatography were purified on a Biotage Isolera One. MilliQ water was purified on a Millipore Biocel A10 water purification system. Norb-acid was prepared as reported in chapter 1 of this thesis.

^{1}H nuclear magnetic resonance (^{1}H-NMR) and ^{13}C nuclear magnetic resonance (^{13}C-NMR) spectra were recorded on Bruker AVANCE-400 MHz NMR spectrometer, or a VARIAN Inova-500 MHz NMR spectrometer. Spectra were analyzed on MestReNova NMR software. Chemical shifts are expressed in parts per million (ppm); splitting patterns are designated as s (singlet), d (doublet), t (triplet), m (multiplet), and br (broad); and coupling constants, J, are reported in Hertz (Hz).

Samples submitted to the MIT Department of Chemistry Instrumentation Facility (DCIF) for high-resolution mass spectrometry (HRMS) were obtained on a Bruker Daltonics APEXIV 4.7 Tesla Fourier Transform Ion Cyclotron Resonance Mass Spectrometer (FT-ICR-MS).

Liquid chromatography-mass spectrometry (LC-MS) was performed on an Agilent 1260 LC system equipped with an Agilent 6130 single quadrupole mass spectrometer. Samples were obtained on an Advanced Materials Technology Halo C18 or an Agilent ZORBAX 300SB-C18 analytical column in a gradient eluent of 0.1% acetic acid in MilliQ purified water to 100% MeCN.

High-pressure liquid chromatography (HPLC) was performed on an Agilent 1260 LC system equipped with an Agilent ZORBAX 300SB-C18 PrepHT (21.2 x 150 mm) preparative column and using a gradient eluent of 0.1% acetic acid in MilliQ purified water to 100% MeCN.

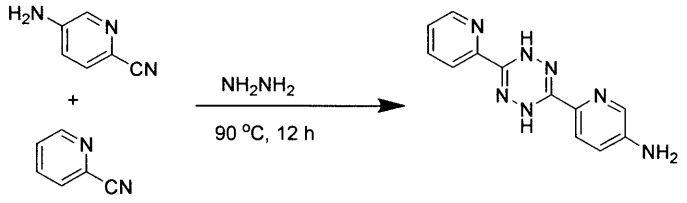

TetrazineH$_2$-Amine: 5-amino-2-cyanopyridine (3.40 g, 28.8 mmol, 1 eq), 2-cyanopyridine (3.00 g, 28.8 mmol, 1 eq), and hydrazine monohydrate (5.8 mL, 120 mmol, 4.2 eq) were heated to reflux at 90 °C under N_2 for 12 h. Then, the orange solids were filtered out and washed with water. The product was dry-loaded onto 2% triethylamine deactivated silica, and purified by column chromatography (50% acetone/Hexanes to 100% acetone). ^{1}H-NMR, ^{13}C-NMR, and HRMS are as reported in literature.[35]

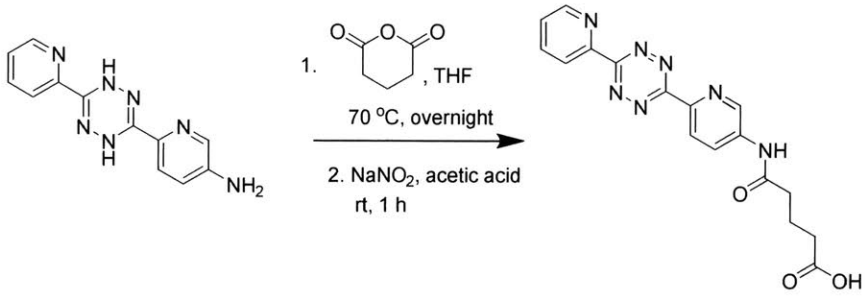

Tetrazine-Acid: Tetrazine-amine (0.93 g, 3.68 mmol, 1 eq) and glutaric anhydride (2.1 g, 18.4 mmol, 5 eq) were dissolved in THF (70 mL) and stirred at 70 °C overnight. The reaction was cooled, followed by addition of acetic acid (36 mL) and sodium nitrite (1.02 g, 14.7 mmol, 4 eq) and stirring for 1 h. Next, water was added and the reaction was stirred for 30 min. The purple-red precipitate was collected by filtration and washed with acetone (50 mL x 5), ethyl acetate (50 mL x 3), and diethyl ether (50 mL x3) to yield tetrazine-acid. ^{1}H-NMR, ^{13}C-NMR, and HRMS are as reported in literature.[25]

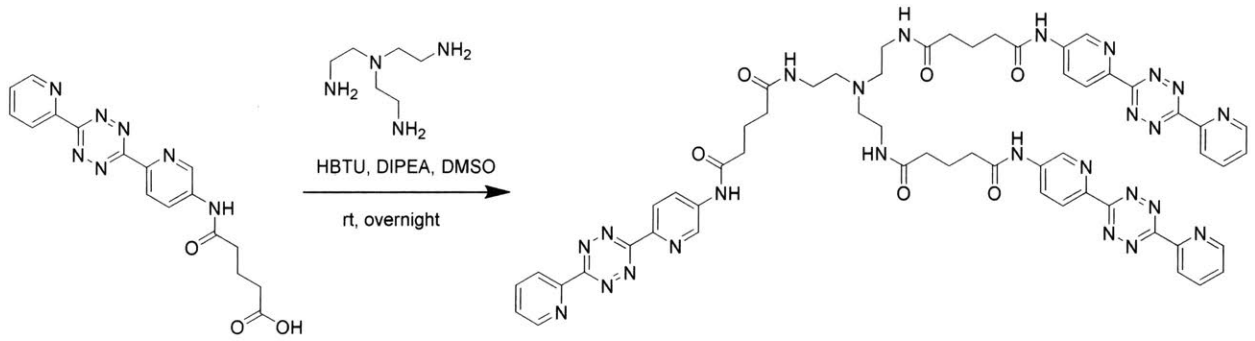

Tri-Tetrazine: Tris(2-aminoethyl)amine (73.7 µL, 0.492 mmol, 1 eq), tetrazine-acid (720 mg, 1.97 mmol, 4 eq), HBTU (747 mg, 1.97 mmol, 4 eq), and DIPEA (0.515 mL, 2.96 mmol, 6 eq) dissolved in DMSO (15 mL) were stirred overnight. MilliQ water (500 mL) was added to precipitate out brightly colored solids, which were collected by filtration and washed with water (200 mL), methanol (200 mL), acetone (200 mL x3), dichloromethane (200 mL x3), and diethyl ether (200 mL x 3). The product was redissolved in DMSO with heating and re-precipitated until impurities were removed to yield tri-tetrazine. ^{1}H-NMR, ^{13}C-NMR, and HRMS are as reported in literature.[25]

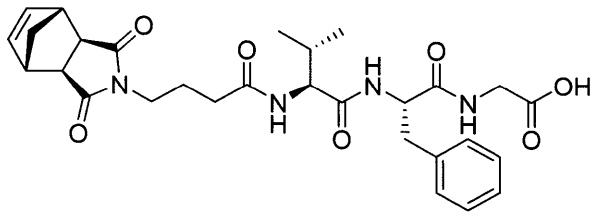

Norb-val-phe-gly: The norb-val-phe-gly peptide was synthesized using solid phase peptide synthesis. FMOC-gly wang resin (0.47 mmol/g loading of FMOC-gly, 10 g, 4.7 mmol, 1 eq) was swollen in dimethylformamide (30 mL) in a solid phase peptide synthesis vessel. The DMF was drained and the resin was incubated in 1:4 piperidine: DMF (100 mL) for 15 min twice in order deprotect the glycine, then the beads were washed with five rounds of DMF (100 mL each) and drained of DMF. In a vial, FMOC-Phe-OH (5.46 g, 14.1 mmol, 3 eq), HBTU (5.35 g, 14.1 mmol, 3 eq), and DIPEA (5 mL, 28.2 mmol, 6 eq) were dissolved in DMF (20 mL) and incubated for 10 min before adding to the resin. The resin was incubated for an hour or until all amine was consumed as monitored by ninhydrin staining. The beads were washed with five rounds of DMF (100 mL each) and drained of DMF before incubating in 1:4 piperidine: DMF (100 mL) for 15 min twice, and then washed again with five rounds of DMF (30 mL each). The coupling step, wash step, deprotection step, and wash steps were repeated, but with FMOC-Val-OH (4.78 g, 14.1 mmol, 3 eq) and then norb-acid (3.5 g, 14.1 mmol, 3 eq) as the amino acids. Instead of a final deprotection step, the peptide resin was washed with DMF (100 mL), DCM (100 mL x 2), and methanol (100 mL x 2) and dried under vacuum. Then the resin was incubated with 9:1 TFA: H_2O solution (10 mL each) twice for 30 min, and the acidic solution was collected. The solution was concentrated in vacuo, then purified by HPLC (10% MeCN and 0.1% acetic acid in MilliQ deionized water to 100% MeCN) to yield norb-val-phe-gly (1.3 g, 49%). ^{1}H NMR (500 MHz, CD_3OD) δ 8.1 – 7.95 (m, 1H), 7.30 – 7.17 (m, 5H), 6.34 (s, 2H), 4.75– 4.71 (m, 1H), 4.03– 4.00 (m, 1H), 3.95 (d, J = 17.6 Hz, 1H), 3.86 (d, J = 17.6 Hz, 1H), 3.55 – 3.45 (m, 2H), 3.29 – 3.20 (m, 3H), 2.93 (dd, J = 10.3, 14 Hz, 1H), 2.76 (s, 2H), 2.26 (t, J = 7.1 Hz, 2H), 1.99 – 1.73 (m, 3H), 1.51 (d, J = 10 Hz, 1H), 1.28 (d, J = 10 Hz, 1H), 0.80 – 0.76 (m, 6H).

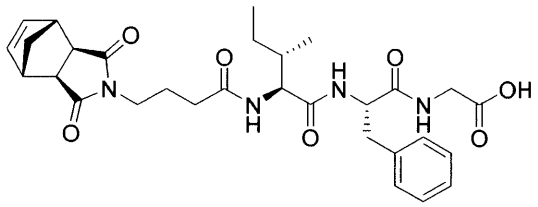

Norb-ile-phe-gly: The norb-ile-phe-gly peptide was synthesized using solid phase peptide synthesis. FMOC-gly wang resin (0.31 mmol/g loading of FMOC-gly, 3g, 0.93 mmol, 1 eq) was swollen in dimethylformamide (30 mL) in a solid phase peptide synthesis vessel. The DMF was drained and the resin was incubated in 1:4 piperidine: DMF (30 mL) for 15 min twice in order deprotect the glycine, then the beads were washed with five rounds of DMF (30 mL each) and drained of DMF. In a vial, FMOC-Phe-OH (1.08 g, 2.79 mmol, 3 eq), HBTU (1.06 g, 2.79 mmol, 3 eq), and DIPEA (0.97 mL, 5.58 mmol, 6 eq) were dissolved in DMF (10 mL) and incubated for 10 min before adding to the resin. The resin was incubated for an hour or until all amine was consumed as monitored by ninhydrin staining. The beads were washed with five rounds of DMF (30 mL each) and drained of DMF before incubating in 1:4 piperidine: DMF (30 mL) for 15 min twice, and then washed again with five rounds of DMF (30 mL each). The coupling step, wash step, deprotection step, and wash steps were repeated, but with FMOC-Ile-OH (0.99g, 2.79 mmol, 3 eq) and then norb-acid (0.70 g, 2.79 mmol, 3 eq) as the amino acids. Instead of a final deprotection step, the peptide resin was washed with DMF (30 mL), DCM (30 mL x 2), and methanol (30 mL X 2) and dried under vacuum. Then the resin was incubated with 9:1 TFA: H_2O solution (10 mL each) twice for 30 min, and the acidic solution was collected. The solution was concentrated in vacuo, then purified by HPLC (10% MeCN and 0.1% acetic acid in MilliQ deionized water to 100% MeCN) to yield norb-ile-phe-gly. ^{1}H NMR (500 MHz, CD_3OD) δ 7.31 – 7.17 (m, 5H), 6.34 (s, 2H), 4.75– 4.72 (m, 1H), 4.05 (d, J = 6.5 Hz, 1H), 3.96 (d, J = 17.5 Hz, 1H), 3.86 (d, J = 17.5 Hz, 1H), 3.55 – 3.45 (m, 2H), 3.30 – 3.20 (m, 3H), 2.92 (dd, J = 10.6, 14 Hz, 1H), 2.76 (s, 2H), 2.25 (t, J = 7.1 Hz, 2H), 1.93 – 1.67 (m, 3H), 1.51 (d, J = 9.6 Hz, 1H), 1.28 (d, J = 9.6 Hz, 1H), 1.22 – 1.00 (m, 2H), 0.81 – 0.72 (m, 6H). ^{13}C-NMR (125 MHz, CD_3OD) δ 180.50, 180.43, 176.04, 173.90, 173.86, 172.20, 139.07, 139.04, 138.94, 130.46,129.58, 127.82, 60.62, 55.92, 49.25, 46.50, 46.46, 43.82, 41.95, 38.90, 38.29, 37.66, 33.29, 25.83, 24.75, 15.92, 11.86.

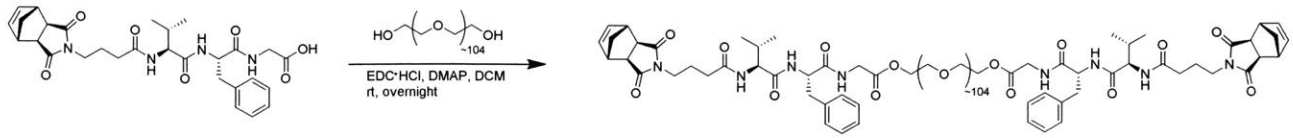

Val-PEG-Val: Norb-val-phe-gly (142 mg, 0.256 mmol, 6 eq), EDC·HCl (49.1 mg, 0.256 mmol, 6 eq), and DMAP (3.1 mg, 0.0254 mmol, 0.6 eq) were dissolved in dichloromethane (10 mL) in a dry flask equipped with a stirbar. After stirring for 30 min, PEG-4.6kDa (196mg, 0.0426 mmol, 1eq) was added and the reaction stirred at room temperature overnight. The reaction was concentrated by rotary evaporation, and the residuals were redissolved in methanol and purified by HPLC (10% MeCN and 0.1% acetic acid in MilliQ deionized water to 100% MeCN) to yield Val-PEG-Val.

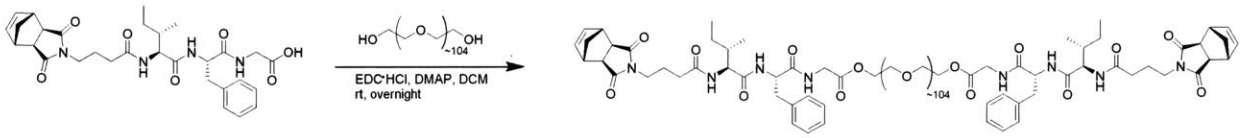

Ile-PEG-Ile: Norb-ile-phe-gly (321 mg, 0.566 mmol, 6 eq), EDC·HCl (109 mg, 0.568 mmol, 6 eq), and DMAP (7 mg, 0.0573 mmol, 0.6 eq) were dissolved in dichloromethane (10 mL) in a dry flask equipped with a stirbar. After stirring for 30 min, PEG-4.6kDa (435 mg, 0.946 mmol, 1 eq) was added and the reaction stirred at room temperature overnight. The reaction was concentrated by rotary evaporation, and the residuals were redissolved in methanol and purified by HPLC (10% MeCN and 0.1% acetic acid in MilliQ deionized water to 100% MeCN) to yield Ile-PEG-Ile.

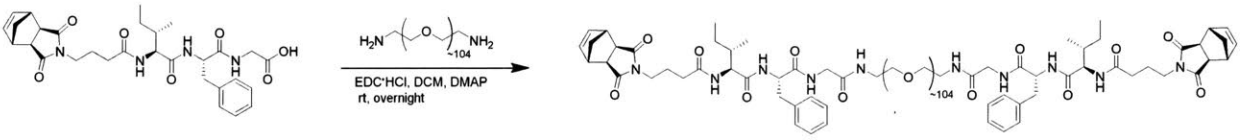

Ile-NH-PEG-NH-Ile: Norb-ile-phe-gly (200 mg, 0.353 mmol, 6 eq), EDC·HCl (67.7 mg, 0.353 mmol, 6 eq), and DMAP (4.3 mg, 0.0353 mmol, 0.6 eq) were dissolved in dichloromethane (10 mL) in a dry flask equipped with a stirbar. After stirring for 30 min, PEG-4.6kDa-diamine (294.2

mg, 0.059 mmol, 1eq) was added and the reaction stirred at room temperature overnight. The reaction was concentrated by rotary evaporation, and the residuals were redissolved in methanol and purified by HPLC (10% MeCN and 0.1% acetic acid in MilliQ deionized water to 100% MeCN) to yield Ile-NH-PEG-NH-Ile (206 mg, 57% yield).

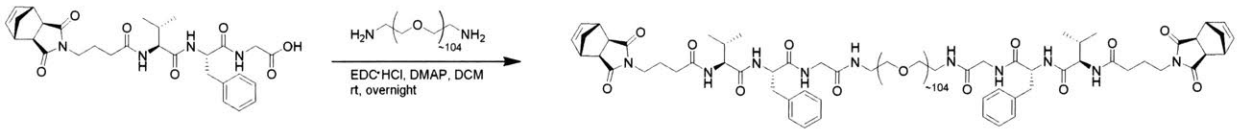

Val-NH-PEG-NH-Val: Norb-val-phe-gly (200 mg, 0.362 mmol, 6 eq), EDC·HCl (69.4 mg, 0.362 mmol, 6 eq), and DMAP (4.42 mg, 0.0362 mmol, 0.6 eq) were dissolved in dichloromethane (10 mL) in a dry flask equipped with a stirbar. After stirring for 30 min, PEG-4.6kDa-diamine (301.7 mg, 0.060 mmol, 1eq) was added and the reaction stirred at room temperature overnight. The reaction was concentrated by rotary evaporation, and the residuals were re-dissolved in methanol and purified by HPLC (10% MeCN and 0.1% acetic acid in MilliQ deionized water to 100% MeCN) to yield Val-NH-PEG-NH-Val (209 mg, 57% yield).

General procedure for hydrogel formation (x= 0.5):

Val-PEG-Val (1.5 eq) and Ile-PEG-Ile (1.5 eq) were weighed out and dissolved in DMSO at the desired concentration (eg. 15.8 mM) minus the volume to be added from the tri-tetrazine crosslinker stock solution. Next tri-tetrazine crosslinker (2 eq) is added from a stock solution, such that the ratio of norbornene to tetrazine groups should be 1:1. The reaction is gently mixed and allowed to react for 2 d. An excess of small molecule, norb-acid, is added to fully react any remaining tetrazine groups, and one volume equivalent of 1 M DDQ is added to the hydrogels. The DDQ oxidation is allowed to take place overnight, and the gel is washed by either using a Soxhlet extractor or rinsing the gel with DMSO multiple times carefully.

General procedure for chymotrypsin and base digest:

Chymotrypsin (Sigma Aldrich, 40 units/mg lyophilized enzyme) was weighed out and dissolved in cold 1 mM HCl at an approximate concentration of 5 units per mL to make a stock solution. Chymotrypsin from stock solution was diluted in buffer (38 mM Tris, 53 mM calcium chloride, pH 7.8), so that the final concentration of chymotrypsin is 0.1 units/mL. Chunks of gel were added to the chymotrypsin solution. The solution was incubated at room temperature overnight or until dissolution of gel, and chymotrypsin was quenched by addition of concentrated acid. The solution is filtered through a syringe filter and analyzed on LCMS (**Figure 5.8A**).

For base digestion, gel chunks are added to a 1 M LiOH solution and solution was stirred for a few hours or until dissolution of gel. The base is quenched with 1 M HCl before filtering and analysis by LCMS (**Figure 5.8B**).

5.5 References

1 Kawamoto, K., Grindy, S. C., Liu, J., Holten-Andersen, N. & Johnson, J. A. Dual Role for 1, 2, 4, 5-Tetrazines in Polymer Networks: Combining Diels–Alder Reactions and Metal Coordination To Generate Functional Supramolecular Gels. *ACS Macro Letters* **4**, 458-461 (2015).

2 Seliktar, D. Designing cell-compatible hydrogels for biomedical applications. *Science* **336**, 1124-1128 (2012).

3 Lutolf, M. & Hubbell, J. Synthetic biomaterials as instructive extracellular microenvironments for morphogenesis in tissue engineering. *Nature Biotechnology* **23**, 47-55 (2005).

4 Lee, K. Y. & Mooney, D. J. Hydrogels for tissue engineering. *Chemical Reviews* **101**, 1869-1880 (2001).

5 Kopeček, J. Hydrogel biomaterials: a smart future? *Biomaterials* **28**, 5185-5192 (2007).

6 Frantz, C., Stewart, K. M. & Weaver, V. M. The extracellular matrix at a glance. *Journal of Cell Science* **123**, 4195-4200 (2010).

7 Alberts, B. et al. *Molecular biology of the cell.* (Garland Science, 2002).

8 Brandl, F., Sommer, F. & Goepferich, A. Rational design of hydrogels for tissue engineering: impact of physical factors on cell behavior. *Biomaterials* **28**, 134-146 (2007).

9 Drury, J. L. & Mooney, D. J. Hydrogels for tissue engineering: scaffold design variables and applications. *Biomaterials* **24**, 4337-4351 (2003).

10 Geiger, B., Bershadsky, A., Pankov, R. & Yamada, K. M. Transmembrane crosstalk between the extracellular matrix and the cytoskeleton. *Nature Reviews Molecular Cell Biology* **2**, 793-805 (2001).

11 Hern, D. L. & Hubbell, J. A. Incorporation of adhesion peptides into nonadhesive hydrogels useful for tissue resurfacing. *Journal of Biomedical Materials Research* **39**, 266-276 (1998).

12 Halstenberg, S., Panitch, A., Rizzi, S., Hall, H. & Hubbell, J. A. Biologically engineered protein-graft-poly (ethylene glycol) hydrogels: a cell adhesive and plasmin-degradable biosynthetic material for tissue repair. *Biomacromolecules* **3**, 710-723 (2002).

13 West, J. L. & Hubbell, J. A. Polymeric biomaterials with degradation sites for proteases involved in cell migration. *Macromolecules* **32**, 241-244 (1999).

14 Lutolf, M. *et al.* Synthetic matrix metalloproteinase-sensitive hydrogels for the conduction of tissue regeneration: engineering cell-invasion characteristics. *Proceedings of the National Academy of Sciences* **100**, 5413-5418 (2003).

15 Lutolf, M. P., Raeber, G. P., Zisch, A. H., Tirelli, N. & Hubbell, J. A. Cell-responsive synthetic hydrogels. *Advanced Materials* **15**, 888-892 (2003).

16 Kraehenbuehl, T. P. *et al.* Three-dimensional extracellular matrix-directed cardioprogenitor differentiation: systematic modulation of a synthetic cell-responsive PEG-hydrogel. *Biomaterials* **29**, 2757-2766 (2008).

17 Kraehenbuehl, T. P., Ferreira, L. S., Zammaretti, P., Hubbell, J. A. & Langer, R. Cell-responsive hydrogel for encapsulation of vascular cells. *Biomaterials* **30**, 4318-4324 (2009).

18 DeForest, C. A., Polizzotti, B. D. & Anseth, K. S. Sequential click reactions for synthesizing and patterning three-dimensional cell microenvironments. *Nature Materials* **8**, 659-664 (2009).

19 Kloxin, A. M., Kasko, A. M., Salinas, C. N. & Anseth, K. S. Photodegradable hydrogels for dynamic tuning of physical and chemical properties. *Science* **324**, 59-63 (2009).

20 Burdick, J. A. & Anseth, K. S. Photoencapsulation of osteoblasts in injectable RGD-modified PEG hydrogels for bone tissue engineering. *Biomaterials* **23**, 4315-4323 (2002).

21 Cushing, M. C. & Anseth, K. S. Hydrogel cell cultures. *Science* **316**, 1133-1134 (2007).

22 Tibbitt, M. W. & Anseth, K. S. Hydrogels as extracellular matrix mimics for 3D cell culture. *Biotechnology and Bioengineering* **103**, 655-663 (2009).

23 Trappmann, B. *et al.* Extracellular-matrix tethering regulates stem-cell fate. *Nature Materials* **11**, 642-649 (2012).

24 Bott, K. *et al.* The effect of matrix characteristics on fibroblast proliferation in 3D gels. *Biomaterials* **31**, 8454-8464 (2010).

25 Zhou, H. *et al.* Counting primary loops in polymer gels. *Proceedings of the National Academy of Sciences* **109**, 19119-19124 (2012).

26 Petka, W. A., Harden, J. L., McGrath, K. P., Wirtz, D. & Tirrell, D. A. Reversible hydrogels from self-assembling artificial proteins. *Science* **281**, 389-392 (1998).

27 Shen, W., Zhang, K., Kornfield, J. A. & Tirrell, D. A. Tuning the erosion rate of artificial protein hydrogels through control of network topology. *Nature Materials* **5**, 153-158 (2006).

28 Shen, W., Kornfield, J. A. & Tirrell, D. A. Structure and mechanical properties of artificial protein hydrogels assembled through aggregation of leucine zipper peptide domains. *Soft Matter* **3**, 99-107 (2007).

29 Shen, W., Kornfield, J. A. & Tirrell, D. A. Dynamic properties of artificial protein hydrogels assembled through aggregation of leucine zipper peptide domains. *Macromolecules* **40**, 689-692 (2007).

30 Zhou, H. *et al.* Crossover experiments applied to network formation reactions: improved strategies for counting elastically inactive molecular defects in PEG gels and hyperbranched polymers. *Journal of the American Chemical Society* **136**, 9464-9470 (2014).

31 Kiick, K. L., Saxon, E., Tirrell, D. A. & Bertozzi, C. R. Incorporation of azides into recombinant proteins for chemoselective modification by the Staudinger ligation. *Proceedings of the National Academy of Sciences* **99**, 19-24 (2002).

32 Roth, S., Drewe, W. C. & Thomas, N. R. A concise and scalable route to L-azidohomoalanine. *Nature Protocols* **5**, 1967-1973 (2010).

33 Soundrarajan, N. et al. Conjugation of proteins by installing BIO-orthogonally reactive groups at their N-termini. *PloS ONE* 7, e46741 (2012).

34 Ayyadurai, N. *et al.* Importance of expression system in the production of unnatural recombinant proteins in Escherichia coli. *Biotechnology and Bioprocess Engineering* **14**, 257-265 (2009).

35 Blackman, M. L., Royzen, M. & Fox, J. M. Tetrazine ligation: fast bioconjugation based on inverse-electron-demand Diels– Alder reactivity. *Journal of the American Chemical Society* **130**, 13518-13519 (2008).

5.6 Supplemental Figures and Spectra

AHA-P gene:

5'-
CCATGGAACATCATCATCATCATCATGCGGGTGCTGGTGCGGGTCCGGAAGGTCGTGGCGATAGTGCTGGTGCGG
GCGCTGGTCCGGAAGGTTTTGCGGGCGCCGGTGCAGGCCCGGAAGGTGCTGGCGCGGGTGCCGGCCCGGAAGG
TGCAGGCGCTGGTGCGGGCCCGGAAGGTGCCGGCGCAGGTGCTGGCCCGGAGGGCGCCGGTGCGGGTGCAGGC
CCGGAAGGCTTCGCTGGTGCCGGCGCAGGTCCGGAAGGCGCGGGTGCCGGCGCGGGTCCGGAAGGCCGTGGTG
ACTCGGCTGGCGCAGGCGCAGGCCCGGAAGGTCATCACCATCACCACCACGAAATGTAAAAGCTT-3'

Translates to:

M E HHHHHH AGAGAGPEG RGDS AGAGAGPEG F AGAGAGPEG AGAGAGPEG AGAGAGPEG AGAGAGPEG
AGAGAGPEG F AGAGAGPEG AGAGAGPEG RGDS AGAGAGPEG HHHHHH E M

Supplemental Figure 5.S1: Gene and protein sequence for AHA-P.

CYS-P gene:

5'-
CCATGGAATGTATTGCAGGTGCGGGCGCTGGTCCGGAAGGCGGTCCGCAGGGTATTTGGGGTCAGGCTGGTGCC
GGTGCGGGTCCGGAAGGCATGGCGGGTGCAGGCGCCGGTCCGGAGGGCCGTGGTGATAGCGCCGGCGCTGGTG
CAGGCCCAGAAGGTGCAGGCGCGGGCGCTGGTCCGGAAGGTGCTGGCGCCGGTGCGGGTCCGGAGGGTGCGG
GTGCAGGCGCCGGTCCGGAAGGCGCCGGTGCTGGTGCAGGTCCAGAAGGCCGTGGCGATTCTGCAGGTGCGGG
CGCTGGCCCAGAAGGCGCTGGCGCCGGTGCGGGTCCGGAGGGTATGTGGGCGGGCGCAGGCGCCGGTCCGGAA
GGTATTTGTGAAATGTGGCACCATCACCACCATCATTAAAAGCTT- 3'

Translates to:

MECI AGAGAGPEG GPQG IWGQ AGAGAGPEG M AGAGAGPEG RGDS AGAGAGPEG AGAGAGPEG
AGAGAGPEG AGAGAGPEG AGAGAGPEG RGDS AGAGAGPEG AGAGAGPEG MW AGAGAGPEG ICEMW
HHHHHH

Supplemental Figure 5.S2: Gene and protein sequence for CYS-P.

A

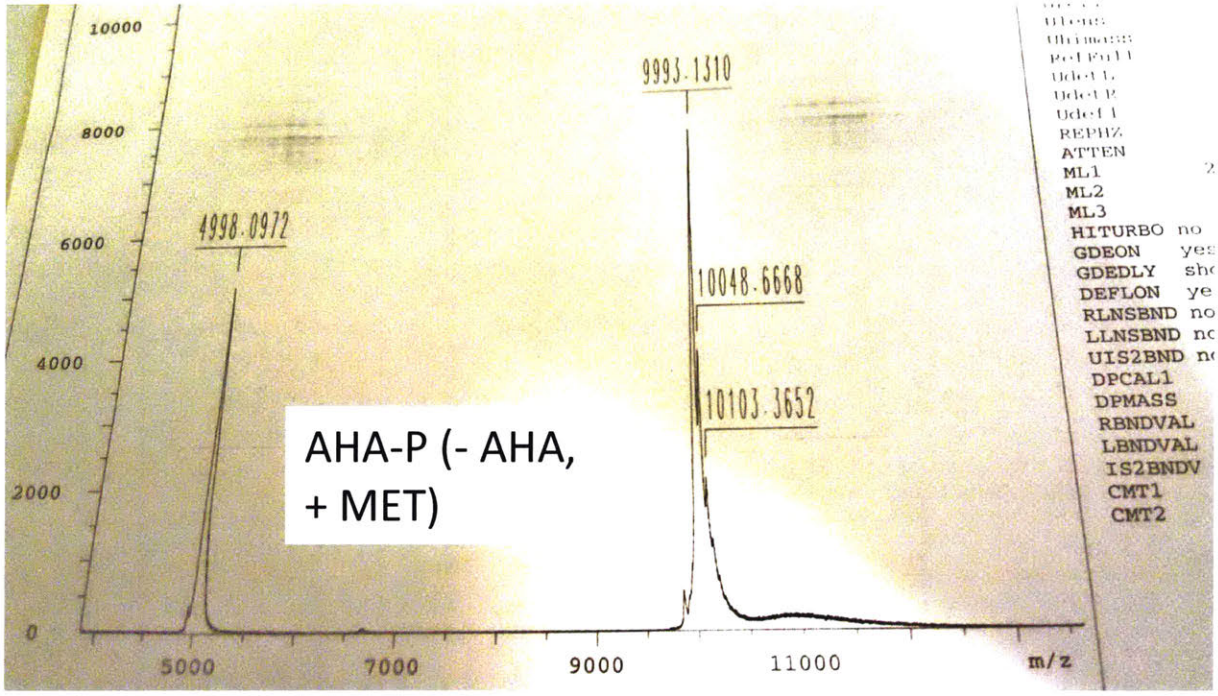

B

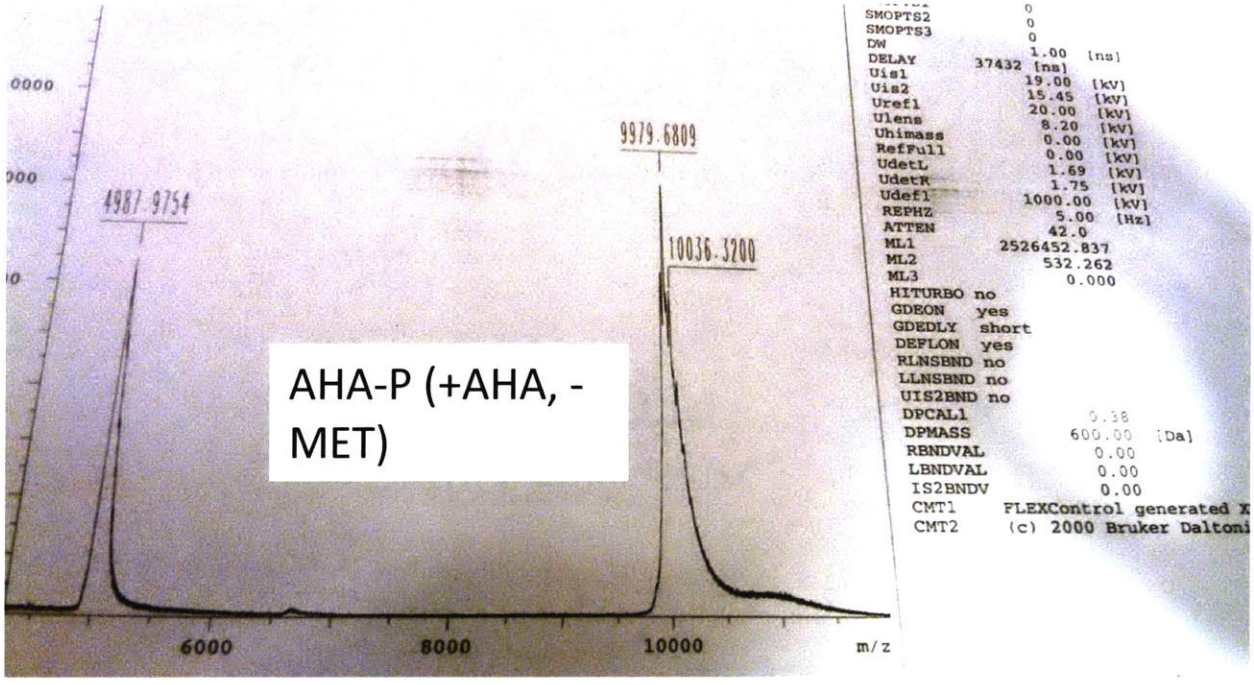

Supplemental Figure 5.S3: MALDI-TOF of AHA-P. A) Control using MET instead of AHA for the expression. B) AHA-P with AHA in place of MET.

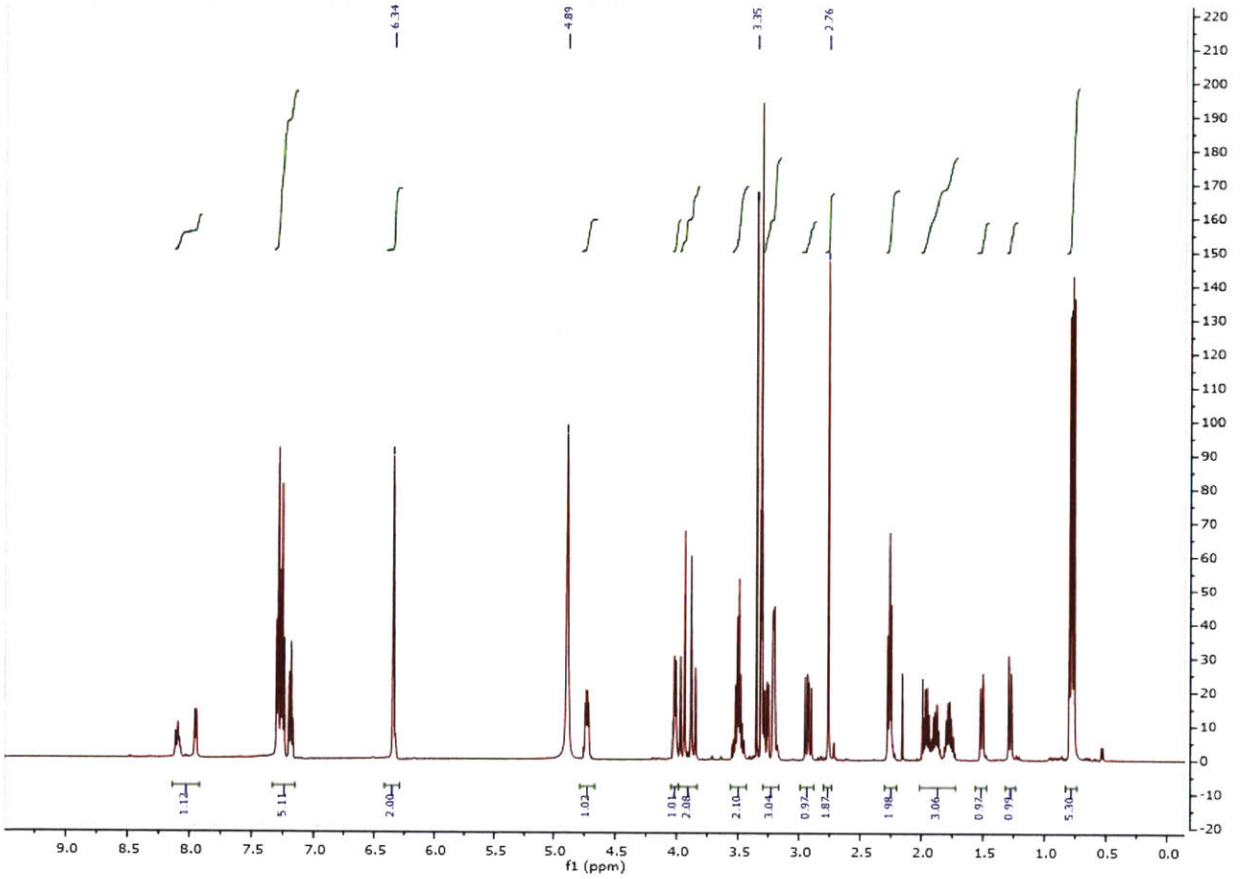

Supplemental Figure 5.S4: ^{1}H-NMR of Norb-val-phe-gly in CD_3OD taken on a 500 MHz spectrometer.

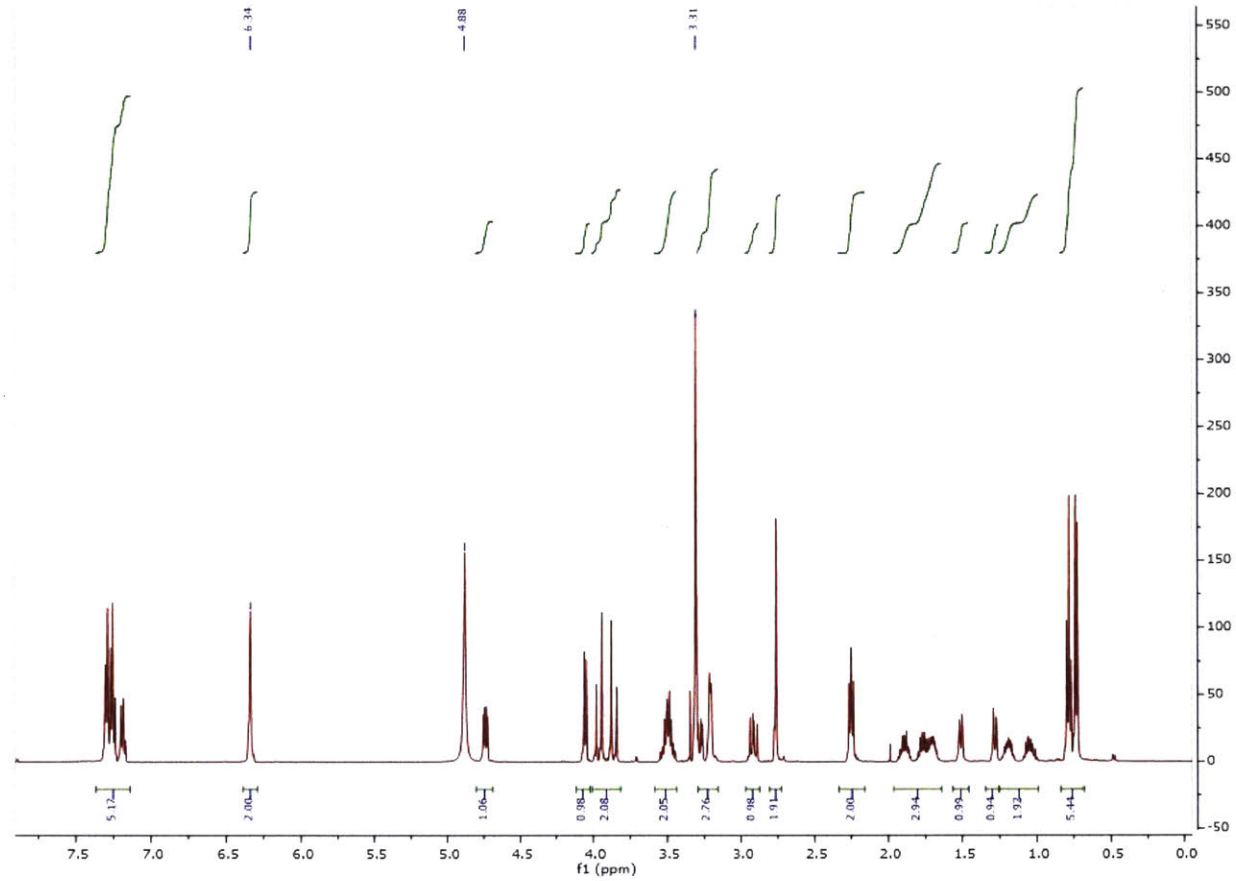

Supplemental Figure 5.S5: ^{1}H-NMR of Norb-ile-phe-gly in CD_3OD taken on a 500 MHz spectrometer.

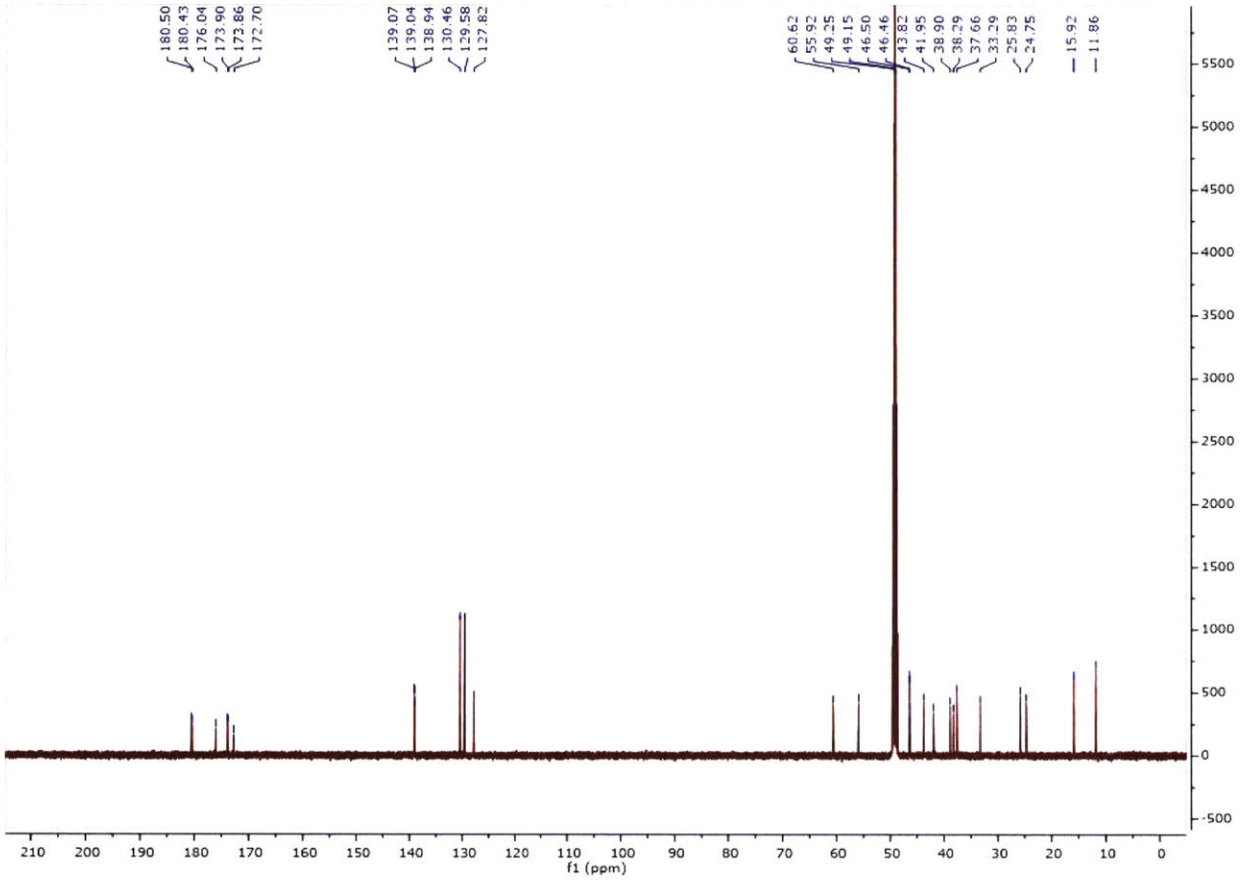

Supplemental Figure 5.S6: ^{13}C-NMR of Norb-ile-phe-gly in CD_3OD taken on a 500 MHz spectrometer.